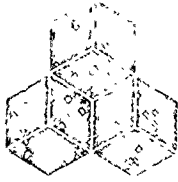


AD 712852



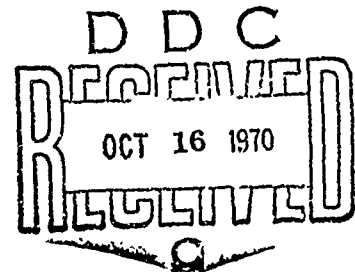
SYSTEMS, SCIENCE AND SOFTWARE

DASA 2498

3SR-267

STRESS WAVE EFFECTS IN INHOMOGENEOUS AND POROUS EARTH MATERIALS

BY
T.D. RINEY
S.K. GARG
J.W. KIRSCH
L.W. MORLAND
C.R. HASTINGS



FORMAL REPORT

FOR PERIOD 15 MAY 1969 - 14 MARCH 1970

PRINCIPAL INVESTIGATOR: T. DAVID RINEY (714) 453-0060
PROJECT SCIENTIST: MR. C.B. MCFARLAND, DASA

SPONSORED BY ADVANCED RESEARCH PROJECTS AGENCY
ARPA ORDER NO. 1438

PROGRAM CODE NUMBER 9F10
CONTRACT NO. DASA 01-69-C-0159
EFFECTIVE DATE OF CONTRACT: 15 MAY 1969

This document has been approved for public release and sale; its distribution is unlimited.

S³PROJECT 119

MARCH 31, 1970

Reproduced by the
CLEARINGHOUSE
for Federal Scientific & Technical
Information Springfield Va. 22151

P.O. BOX 1620, LA JOLLA, CALIFORNIA 92037, TELEPHONE (714) 453-0060

DISCLAIMER NOTICE

THIS DOCUMENT IS BEST QUALITY PRACTICABLE. THE COPY FURNISHED TO DTIC CONTAINED A SIGNIFICANT NUMBER OF PAGES WHICH DO NOT REPRODUCE LEGIBLY.

DASA 2498

SYSTEMS, SCIENCE AND SOFTWARE

3SR-267

**STRESS WAVE EFFECTS IN INHOMOGENEOUS
AND POROUS EARTH MATERIALS**

**BY
T.D. RINEY
S.K. GARG
J.W. KIRSCH
L.W. MORLAND
C.R. HASTINGS**

FORMAL REPORT

FOR PERIOD 15 MAY 1969 - 14 MARCH 1970

**PRINCIPAL INVESTIGATOR: T. DAVID RINEY (714) 453-0060
PROJECT SCIENTIST: MR. C.B. McFARLAND, DASA**

**SPONSORED BY ADVANCED RESEARCH PROJECTS AGENCY
ARPA ORDER NO. 1438**

PROGRAM CODE NUMBER 9F10

CONTRACT NO. DASA 01- 69-C-0159

EFFECTIVE DATE OF CONTRACT: 15 MAY 1969

S³PROJECT 119

MARCH 31, 1970

P. O. BOX 1620, LA JOLLA, CALIFORNIA 92037, TELEPHONE (714) 453-0060

CONTENTS

FOREWORD	v
I. INTRODUCTION AND SUMMARY.	1
II. EQUATION OF STATE OF WATER.	5
2.1 Introduction	5
2.2 Compressed States.	8
2.2.1 Theory.	8
2.2.2 Analysis.	11
2.2.1 Mie-Gruneisen Formulation.	12
2.2.2 Born Equation of State	19
2.2.3 Final Selection of Equation of State for Compressed Water.	34
2.3 Expanded States.	37
2.3.1 Expanded Liquid States.	39
2.3.1.1 p-V-E Equation of State.	41
2.3.1.2 E-V-T (Caloric Equation of State	44
2.3.2 Liquid-Vapor Equilibrium States	47
2.3.2.1 Basic Theory	47
2.3.2.2 Calculations	51
III. CHARACTERIZATION OF NTS TUFF.	59
3.1 Introduction	59
3.2 Dry Tuff	60
3.2.1 Porous, Dry Tuff Data	60
3.2.2 S ³ Compacted Dry Tuff	64
3.2.3 Schooner Tuff Hydrostat	70
3.3 Wet Tuff Data.	73

IV.	HOMOGENIZED EQUATION OF STATE FOR TUFF TUFF/WATER MIXTURES	77
4.1	Basic Considerations	77
4.2	Pressure Equilibrium (p-V Equations of State).	83
4.3	Equilibrium States—Energy Effects	88
4.3.1	PTEQ Calculations	89
4.3.1.1	Shock Hugoniots.	89
4.3.1.2	Release Adiabats	95
4.3.2	Additional Comments	102
V.	1-D COMPOSITE CONFIGURATIONS.	117
5.1	Introduction	117
5.2	Linear Fluid Model	121
5.2.1	Effect of Artificial Viscosity.	123
5.2.2	Laminated Composite	126
5.3	Volumetric Fluid Models.	134
5.3.1	Preliminary Considerations.	134
5.3.2	Pulse Propagation Normal to Laminates.	135
5.3.3	Step Pulse Normal to Laminates.	144
5.4	Thermodynamic Fluid Model.	150
5.5	Fourier Synthesis Method	157
5.5.1	Analysis.	157
5.5.2	The WARP Computer Program	159
VI.	2-D COMPOSITE CONFIGURATIONS.	161
6.1	Introduction	161
6.2	Wave Propagation Parallel to Bilaminates	162
6.2.1	Simplified Analytic Solutions	162
6.2.2	Detailed Computer Solutions	167

6.3	Wave Propagation Transverse to Parallel Pores	178
6.3.1	Computer Solutions.	178
6.3.2	Periodicity of Oscillations	181
VII.	THEORY OF INTERACTING CONTINUA.	191
7.1	Introduction	191
7.2	Equations of Theory of Interacting Continua	193
7.3	Constitutive Laws for Interacting Continua	210
7.3.1	Formulation of Mechanical Theory.	210
7.3.2	Interacting Continua under Simple Deformation.	217
7.4	Plane Wave Propagation	229
7.4.1	Governing Relations	229
7.4.2	Non-Dimensional Formulation	232
7.4.3	Initial and Boundary Conditions	235
7.5	Experimental Data Analysis	236
7.6	Finite Difference Scheme	244
7.6.1	Provisional Values at ($j+\frac{1}{2}$, $n+\frac{1}{2}$).	244
7.6.2	Final Values at (j , $n+1$).	245
7.6.3	Velocity Boundary Conditions.	246
7.6.4	Artificial Viscosity.	247
7.7	Numerical Results.	248
7.7.1	Minimal Principle vs Pressure Equilibrium.	249
7.7.2	Inclusion of Dilatational Difference Term $k(\lambda-\gamma)$ in the Constitutive Law.	254
7.7.3	Effect of Diffusive Resistance.	258
7.7.4	Inclusion of Strength Effects	263

VIII. DISCUSSION. 269

REFERENCES 273

APPENDIX A. Derivation of the Hydrodynamic
Equation of State for a Mixture from the
Given Equation of State of the Constituent
Materials 281

APPENDIX B. NTS Tuff Data 287

FOREWORD

This formal technical report entitled "Stress Wave Effects in Inhomogeneous and Porous Earth Materials," is submitted by Systems, Science and Software (S³) to the Advanced Research Projects Agency (ARPA) and the Defense Atomic Support Agency (DASA). The report presents the results of the first ten-month period of a continuing study to develop reliable material models to predict the response of geologic media in the transition regime which lies between the high pressure hydrodynamic and low pressure elastic regimes. This work, in support of the PRIME ARGUS research program, was accomplished under Contract No. DASA 01-69-C-0159, which was funded by ARPA. Dr. Stanley Ruby was the ARPA Program Manager and Mr. Clifton B. McFarland was DASA Project Scientist. Dr. T. David Riney was the S³ Principal Investigator for this study.

The technical results presented in Sections II through VII represent the work of a number of S³ staff members. It is appropriate to list here both the principal authors of these sections and the other contributors to that work:

	<u>Authors</u>	<u>Contributors</u>
Section II	J. W. Kirsch	G. A. Gurtman C. R. Hastings M. L. Gittings
Section III	C. R. Hastings	
Section IV	J. W. Kirsch	C. R. Hastings L. J. Hageman
Section V	T. D. Riney	K. G. Hamilton G. A. Gurtman

	<u>Authors</u>	<u>Contributors</u>
Section VI	T. D. Riney	E. J. Halda J. K. Dienes
Section VII	L. W. Morland* S. K. Garg	K. G. Hamilton

Dr. J. M. Walsh contributed to the thermodynamic studies and Dr. D. H. Brownell, Jr., contributed to the choice of numerical schemes utilized in some of the calculations. The authors are also indebted to Dr. G. D. Anderson for technical review of this report.

*Work done during the summer of 1969 when Dr. Morland, University of East Anglia, served as a consultant on this project.

I. INTRODUCTION AND SUMMARY

The PRIME ARGUS program is concerned with the detection, identification and interpretation of the teleseismic signals which emanate from an underground nuclear explosion. Because detection stations are necessarily at remote locations from the event, the detected signals are weak, well within the apparent elastic regime of earth media. Thus, one is concerned with a signal which has attenuated from stress levels, at close distances, which may be megabars, to stresses, at detection distances, which are small compared to strengths of earth media.

In the PRIME ARGUS program, it has been recognized that a basic problem in relating the yield of a device to the observed seismic signal magnitude is the lack of understanding of the phenomena that occur in geologic materials under shock conditions in the pressure range from 300 kbar down to a few bars.⁽¹⁾ This is the transition region between the hydrodynamic regime, in which strength effects may be ignored, and the elastic regime. In the transition region complex phenomena such as those associated with dynamic void compaction, heterogeneity, pore water pressure and diffusion, fracture phenomena, material phase changes, and dependence of strength parameters on thermodynamic state can become so important as to dominate the attenuation of the signal.⁽²⁾ Current uncertainties in modeling these effects in continuum mechanics computer codes, coupled with the usual difficulties of shock hydrodynamics, render it hazardous to predict ground shock effects in the critical pressure range.

A typical geologic material consists of a rock matrix containing voids or cracks that may be partially filled with water in one of its thermodynamic states. Even if the basic

matrix material is unchanged, the porosity and the water content will vary significantly with depth and with surface distance and the propagation characteristics of the medium will vary accordingly. The theoretical studies described in this report, in support of the PRIME ARGUS program, are directed to the construction of reliable techniques for predicting wave propagation in a geologic medium which contains a specified amount of water in its pores.

The geologic medium is considered to be a composite and a description of its wave propagation characteristics is sought in terms of the behavior of the isolated matrix and water components. The general approach is to construct material models of increasing sophistication from available material properties data and to use analytical and numerical methods to evaluate stress wave phenomena as each additional physical effect is introduced into the model. Nevada tuff was selected as the matrix rock in order to be specific, but the basic methods should be applicable to other porous and heterogeneous geologic media.

In Section II, the thermodynamic equation of state for water is constructed in convenient analytic forms for the critical transition pressure regime. Both the expanded and condensed states of water are treated as well as the transition through the steam dome. In Section III, an equation of state for compacted dry tuff is formulated for the transition pressure regime. These analytic forms are used in Section IV to implement a computer program which calculates an homogenized equation of state for a water/rock composite medium from the equations of state of the components under the assumption that the components of the composite are in pressure and thermal equilibrium. The program is applied to predict the shock response of saturated wet tuff media with varied mass fractions of water.

The homogenized equation of state for the water/rock composite ignores the substructure of the medium which can scatter or disperse a wave. Detailed finite difference calculations have been made to examine this effect for water/tuff configurations in which both materials are treated as fluids. In Section V calculations are presented describing the propagation of pressure pulses in a direction normal to the layers of bilaminate composite configurations. Calculations treating wave propagation parallel to the layers of a bilaminate configuration are presented in Section VI. Numerical results for a step pulse propagating through a tuff matrix with periodic water-filled pores are also presented in this section.

The adaptation and application of the Theory of Interacting Continua to study non-linear wave propagation through a water/rock composite medium is described in Section VII. This analysis permits the treatment of the motion (diffusion) of water relative to the rock matrix without explicit treatment of the substructure of the medium as would be required by conventional continuum mechanical models. A computer program implemented to study wave propagation within this theoretical framework is applied to study diffusion effects in a water-saturated tuff matrix with shear strength. Finally, in Section VIII, the status of the work is summarized and suggestions are made for the direction of the effort during the next contract period.

II. EQUATION OF STATE OF WATER^{*}

2.1 INTRODUCTION

Numerical calculations to predict shock wave propagation in various media require that an equation of state for the materials be known. In particular, such computer codes as SKIPPER, CRAM, and POROUS (which have been employed in the course of the present program) are typical of shock propagation codes which are dependent on an equation of state of the form

$$p = p(V, E) . \quad (2.1a)$$

An adequate equation of this form is not readily available for pure water. Moreover, the consideration of thermal equilibrium between tuff and water in Section IV requires that a caloric equation of state also be determined, i.e.,

$$E = E(V, T) . \quad (2.1b)$$

In this section, new equations of state for water in the compressed and expanded regions are presented. They are of the required forms, (2.1, a and b), and are based on a physical model of water which is compatible with experimental results. Within the framework of this model the double formulation of the equilibrium states implicitly guarantees that the results will be internally consistent.

Compatible with the pressure-volume range of interest noted in Section I, the proposed equations of state have been developed for application to the thermodynamic region with entropies less than the value at 200 kbars on the shock Hugoniot. This would include the liquid-vapor transition at low pressures, but no attempt has been made to characterize the solid phases of water.

^{*} Author: J. W. Kirsch

Considerable effort has been expended in the characterization of water by numerous investigators and is available in the open literature. However, most of the experimental data on equilibrium states are concentrated in low pressure regimes⁽³⁾ (below 2.5 kilobars), low temperature regions,^(4,5) and the thermodynamic vicinity of the saturation line.^(6,7,8) Unfortunately, the peculiar qualities of water are most evident in these regimes and precise characterization of the molecular physics of water has not been possible.

A review of the literature on water was undertaken to ascertain the extent of previous investigations in the range of interest. The major contribution to our understanding of high pressure (250 kbar) thermodynamic states was made by Rice and Walsh.^(9, 10) Their experiments on water were conducted to determine the shock Hugoniot. The experimental results were interpreted under the simplifying assumption that, above 25 kbar, the specific heat at constant pressure is constant and that $\left(\frac{\partial V}{\partial T}\right)_p$ is, at most, a function only of the pressure. Their analysis provides a numerical method by which p , V , E states may be computed (as well as the temperature, T) for the compressed states of water. Under certain additional approximations, Papetti and Fujisaki⁽¹¹⁾ have reduced the Rice and Walsh⁽¹⁰⁾ numerical method to a still simpler, analytic form. The equation of state, however, is not written in the form $p(V, E)$, but rather $V(p, E)$, and does not lend itself, directly, to use in the continuum mechanics computer codes.

Walker and Sternberg⁽¹²⁾ have developed a $p(V, E)$ equation of state for water. These equations have the form

$$p = \frac{f_1(E)}{V} + \frac{f_2(E)}{V^3} + \frac{f_3(E)}{V^5} + \frac{f_4(E)}{V^7}$$

where the $f_i(E)$ are polynomials in E , and have been fit

to the Rice and Walsh data. Although such a form is convenient for p-V-E calculations, the complexity of the relations and the lack of a direct E-V-T relationship precluded (immediate) use of this analytic form of the equation of state of water.

Tabular arrays^(13,14) of equilibrium states of water are available which supply data in the range of interest. These tables have been developed from the same data⁽³⁻¹⁰⁾ and present no new information or physical insight into the physics of water states. In any case, the tables contain only a limited amount of data* and considerable effort would be required to "fill" in the gaps. There is in progress (at the RAND Corporation) a compilation of water states.⁽¹⁶⁾ This work covers, effectively, the entire range of thermodynamic variables encountered in nuclear bursts. However, in the range of interest in this study, the compilation contains data based on the work of Papetti and Fujisaki,⁽¹¹⁾ and Walker and Sternberg⁽¹²⁾ (both of which are derived from the Rice and Walsh⁽¹⁰⁾ data). These states have been presented elsewhere⁽¹⁷⁾ (in graphical form). The RAND tables are not presently available and it is not known as to how much of an improvement they represent over that already in the literature.⁽¹²⁻¹⁴⁾

As a result of these findings, effort has been concentrated on constructing an analytic equation of state which affords considerable simplification relative to previous models, yet yields results which agree with the available data.

* Moreover, Sharp's^(13,14) tables contain some inconsistencies and a certain degree of inaccuracy is implicit in his method of calculation. Howard⁽¹⁵⁾ presents only p-V-T data.

2.2 COMPRESSED STATES

A new equation of state for compressed water is developed on the basic assumption that in the thermodynamic vicinity of the Hugoniot, water can be considered to behave in a pseudo-crystalline manner. (Actual phase transitions (to Ice-VII), however, are not considered.) The analysis, relies heavily on the experimental data and theoretical calculations presented by Rice and Walsh⁽¹⁰⁾ for pressures between 2 and 200 kilobars. In this regime, it is assumed that the specific heat at constant volume, C_V , is constant. This assumption implies an equivalence between the Mie-Gruneisen formulation often applied to solids and the p-T-V equation of state suggested by Born⁽¹⁸⁾ for crystalline materials at the melting point.

It should be noted that most of the numerical pulse propagation work presented in other sections of this report was conducted under the assumption of a relatively simpler form of the equation of state than in Eq. (2.1a). In the spirit of step-by-step consideration of the various factors affecting shock wave propagation in geologic composites, first consideration has been given to idealized forms for the equation of state for compressed water, i.e., $p = p(V)$. These equations of state and the p-V-E, E-V-T expressions that have been developed for later inclusion in numerical experiments are presented in this section.

2.2.1 Theory

Analytical expressions for the equation of state of water in the thermodynamic vicinity of the shock Hugoniot have been proposed by Papetti and Fujisaki⁽¹¹⁾ and most recently, Cowperthwaite and Shaw.⁽¹⁹⁾ As noted previously,

the Papetti-Fujisaki⁽¹¹⁾ model is based on the Hugoniot data published by Rice and Walsh,⁽¹⁰⁾ and is limited to pressures greater than 25 kbar. Cowperthwaite and Shaw⁽¹⁹⁾ hypothesize an equation of state for a number of liquids based on the Walsh-Christian⁽²⁰⁾ model for metals. Their approach is to assume C_V is (at most) dependent only on temperature and that $\left(\frac{\partial p}{\partial T}\right)_V$ is constant.

An alternate view of the physics underlying water's behavior can be deduced from the fact that extrapolations of Bridgman's phase transition data by Snay and Rosenbaum⁽²¹⁾ lay immediately adjacent to the experimentally determined Hugoniot in the pressure range from 20 to 30 kilobars.* Moreover, in a subsequent set of shock propagation experiments, Altshuler, et al.,⁽²²⁾ report data from which they concluded that a phase transition (to Ice-VII) had occurred at about 120 kbar.

Within this framework, it is quite relevant to note that Born,⁽¹⁸⁾ in his paper on the thermodynamics of crystal melting, hypothesized that liquids in states near the melting transition may retain the basic lattice structure similar to the solid phase, although the ordered geometric arrangement of the lattices may be lost. This suggests that, at least in the vicinity of the Hugoniot curve, the equation of state for water may be describable by a functional form similar to that derived by Born for melting crystals, i.e.,

$$p(V, T) = h_1(V) + T h_2(V)** \quad (2.2)$$

* Phase change effects were not considered by Rice and Walsh.

** An equivalent expression was proposed by Schall⁽²³⁾ in 1949 for employment in the interpretation of the results of his experimental investigation of shock propagation in pure water. The physical justification for this equation is vague (perhaps due to losses in translation) and his resulting expressions appear to be inaccurate (vis-a-vis the experimental data of Rice and Walsh.^(9,10))

Implicit in this form of an equation of state is the partitioning of a material's internal energy into harmonic thermal motion of its molecules and the compressional potential energy of its lattice. This can be readily demonstrated by invoking the identity,

$$\left(\frac{\partial E}{\partial V}\right)_T \equiv -p + T \left(\frac{\partial p}{\partial T}\right)_V = -h_1(V) \quad (2.3)$$

i.e., the compressional energy of such materials is solely a function of the degree of compression (of its lattice). Moreover, Eq. (2.3) can be integrated to yield

$$E(V,T) = -\int_{V_0}^V h_1(V) dV + f(T) \quad (2.4)$$

where $f(T)$ represents the contribution of the thermal motion of the molecules within the lattice.

In the calculations which follow, we have assumed that this thermal contribution to the internal energy is linear with T , i.e.,

$$\left(\frac{\partial E}{\partial T}\right)_V = C_V = \text{constant} \quad (2.5)$$

This assumption admits a functional form of (2.4) and

$$E(V,T) - E_0(V_0, T_0) = C_V(T - T_0) - \int_{V_0}^V h_1(V) dV \quad (2.6)$$

It may be observed that if C_V is considered a constant, the Born form of the equation of state (2.2, 2.6) is equivalent to the Mie-Gruneisen formulation often applied to solids subjected to high pressures. The Mie-Gruneisen equation of state can be written as

$$p = p_H(V) + \frac{G(V)}{V} \left(E - E_H(V) \right) \quad (2.7)$$

where the subscript H refers to the Hugoniot curve. Substituting the expression for energy (Eq. 2.6) into this relation, gives

$$p = \left\{ p_H(V) - \frac{G(V)}{V} E_H(V) + \frac{G(V)}{V} \left(E_0 - \int_{V_0}^{V_1} h_1(V) dV \right) - \frac{G(V)}{V} C_V T_0 \right\} + T \left(\frac{C_V G(V)}{V} \right) \quad (2.8)$$

This expression for pressure, in terms of T and V, is equivalent to the Born form with the following identifications.

$$h_1(V) = p_H(V) + \frac{G(V)}{V} \left(E_0 - E_H(V) - \int_{V_0}^{V_1} h_1(V) dV - C_V T_0 \right) \quad (2.9)$$

$$h_2(V) = \frac{C_V G(V)}{V} \quad (2.10)$$

Thus, in the limit that C_V is constant, the Mie-Gruneisen formulation is equivalent to the Born model. This is significant in that one can construct a self-consistent equation of state (for such materials) based on either isothermal data or Hugoniot-release isentrope information.

2.2.2 Analysis

The available information on compressed water enables the development of an equation of state based on either of the two methods noted above. In the present work, a "hybrid" equation of state, derived from both types of data, has been selected for use in the numerical experiments dealing with energy effects. Presentation of the analysis from which this

equation of state has been constructed is given in separate sections dealing with the two component formulations.

2.2.2.1 Mie-Gruneisen Formulation

The cornerstone of this analysis is to characterize the Hugoniot with analytic expressions. A least square, cubic fit to the Rice-Walsh data⁽¹⁰⁾ has been obtained for $p_H(V)$, (see Fig. 2.2), i.e.,

$$p_H(V) = A\mu + B\mu^2 + F\mu^3, \quad (2.11)$$

$$A = 21.9534 \text{ kbar}$$

$$B = 52.138 \text{ kbar}$$

$$F = 231.81 \text{ kbar}$$

where $\mu = \frac{V_0 - V}{V}$, and $E_H(V)$ is determined from the Hugoniot relation

$$E_H(V) = + \frac{p_H(V)}{2} (V_0 - V) \quad (2.12)$$

The expression in Eq. (2.11) has been used as the non-linear, volumetric equation of state in a portion of the calculations presented in Sections V, VI, and VII.*

Since $E_H(V)$ and $p_H(V)$ are known, the only unknown in the Mie-Gruneisen formulation is the Gruneisen ratio, $G(V)$. It is possible to explicitly determine $G(V)$ on the Hugoniot within the framework of the analysis (above 25 kbar). These calculations are graphically presented in Fig. 8 of the Papetti and Fujisaki paper⁽¹¹⁾.

* A linear, volumetric equation of state, $P = A (1 - V/V_0)$, has also been utilized in the first phase of the numerical work presented in Section V.

It is of interest to determine if the Rice-Walsh⁽¹⁰⁾ isentropic data could be reduced to the Mie-Gruneisen form. This is accomplished by calculating the value of $G(V)$ which is required to satisfy Eq. (2.7) at a given value of V and entropy, S_H . From Eq. (2.7),

$$G(V) = \left\{ \frac{p_{S_H}(V) - p_H(V)}{E_{S_H}(V) - E_H(V)} \right\} V \quad (2.13)$$

where the subscript S_H refers to a specific isentrope which intersects the Hugoniot as V_{S_H} , and

$$E_{S_H}(V) = E_H(V_{S_H}) - \int_{V_{S_H}}^V p_{S_H}(V) dV. \quad (2.14)$$

The five series of $G(V)$ points obtained in this fashion are displayed in Fig. 2.1. It can be seen that the points do not lie on a single curve, nor are they coincident with the Hugoniot values for $G(V)$ ⁽¹¹⁾. These results indicate that the Gruneisen ratio based on the constant C_p data⁽¹⁰⁾ is somewhat dependent on the energy. The dependence must be small, however, since the series of points in Fig. 2.1 trace out curves that are in reasonable agreement.

The data presented in Fig. 2.1 can be represented by the following form

$$G(V) = a \sin (bV + c) + h \quad (2.15)$$

where

$$a = .41 \quad b = 9.52 \quad c = -4.5676 \quad h = .94$$

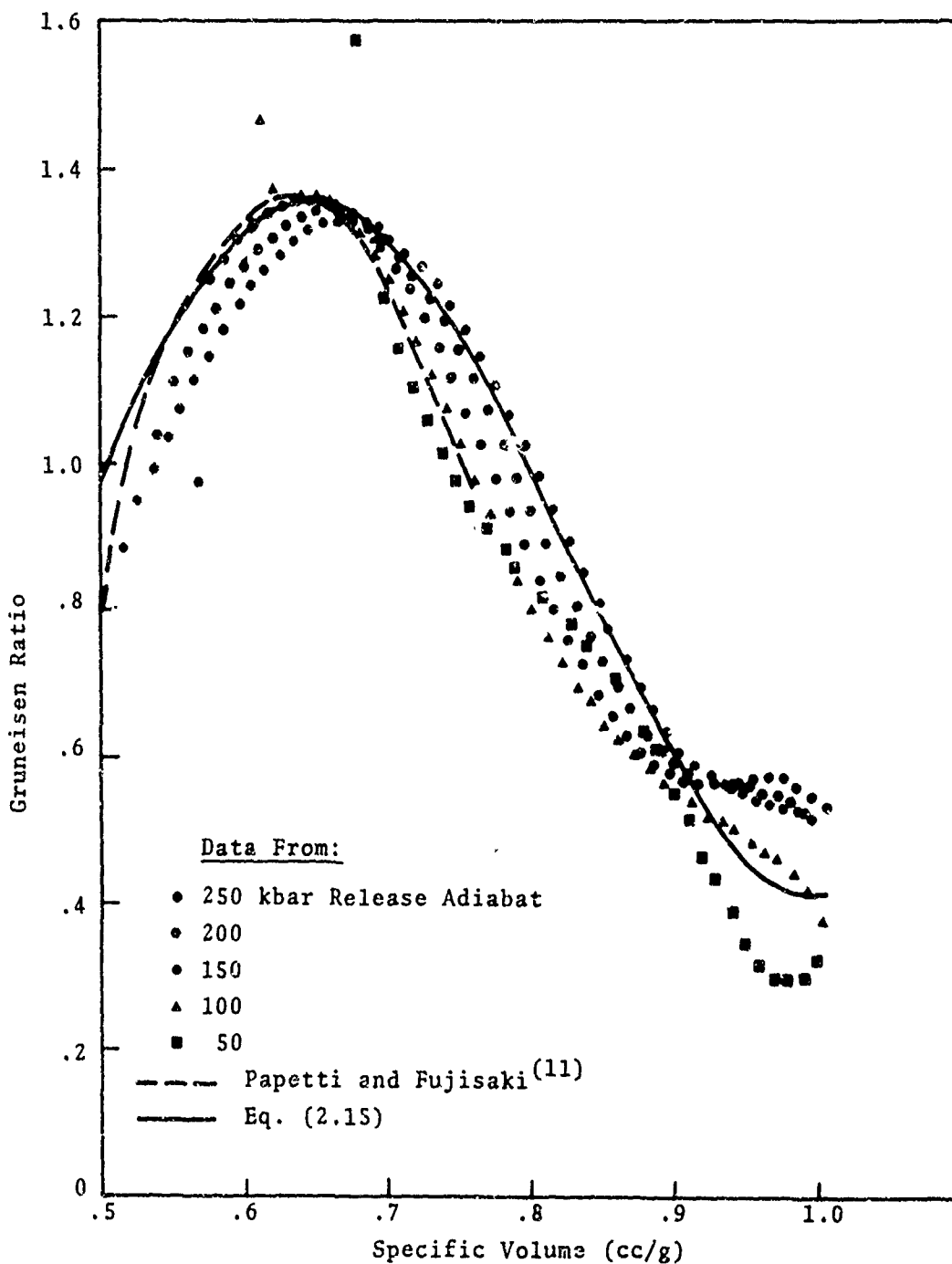


Fig. 2.1--Gruneisen ratio for water plotted as a function of volume. Calculations of $G(V)$ on the Hugoniot⁽¹¹⁾ are compared to those computed from release adiabats (Eq. 2.13). Also shown is $G(V)$ used in subsequent calculations (Eq. 2.15).

This expression is plotted in Fig. 2.1 for comparison to the various curves for $G(V)$. Using this expression for $G(V)$, and Eqs. (2.11, 2.12), a complete p - V - E equation of state can be written for the compressed states of water, i.e.,

$$p(V,E) = p_H(V) \left(1 - \frac{G(V)\mu}{2} \right) + \frac{G(V)}{V} E \quad (2.16)$$

As a check on the sufficiency of this equation of state, a set of release isentropes have been calculated by substituting Eq. (2.16) into the differential equation

$$dE = -p(V,E) dV \quad (2.17)$$

and integrating this equation from various starting points on the Hugoniot. The comparison of these calculations to the isentropes calculated by Rice and Walsh⁽¹⁰⁾ is given in Fig. 2.2 wherein the excellent agreement between the two sets of data is clearly indicated.

It should be noted that it was not, strictly speaking, necessary to use the $G(V)$ derived from the release isentropes. The Gruneisen ratio determined by Papetti and Fujisaki⁽¹¹⁾ is dependent only on the Hugoniot values of p, V, E . Although this method has been applied to the region above 25 kbar, it would, no doubt, be possible to extend this curve to V_0 (under some sort of simplifying thermodynamic assumption). However, the advantage in using Eq. (2.15) is that the original release isentrope data⁽¹⁰⁾ are more closely approximated than with the $G(V)$ computed on the Hugoniot.

Caloric Equation of State -- Complete formulation of the water equation of state must include some additional relationship which includes temperature. The specific heat at constant volume and $h_1(V)$, are all that are needed to provide an E - V - T equation of state (see Eq. 2.6). The

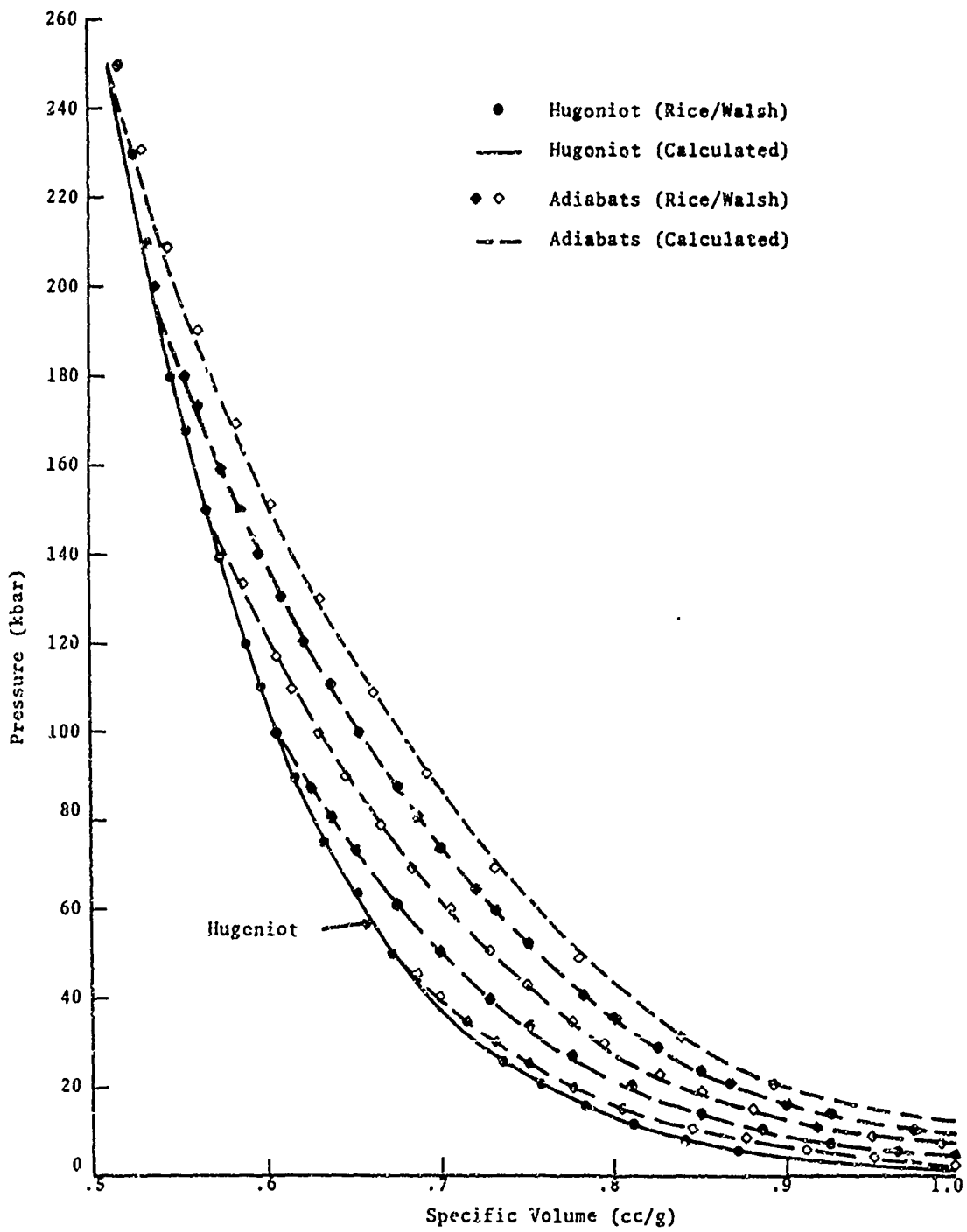


Fig. 2.2--Hugoniot and release adiabat curves for water calculated from Eq. (2.13) compared to the Rice and Walsh⁽¹⁰⁾ values.

specific heat at constant volume is taken as being between .7 and .8 based on Bridgman's data reported by Dorsey⁽²⁴⁾. For C_V independent of volume, the compressional energy derivative, $h_1(V)$, is just the 0°K isotherm.* Since the p-V-E equation of state is known and the 0°K isotherm is equivalent to an isentrope passing through $V = V_0$ at $T = 0^\circ\text{K}$, $h_1(V)$ may be directly determined by integrating the isentropic equation (2.17). The p-V relation resulting from this integration has been fit to a six-degree polynomial. This is then integrated over specific volume to obtain the compression energy integral, $I_1(V)$

$$I_1(V) \equiv - \int_{V_0}^V h_1(V) dV \quad (2.18)$$

where the polynomial is given in Fig. 2.3. Although another form of $I_1(V)$ is determined in the analysis associated with the Born formulation (Eq. 2.22), it is instructive to compute Hugoniot temperatures from the relation

$$\left\{ (E_H - E_0) - I_1(V) \right\} \frac{1}{C_V} = T_H - T_0 \quad (2.19)$$

where E_H is the energy on the Hugoniot⁽⁸⁾ and $I_1(V)$ is given by Eq. (2.18). (For comparative purposes, a $C_V = .78 \text{ cal/g}$ ($\sim 3.265 \times 10^{-7} \text{ ergs/gm}$) has been utilized to find T_H .) These values are plotted vs specific volume in Fig. 2.3, and compared to the Rice and Walsh theoretical values. It can be seen that there is excellent agreement

* It should be noted that this same form of the thermal equation of state (Eq. 2.6) has been applied to non-metallic geologic materials with low thermal expansion coefficients, by Ahrens, et al.,⁽²⁵⁾. For such materials, substitution of a room temperature isotherm for the compressional shock energy derivative, $(\partial E/\partial V)_T$, is a good approximation.

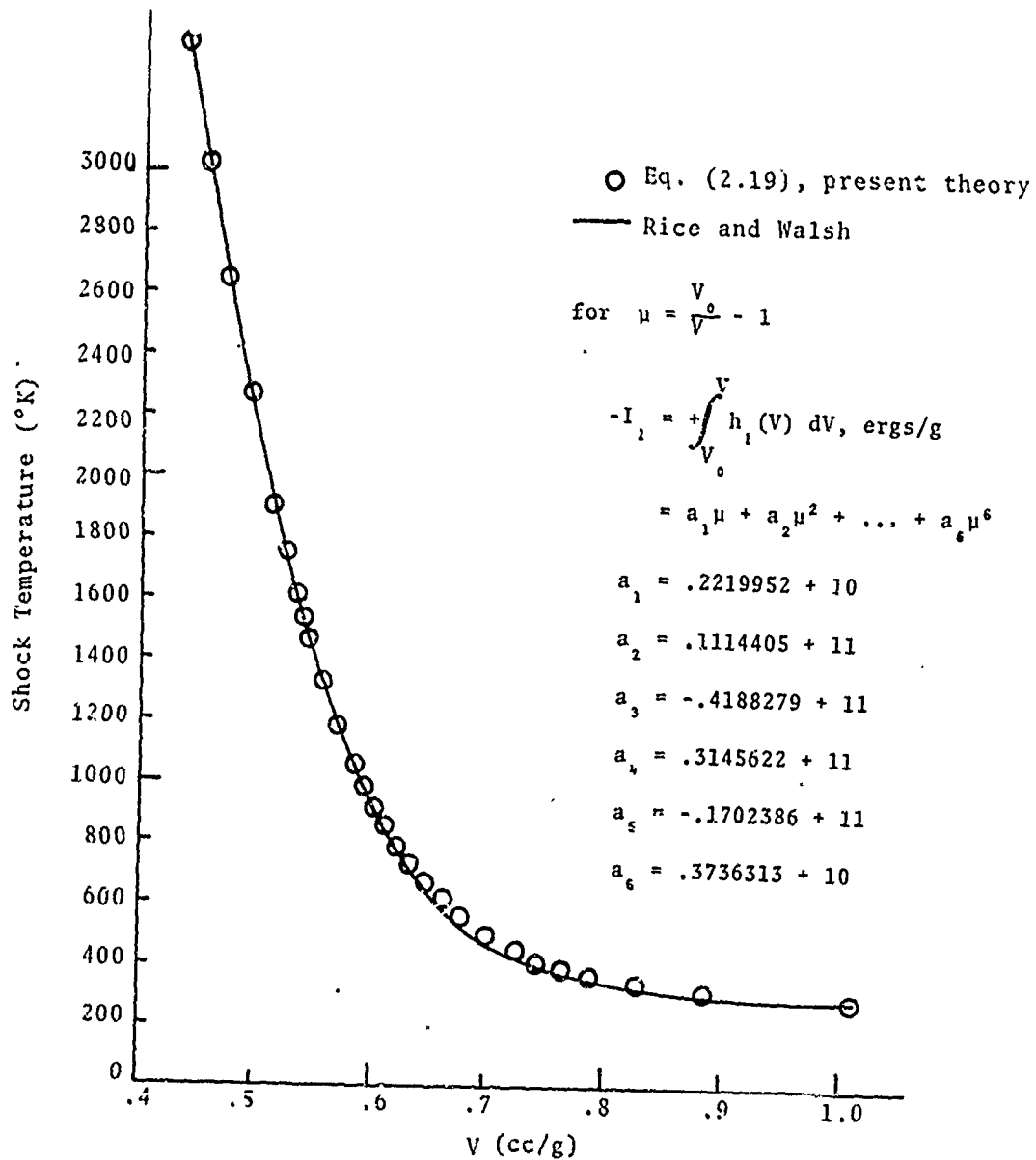


Fig. 2.3--Temperatures on the water Hugoniot computed from Eq. (2.19) (using the Rice and Walsh⁽¹⁰⁾ Hugoniot energies) with $C_V = .78$ cal/g and the $I_1(V)$ determined from the p-V-E equation of state (2.3).

which might be improved in the low pressure range by choosing a different C_V . Further discussion of these results is contained in the following section.

2.2.2.2 Born Equation of State

The p-V-T equation of state requires that $h_1(V)$ and $h_2(V)$ be known. C_V is required to establish the E-V-T state equation, Eq. (2.6). In the case of water, these functions may be deduced from the available data in a number of ways. The most direct method is described below. Essentially, the Rice-Walsh⁽¹⁰⁾ isotherms are demonstrated to conform to the proposed equation of state in the (thermodynamic) vicinity of the Hugoniot. This analytical method, although equivalent to the Mie-Gruneisen formulation, is significant in that it is not necessary to possess an explicit description of the shock Hugoniot to construct a reasonably accurate equation of state.

Compression Energy Function, $h_1(V)$ -- The functional form of $h_1(V)$ was obtained by first taking polynomial fits* to the tabulated⁽¹⁰⁾ isothermal pressure-volume variations. Then, for any two isotherms, (T_i, T_j) , and a given specific volume, Eq. (2.16) yields

$$h_1(V) = \frac{p_i - (T_i/T_j)p_j}{1 - (T_i/T_j)} \quad (2.20)$$

In this manner, polynomial expressions for $h_1(V)$ were obtained for the ten possible combinations of the Rice-Walsh isotherms. One may then compare these curves to ascertain the validity of the assumption that a unique $h_1(V)$ does exist

* Six-degree polynomials were required to fit the Rice-Walsh⁽¹⁰⁾ data.

for water. The ten curves are presented in Fig. 2.4 wherein it can be seen that any pair of isotherms yield an $h_1(V)$ which varies from the mean by only three percent. In Fig. 2.4 the $h_1(V)$ computed from the 448°K and 1273°K isotherms is highlighted because it is employed in subsequent equilibrium state calculations. Expressed in polynomial form, this $h_1(V)$ is given by

$$\left[h_1(V) \right]_{\substack{448^\circ \\ 1273^\circ}} = A_1 + A_2 V + A_3 V^2 + A_4 V^3 + A_5 V^4 + A_6 V^5 + A_7 V^6 \quad (2.22)$$

where A_i are presented in Table 2.1.

As a check on the E-V-T equation of state the thermodynamic data for water computed by Sharp⁽¹⁴⁾ could be used to verify the form of the compressional energy integral $\left(- \int h_1(V) dV \right)$. Sharp has fit $V(T,p)$ between neighboring isobars and isotherms and then integrated $(\partial V/\partial T)_p$ and V to obtain the entropy (S) and Gibbs free energy (G).

From S and G, Sharp⁽¹⁴⁾ calculated the other thermodynamic variables. The basic data input of his calculations is from Rice and Walsh⁽¹⁰⁾ above 2.5 kbars, and the various "standard" sources on water data for the lower pressures. For a number of condensed state isotherms, Sharp has computed the internal energy. In the present formulation, these energy isotherms should have the same variation with V , and their shape would be identical to that of $h_1(V)$ defined by Eq. (2.18). A comparison of Sharp's data with the compression energy curves obtained from the volumetric integration of the two expressions for $h_1(V)$, Eqs. (2.18) and (2.22), is presented in Fig. 2.5. (The energy points from Sharp's isotherms over 160°C were normalized by setting the internal energy equal to zero at $V = .675$. Lower temperature isotherms tabulated by Sharp⁽¹⁴⁾ were normalized at $V = 1.0018$.) It may be concluded from Fig. 2.5 that the variation of

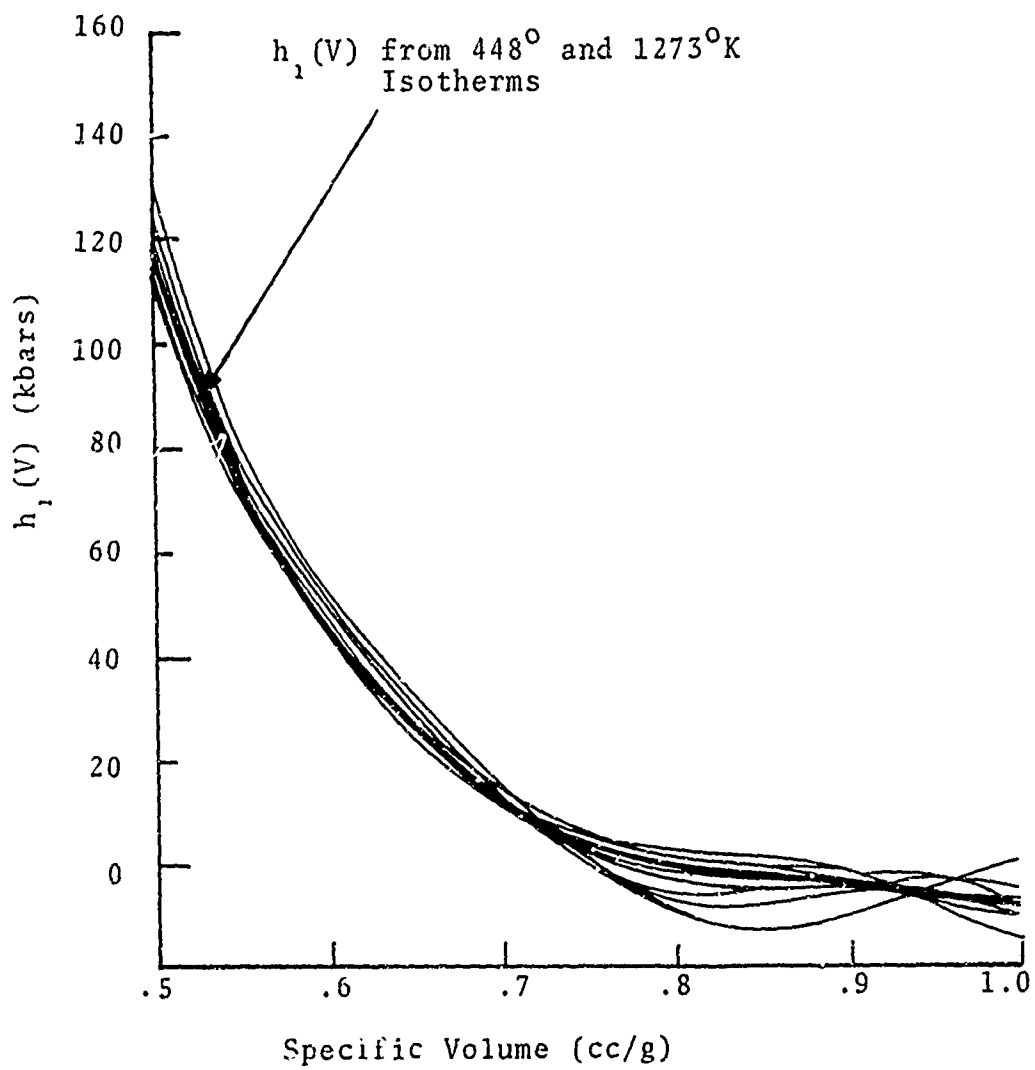


Fig. 2.4--Zero degree K isotherms ($h_1(V)$) for water plotted vs volume. Each curve is determined from two of the isotherms computed by Rice and Walsh⁽¹⁰⁾.

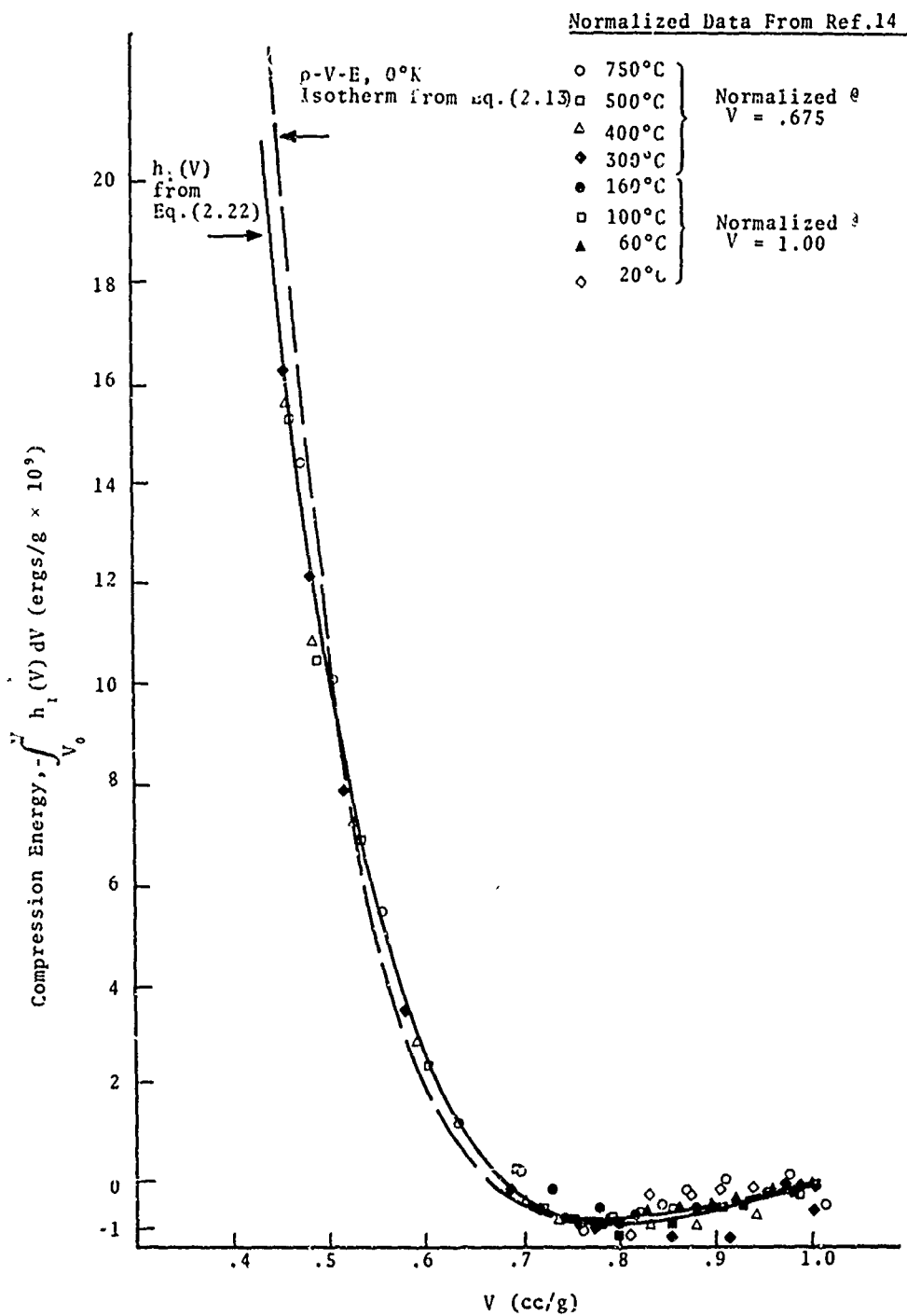


Fig. 2.5--Comparison of compression energy integrals, $I_1(V)$, determined from the p-V-E state equation (2.13) and that derived from $[h_1(V)]_{12780K}^{4480K}$, Eq. (2.22), with the energy isotherms tabulated by Sharp⁽¹⁴⁾.

TABLE 2.1
 POLYNOMIAL EXPRESSIONS FOR $h_1(V)$, $\int_{V_0}^V h_1(V) dV$, AND $h_2(V)$
 DERIVED FROM THE 448°K AND 1273°K RICE AND WALSH⁽¹⁰⁾ ISOTHERMS

$$f^*(V) = a_0 + a_1 V + a_2 V^2 + a_3 V^3 + a_4 V^4 + a_5 V^5 + a_6 V^6 + a_7 V^7$$

a_n	$h_1(V), \text{ kbars}$	$\int_{V_0}^V h_1(V) dV, \text{ kbars-cc}$	$h_2(V), \frac{\text{kbars}}{^\circ\text{K}}$
a_0	= 2.1151485352+04	= -2.3440333252+03	= -1.0418174624+01
a_1	= -1.6696763086+05	= 2.1151485352+04	= 9.2393991470+01
a_2	= 5.5372096875+05	= -8.3483815430+04	= -3.3131429672+02
a_3	= -9.7904692187+05	= 1.8457365625+05	= 6.2118081665+02
a_4	= 9.6834446875+05	= -2.4476173047+05	= -6.4345397186+02
a_5	= -5.0652573047+05	= 1.9366889258+05	= 3.4930139542+02
a_6	= 1.0931559375+05	= -8.4420955078+04	= -7.7670559883+01
a_7	= 0.0000000000	= 1.5616513306+04	= 0.0000000000

* V in cc/g

energy with volume indicated by Sharp's data is in reasonable agreement with both of the present theory's energy compression curves from the present theory.

It should be remarked that the increased scatter in the energy curve data for $V > .7$ can be interpreted as an indication of a transitional molecular structure of water. The hypothesized lattice-like structure of the more compressed water states appears to break down in this regime, being replaced by more gas-like behavior as the molecules separate.

Determination of $h_2(V)$ -- Analogous to the determination of $h_1(V)$, one may compute curves for $h_2(V)$ from the relation

$$h_2(V) = \frac{p_i(V) - p_j(V)}{T_i - T_j} \quad (2.23)$$

where the subscripts connote particular isotherms. Although the degree of convergence of these $h_2(V)$ curves is seen in Fig. 2.6 to be slightly less satisfactory than the $h_1(V)$ curves (see Fig. 2.4), it can be claimed that one may represent $h_2(V)$ by a single curve within the limits of the present theory. The highlighted curve in Fig. 2.6 is $h_2(V)$ computed from the 448°K and 1273°K isotherms and has been employed in subsequent calculations of equilibrium states. In polynomial form, $h_2(V)$ is

$$\left[h_2(V) \right]_{\substack{448^\circ \\ 1273^\circ}} = c_1 + c_2 V + c_3 V^2 + c_4 V^3 + c_5 V^4 + c_6 V^5 + c_7 V^6 \quad (2.24)$$

where c_i are given in Table 2.1.

Selection of C_V -- The last parameter required to characterize water is its specific heat at constant volume. There exists little experimental information on the C_V for water. It has already been pointed out that values

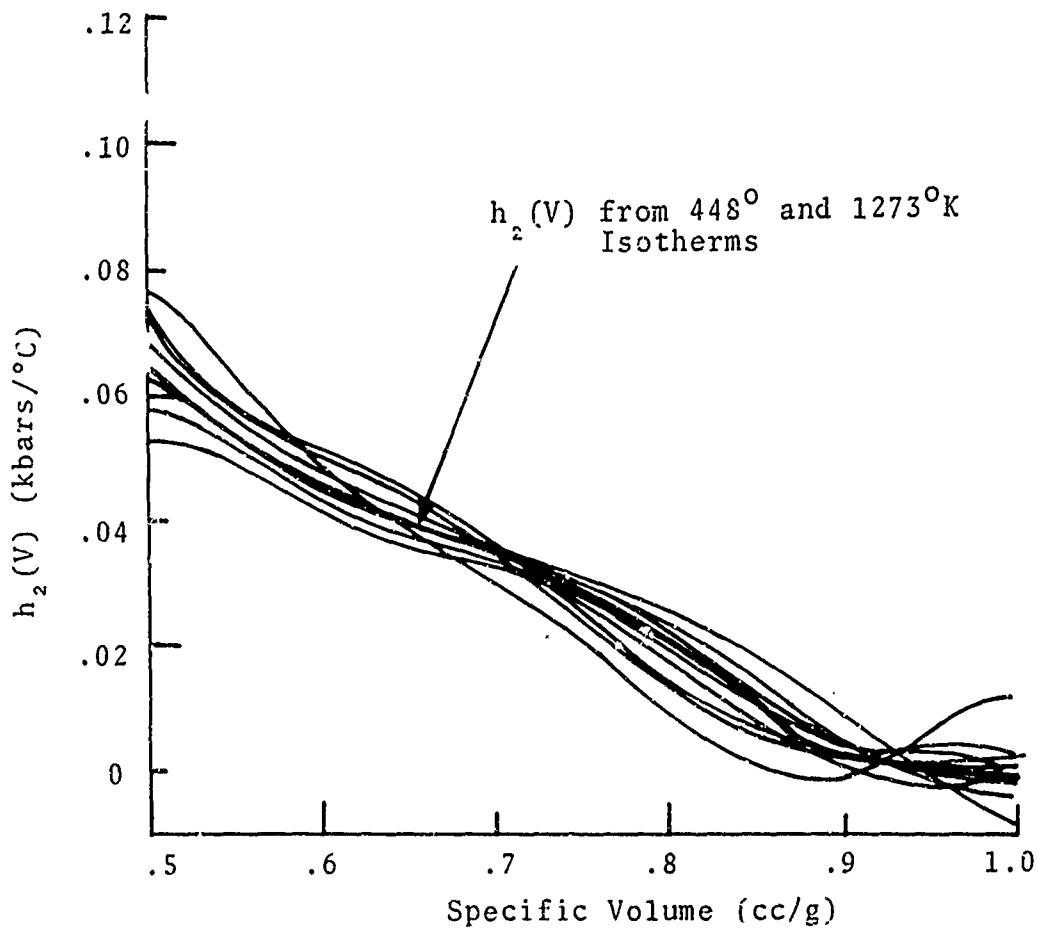


Fig. 2.6-- $h_2(V)$ for water plotted vs volume. Each curve is determined from two of the isotherms computed by Rice and Walsh⁽¹⁰⁾.

between .7 and .8 cal/g have been reported by Dorsey⁽²⁴⁾. Near the critical region, values within 10% of .7 have been computed from an equation of state developed by Watanabe, et al⁽²⁶⁾.

In the absence of any additional experimental or theoretical values, it is perhaps most appropriate to use the compression energy curve in Fig. 2.5 to determine an appropriate value of C_V . This method involves drawing the (isothermal) compression energy curve through the various points on the water Hugoniot in the E-V plane (as in Fig. 2.7). Then C_V is computed from

$$C_V = \left(\frac{\Delta E}{\Delta T} \right)_V \quad (2.25)$$

where the ΔT 's are taken from the Rice-Walsh⁽¹⁰⁾ values (see Fig. 2.7). The variation of C_V with T determined by this graphical method is depicted in Fig. 2.8. It can be seen that C_V exhibits a slight temperature dependence, but in the spirit of using single curves for $h_1(V)$ and $h_2(V)$, a single value of C_V (equal to 78 cal/g) is sufficiently accurate.

p-V-T Calculations -- It is a straightforward matter to calculate the Hugoniot, release adiabats, and isotherms from the two expressions

$$p = h_1(V) + Th_2(V) \quad (2.2)$$

$$E - E_0 = C_V(T - T_0) - \int_{V_0}^V h_1(V) dV \quad (2.6)$$

where $h_1(V)$ and $h_2(V)$ are given in Eqs. (2.22) and (2.24).

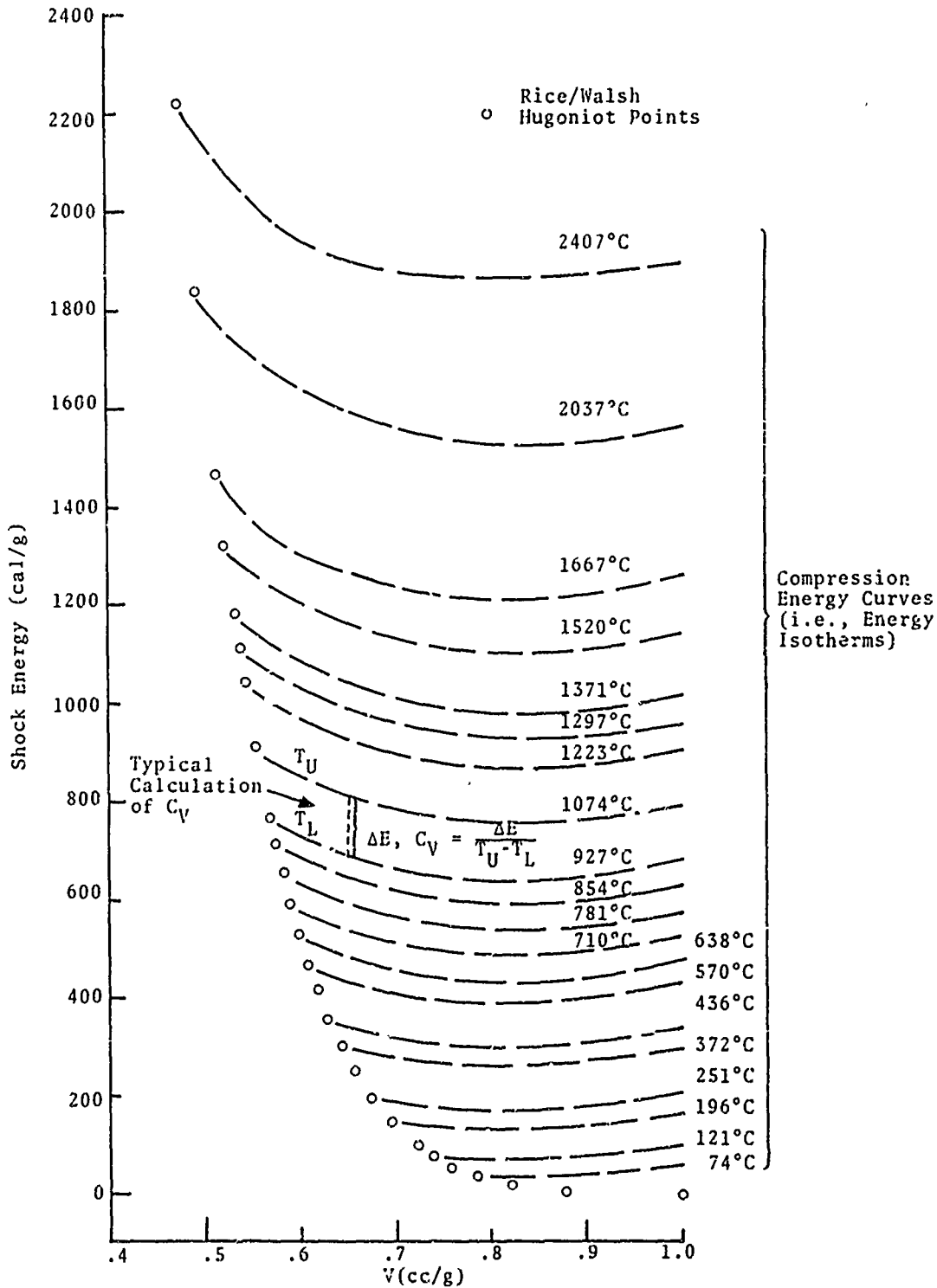


Fig. 2.7--Graphical description of C_V calculation from Rice and Walsh⁽¹⁰⁾ Hugoniot data. (The compression energy curves are only qualitative in this figure.)

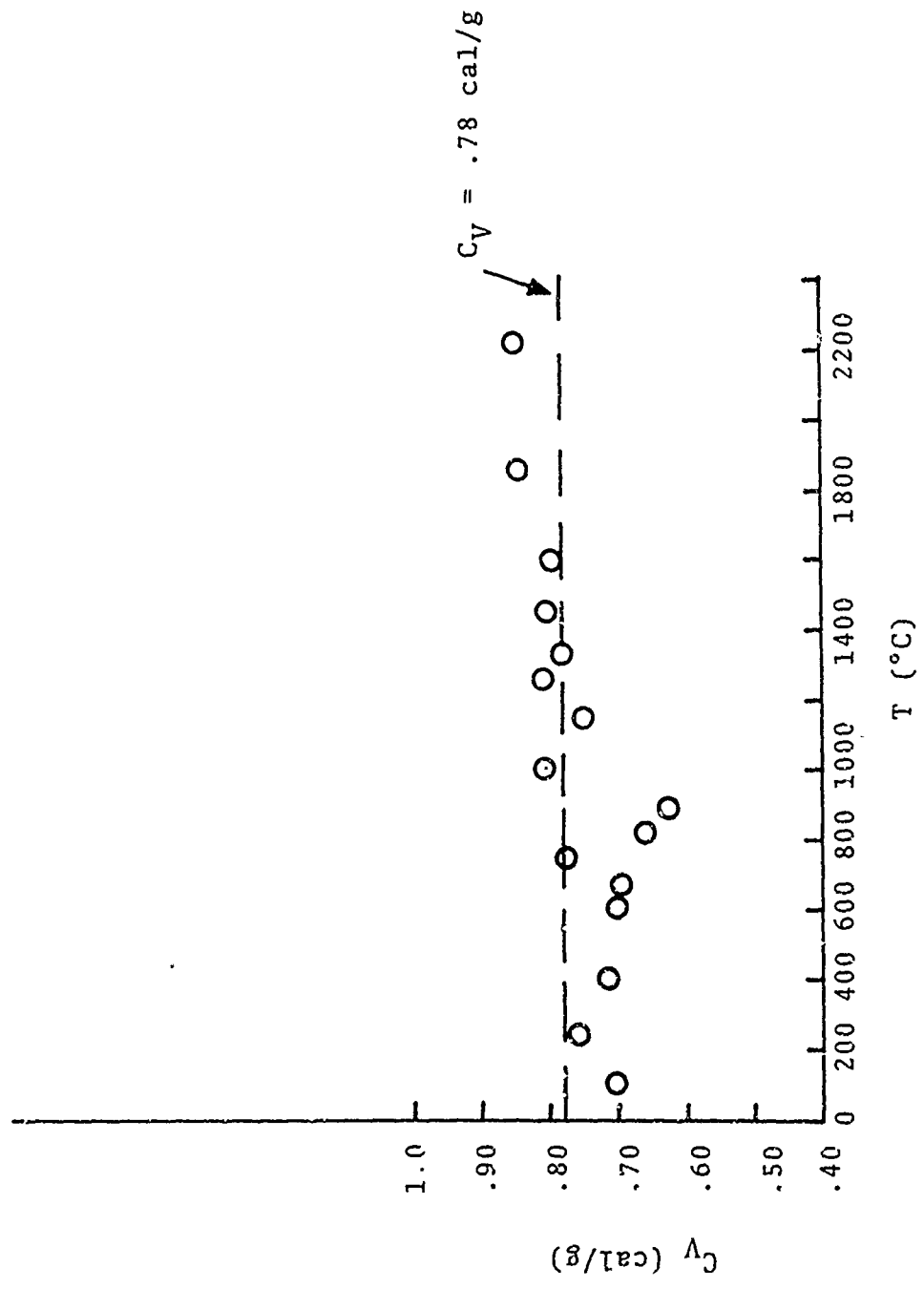


Fig. 2.8-- C_V of water as a function of T.

A comparison of the calculated pressure-volume variation for the Hugoniot to that measured by Rice and Walsh is presented in Fig. 2.9. For pressures above 200 kilobars, there is a mild departure between the calculated curve and the experimental values. Overall, the agreement is comparable to that of the Hugoniot curve used in the p-V-E formulation which is a (least-squares) cubic fit to the Rice-Walsh data.

The release adiabats from 50, 100, 150, and 200 kbars are depicted in Fig. 2.10. Comparable Rice-Walsh data are also plotted, which are seen to be in reasonable agreement with the present calculations.

To best compare the caloric equation of state, temperatures on the Hugoniot have been calculated from Eq. (2.19) using the Hugoniot energies and specific volumes reported by Rice and Walsh⁽¹⁰⁾. In Fig. 2.11, the Hugoniot temperatures computed by Rice and Walsh (constant C_p), Cowperthwaite and Shaw⁽¹⁹⁾ (constant C_v , constant $(\partial p/\partial T)_v$) are plotted against shock pressure and compared to the results of the present theory. The excellent agreement between the Rice-Walsh values and the present theory demonstrates that it is possible to represent water as having a constant C_v ; yet still predict temperatures compatible with the results of Rice and Walsh. The difference between the present calculations and those of Cowperthwaite and Shaw⁽¹⁹⁾ can be attributed directly to the inclusion of the compression energy integral in the present theory, since the same value of C_v was employed in both sets of computations.

Finally, it is of interest to see how satisfactorily the $h_1(V)$ and $h_2(V)$ computed from two isotherms can be employed to predict the shape of other isotherms. Using the $h_1(V)$ and $h_2(V)$ derived from the 448°K and 1273°K isotherms, the pressure-volume traces for 448, 523, 773, 1023, and 1273°K are plotted in Fig. 2.12 and compared to the Rice-Walsh results. The two sets of data are very nearly coincident.

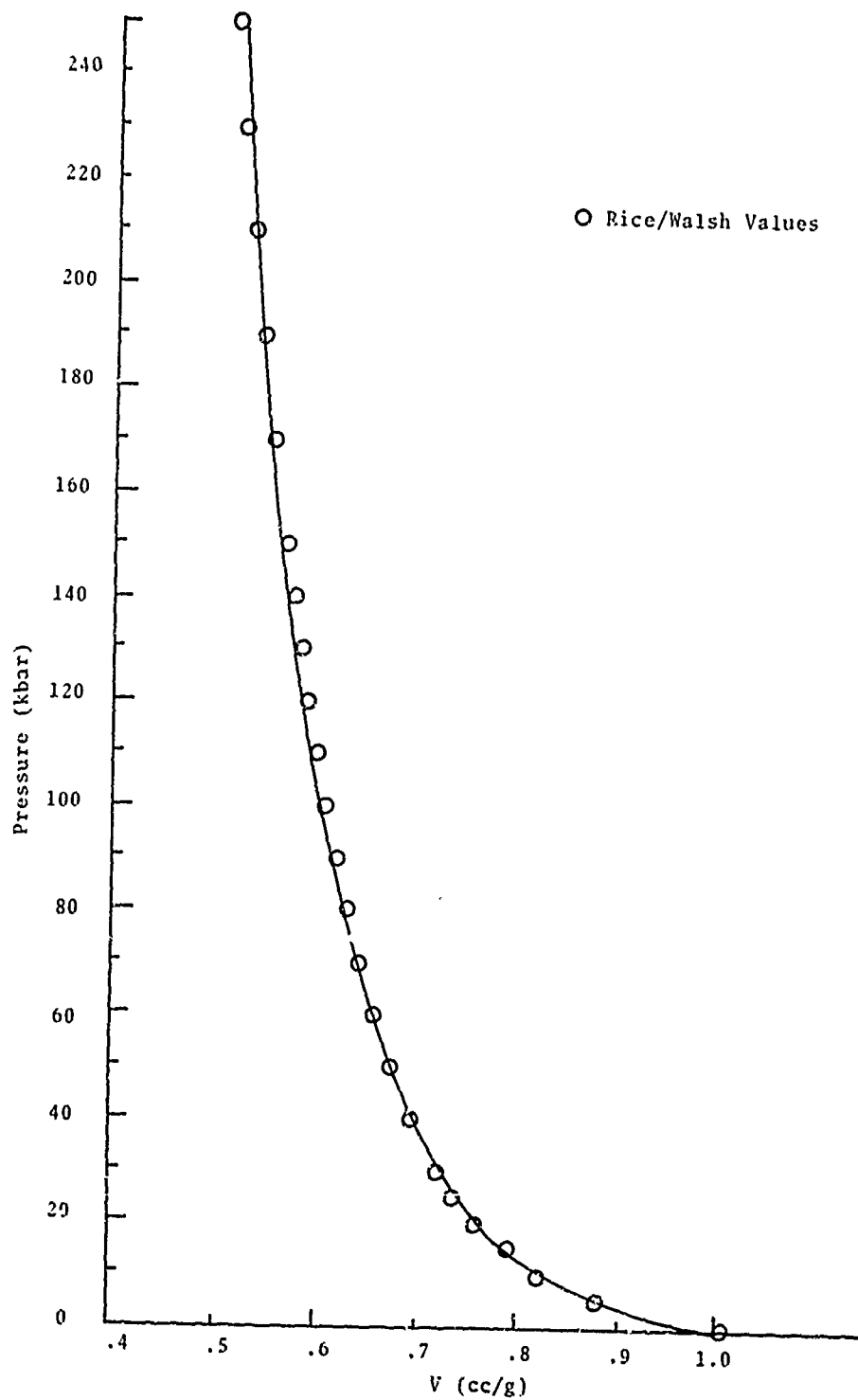


Fig. 2.9--The water shock Hugoniot computed from Eq. (2.2), (2.6) (using h_1 , h_2 , I_1 in Table 2.1, and $C_V = .78$ cal/g). Also shown are Rice and Walsh⁽¹⁰⁾ points.

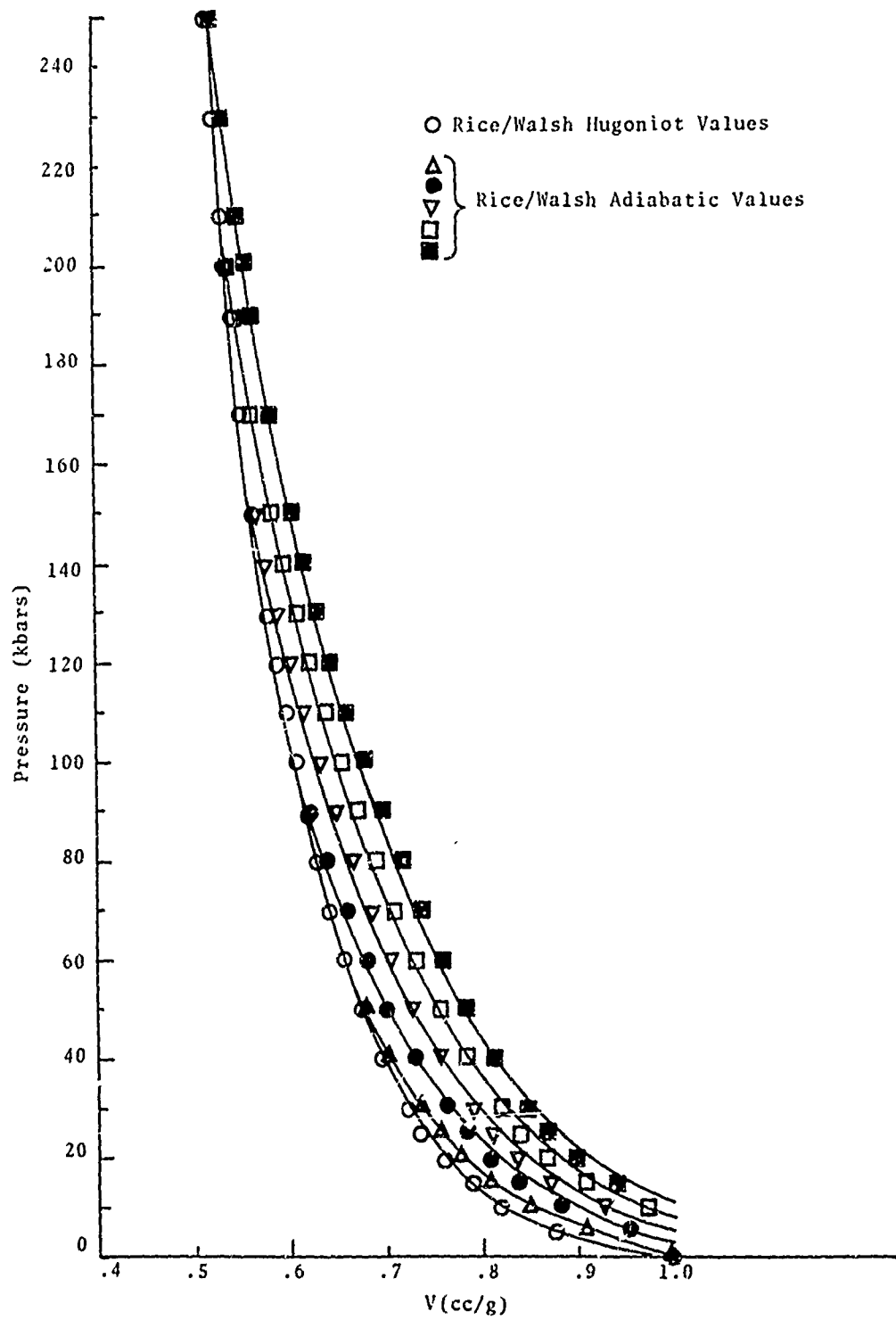


Fig. 2.10--Release adiabats of water computed from Eq. (2.2), (2.6) (using h_1 , h_2 , I_1 in Table 2.1 and $C_V = .78$ cal/g) compared to Rice and Walsh⁽¹⁰⁾ calculations.

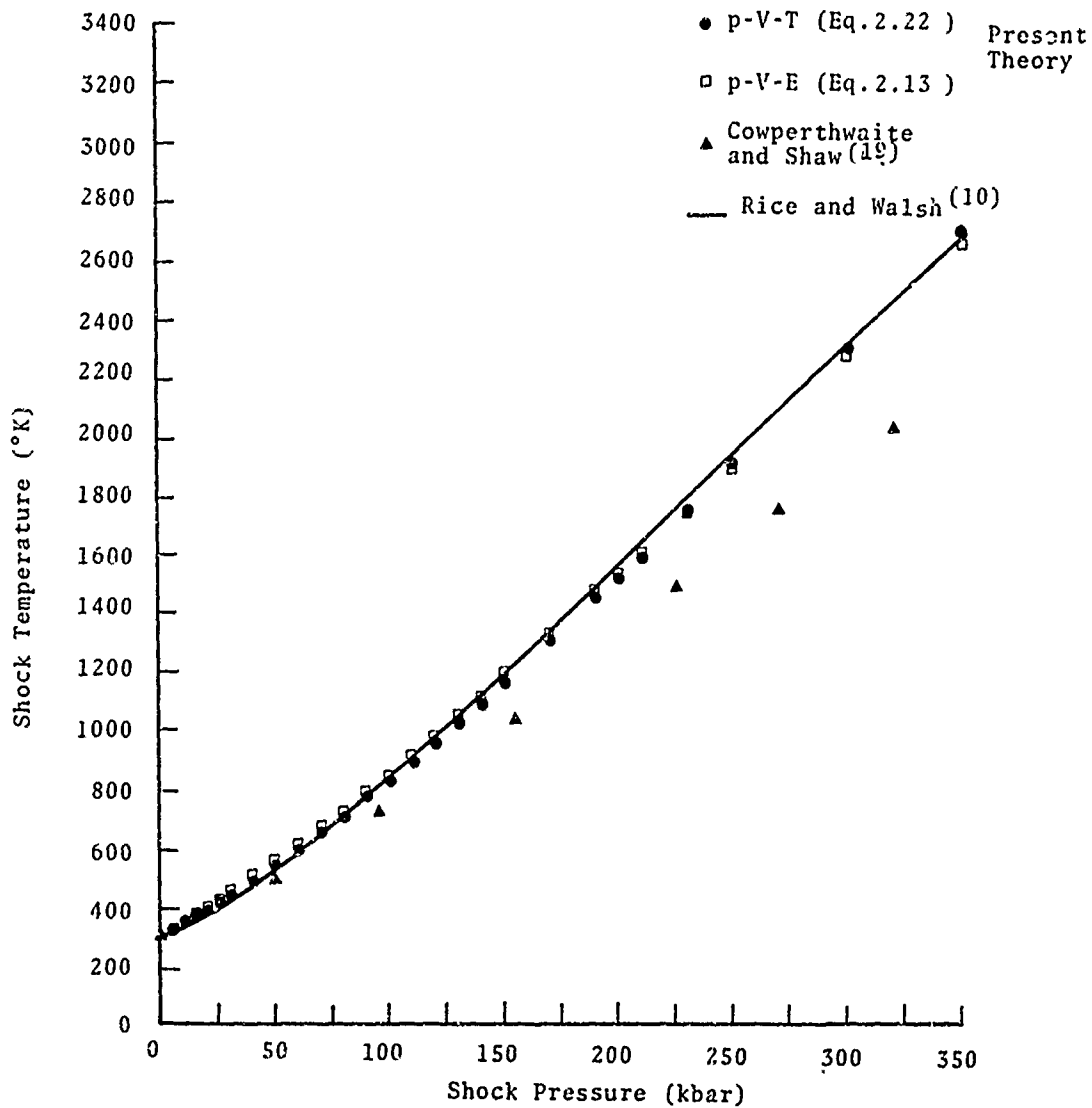


Fig. 2.11--Temperatures on the water Hugoniot computed from Eq. (2.19), (2.22) (using the Rice and Walsh⁽¹⁰⁾ Hugoniot energies and $C_V = .78$ cal/g) compared to the Rice and Walsh values ($C_p = \text{constant}$) and the calculations by Cowperthwaite and Shaw⁽¹⁹⁾ ($C_V = .78$ cal/g, $(\partial p / \partial T)_V = \text{const.}$)

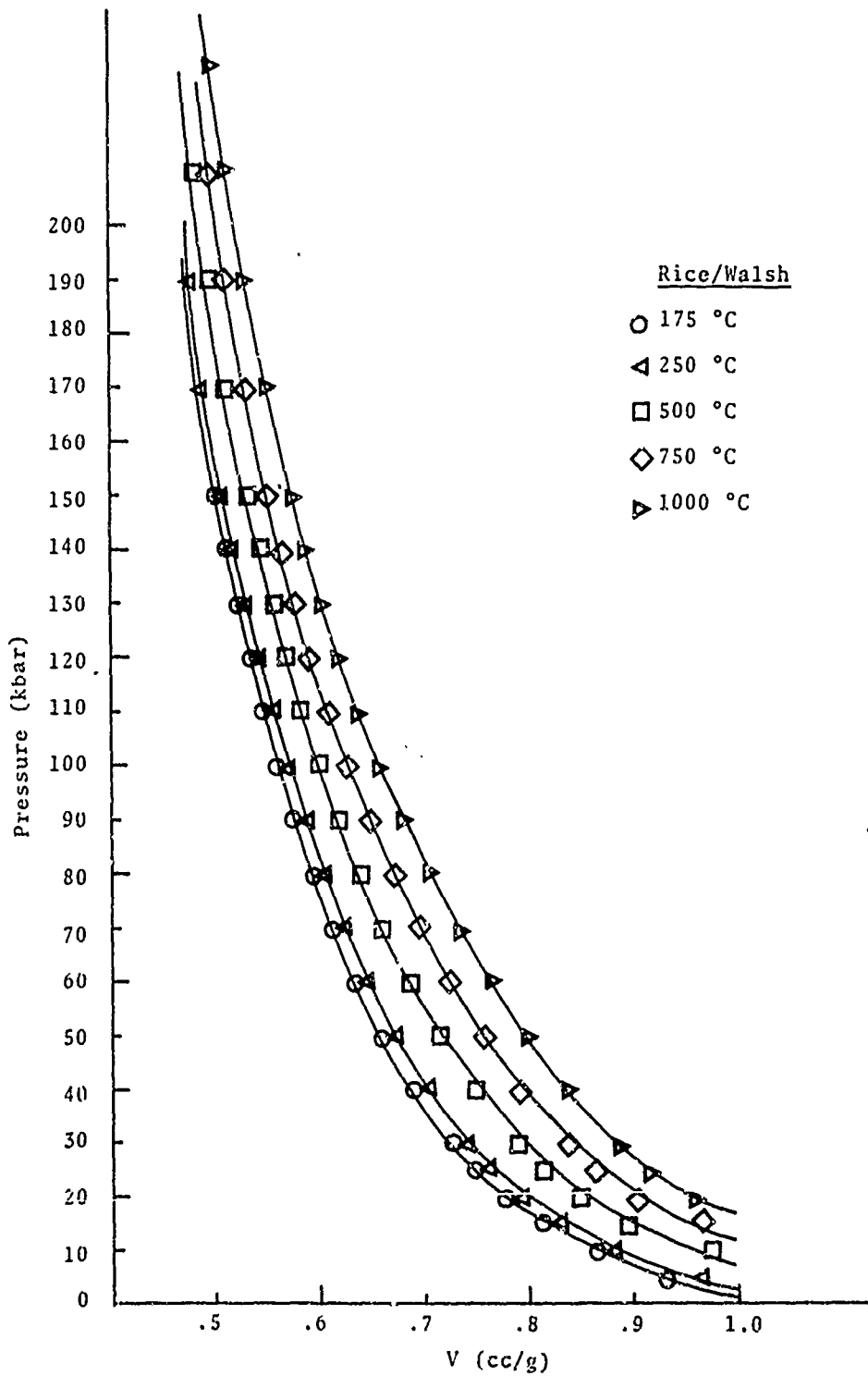


Fig. 2.12--A comparison of the water isotherms computed from $p(V,T) = h_1(V) + Th_2(V)$, using $h_1(V)$, $h_2(V)$ in Table 2.1 to the values reported by Rice and Walsh⁽¹⁰⁾.

However, there is some mild disagreement in the low-pressure (high-specific volume) range of the calculations. This is to be expected vis-a-vis the aforementioned scatter around $h_1(V)$ in this regime.

2.2.3 Final Selection of Equation of State for Compressed Water

It can be concluded from the results presented in the preceding sections, that the simplifications accrued by the present theory do not greatly alter the thermodynamic representation of equilibrium states from that of other investigators⁽¹⁰⁻⁻¹⁵⁾. The two equations of state formulations presented are (in principle) equivalent. However, they do exhibit (expected) minor quantitative differences since the analytic expressions were derived from different forms of the Rice-Walsh data⁽¹⁰⁾. For the purposes of this contract, it is perhaps most convenient to use a hybrid form developed from these two methods of characterizing pure water substance. This selected form would have the quality of most accurately matching the Rice-Walsh data (the more-or-less accepted "standard" for high-pressure (up to 250 kbar) water calculations) while retaining the simplicity of the overall theory. The most appropriate equation of state (from this viewpoint) is the p-V-E relation (Eq. 2.16) in combination with the E-V-T relation developed from the isotherm data (2.6, 2.22):

$$p = \left\{ 21.9543\mu + 52.138\mu^2 + 231.81\mu^3 \right\} \left(1 - \frac{G(V)\mu}{2} \right) + \frac{G(V)}{V} E \quad (2.16)$$

$$E = E_0 + C_V(T - T_0) - \int_{V_0}^V h_1(V) dV \quad (2.26)$$

where

$$G(V) = .41 \sin(9.52 V - 4.5676) + .94 \quad (2.15)$$

$$- \int_{V_0}^V h_1(V) dV = B_1 + B_2 V^1 + B_3 V^2 + B_4 V^3 + B_5 V^4 + B_6 V^5 + B_7 V^6 + B_8 V^7, B_i \text{ given in Table 2.1} \quad (2.27)$$

$$C_V = .78 \text{ cal/gm} = 3.26 \times 10^7 \text{ ergs/gm} \quad (2.28)$$

This set of expressions adequately represent the thermodynamic states on the Hugoniot and release adiabats (see Figs. 2.2, 2.11). Additionally, the isotherms computed from this state equation are in reasonable agreement with the Rice and Walsh calculations as may be observed in Fig. 2.13.*

* The choice of Eq. (2.22) for $h_1(V)$, as opposed to Eq. (2.18), was made on the basis that the predicted shock temperatures are in better agreement with the Rice and Walsh values at pressures less than 150 kbar.

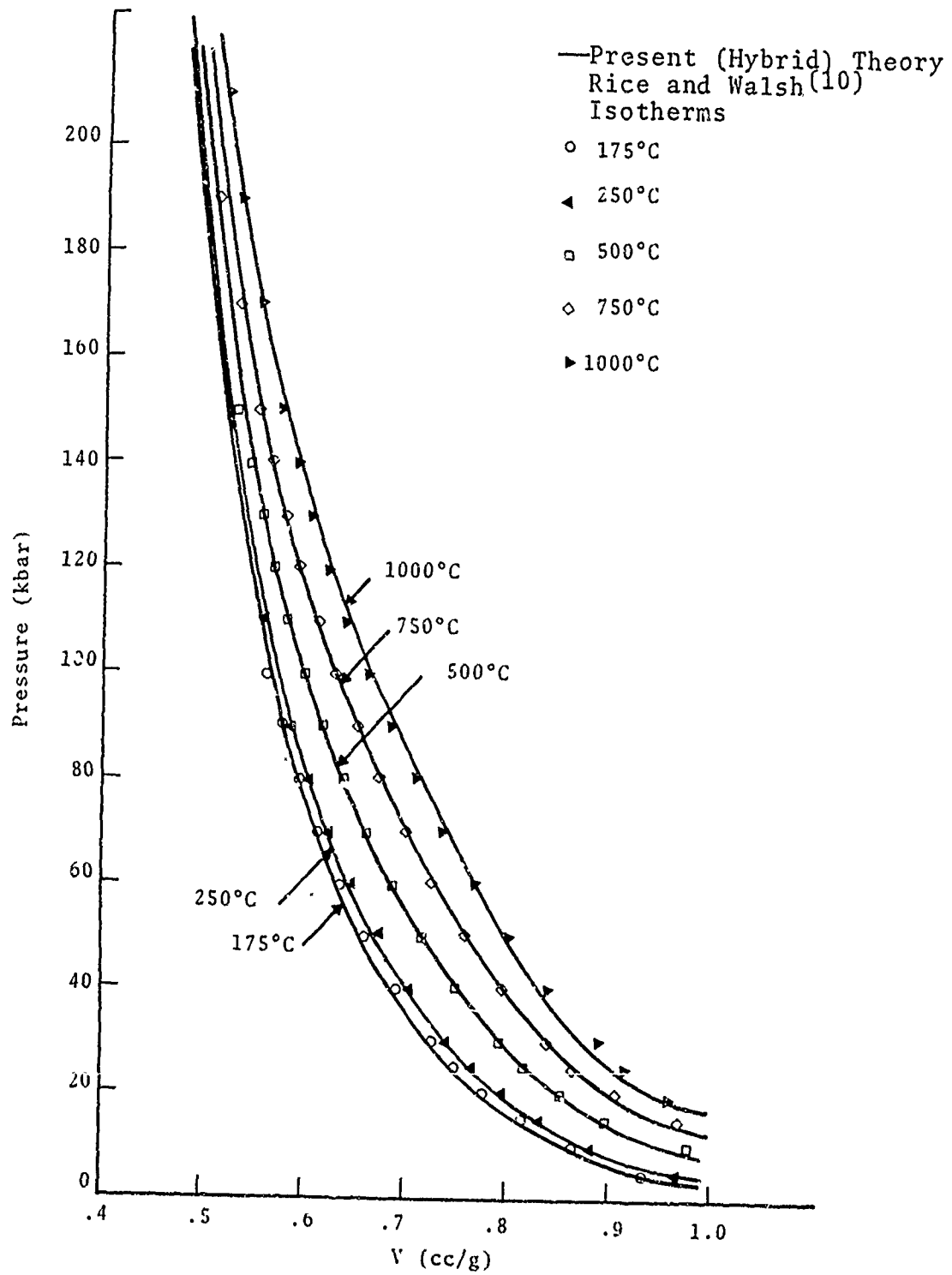


Fig. 2.13--Isotherms determined from "hybrid" equation of state of compressed water (2.16), (2.26) compared to Rice and Walsh⁽¹⁰⁾ results.

2.3 EXPANDED STATES

It can be anticipated that knowledge of the expanded states of water, similar to that obtained about the compressed states near the Hugoniot, will be required to completely describe pulse propagation effects in geologic composites. The particular regime to be characterized is that between the 200 kbar release isentrope and the saturation line, as well as the two phase region under the steam dome (see Fig. 2.14).

In light of the conclusions concerning the physical state of compressed water as the specific volume increases, it could be expected that water exhibits more gas-like behavior as it is expanded.

Thus, the compressed equation of state would have to be modified to mirror the drastically different physics of the water equilibrium states. (Once again, however, the equations of state must be suitable for use in thermal equilibrium calculations.) The general lack of simple (or even complicated), consistent thermal equations of state that existed for water in the compressed state is also evident in the expanded regions. It was necessary, therefore, to develop a thermal equation of state.

The following section describes the development of an equation of state for water in the range in interest. Emphasis has been placed on reproducing the qualitative trends of the available (extrapolated) data, simplicity, and compatibility with the Keenan-Keyes⁽⁶⁾ steam dome data. The expanded liquid phase is treated in a manner analogous to the compressed states described in the preceding section. Two-phase conditions in the steam dome are determined under the assumption of pressure and thermal equilibrium between the phases.

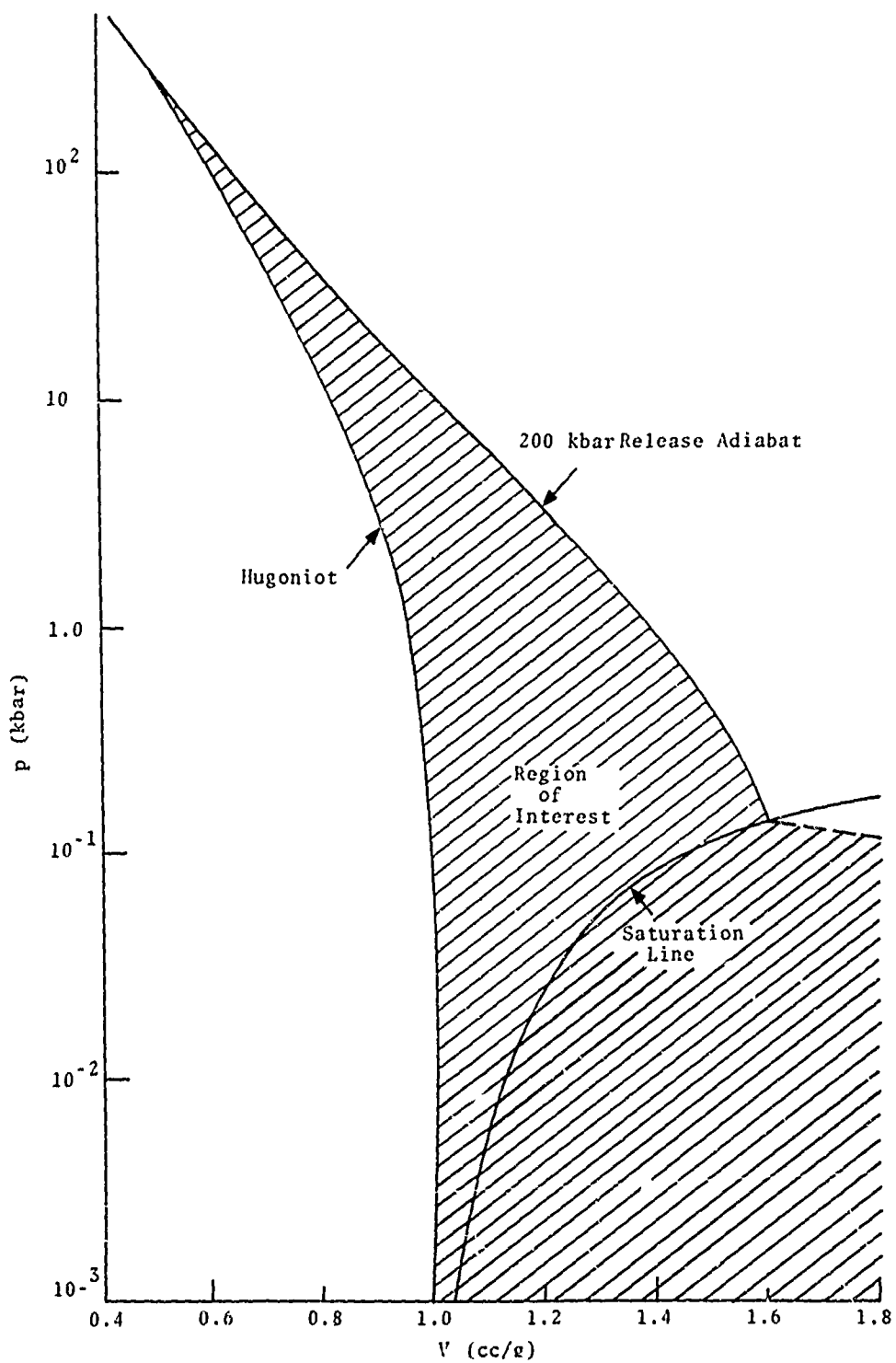


Fig. 2.14--Region of interest for the expanded states of water.

2.3.1 Expanded Liquid States

The Mie-Gruneisen (-Born) form of the equation of state developed for the condensed states of water may be employed to compute various release adiabats which extend into the expanded state regime. Three of these isen⁴ropes are shown in Fig. 2.15 and compared to those presented by Walker and Sternberg⁽¹²⁾. The latter calculations are based on multi-staged p-V-E equations of state which represent fits to experimental data near the saturation line (and a meager amount of data from the work of Kennedy, et al.^(3,27-31)). It can be seen that the extrapolated adiabats using the compressed equation of state are qualitatively similar to the Walker-Sternberg curves, but their intersection with the saturation line is markedly inaccurate.

To remedy this situation and yet retain the basic simplicity of the form used in the condensed states, a new p-V-E equation of state has been constructed based on an extrapolation of the water shock Hugoniot into the expanded state regime. The Walker-Sternberg equations were not used because energy levels of the release adiabats would require a number of states in which portions of the equation would have to be changed. Moreover, the present form facilitated a smooth transition to the condensed states data at $V_0 = 1.0018$. The new equation of state has been developed (implicitly) to assure isentrope intersection with the saturation line at the proper entropy value. Similarly, a caloric equation of state is constructed using the isothermal compression energy term. Employment of such an energy equation maintains the fundamental partition of the internal energy between a strictly thermal portion and the compressional energy.

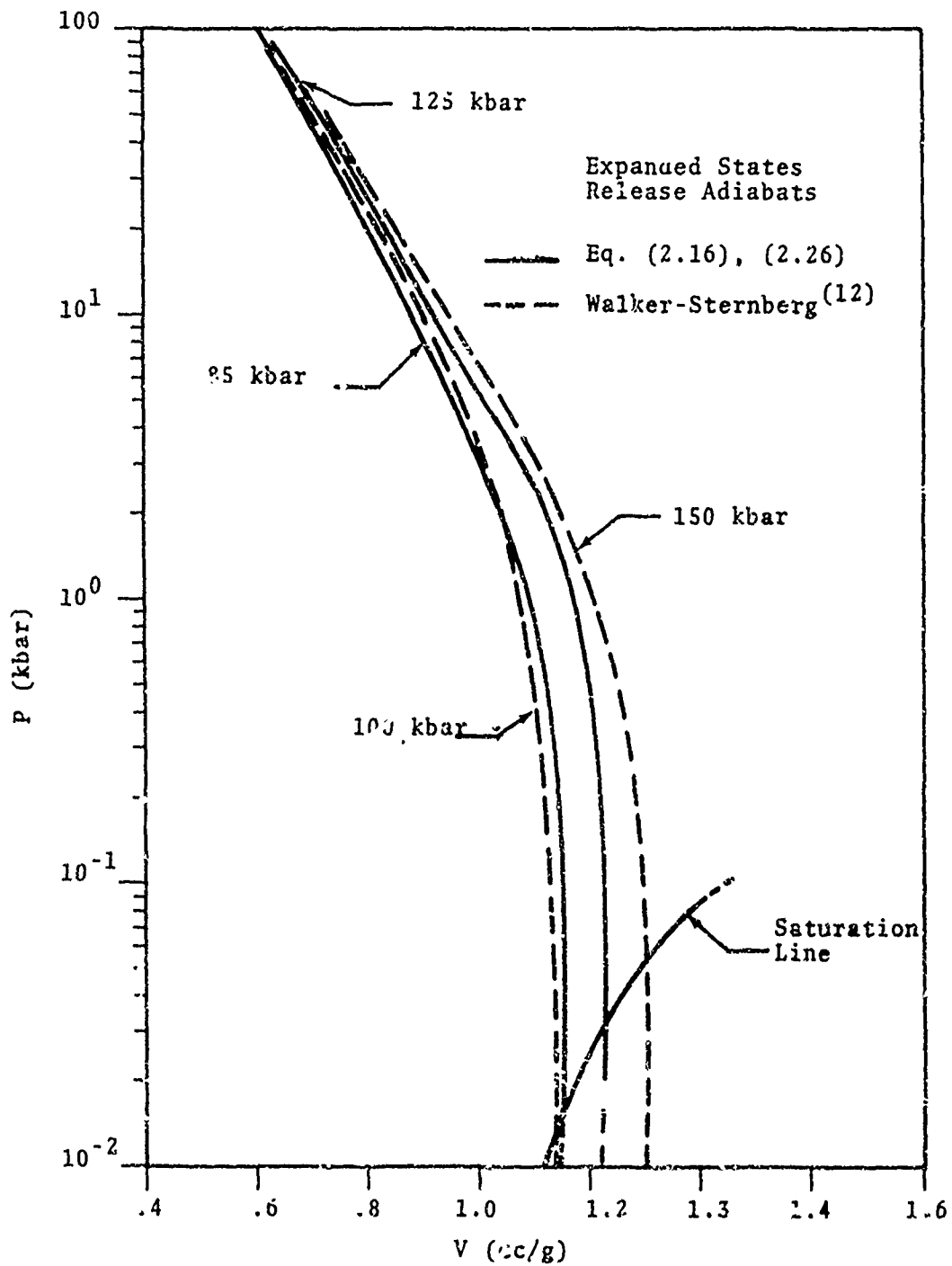


Fig. 2.15--Release adiabats for water in the expanded states region as computed from the (compressed) state equation (Eqs. 2.16, 2.26).

2.3.1.1 p-V-E Equation of State

A hypothetical shock Hugoniot has been constructed for $V > 1$ which is centered on the ambient equilibrium state ($V = 1.0018$, $T = 293^\circ\text{K}$, $p = 1$ bar). The development of this curve was based on the method described for the compressed states (see Section 2.3.2.1). A Mie-Gruneisen form of the state equation, with the Gruneisen ratio set at .54, is used to generate the p-V relation describing the (extrapolated) Hugoniot. The only data input was the saturation line⁽⁶⁾. Continuity of the shock Hugoniot's first derivative was imposed at the cross-over point ($V_0 = 1.0018$). It was found necessary to include an exponential function near $V = V_0$ to smoothly join the two Hugoniots.

The resulting Hugoniot curve plotted in Fig. 2.16 is represented by the analytic expression

$$p = \tilde{\mu}^{-3} \sum a_i \tilde{\mu}^i + A\mu \exp(b|\mu|^c) \quad (2.29)$$

where $\tilde{\mu} = \mu + \text{constant}$. The coefficients in (2.29) are given in Table 2.2. The usefulness of such a straightforward construction is apparent in Fig. 2.17 where the release adiabats (from 50, 100, 150, 200 kbar) are plotted on a logarithmic pressure scale. These compare favorably to the results of the Walker-Sternberg⁽¹²⁾ calculations, and are seen to intersect the saturation line within one percent of the correct specific volume (up to the 150 kbar release adiabat). For higher shock pressure isentropes, there is more divergence in the specific volume intersection (the 200 kbar case is shown in Fig. 2.17). However, the pressures are within the same accuracy as those for the lower valued isentropes.

Although one may improve on the present expression by a number of methods (e.g., admit volumetric dependence in the Gruneisen ratio or perhaps use some Walker-Sternberg data to

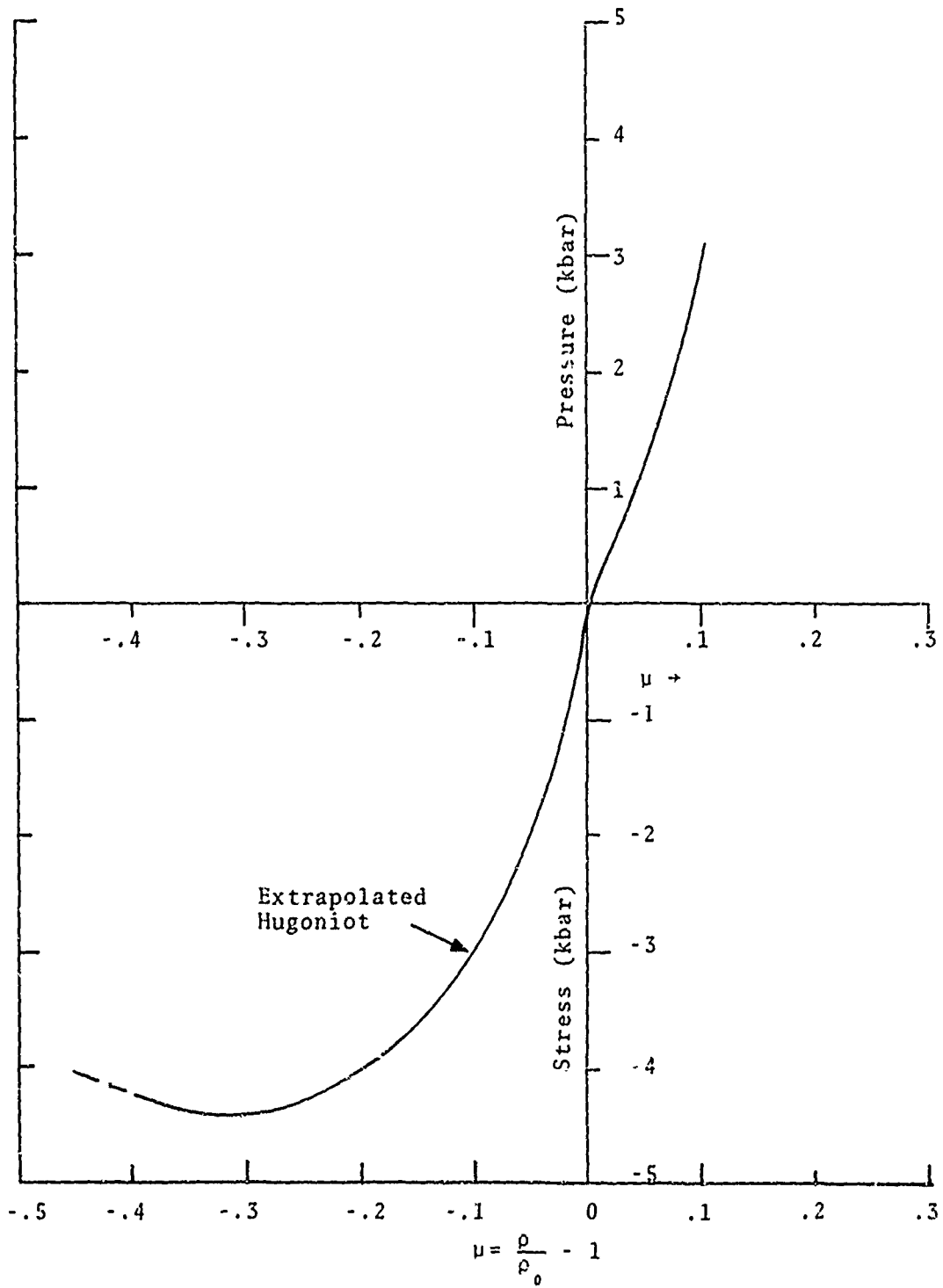


Fig. 2.16--Extrapolation of the water shock Hugoniot to the expanded states regime.

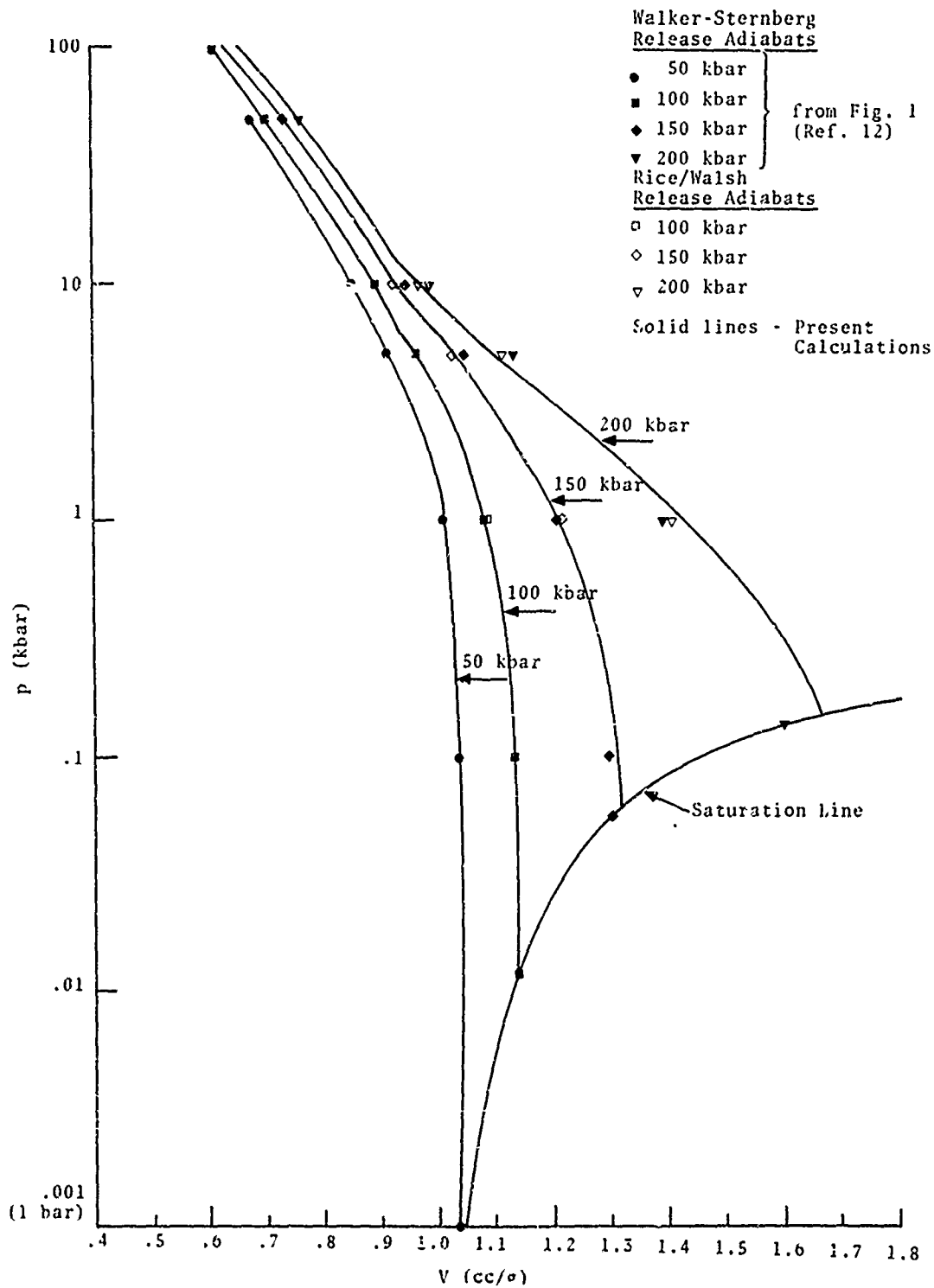


Fig. 2.17--Release adiabats for water based on the Mie-Gruneisen form of expanded (states) equation of state compared to results published by Walker and Sternberg(12).

curve fit the extrapolated Hugoniot), it can be concluded that up to the 150 kbar release adiabat, the expanded p-V-E equation of state (Eq. 2.29) provides sufficiently accurate representation of the available state information on water in the regime of interest.

2.3.1.2 E-V-T (Caloric) Equation of State

An analogous approach to the construction of a p-V-E form of the equation of state may be employed for the thermal formulation. Water is still presumed to exhibit a thermal behavior represented by

$$E = f(T) - \int_{V_0}^V h_1 dV \quad (2.4')$$

(as in the compressed states). The compressional energy term for the expanded states must now be determined and should be expected to continue the gas-like behavior noted in the (less) compressed states (see Section 2.2.2).

Consistent with the proposed p-V-E Mie-Gruneisen formulation and Eq. (2.4'), C_V is assumed constant. For continuity of the energy expressions, C_V is once again taken as .78 cal/g. This value is chosen out of convenience and taken to be representative of water in this limited regime. The data of Bridgman reported by Dorsey⁽²⁴⁾ indicate a temperature dependence and infer that slightly higher values would be appropriate, whereas data in the critical region⁽²⁶⁾ indicate that C_V has dropped below the value used in our calculations.

The compression energy integral $-\int_{V_0}^V h_1 dV$ has been determined by satisfying energy requirements on the saturation line, i.e.,

$$\begin{aligned}
 [E_{\text{SAT}}(T) - E_0] - C_V [T - T_0] &= - \int_{V_0}^{V_{\text{SAT}}(T)} h_1(V) dV & (2.30) \\
 &= I_{\text{EX}}(V)
 \end{aligned}$$

where the subscript EX connotes expanded states. With such a construction, the thermal equation of state will assuredly be accurate in the vicinity of the saturation line and will be continuous with the compressed state values at $V = V_0$. In Fig. 2.18, $I_{\text{EX}}(V)$ determined from this set of hypotheses is compared to the normalized energy isotherms taken from Sharp's⁽¹⁴⁾ tabular data. The normalization of the data was accomplished as in the compressed states (by taking the zero energy point at $V = .685$ for high temperatures ($t > 160^\circ\text{C}$), and at $V = 1.0018$ for lower temperatures).

The normalized compression energy points of Sharp⁽¹⁴⁾ are lower (by $\sim 25\%$) than the $I_{\text{EX}}(V)$ calculated from the constant C_V form of the thermal equation of state. However, the data in Sharp's tables does appear to be in agreement on the shape of an $I_{\text{EX}}(V)$, which is an indication that the Born form of the equation of state is appropriate (i.e., the internal energy is partitioned into volumetric and thermal components). This result is not unreasonable for a "gas-like liquid" since a van der Waals gas exhibits similar behavior and satisfies the proposed form of the p-V-T equation of state.

It is apparent that if the tabulated data⁽¹⁴⁾ are a good representation of the equilibrium states of pure water (in this regime), the constant C_V model is not entirely satisfactory. Modifications of the thermal contribution to internal energy can be considered (e.g., an additional logarithmic contribution to the thermal energy would fit the data). The present formulation, however, should also be

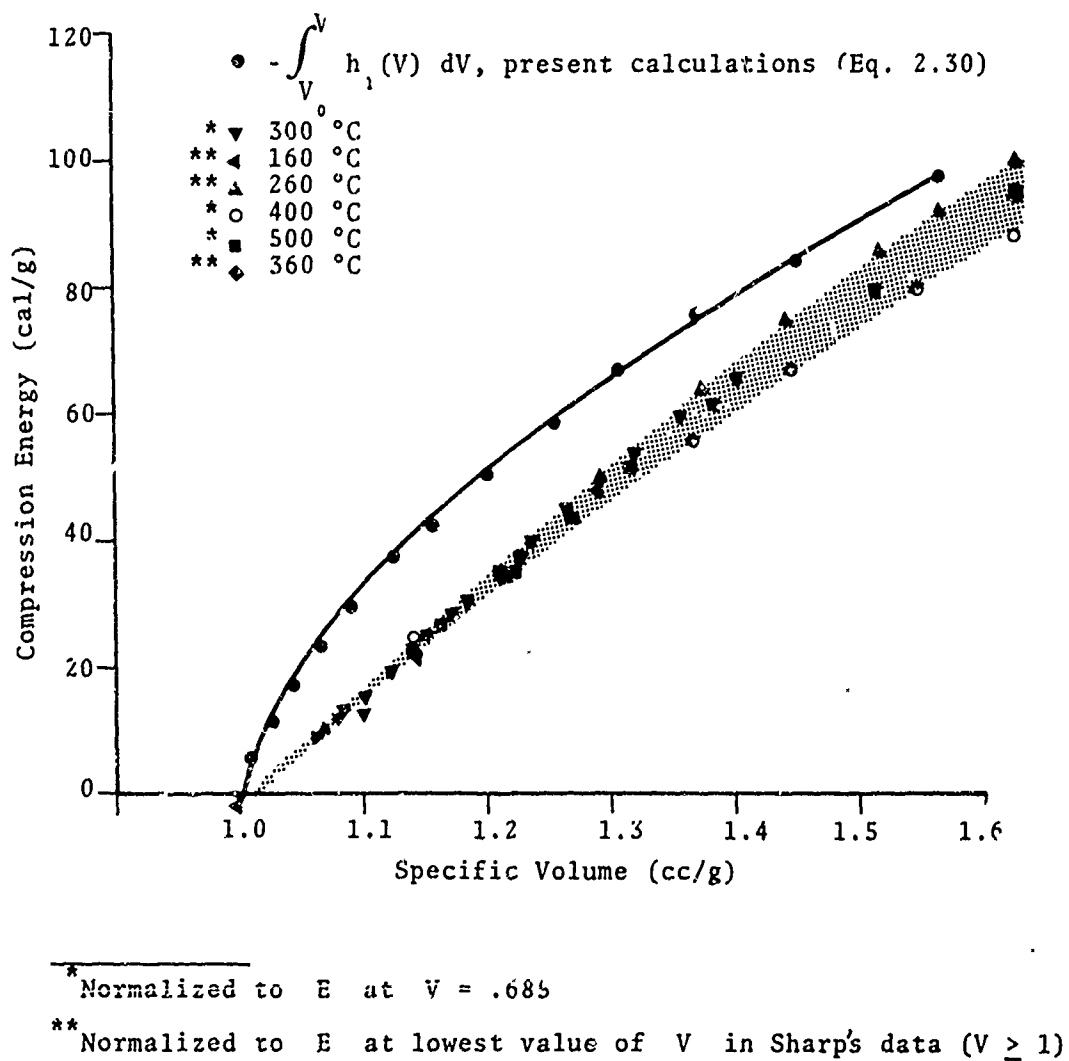


Fig. 2.18--Compression energy curve for the expanded states of water based on constant $C_V (= .78)$ compared to normalized energy isotherms reported by Sharp⁽¹⁴⁾

judged on its p-V-T comparison with the work of other investigators^(3, 10, 12). In Figs. 2.19, the expanded state (p-V) isotherms calculated from Eqs. (2.29, 2.30) are compared to the experimental data⁽³⁾ and the theoretical points^(10, 12). There is good agreement over most of the range of interest. The relatively poor correlation of the $I_{\ell, \text{EX}}(V)$ does not greatly affect temperature calculations, since the internal energy of the liquid states in this thermodynamic region are primarily determined by the $C_V(T)$ term in Eq. (2.30). Moreover, when the compressional energy input becomes significant ($V > 1.3$), the present form for $I_{\ell, \text{EX}}(V)$ does give compressional energy values which are reasonably consistent with the data in Sharp's tables⁽¹⁴⁾.

2.3.2 Liquid-Vapor Equilibrium States

It has been reported in previous investigations^(12, 17) that the adiabatic expansion of water which has undergone a shock compression contains a regime wherein the expanded water may undergo a phase transition. This is demonstrated by the intersection of the release adiabats (from 50 to 200 kbar) with the saturation line (on a p-V plot, for example). In the following section, an equation of state for liquid-vapor equilibrium states is developed under the assumption of pressure and thermal equilibrium. It should be mentioned that, fundamentally, this approach is identical to that previously used⁽¹⁷⁾, but the final form of the equation of state is different (and more appropriate for our tuff/water mixture study (Section IV)).

2.3.2.1 Basic Theory

In principle, the characterization of equilibrium mixtures (of saturated) liquid and gaseous water may be accomplished in a straightforward (albeit numerically

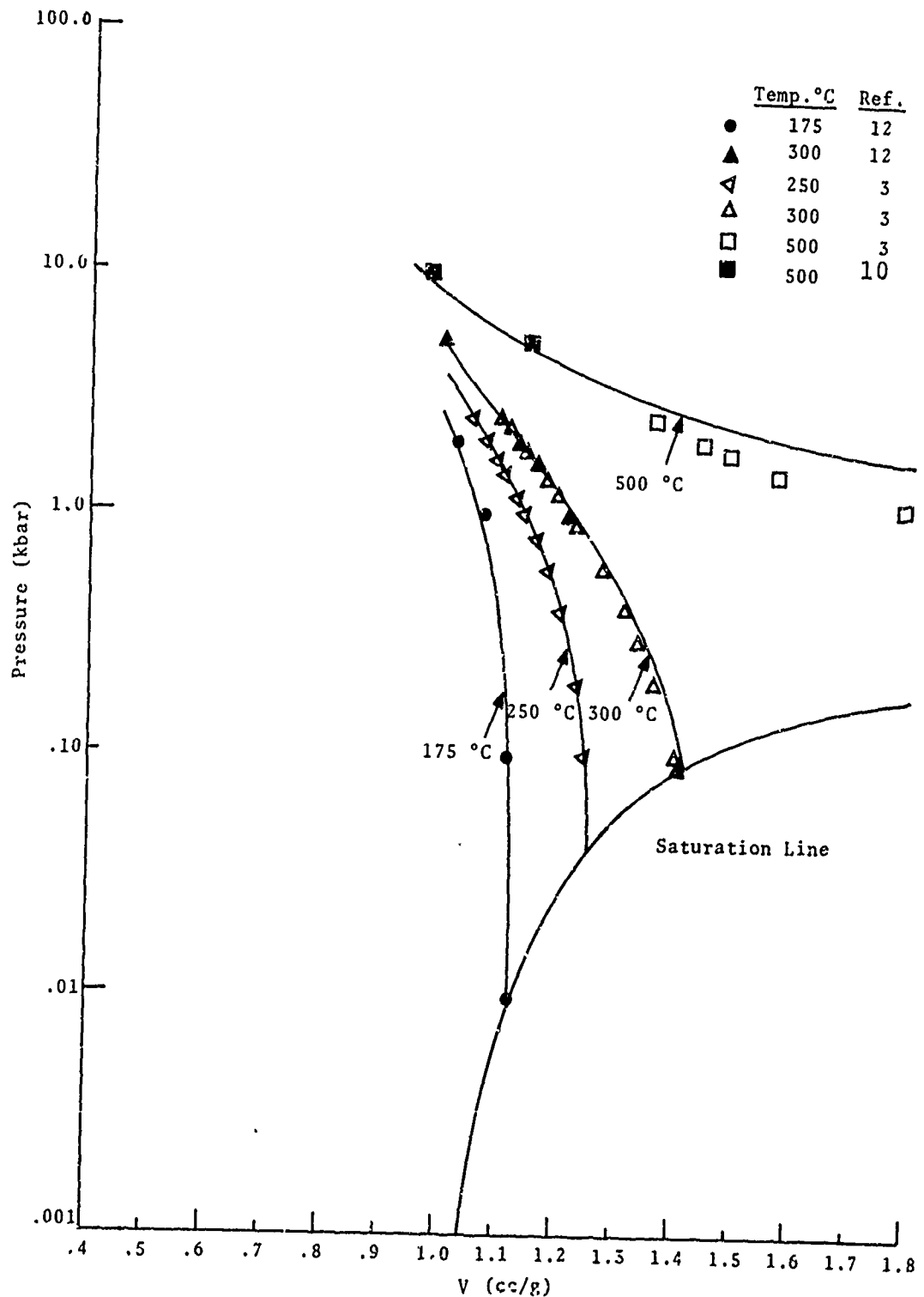


Fig. 2.19--Expanded states isotherms from the present theory compared to available experimental⁽³⁾ and theoretical^(10,12) data.

complicated) manner. Equilibrium mixtures of co-existent states differ from homogeneous equilibrium states in that the two phases have separate state equations. A two-phase system in equilibrium is (strictly speaking) not represented by a single point on the p-V-T surface, but rather by the two points on the phase lines of the saturated liquid and vapor.

If we restrict the analysis to phase mixtures in thermal and pressure equilibrium wherein the vapor is free to expand, the Gibbs phase rule states that equilibrium is possible at a definite pressure once the temperature is specified. More generally, the phase transition occurs along a line on a thermodynamic variable plane (i.e., p-V plane, etc.), and can be characterized as a function of one state variable. For our purposes, temperature is the desired choice since it will facilitate the incorporation of phase change effects into the pressure-thermal equilibrium tuff/water mixtures described in Section IV.

As presented in most thermodynamic text books^(32, 33) the well-known Clausius-Clapeyron relation for the pressure on the phase line is

$$\left(\frac{dp}{dT}\right)_{\text{SAT}} = \frac{L(T)}{T(V_g - V_\ell)} \quad (2.31)$$

where $L(T)$ = (latent) heat of vaporation and the subscripts denote: g(gas), ℓ (liquid) and SAT (phase line). Eq. (2.31) yields $p_{\text{SAT}}(T)$, the saturation (or phase) line for water in the p-T plane. Expressions for $p(T)_{\text{SAT}}$ are available^(6, 8) which have been derived from analytical and empirical expressions for $L(T)$, $V_g(T)$, and $V_\ell(T)$.

Complete specification of an equilibrium liquid/water mixture is accomplished when the relative amount of water in the gaseous state is known. Let us introduce ζ as the

fraction of the mass of a system which has changed phase,
i.e.,

$$\zeta \equiv \frac{M_g}{M_g + M_l} \quad (2.32)$$

where $M_{g,l}$ is the mass of gas or liquid. It is easily shown that ζ may be represented in terms of the mixture's specific volume by

$$\zeta(V,T) = \frac{V - V_l(T)}{V_g(T) - V_l(T)} \quad (2.33)$$

where, V , the specific volume of the liquid/vapor mixture is

$$V \equiv \frac{M_g V_g(T) + M_l V_l(T)}{M_g + M_l} \quad (2.34)$$

and $V_{g,l}(T)$ is the specific volume of the gas or liquid on the phase line. The total energy of an equilibrium mixture is given by

$$E = E_l(T) + \zeta(V,T) (E_g(T) - E_l(T)) \quad (2.35)$$

(The specific energy of the gas or liquid, $E_{g,l}$, is written as a function of temperature on the phase line just as one may write any other thermodynamic state variable in terms of T .) Substitution of Eq. (2.33) into this last equation and re-writing it in a more convenient form results in,

$$E = F_1(T) + V F_2(T) \quad (2.36)$$

where

$$F_1(T) = E_l(T) - \frac{V_l(T)}{(V_g - V_l)} (E_g - E_l) \quad (2.37)$$

$$F_2(T) = \frac{E_g - E_l}{V_g - V_l} \quad (2.38)$$

Admittedly, the preceding analysis is based on an idealized model of the phase change. It is not obvious that the conditions of pressure and thermal equilibrium may be extended to include changes of phase in water when absorbed in pores of a geologic material. However, the energy-absorbing significance of vaporization can be readily studied within such approximations.

2.3.2.2 Calculations

Once $p_{SAT}(T)$, $F_1(T)$, and $F_2(T)$ are determined, the equation of state for water in the two-phase region (i.e., the steam dome) is specified. As mentioned previously, expressions for $p_{SAT}(T)$ are available in the literature, but these are quite cumbersome for our purposes. If it is assumed that $V_g \ll V_l$, then Eq. (2.31) becomes

$$dp \approx dT \left\{ \frac{L(T)}{T V_g(T)} \right\} \left(1 + O\left(\frac{V_g}{V_l}\right) \right) \quad (2.39)$$

Furthermore, in the region where $V_l \ll V_g$, it is observed that one may fit the available data for $L(T)$ and $V_g(T)$ to analytical expressions such as

$$L(T) \approx L_0 \left(1 - \frac{t}{t_c} \right)^{k_1}, \quad (2.40)$$

$$V_g(T) \approx \frac{k_t}{p_{SAT}(T)} \left(1 - \frac{t}{t_c} \right)^{k_2} \quad (2.41)$$

where k_1 and k_2 are constants, t is degrees F, t_c is the critical temperature, and T is the absolute temperature. A comparison of such expressions with the available data⁽⁶⁾ is given in Fig. 2.20.

The integration of Eq. (2.39) with these substitutions for $L(T)$ and $V_g(T)$ results in

$$p(T) = e^{-k \left\{ \frac{a}{T} + b \ln T + c + dT \right\}} \quad (2.42)$$

where a , b , c , and d are constants. It was then determined that by properly choosing these constants, an expression is obtained for $p_{SAT}(T)$ which is accurate to about one percent (in pressure) up to a temperature of 300°C. The final form of $p_{SAT}(T)$ used in these calculations is given in Table 2.2, and its accuracy is graphically depicted in Fig. 2.21(a). This latter expression differs (in form) from Eq. (2.42) only in a small correction term to the exponent.

For the components of $F_1(T)$, $F_2(T)$, expressions have been constructed (see Table 2.2) which fit the saturation data⁽⁶⁾ to within a percent from 20°C to 300°C. The representation of $V_g(T)$ is similar to that postulated in Eq. (2.41). Polynomials in T have been fit to the E_g and E_g data. Finally, the expression for $V_g(T)$ is taken directly from Keenan and Keyes⁽⁶⁾ and is that which is used to develop the steam tables. These analytic forms are compared to the saturation line data in Fig. 21(b-d).

The pressure-volume traces of the expanded state release adiabats extending well in to the two-phase region are presented in Fig. 2.22. These isentropes are in agreement with the results previously reported⁽¹⁷⁾. Moreover, numerous hand calculations were performed to check the validity of the E-V-T relationship. The accuracy of the present calculations was found to be within one percent (in energy).

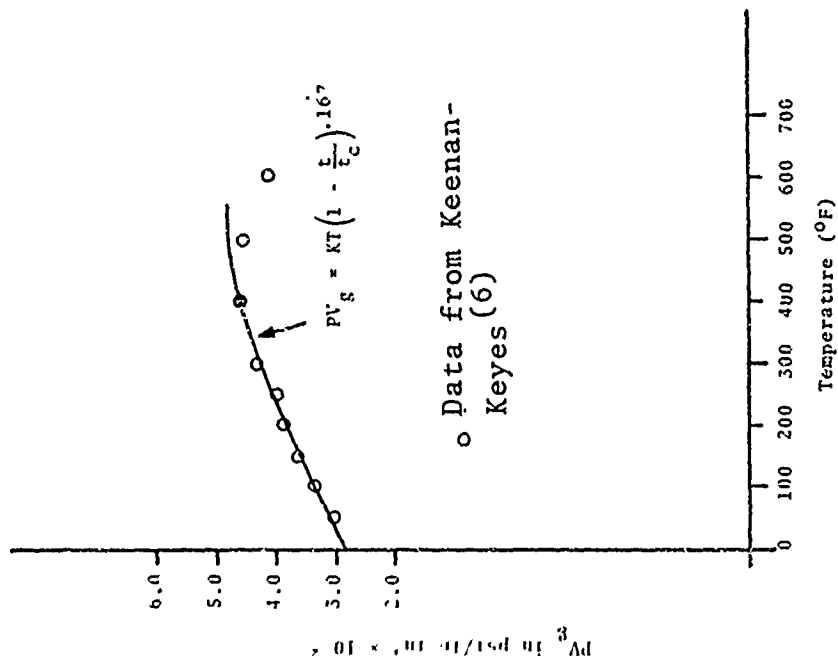


Fig. 2.20(a) -- Latent heat of vaporization vs temperature for water.

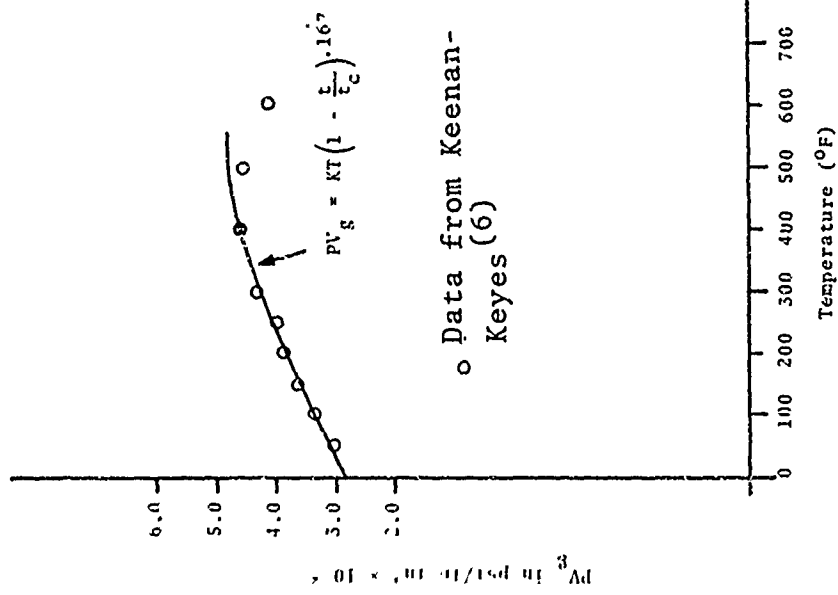


Fig. 2.20(b) -- Pressure-volume product (PV_g) for water vapor on the saturation line.

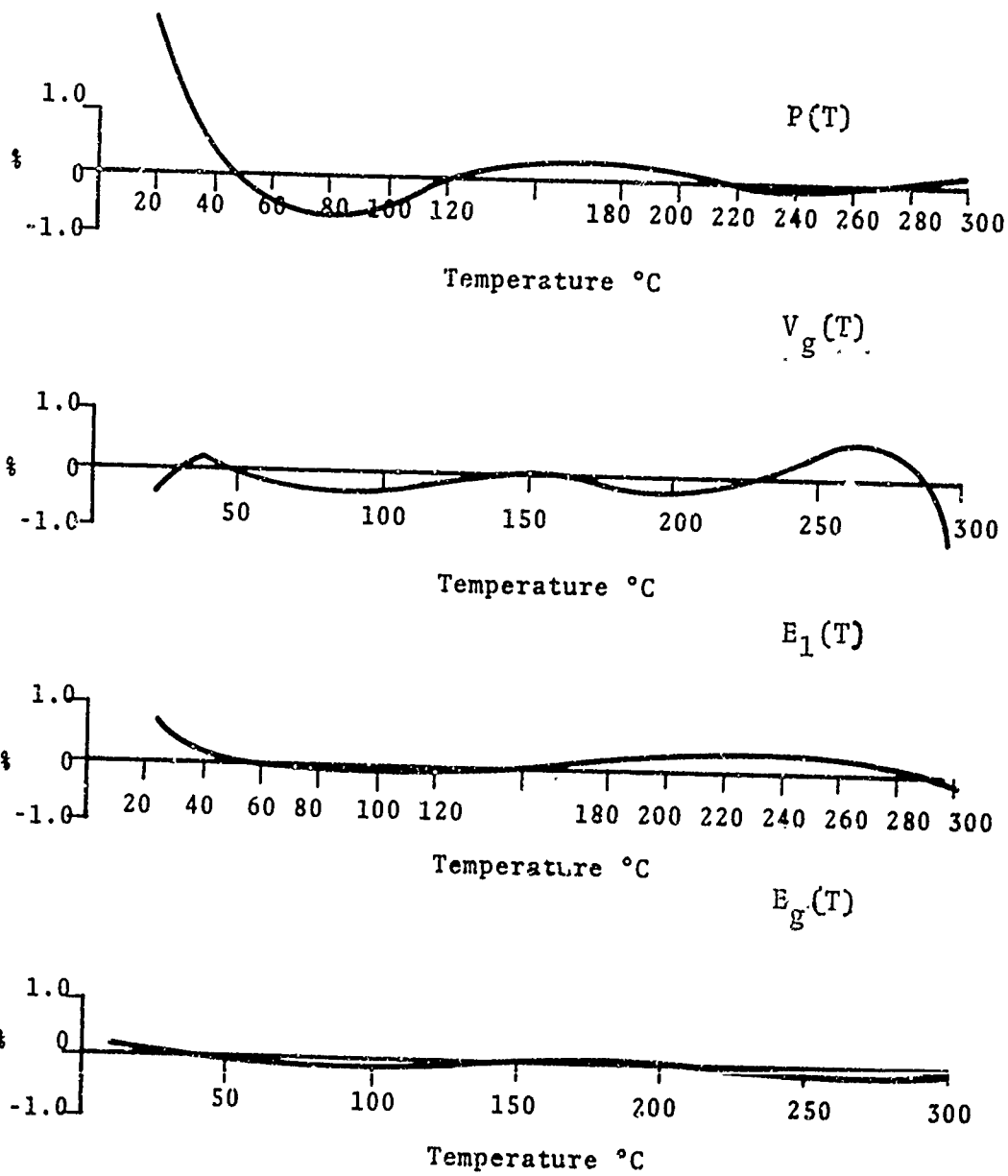


Fig. 2.21--Accuracy of the analytic fits in Table 2.1 compared to the saturation data of Keenan and Keyes⁽⁶⁾

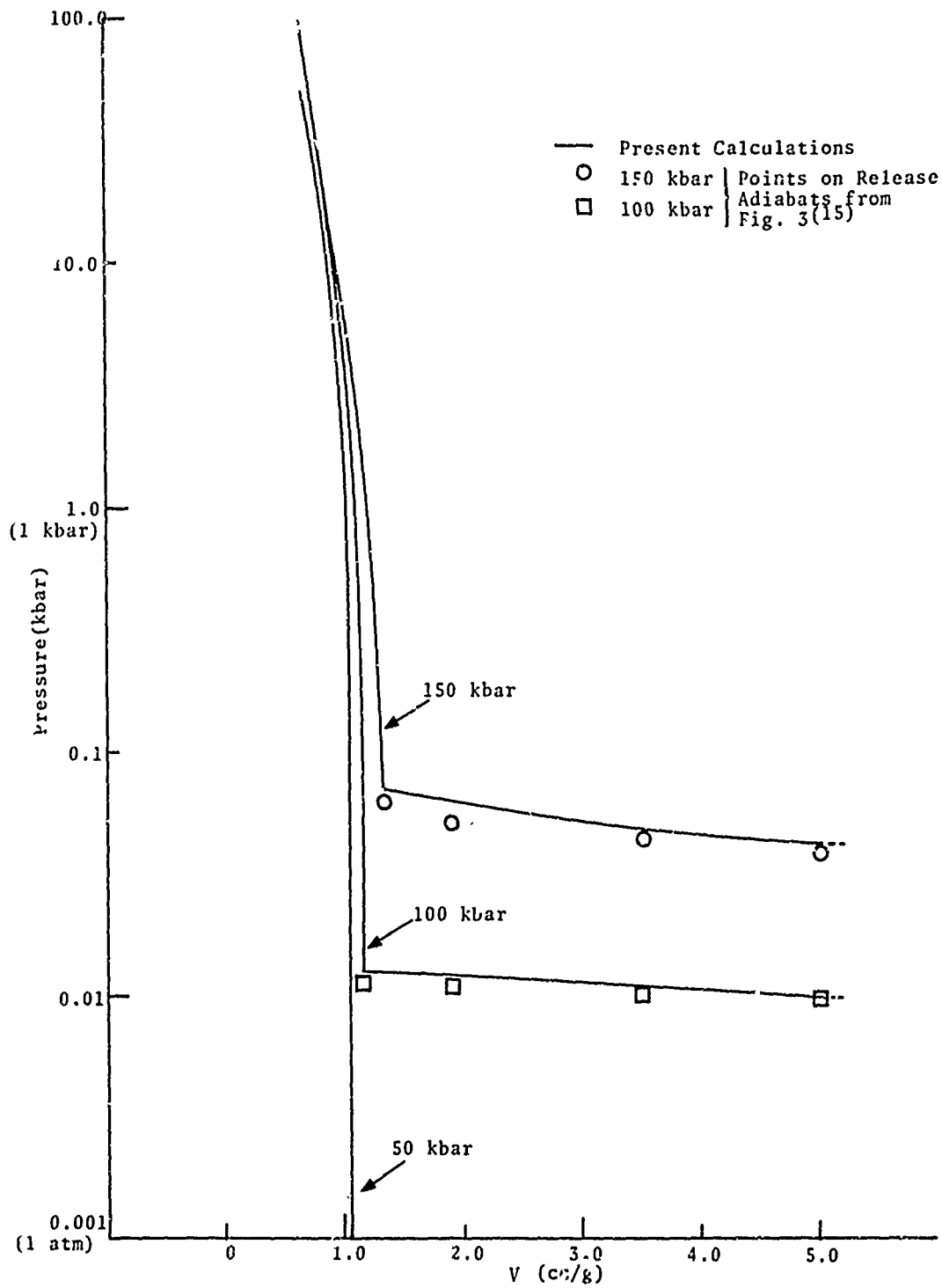


Fig. 2.22--Release adiabats for water extending into the steam dome. Also shown are representative points from a graphical presentation of previous calculations⁽¹⁷⁾.

TABLE 2.2

ANALYTIC EXPRESSIONS FOR SATURATION STATES
AND THE EXTRAPOLATED HUGONIOT

(T = temperature in °K, $T_0 = 293.16$ °K, T_C = critical temperature, °K)

SPECIFIC ENERGY OF LIQUID:

$$E_l(T) = K_{1l}(T-T_0) + K_{2l}(T-T_0)^2 + K_{3l}(T-T_0)^3, \text{ ergs/g}$$

$$K_{1l} = 4.1842 \times 10^7$$

$$K_{2l} = -4.132 \times 10^3$$

$$K_{3l} = 4.8754 \times 10$$

SPECIFIC ENERGY OF GAS:

$$E_g(G) = K_{1g} + K_{2g}T + K_{3g}T^2 + K_{4g}T^3, \text{ ergs/g}$$

$$K_{1g} = 2.56886 \times 10^{10}$$

$$K_{2g} = -4.156137 \times 10^7$$

$$K_{3g} = 1.58541 \times 10^5$$

$$K_{4g} = -1.55021 \times 10^2$$

(Table 2.2 continued)

SPECIFIC VOLUME OF GAS:

$$V_g(T) = \frac{K_1 T}{P_{SAT}(T)} \left(1 - .167 \tilde{T} + .01 \tilde{T}^2 - .01 \tilde{T}^3 \right. \\ \left. - .1 \tilde{T}^4 - .5 \tilde{T}^5 \right) \\ \times \left(1 - .0093 \sin \left\{ \frac{6}{160} \frac{28}{160} (t-300) \right\} \right), \text{ cc/g}$$

$$K_1 = 4.7 \times 10^6 ; \quad \tilde{T} = \frac{T - T_0}{T_C - T_0}$$

SATURATION PRESSURE:

$$p(T) = 5.343439 \times 10^{12} \left[\exp \left(- \frac{.5222 \times 10^4}{T} \right) \right. \\ \left. \times \left(1.13 + .2 T' \ln T' - .0145 T'^2 \right) \right] \\ \times \left(1 + .018 \sin \left(\frac{6.28(T-320)}{280} \right) \right), \text{ ergs/cc}$$

$$T' = \frac{9T}{3527}$$

$$V_l^*(T) = \frac{V_C + K_1 (T_C - T)^{1/3} + K_2 (T_C - T) + K_3 (T_C - T)^4, \text{ cc/g}}{1 + K_4 (T_C - T)^{1/3} + K_5 (T_C - T)}$$

$$V_C = 3.1975 \text{ cc/g}$$

$$K_2 = 1.203374 \times 10^{-3}$$

$$T_C = 647.27 \text{ }^\circ\text{K}$$

$$K_3 = 7.48908 \times 10^{-13}$$

$$K_1 = -0.3151548$$

$$K_4 = .1342489$$

$$K_5 = -3.945263 \times 10^{-13}$$

EXTRAPOLATED HUGONIOT:

$$P_H = \text{COR} + \tilde{\mu}^{-3} d_1 \tilde{\mu} + d_2 \tilde{\mu}^2 + \dots + d_9 \tilde{\mu}^9 \\ + A\mu \exp(b|\mu|^c), \text{ ergs/cc}$$

where

$$\mu = \frac{\rho}{\rho_0} - 1$$

$$\tilde{\mu} = \mu + \text{OFF}$$

$$\begin{aligned} a &= -8.0719379 \times 10^{10} \\ b &= -4.29432294 \times 10^3 \\ c &= 1.11758514 \\ \text{OFF} &= -3.5 \times 10^{-3} \\ \text{COR} &= -3.63648578 \times 10^5 \\ d_1 &= -4.95410061 \times 10^1 \\ d_2 &= -2.81642881 \times 10^4 \\ d_3 &= -7.29095512 \times 10^6 \\ d_4 &= -6.12098976 \times 10^8 \\ d_5 &= 3,35998868 \times 10^{10} \\ d_6 &= 1.22992201 \times 10^{11} \\ d_7 &= 2.75208479 \times 10^{11} \\ d_8 &= 4.05505393 \times 10^{11} \\ d_9 &= 2.59487478 \times 10^{11} \end{aligned}$$

* From Keenan-Keyes (6)

III. CHARACTERIZATION OF NTS TUFF*

3.1 INTRODUCTION

A qualitative definition of tuff has been given by Allen:⁽³⁴⁾

"Newly fallen volcanic ash is a fine white or gray powder which may also contain small fragments or other pyroclastic matter. This material is called tuff when it becomes moderately compacted."

Take the phrase "moderately compacted," add to that the variation in the composition and combination of "volcanic ash" and "pyroclastic matter," throw in the fact that tuff has a chemical affinity for water,⁽³⁵⁾ and it becomes clear that tuff is not a well-defined material. The variation in the properties of tuff will be presented and discussed in this section. Also presented in this section will be a set of parameters representing a completely compacted or non-porous, dry tuff. Since the parameters of this representative tuff will be used extensively in the remainder of this report, and because its description is lengthy and cumbersome, it will be referred to as "S³ compacted dry tuff."

* Author: C. R. Hastings

3.2 DRY TUFF

Tuff in its natural state is very rarely found in the absence of water; however, the majority of the laboratory data is on dry tuff. Furthermore, completely compacted or non-porous, dry tuff, does not appear to exist in a natural state and there are little or no data on this material. In the sequel, data for porous, dry tuffs are presented and discussed. Also, the development of an equation of state and estimation of the critical constitutive parameters for S^3 compacted dry tuff are described.

3.2.1 Porous, Dry Tuff Data

The available hydrostatic, pressure-volume data for dry tuffs of various densities and porosities are shown in Fig. 3.1. A third-degree polynomial fit to the Schooner tuff data (required in Section VII of this report) is also shown. The spread in the specific volume at higher pressures (.36 to .41 cc/g at 40 kbar) seems to indicate that all of the pores have not been collapsed in tuff at 40 kilobars. However, the initial porosity and the chemical (or geological) composition (seldom reported) must be taken into account before any meaningful conclusions can be made. The irreversible crushup of the pores has not been treated during the past contract period.

The available Hugoniot data below 200 kilobars for various dry tuffs are shown in Fig. 3.2(a) (shock velocity vs particle velocity) and Fig. 3.2(b) (stress vs volume). The crystal or non-porous density of tuff varies from 2.0 to 2.7 g/cc (see Appendix B.1). The grain size varies considerably in a single sample (see Appendix B.2); however, the matrix of tuff appears to be a very fine grained powder with an average diameter of 0.01 mm or less. The reported

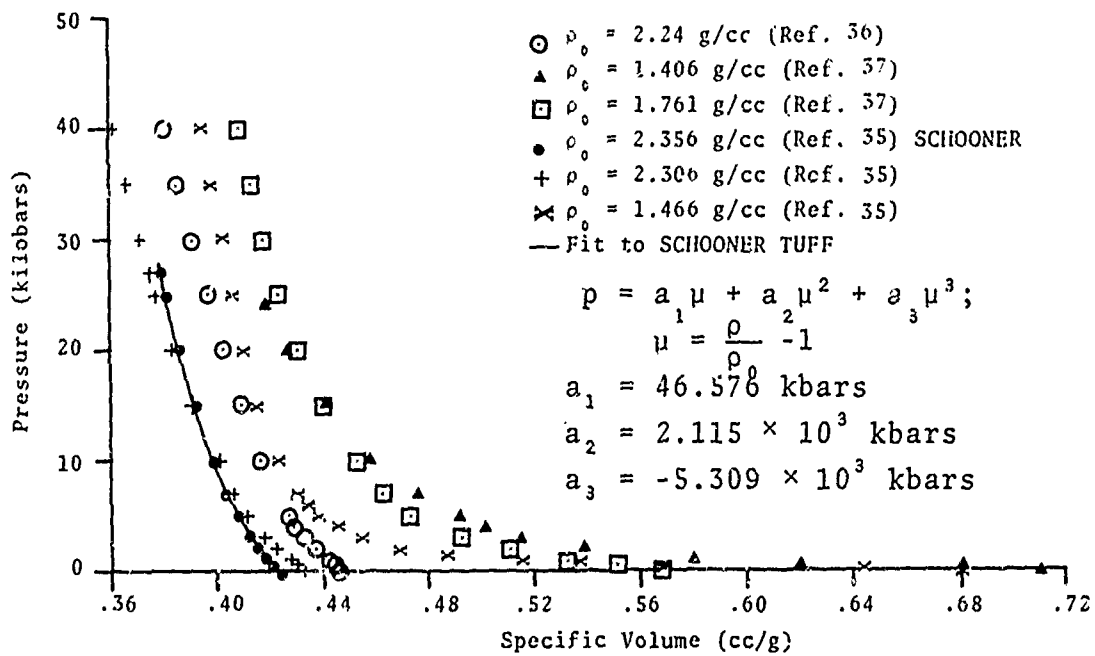


fig. 3.1--Hydrostatic pressure-volume data for dry, porous tuffs.

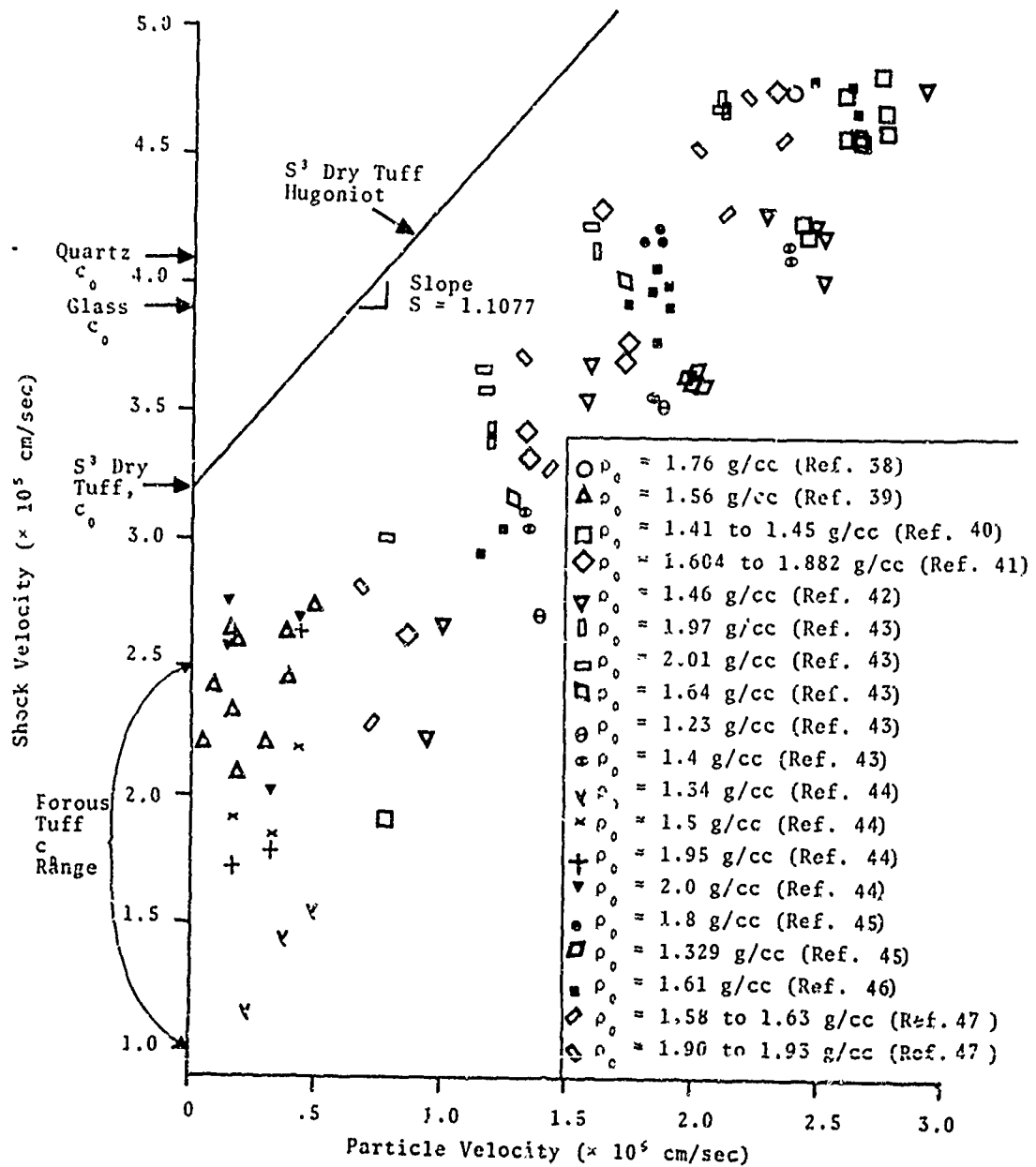


Fig. 3.2(a)--Hugoniot shock velocity-particle velocity data for dry, porous tuffs.

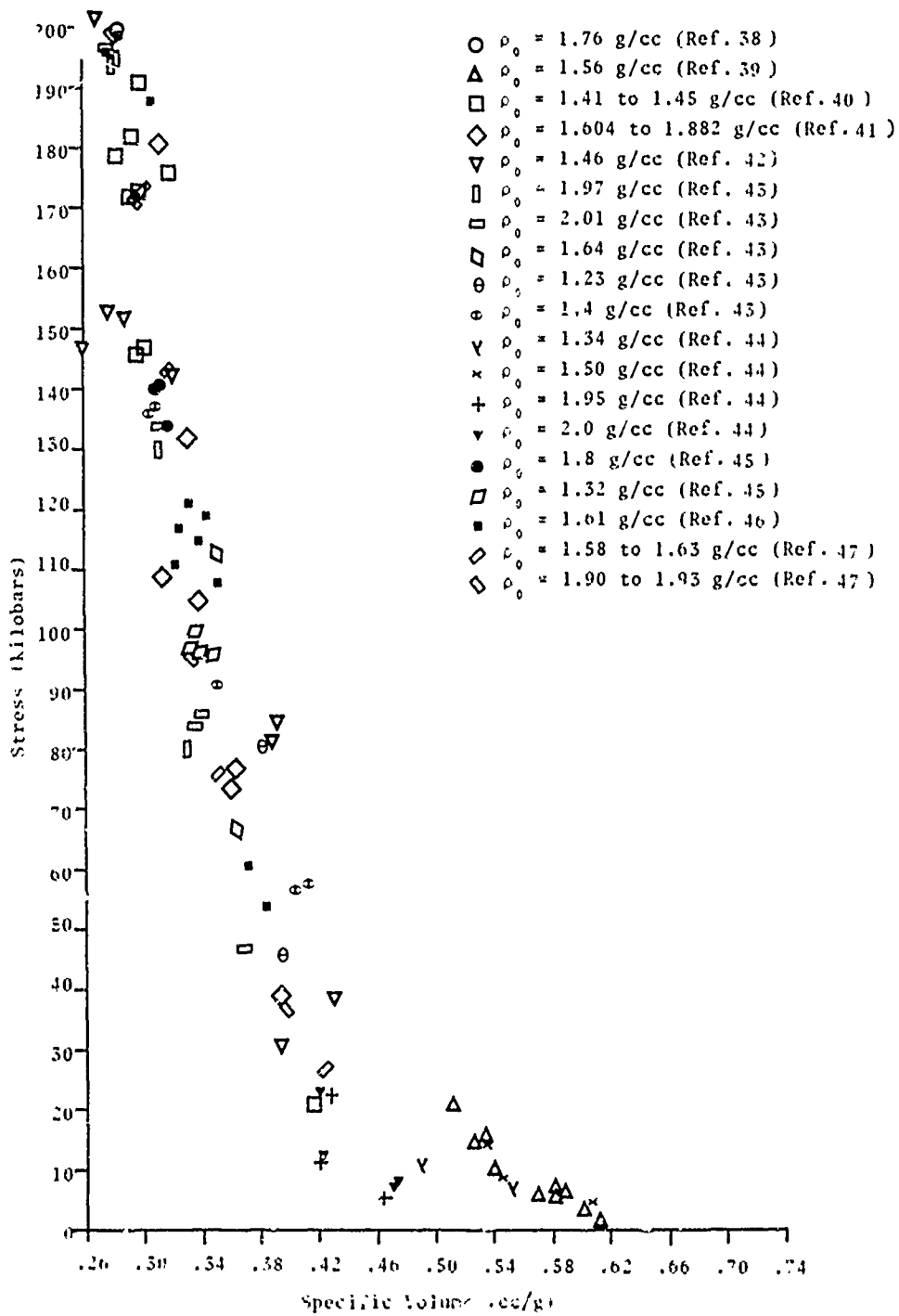


Fig.3.2(b)--Hugoniot stress-specific volume data for dry, porous tuffs.

values of the hydrodynamic sound speed, c_0 , for porous dry tuff, varies from 1.03 to 2.56×10^5 cm/sec (see Appendix B.3).

3.2.2 S³ Compacted Dry Tuff

The density chosen for S³ compacted dry tuff is $\rho_0 = 2.4$ g/cc. A reasonable representation of the composition is:

80% by weight	Glass
10% by weight	Quartz
10% by weight	Clay

(See Appendix B.4 for compositions found in the literature.) The hydrodynamic sound speeds of quartz and a typical glass are 4.09×10^5 cm/sec and 3.9×10^5 cm/sec.⁽⁴⁸⁾ A value of $c_0 = 3.2 \times 10^5$ cm/sec, required in constructing the equation of state, is felt to be a reasonable estimate for the hydrodynamic sound speed of S³ compacted dry tuff.

Hugoniot Fit -- The procedure used to obtain a Hugoniot fit, of the form of Eq. (2.11), for S³ compacted dry tuff is as follows. At a Hugoniot stress of 200 kbars, the specific volumes of several porous dry tuffs are close to .28 cm/g. This point, and the initial density of 2.4 g/cc were used in the standard mass and momentum jump relations,

$$\text{Mass:} \quad \rho_0 D = \rho(D - u) \quad (3.1)$$

$$\text{Momentum:} \quad p = \rho_0 Du \quad (3.2)$$

where

ρ_0 = initial density

ρ = shock density

D = shock velocity

u = particle velocity

p = Hugoniot stress or pressure,

to obtain a D, u point. A straight line (with a slope s, of 1.1077) is drawn from this point to the sound speed, c_0 , in the D, u plane (see Fig. 3.2(a)). The following relations, from Bakken and Anderson,⁽⁴⁹⁾ are all that are needed to evaluate the constants in the Hugoniot fit in the required form:

$$p = A\mu + B\mu^2 + F\mu^3, \quad \mu = (\rho/\rho_0) - 1 \quad (3.3)$$

where the constants in the cubic approximation are

$$\begin{aligned} A &= \rho_0 c_0^2 \\ &= 2.4576 \times 10^{11} \text{ ergs/cc} \end{aligned}$$

$$\begin{aligned} B &= A[1+2(s-1)] \\ &= 2.98697 \times 10^{11} \text{ ergs/cc} \end{aligned}$$

$$\begin{aligned} F &= A[2(s-1) + 3(s-1)^2] \\ &= 6.14886 \times 10^{10} \text{ ergs/cc} \end{aligned}$$

This fit is illustrated along with the Hugoniot and hydrostatic data in Fig. 3.3.

Thermal Description -- Data for the volumetric thermal expansion coefficient, β , and the constant pressure and constant volume specific heats, C_p and C_v , could not be found for tuff. Estimates were made from handbook values given

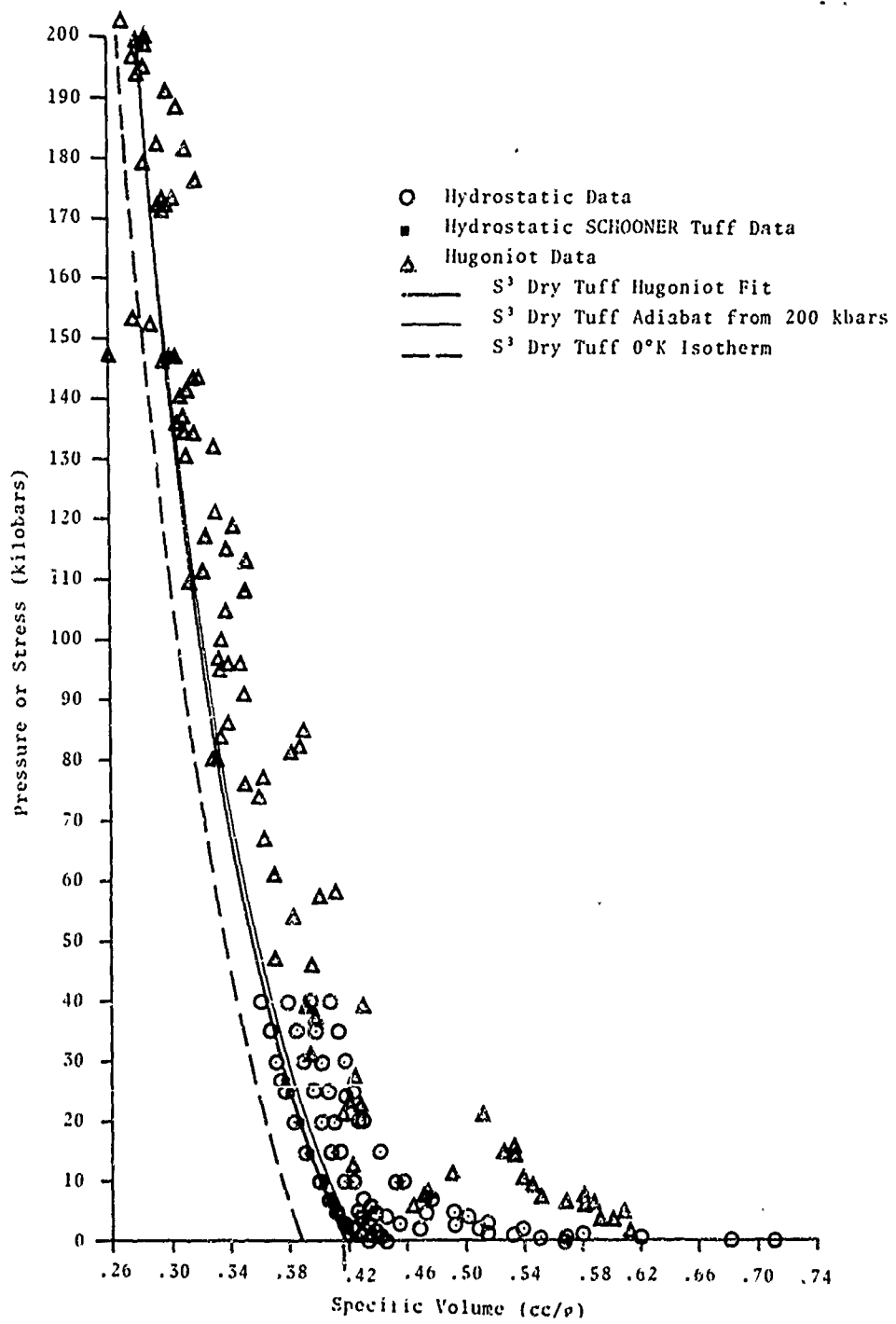


Fig. 3.3--Hugoniot and hydrostatic data and calculated curves for dry tuffs.

for similar materials and from values cited for its assumed components (glass, 80%; quartz, 10%; clay, 10%). The estimated values for S³ compacted dry tuff are as follows (see Appendix B.5 for summary of data):

$$\beta = 27. \times 10^{-6} \text{ cc/cc } ^\circ\text{C} \quad (3.4)$$

$$C_p = 0.2 \text{ cal/g } ^\circ\text{C} \text{ (or } 8.372 \times 10^7 \text{ ergs/g } ^\circ\text{C)} \quad (3.5)$$

$$C_V = 0.2 \text{ cal/g } ^\circ\text{C} \text{ (or } 8.372 \times 10^7 \text{ ergs/g } ^\circ\text{C)} \quad (3.6)$$

Gruneisen Ratio -- The Gruneisen ratio for S³ compacted dry tuff can be obtained from the thermodynamic relation⁽⁴⁹⁾

$$G = \frac{\beta c_0^2}{C_p} . \quad (3.7)$$

Using the values given above, the Gruneisen ratio was found to be

$$G = 0.33 . \quad (3.8)$$

This value is assumed to be constant over the entire pressure-volume range of interest. The Gruneisen ratio and the Hugoniot fit were used to calculate a release adiabat from the 200-kbar Hugoniot state. The calculated curve is shown in Fig. 3.3.

Isotherm -- The thermal expansivity is assumed to be sufficiently small such that a good estimate of $h_1(V)$ (see Eq. (2.2)) is given by the zero degree isotherm,

$$h_1(V) = [p(V,E)]_{T=0^\circ\text{K}} \quad (3.9)$$

The value of $[p(V,E)]_{T=0^\circ K}$ has been determined by numerically integrating the pdV work on the zero degree isotherm,

$$E^n = E^{n-1} + p^n (V^{n-1} - V^n) , \quad (3.10)$$

where $p^n = p(V^{n-1}, E^{n-1})$ as evaluated from Eq. (2.7), using the parameters for S^3 compacted dry tuff given above. The integration is initiated at the state $p = -19.4$ kbar, $E = -2.45 \times 10^{10}$ ergs/g, $\rho = 2.4$ g/cc.* The resulting isotherm is shown in Fig. 3.3. A fit to the integral of the isotherm (see Eq. 2.6) is

$$\int_{V_0}^V h_1(V) dV = a_1 \mu + a_2 \mu^2 + \dots + a_7 \mu^7 \quad (3.11)$$

* An approximate value of the internal energy, E , at $\rho = 2.4$ g/cc on the $0^\circ K$ isotherm can be obtained from the expression (see Eq. 2.6)

$$E = E_0 + C_V(T - T_0) - \int_{V_0}^V h_1(V) dV .$$

The values of E_0 , T and the integral are all zero, leaving

$$\begin{aligned} E &= - C_V T_0 \\ &= -2.45 \times 10^{10} \text{ ergs/g} . \end{aligned}$$

The corresponding pressure can be obtained from the expression, (see Eq. 2.7)

$$p = f(V) + G\rho E .$$

The function, $f(V)$, is zero at $\rho = 2.4$ g/cc; therefore,

$$\begin{aligned} p &= G\rho E \\ &= -19.4 \text{ kilobars} . \end{aligned}$$

where

$$a_1 = 8.0746633 \times 10^9 \text{ ergs/g}$$

$$a_2 = -5.3895904 \times 10^{10} \text{ ergs/g}$$

$$a_3 = 2.8099165 \times 10^{10} \text{ ergs/g}$$

$$a_4 = -1.784375 \times 10^{10} \text{ ergs/g}$$

$$a_5 = 1.14124046 \times 10^{10} \text{ ergs/g}$$

$$a_6 = -5.47535341 \times 10^9 \text{ ergs/g}$$

$$a_7 = 1.341517856 \times 10^9 \text{ ergs/g}$$

Strength -- Data on the strength of dry, non-porous tuff have not been found. There is a limited amount of strength data on dry, porous tuffs (see Appendix B.6). Reasonable estimates of Poisson's ratio, ν , and the unconfined shear strength, Y of S^3 compacted dry tuff, based on existing data, are

$$\nu = 0.15 \quad (3.12)$$

$$Y = 1. \text{ kilobar} . \quad (3.13)$$

Equation of State -- For easy reference, all of the parameters presented above for S^3 compacted dry tuff are tabulated in Table 3.1. These may be employed in a Mie-Gruneisen formulation of the equation of state:

$$p = p_H \left(1 - \frac{G_H}{2} \right) + \frac{G}{V} E \quad (3.14)$$

and the constant C_V form of the caloric equation of state

$$E - E_0 = C_V(T - T_0) - \int_{V_0}^V h_1(V) dV \quad (3.15)$$

where E_0 is taken to be zero, $T_0 = 293^\circ\text{K}$, and $p_H, G, C_V, \int_{V_0}^V h_1(V) dV$ are given in Table 3.1.

3.2.3 Schooner Tuff Hydrostat

An extension to 200 kbars of the hydrostatic fit to Schooner tuff (shown in Fig. 3.1) is required later in Section VII of this report. The high pressure portion of the Hugoniot curve, obtained in Section 3.2.2, is considered to be a reasonable representation of the high pressure states of this material. The following is a fit to the low pressure hydrostatic data and the high pressure points computed from the S^3 compacted dry tuff Hugoniot:

$$p = a_1 \mu + a_2 \mu^2 + a_3 \mu^3 + a_4 \mu^4; \quad \mu = \frac{\rho}{\rho_0} - 1 \quad (3.16)$$

where

$$a_1 = 4.8851 \times 10^{10} \text{ ergs/cc}$$

$$a_2 = 1.9868 \times 10^{12} \text{ ergs/cc}$$

$$a_3 = -4.6715 \times 10^{12} \text{ ergs/cc}$$

$$a_4 = 4.3406 \times 10^{12} \text{ ergs/cc}$$

TABLE 3.1
PARAMETERS FOR S³ COMPACTED DRY TUFF

Parameter	Description	Value	Units
G. S.	Grain Size	< 0.01	mm
ρ_0	Initial Density	2.4	g/cc
Composition	Glass	80	% by weight
	Quartz	10	% by weight
	Clay	10	% by weight
c_0	Hydrodynamic sound speed	3.2×10^5	cm/sec
s	Slope of the Hugoniot curve in the D, u plane	1.1077	--
A } B } F }	Coefficients of the Hugoniot fit, $P_H = A\mu + B\mu^2 + F\mu^3$ $\mu = \rho/\rho_0 - 1$	2.4576×10^{11}	ergs/cc
		2.98697×10^{11}	ergs/cc
		6.14886×10^{10}	ergs/cc
β	Volumetric thermal expansion coefficient	2.7×10^{-5}	cc/cc °C
C_p	Constant pressure specific heat	8.372×10^7	ergs/g °C
C_v	Constant volume specific heat	8.372×10^7	ergs/g °C
G	Gruneisen ratio	0.33	--

(Table 3.1 Continued)

Parameters for S³ Compacted Dry Tuff

Parameter	Description	Value	Units
$\int_{V_0}^V h_1(V) dV$	Integral of the zero degree isotherm		
a_1		8.0746633×10^9	ergs/g
a_2		$-5.3895904 \times 10^{10}$	ergs/g
a_3		2.8099165×10^{10}	ergs/g
a_4		-1.784375×10^{10}	ergs/g
a_5		$1.14124046 \times 10^{10}$	ergs/g
a_6		-5.47535341×10^9	ergs/g
a_7		1.341517856×10^9	ergs/g
ν	Poisson's ratio	0.15	--
Y	Unconfined shear strength	1.0×10^9	ergs/cc

3.3 WET TUFF DATA

The completely saturated wet tuff data presented in this subsection will be used in following sections as a check on the success of various models to predict the equilibrium states of the water-tuff composite.

The pressure-volume hydrostatic data for various saturated tuffs are shown in Fig. 3.4. The discontinuities at 10 and 24 kilobars are due to the water-ice VI and ice VI-ice VII phase changes.

The available published Hugoniot data for saturated tuffs are shown in Fig. 3.5. The data are not complete enough to indicate whether or not any of the water phase changes take place. Figure 3.6 contains both the Hugoniot and hydrostatic data along with two adiabats released from Hugoniot states of 135 and 146 kilobars. The accuracy of the adiabatic data, as the pressure is released further and further from its associated Hugoniot state, becomes so poor that it can no longer be used to evaluate a composite model.

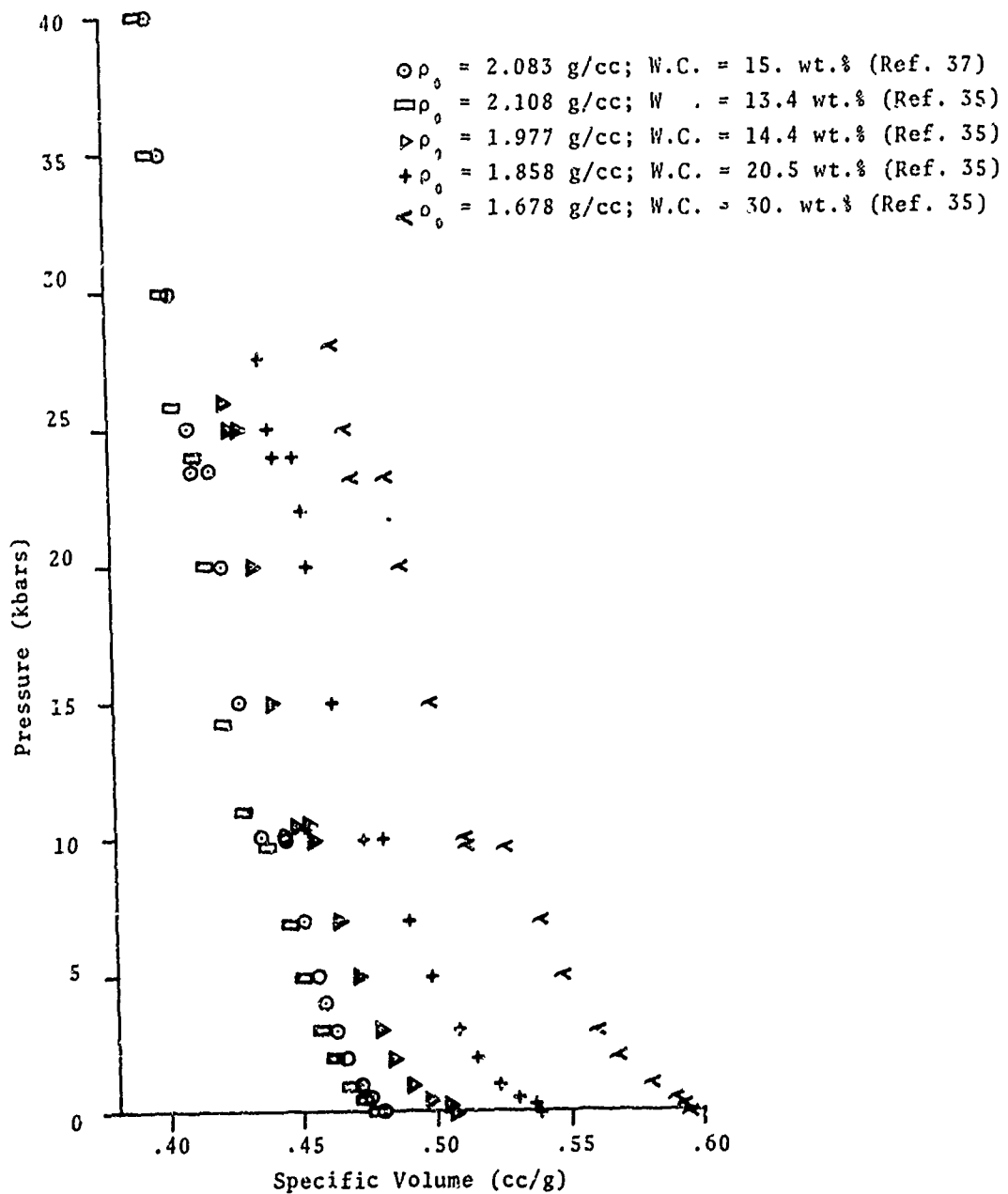


Fig. 3.4--Hydrostatic, pressure-volume data for saturated tuffs of indicated water content.

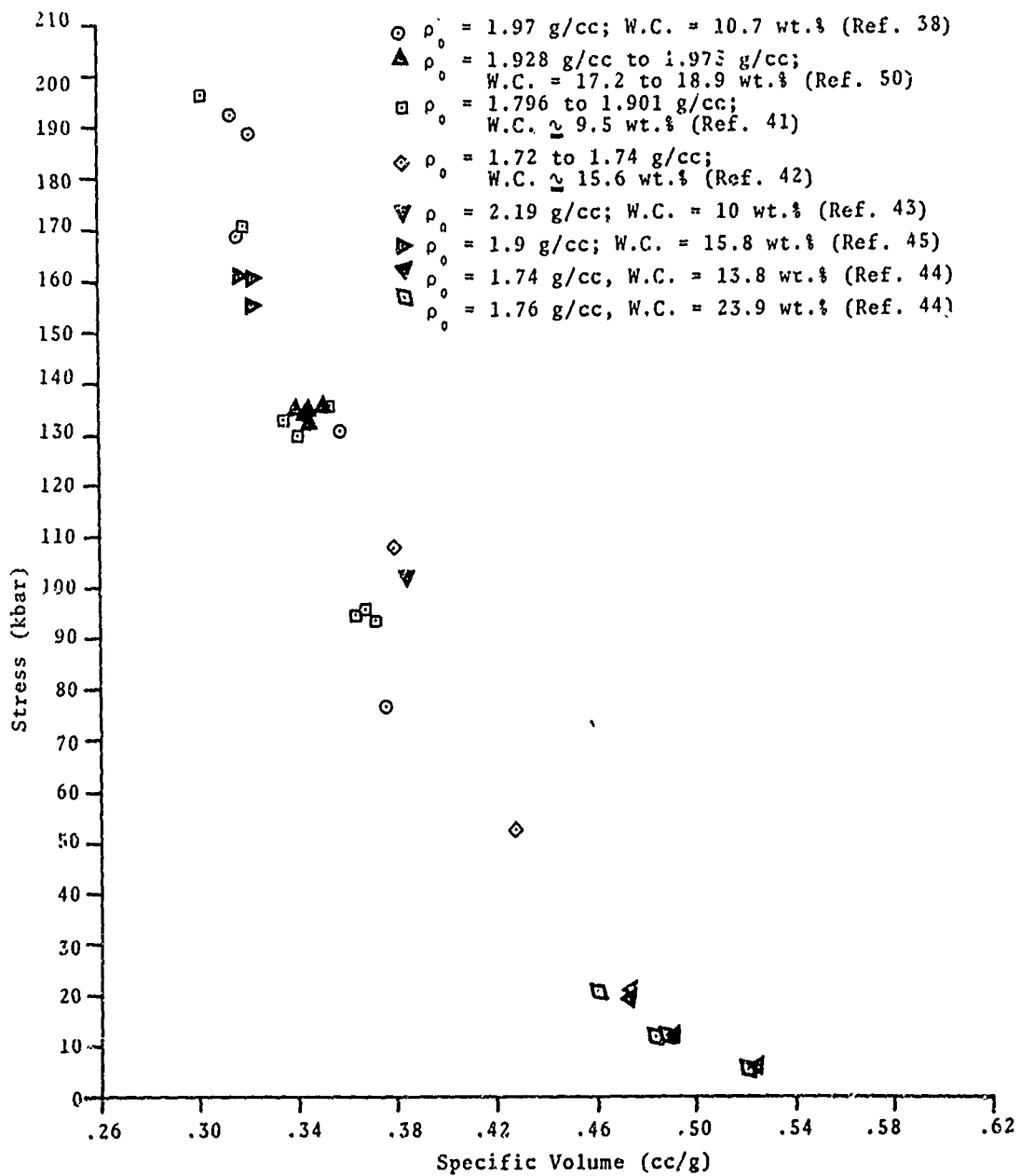


Fig. 3.5--Hugoniot stress-volume data for saturated tuffs of indicated water content.

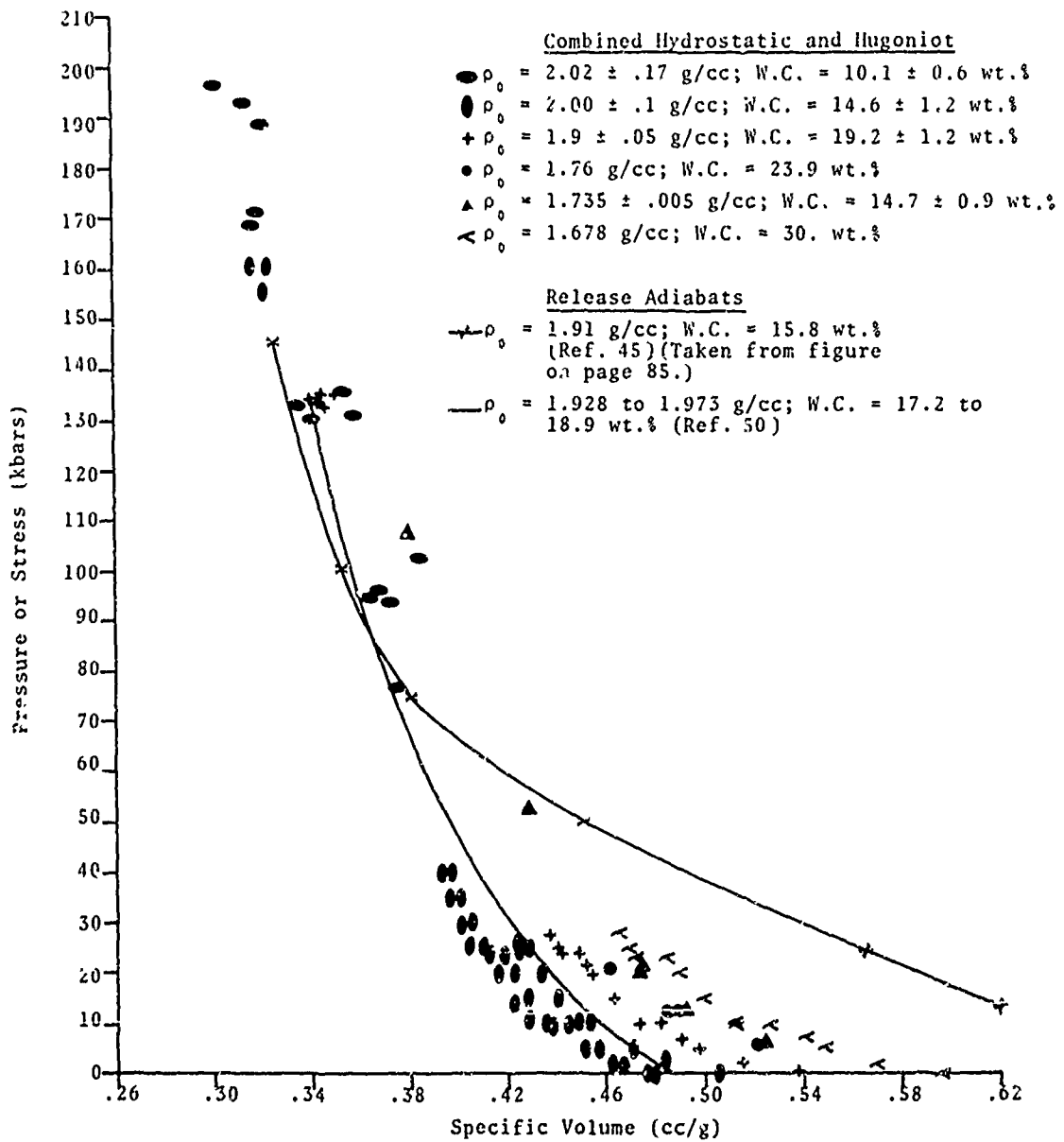


Fig. 3.6--Hydrostatic, Hugoniot and release adiabatic data for saturated tuffs of indicated water content.

IV. HOMOGENIZED EQUATION OF STATE FOR TUFF/WATER MIXTURES*

It is often useful in the study of pulse propagation into composite materials to consider the mixture of constituents to be so thorough as to justify the use of a homogeneous equation of state for the gross material. Such an approximation reduces the complexity of any numerical calculations for such materials. In the case of some extremely complex geologic composites, it is presently the only practical method to model the material. An equation of state for such a geologic material, compacted dry tuff, has been derived which is based on this assumption of homogeneity (Section 3.2). An additional component, i.e., water, is also present in most test site locations. In the following section, a homogeneous equation of state for fully saturated water/tuff mixtures is developed.

4.1 BASIC CONSIDERATIONS

The problem to be considered is the determination of a homogeneous equation of state for a composite consisting of materials which have been characterized by the following relations,

$$p_i = p_i(V_i, E_i) \quad (4.1)$$

$$E_i = E_i(V_i, T_i) \quad (4.2)$$

Since it is necessary that the composite material be characterized by its own p, E, V , and T , certain additional relations are necessary to construct an appropriate equation of state. Namely, if the specific volume and internal energy of the

* Author: J. W. Kirsch

mix is given by

$$V = \sum F_i V_i, \quad E = \sum F_i V_i \quad (4.3)$$

where F_i is the mass fraction of material i , some sort of molecular interchange must be hypothesized to provide the additional equations to enable the calculation of equilibrium states.

The condition of pressure and thermal equilibrium (PTEQ) requires that

$$p_i = p_j = p_k = \dots \quad (4.4)$$

and

$$T_i = T_j = T_k = \dots \quad (4.5)$$

This is an idealized situation wherein the mixture is homogeneous down to such a small scale that the molecular exchange of thermal energy between the components (effectively) occurs instantaneously. One may alternatively propose that no thermal energy is exchanged and that only hydrostatic (pressure) equilibrium occurs.

Each thermodynamic statement above (Eqs. 4.4, 4.5) carries along some implicit statements about the nature of the material. Pressure equilibrium between constituents is justifiable on the grounds that only saturated tuff is under consideration. That is, all pores are taken to be filled with water. Under this assumption, it is a trivial calculation to show that a pressure pulse will travel the order of .15 cm in a microsecond. Since typical pore sizes are between .01 cm and .001 cm, or smaller, ^(36, 40, 45) it is reasonable to assume that pressure equilibrium will occur during a microsecond pulse.

The occurrence of thermal equilibrium, between water and the tuff composite, is more difficult to achieve. A simple model of the thermal situation has been suggested.⁽⁵⁰⁾ The surfaces of spheres of water or quartz are assumed to instantaneously come to the temperature of the material in which it is immersed. The surface temperature is further assumed to remain constant for all time. By using standard heat transfer graphs,⁽⁵¹⁾ it is possible to calculate "effective heat penetration times" for various, simple geometries. It is shown by Rosenberg, et al.,⁽⁵⁰⁾ that for the smallest tuff particles (.03 cm) and available thermal diffusivity data, the time required to reach thermal equilibrium is a couple of orders of magnitude larger than a μ sec.

The basic parameter of these calculations is the Fourier modulus, F_0 , given by

$$F_0 = \frac{\alpha\tau}{d^2} \quad (4.6)$$

where

α = thermal diffusivity, cm^2/sec

τ = time, sec

d = characteristic (particle) dimension, cm

A larger Fourier modulus implies greater thermal penetration. In Fig. 4.1 the temperature distribution in a sphere is graphically depicted under the condition that the surface temperature has been raised to t_0 at $\tau = 0$, and maintained thereafter. With appropriate diffusivity values for water and quartz (i.e., $\alpha_q = .03$, $\alpha_w = .0014$), the Fourier moduli

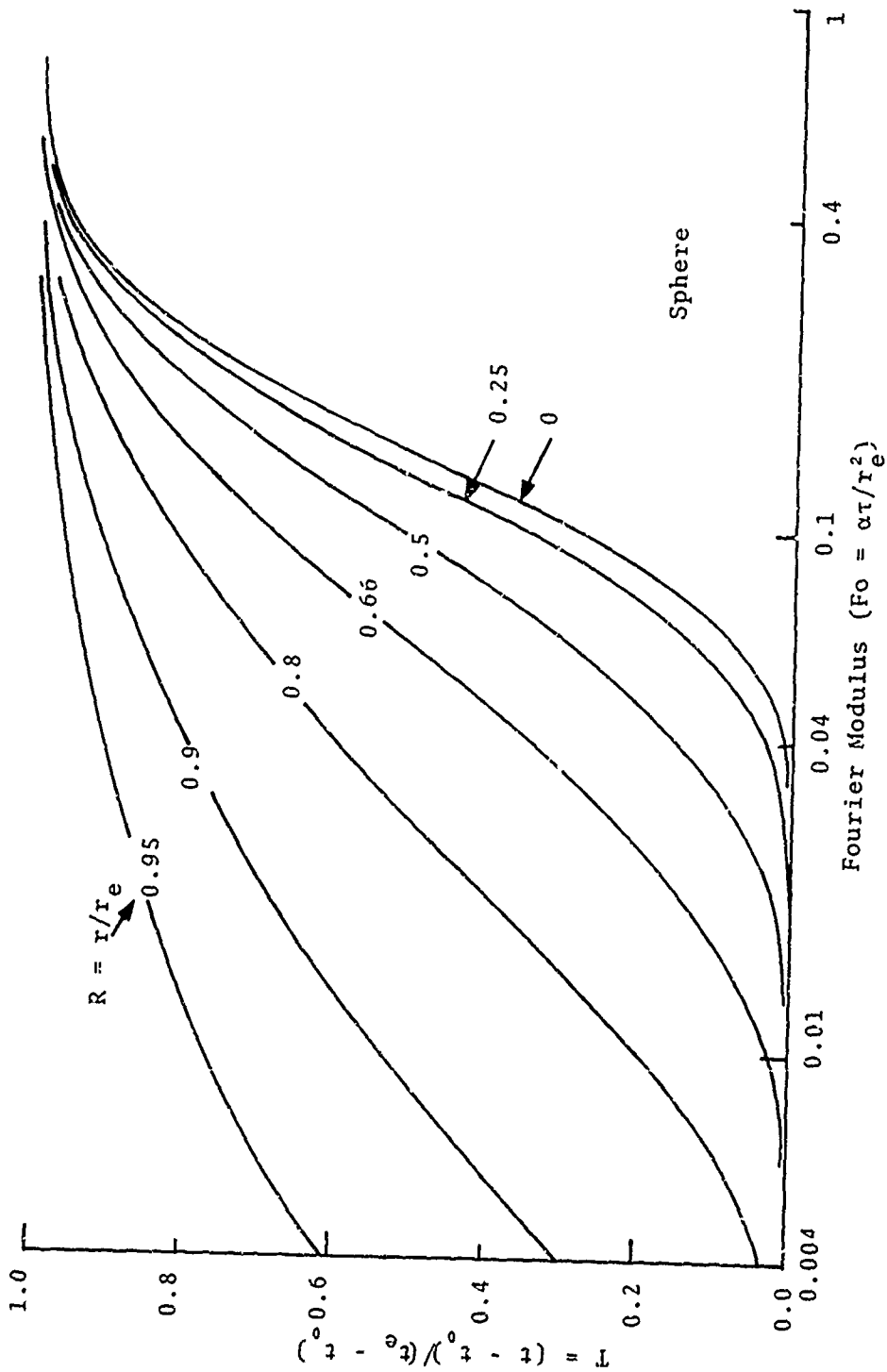


Fig. 4.1--Temperature distribution in a sphere, $0 < r < r_e$, after sudden change in surface temperature at $r = r_e$ from $t < 0$ to t_e for $\tau \geq 0$. (Taken from Schneider(51) charts.)

for .03 cm-diameter particles and $\tau = 1 \mu\text{sec}$ are

$$F_{0T} = .33 \times 10^{-4} \quad (4.7)$$

$$F_{0W} = .014 \times 10^{-4} \quad (4.8)$$

Qualitatively, one can see that only minute thermal penetration is possible under these conditions (as was concluded by Rosenberg, et al.⁽⁵⁰⁾) However, it has been reported by a number of investigators^(36, 40, 45) that tuff consists not only of relatively large grain matter sized between 3 and .03 cm, but also of small grain particles and matrix material sized on the order of tens of microns. It is pointed out in Ref. 40 that about 22% (by weight) of their tuff samples consisted of fine grain particles less than .005 cm. This is significant since 10^{-3} cm pore sizes increase the Fourier moduli (4.7, 4.8) by about three orders of magnitude. Based on the temperature distribution plot in Fig. 4.1, it can be concluded that significant portions of such spheres would experience a marked change in temperature during the microsecond pulse (the fine grain ($d < 1\mu$) material would achieve thermal equilibrium with the water based on this model).

These simple calculations suggest that a partial thermal equilibrium model be considered for tuff wherein the water is in thermal equilibrium with only a portion of the tuff material. However, within the context of the available information on tuff, it may very well be that water in equilibrium with only the fine grain material may lead to even lower water temperatures if that material's thermal capacity is lower than that of the large grain matter.

It should also be mentioned that the thermal material properties and the molecular interaction between various species under high pressure shock conditions is not considered in the simplified model described above. One investigation⁽⁵²⁾ of shock wave propagating into a dust-laden fluid (40% dust, by mass) shows that the solid particles in the flow attain a high degree of thermal equilibrium within the shock itself.

One may conclude from the above discussion that questions concerning thermal equilibrium are directly connected to the overall problem of characterizing the macro- and micro-structure of geologic materials.* The critical physical parameters of a particular model are not available. In the interest of brevity, only the pressure equilibrium and PTEQ models will be considered so as to ascertain the extremes of the thermal behavior to be anticipated in the constituents.

*It should be noted that for millisecond duration pulses, the argument is considerably enhanced in favor of both pressure and thermal equilibrium.

4.2 PRESSURE EQUILIBRIUM (p-V EQUATIONS OF STATE)

Mixtures in pressure equilibrium can be most readily analyzed if there is a single-valued relationship between pressure and volume. Hence, if energy effects are neglected altogether, Eqs. (4.1) through (4.3) reduce to the volumetric equations of state,

$$p(V) = p_i(V_i) \quad (4.9)$$

where

$$V = \sum_i F_i V_i \quad (4.10)$$

Specializing these equations to a two-component mixture (like that proposed for tuff and water),

$$p(V) = p_1(V_1) = p_2(V_2) \quad (4.11)$$

$$V = FV_1 + (1-F)V_2 \quad (4.12)$$

The simplest case to consider is a mixture of two materials described by linear equations of state

$$p_1 = A_1 \frac{V_{01} - V_1}{V_{01}}, \quad p_2 = A_2 \frac{V_{02} - V_2}{V_{02}}, \quad (4.13)$$

where V_{0i} is some initial volume and A_i are constants. Solving each of these expressions for V_i , setting $p_1 = p_2 = p$ (i.e., pressure equilibrium), and substituting the V_i expressions into Eq. (4.12) yields

$$V = V \left(\frac{A_1 V_{01} - pV_{01}}{A_1} \right) + (1-F) \left(\frac{A_2 V_{02} - pV_{02}}{A_2} \right) \quad (4.14)$$

Solving this equation for p results in a linear equation of state for the mix,

$$p = A \left(\frac{V_0 - V}{V_0} \right) \quad (4.15)$$

where

$$V_0 = FV_{01} + (1-F)V_{02} \quad (4.16)$$

$$A = \frac{V_0}{\frac{FV_{01}}{A_1} + \frac{(1-F)V_{02}}{A_2}} \quad (4.17)$$

In general, components with non-linear equations of state do not yield an explicit relation between p and V . The equation of state (of the mix) is a transcendental relationship. For example, the Murnaghan form

$$p = \frac{B}{\psi} \left[\left(V_0/V \right)^{-\psi} - 1 \right] \quad (4.18)$$

of the equation of state is sometimes used to represent the extremes of static compressibility tests and shock measurements at high pressures. The constants B and ψ are related to the sound velocity c_0 and the slope of the shock/particle velocity Hugoniot data according to⁽³⁵⁾

$$c_0 = \sqrt{BV_0}, \quad \psi = 4s-1 \quad (4.19)$$

Pressure equilibrium suffices to construct an homogenized equation of state for a mixture from those of its constituents when substituted into Eq. (4.12).

$$V = F \left[\frac{V_{01}}{\left(1 + \frac{p\psi_1}{A_1} \right)^{1/\psi_1}} \right] + (1-F) \left[\frac{V_{02}}{\left(1 + \frac{p\psi_2}{A_2} \right)^{1/\psi_2}} \right] \quad (4.20)$$

This transcendental relation cannot be solved explicitly for p and, unlike the simple linear case, does not preserve the form of the equations of state for the constituents. Nevertheless, p can be numerically evaluated for specified V and (4.20) represents an homogenized equation of state.

For subsequent calculations it is necessary to consider pressure equilibrium between materials whose pressure varies according to a cubic polynomial in μ ($\equiv \frac{V_0 - V}{V}$). Specifically, the Hugoniot data for both compacted dry tuff and water have both been fitted to the form

$$p = A\mu + B\mu^2 + F\mu^3; \quad (4.21)$$

where A , B , F are given in Eqs. (2.11) and (3.3) respectively). The condition of pressure equilibrium (together with the tacit assumption that the internal energies of the constituents of the mixture are those for the Hugoniots of the pure materials) has been imposed on these fits to construct a p - V relation for completely saturated wet tuff with the following values for the mass fractions of water.

$$F = \frac{M_W}{M_W + M_T} = 0, .5, .10, .15, .20, .25, .30 \quad (4.22)$$

Pressure-volume relationships are obtained for each mix in the same manner. A given pressure implies the specific volumes of the two components from which V is directly calculated (i.e., Eq. (4.12)).

The corresponding p - V curves are shown in Fig. 4.2. The curve for zero water content represents the Hugoniot for compacted dry tuff of density $\rho_0 = 2.4$ g/cc.

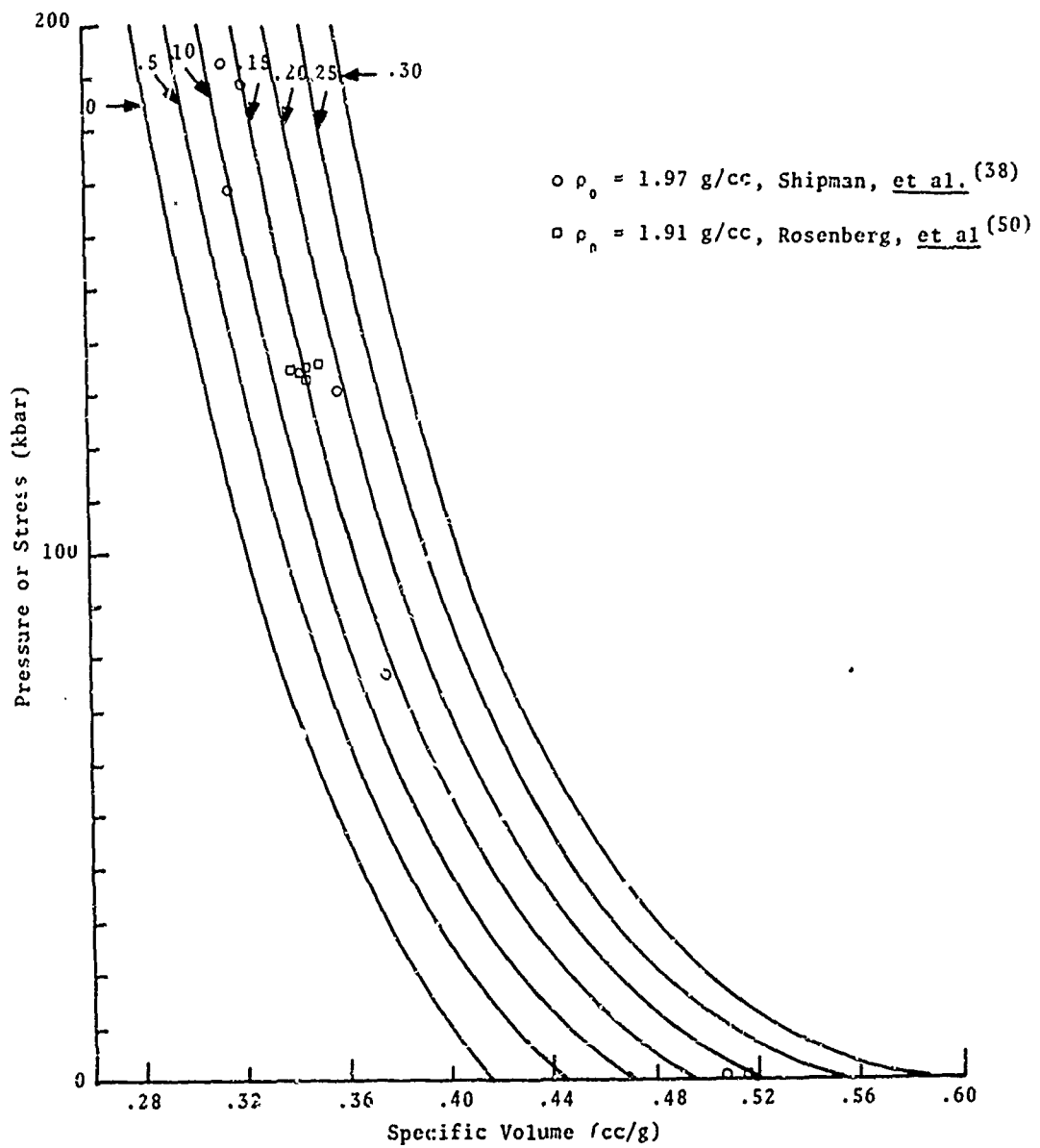


Fig. 4.2--Hugoniot for various water/tuff mixtures computed on the basis of pressure equilibrium.

The available Hugoniot data for saturated wet tuff for $p < 200$ kbar are also shown in Fig. 4.2. The data points are scattered about the $F = .15$ curve which corresponds to the representative value for the water content of wet tuff. This particular curve has also been fitted to the cubic form, i.e.,

$$\begin{aligned} p = & 5.96758 \times 10^{10} \mu \\ & + 6.31245 \times 10^{11} \mu^2 \\ & - 2.60228 \times 10^{11} \mu^3, \text{ ergs/cc} \end{aligned} \quad (4.23)$$

where

$$\rho_0 = 1.9835, \text{ g/cc} \quad (4.24)$$

4.3 EQUILIBRIUM STATES—ENERGY EFFECTS

The calculation of equilibrium states when the constituents are characterized by equations of state of the form (4.1), (4.2), involves the simultaneous solution of a set of algebraic equations. As one might suspect, the "hand" solution of these equations, even for a two-component mixture, can be very complex and time consuming. Consequently, an iteration subroutine from the S³ computer library has been adapted to calculate p-V-E-T data for PTEQ (or, alternatively, pressure equilibrium only) mixtures. This iterative scheme is fully described in Appendix B.

Briefly, the iteration process for PTEQ calculations is initiated for a given E, V by assuming a temperature of the mix, as well as the V_i's. The constituent's energies are then computed (from Eq. (4.2)) and their mass-weighted sum is compared to the original E. The difference between the energies is then divided by an appropriate C_v of the mix to give the first correction to the temperature.

In the next phase of the calculations, the (corrected) temperature is held constant, while the specific volumes are adjusted to assure pressure equilibrium. Thus, new T and V_i's are obtained with which the iteration is continued until a satisfactory answer is obtained. For the present calculations, the iteration is completed when the difference in the energies is less than .05 percent of the desired E.

If thermal equilibrium is not required, the thermal iteration step is omitted. Since the constituents will undergo independent thermal shock transitions, it is possible to adapt the above-described iteration procedure to solve for V_i if (during unloading) the isentropic expression $\int_{V_{H_0}}^V p dV + E_{H_0}(V_0)$, is substituted for E in the p-V-E

equation of state. The subscript H_0 corresponds to the state of the material just behind the shock. In shock loading, the E_{H_0} expression is obtained from the shock Hugoniot. (For the present calculations, the basic iteration scheme has not been used to calculate pressure equilibrium mixtures.)

4.3.1 PTEQ Calculations

A series of PTEQ calculations has been conducted wherein equilibrium states of various mixtures have been computed on the shock Hugoniot and release adiabats. In these calculations, the equations of state developed for S^3 dry compacted tuff (Eqs. 3.14, 3.15) and water (Eqs. 2.16, 2.25) have been employed. It was ascertained that a typical calculation of pressure, after the energy and specific volume of the mix had been specified, requires approximately 10 milliseconds on the UNIVAC 1108 computer.

4.3.1.1 Shock Hugoniots

Shock Hugoniots for the homogenized PTEQ tuff/water mixes have been computed for various mass fractions of water. These are presented in Fig. 4.3. The experimental data for wet tuff is plotted for comparison. The thermodynamic states represented by these curves have been obtained by finding those states which satisfy both the Hugoniot relation,

$$E - E_0 = \frac{(p + p_0)(V_0 - V)}{2} \quad (4.25)$$

and the PTEQ mixture equation of state. The p-V-E-T data (for the components and the mix) are given in Table 4.1.

Qualitatively speaking, these (PTEQ) curves are similar to those obtained on the basis of pressure equilibrium only (see Fig. 4.2). Moreover, the general agreement with the experimental data for $F = .15$ and $.20$ is maintained in

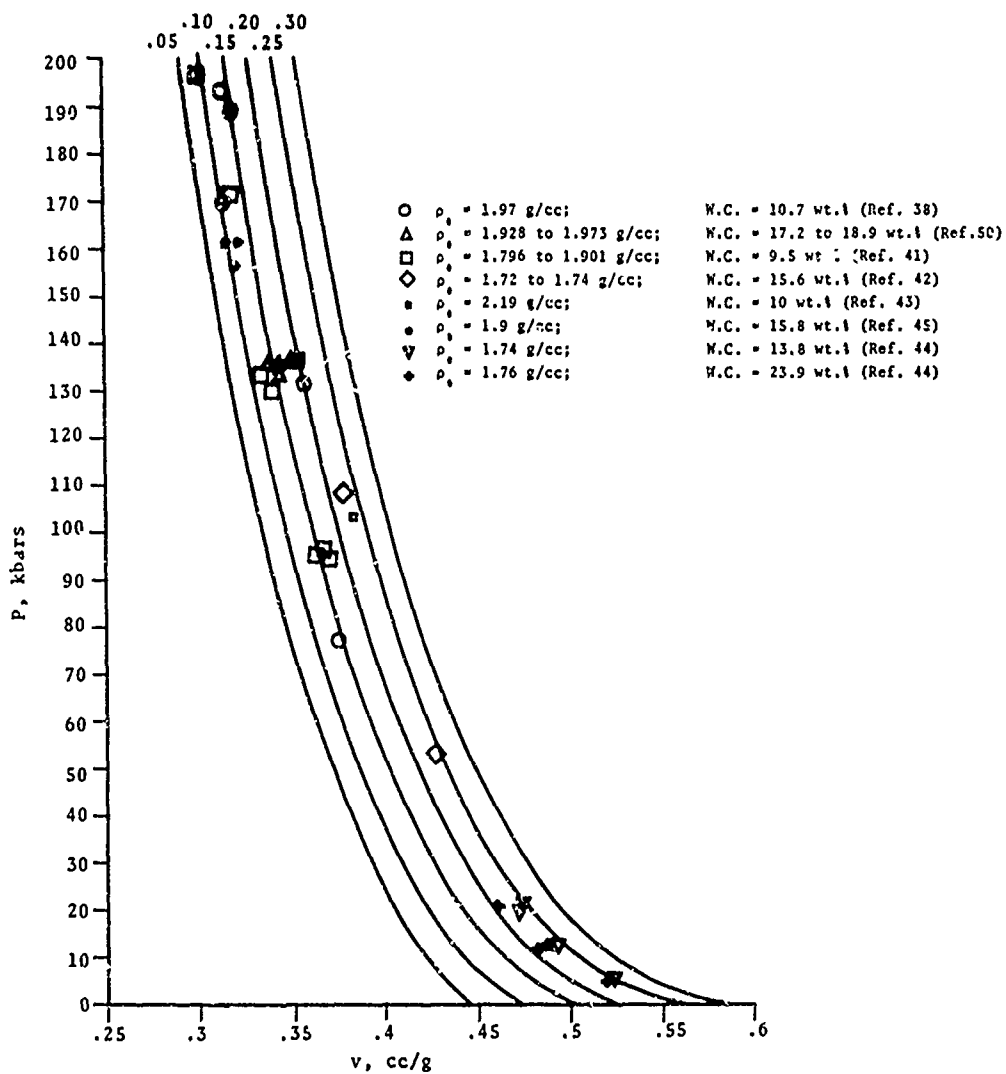


Fig. 4.3--Hugoniot for various water/tuff mixtures computed on the basis of pressure and thermal equilibrium (PTEQ).

the PTEQ calculations. Direct comparison of the results of these calculations, in the p-V plane, is presented in Fig. 4.4 wherein the pressure equilibrium and PTEQ shock Hugoniots for two of the mixes (5, 15%) are plotted on a common set of axes. The PTEQ Hugoniots lie below those determined from pressure equilibrium considerations, indicating that the effect of imposing thermal equilibrium on the mix is to enhance the energy absorption characteristics of the materials.

This effect can be explained by the fact that water, under the same relative compression, heats up to higher temperatures than tuff. Thermal equilibrium requires that the water gives up a significant portion of this thermal energy to the tuff. Although this doesn't greatly affect the compressibility of the tuff, it does result in a sizeable increase in the water's compressibility. (Another way of explaining this result is that the internal energy of the water is dominated by the thermal component ($C_V \Delta T$) wherein for (S^3) tuff, compressional energy ($-\int h_1(V) dV$) is much greater than its thermal component. Temperature equilibrium will thereby greatly reduce the internal energy of the water component (at a given V) while the tuff would exhibit only a small increase in its internal energy.)

To demonstrate this explanation, the locus of equilibrium states computed for the water and tuff components in the 10% and 30% PTEQ mixes are superimposed on the corresponding Hugoniot curves for each of the pure materials in Fig. 4.5. It is readily observed that the water states in the PTEQ mix must be at considerably lower thermal energies than the (thermally independent) pure water case. This can also be seen in the temperatures calculated for the PTEQ Hugoniots. The tuff temperatures are increased over those calculated for the pure tuff Hugoniot whereas the water temperatures in the (shocked) PTEQ mixes are lower. These Hugoniot temperatures are plotted vs specific volume in Fig. 4.6 for the case of the 15% mix.

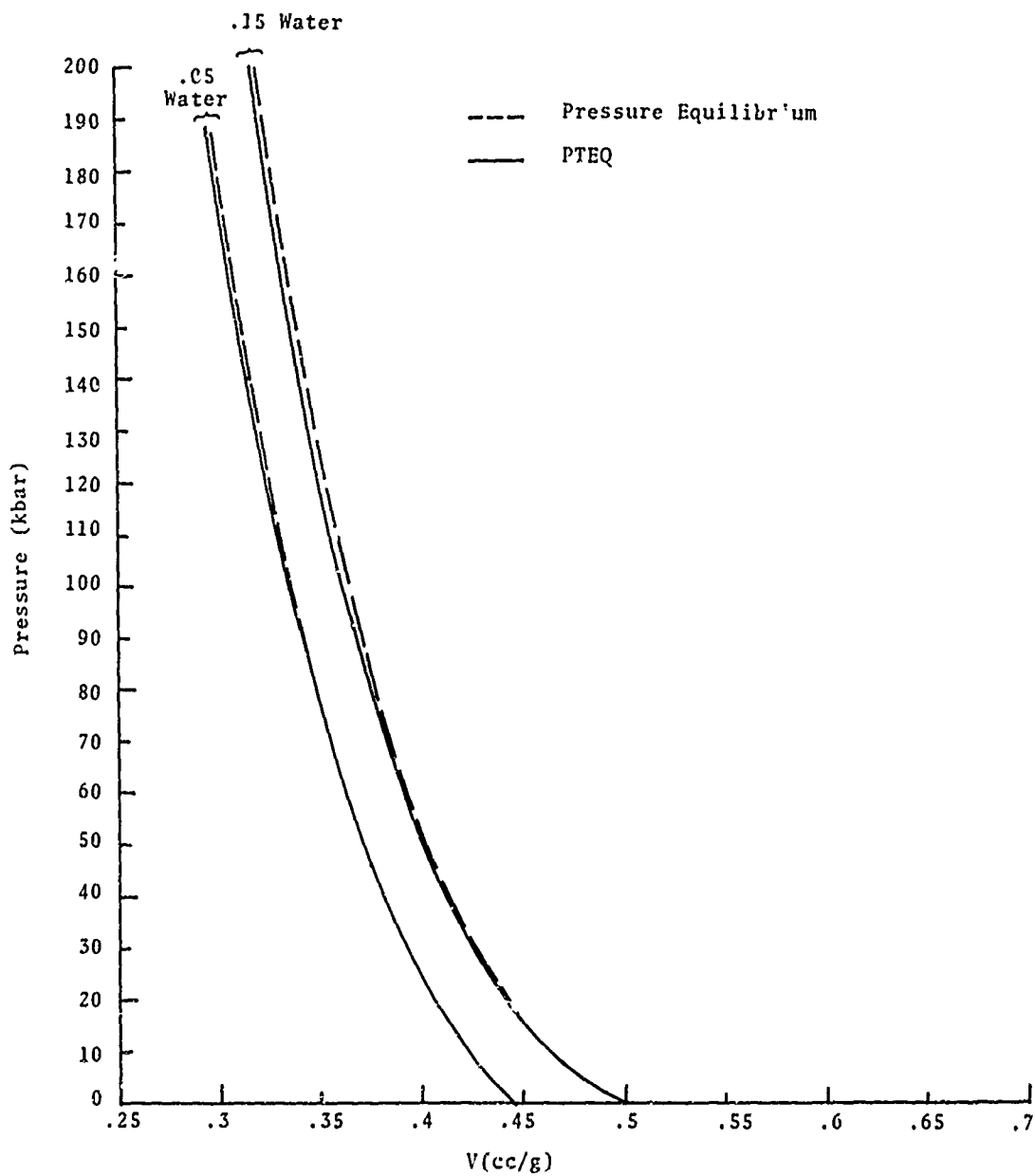


Fig. 4.4--Comparison of the 5% and 15% (by mass) water/tuff Hugoniot curves computed on the basis of PTEQ with the pressure equilibrium curves.

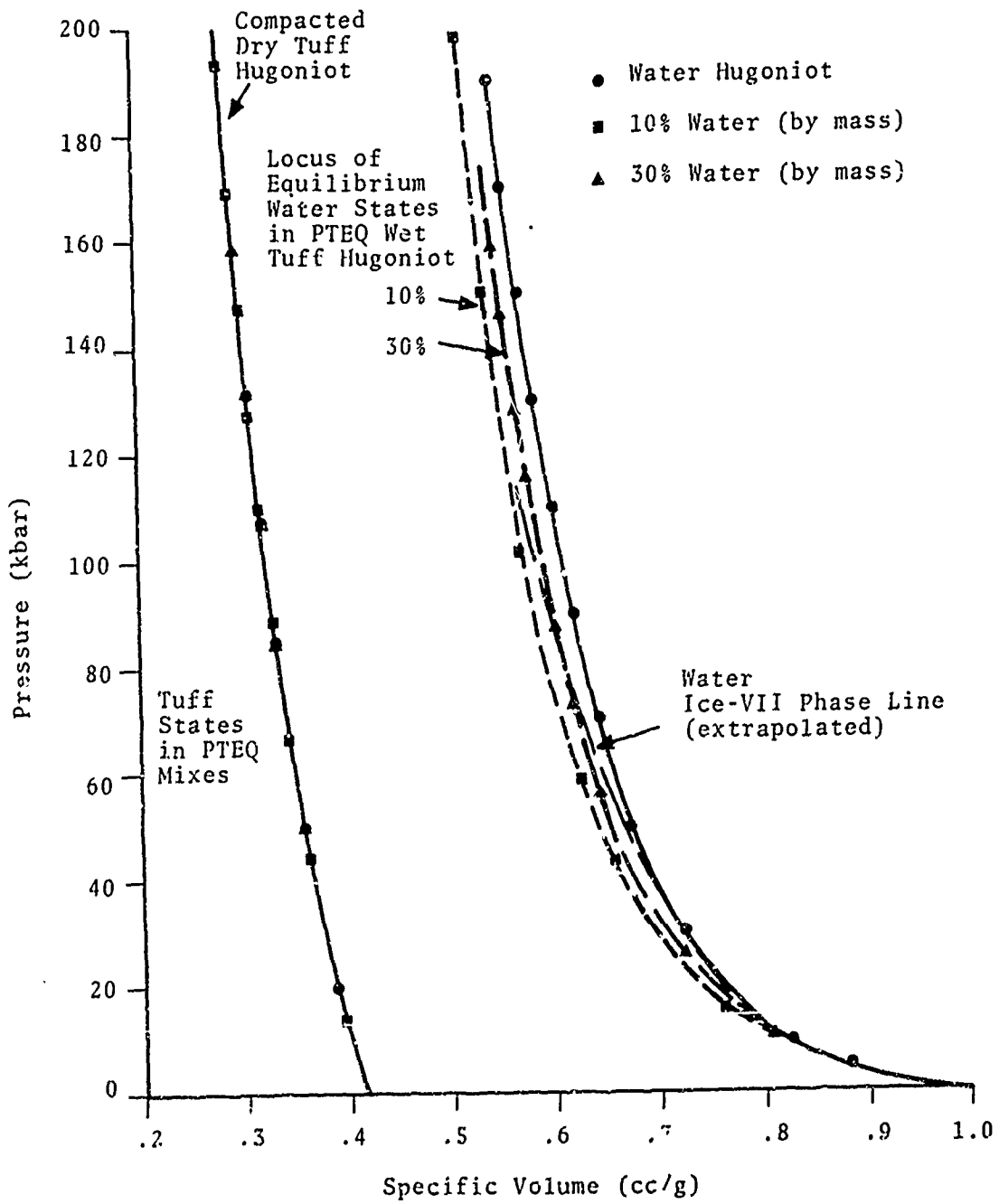


Fig. 4.5--Locus of the water and tuff states on the PTEQ Hugoniot compared to the Hugoniots of the pure materials.

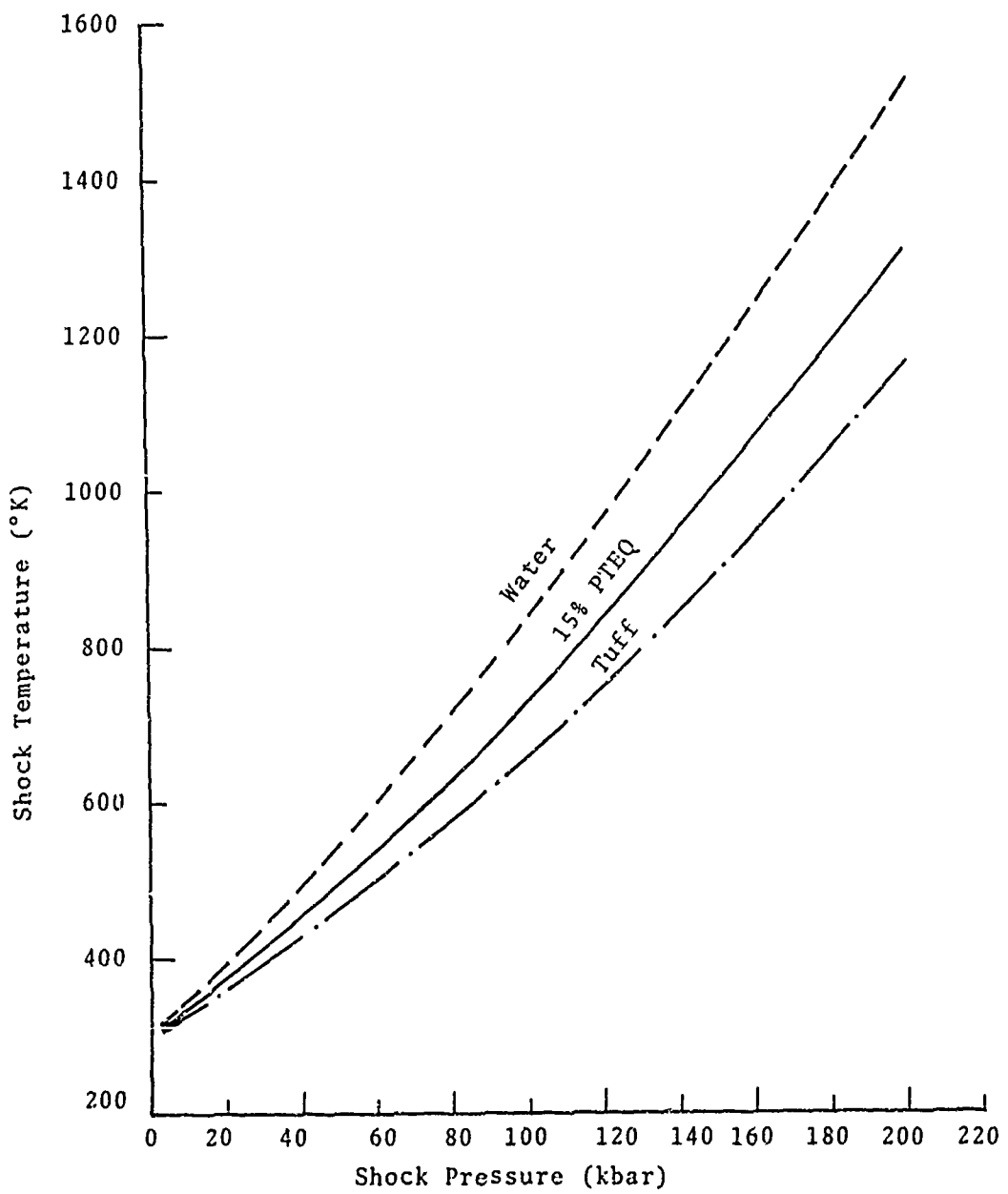


Fig. 4.6--Comparison of the shock temperature for a (15% water) PTEQ mixture to the shock temperatures of the pure materials.

Such behavior of the water and tuff, when in thermal equilibrium, enhances the possibility that the compressed water would undergo a phase change (to ice-VII). The extrapolation of Bridgman's phase transition curve for water⁽²¹⁾ is superimposed on the plots in Fig. 4.5. Clearly, for the lower percentage water mixes, an analysis of phase transition kinetics may be appropriate as the statement that the Hugoniot "skirts the phase transition line" is not applicable. In this regard, it should also be noted that increases in the tuff temperature might have a significant effect on high pressure phase transitions (at pressure about 380 kbar⁽⁵³⁾) and may also induce the debonding of "nonliquid" water contained within tuff's clay lattice (reported by Stephens, et al.⁽³⁵⁾).

4.3.1.2 Release Adiabats

Release adiabats have been calculated for the various percent water mixtures under consideration up to pressures of 150 kbar. In general, the isentropes for the PTEQ mixes lie close to the Hugoniots in the pressure range of interest. However, there are significant differences between these results and those computed for pure tuff. As shown in Fig. 4.8 for the 15% water mixture, the extra energy absorption due to the presence of the water results in "slower" unloading of the shocked composite material than in the pure tuff.

The effects of water concentration on the unloading curves is demonstrated in Fig. 4.8. Three cases (5, 20, 30% water) are considered wherein the release adiabats are presented along with the corresponding Hugoniot curve. It may be readily concluded that as the water concentration goes up, tuff/water mixtures would exhibit more and more energy dependence in an unloading process.

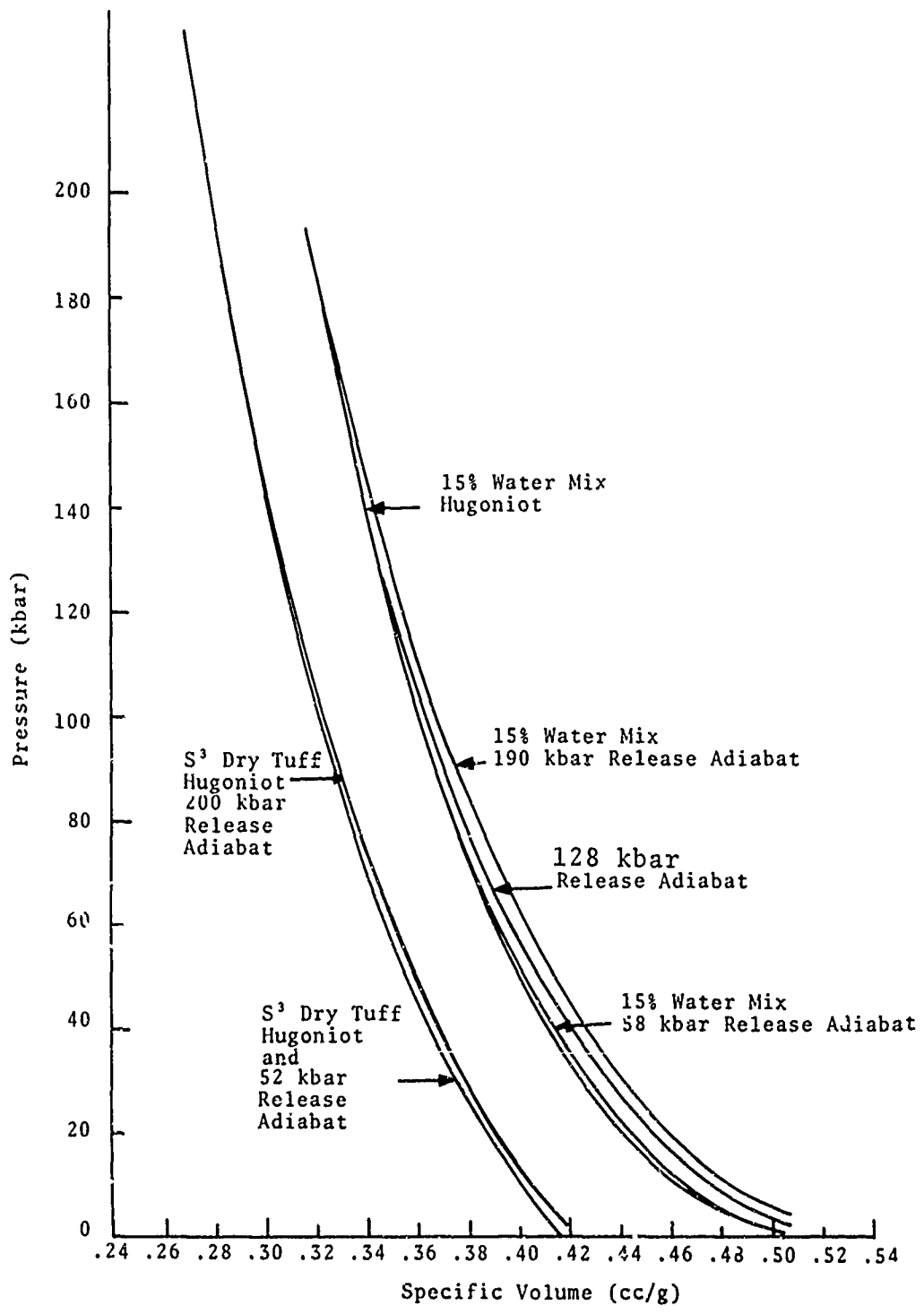


Fig. 4.7--Release adiabats computed for the 15% water PTEQ mixture compared to that of (S³) dry tuff.

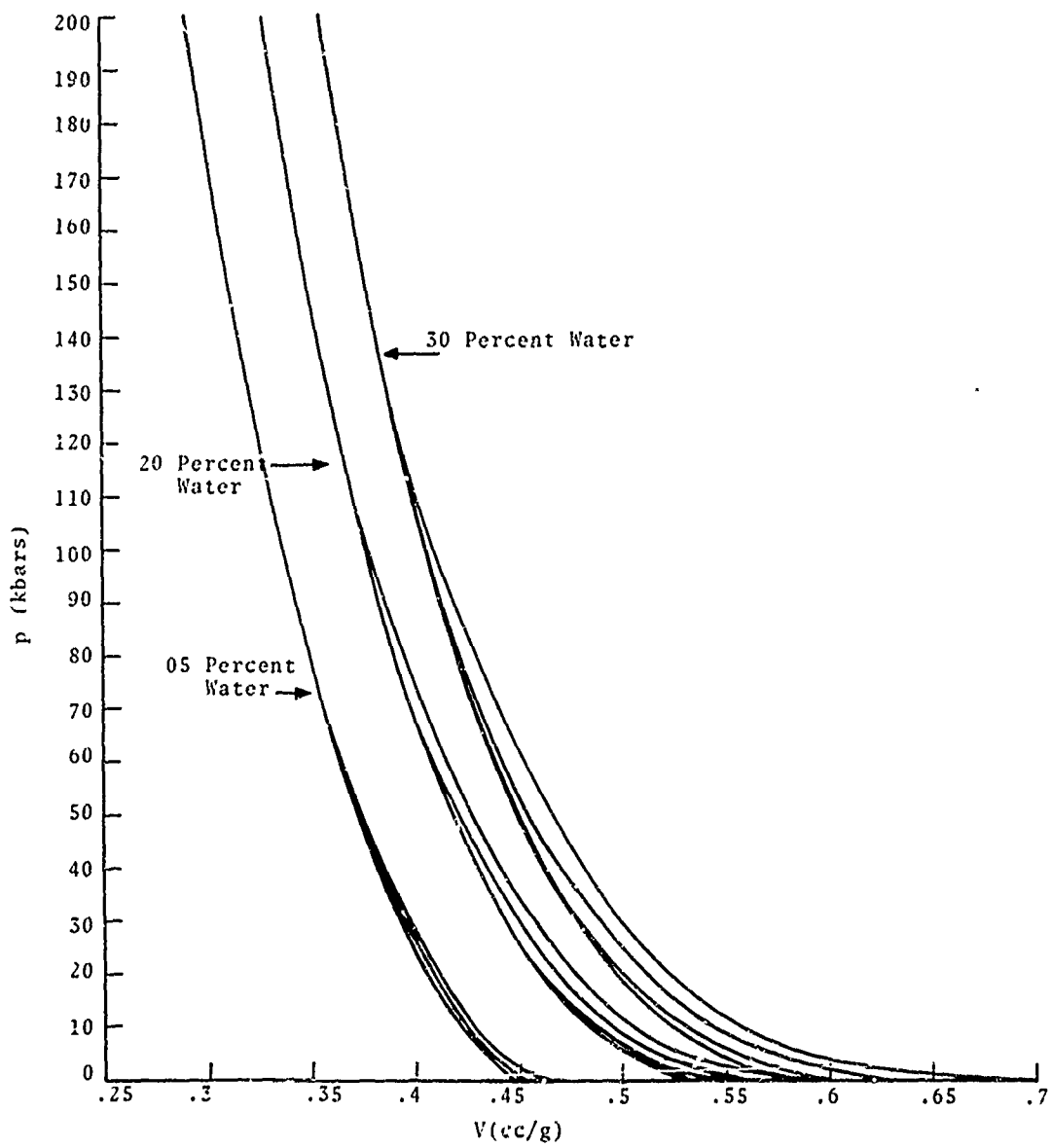


Fig. 4.8--Release adiabats of three PTEQ water/tuff mixtures. Note the increased energy dependence as water concentration is raised.

In Fig. 4.8 the water phase change occurs at pressures too small to be shown. It is not evident from these curves that there is a discontinuity in the p-V trace as the two-phase thermodynamic region is entered. This is seen in Fig. 4.9 wherein the release adiabats for 10 and 25% mixtures are plotted out to specific volumes of 2.5. Essentially, the phase transition is isothermal, and the water component acquires energy from the tuff as the pressure slightly decreases. For example, in the two-phase region of the 150 kbar release adiabat (10% water mix), the temperature changes by only .3°C (.1%) whereas the pressure drops by about 2% at a specific volume (of the mix) equal to 2.5.

There isn't an over-abundance of experimental data to which the present theory can be compared. In Fig. 4.10, the 135-kbar release adiabat measured by Rosenberg, et al.⁽⁵⁰⁾ for a 15% water/tuff mix (fully saturated) is compared to the Hugoniot and 135-kbar release adiabat for the 15% (by mass) PTEQ water/tuff mixture. There is reasonable qualitative agreement. In fact, the shape of the curves is very nearly identical.* However, the other set of experimental points,⁽⁴⁵⁾ plotted in Fig. 4.11, illustrates that the simple homogenized model may not be appropriate in all cases. (It should be remarked that in both sets of experimental release data the p-V relationship below 80 kbar is difficult to infer from the experimental data). This disparity in experimental results is one indication that to fully characterize the effect of the presence of water in geologic material one will also require more exact knowledge of the geologic composite itself.

*The S^3 compacted dry tuff Hugoniot could be slightly displaced (to the left in the p-V plane) to more exactly reproduce the experimental results.

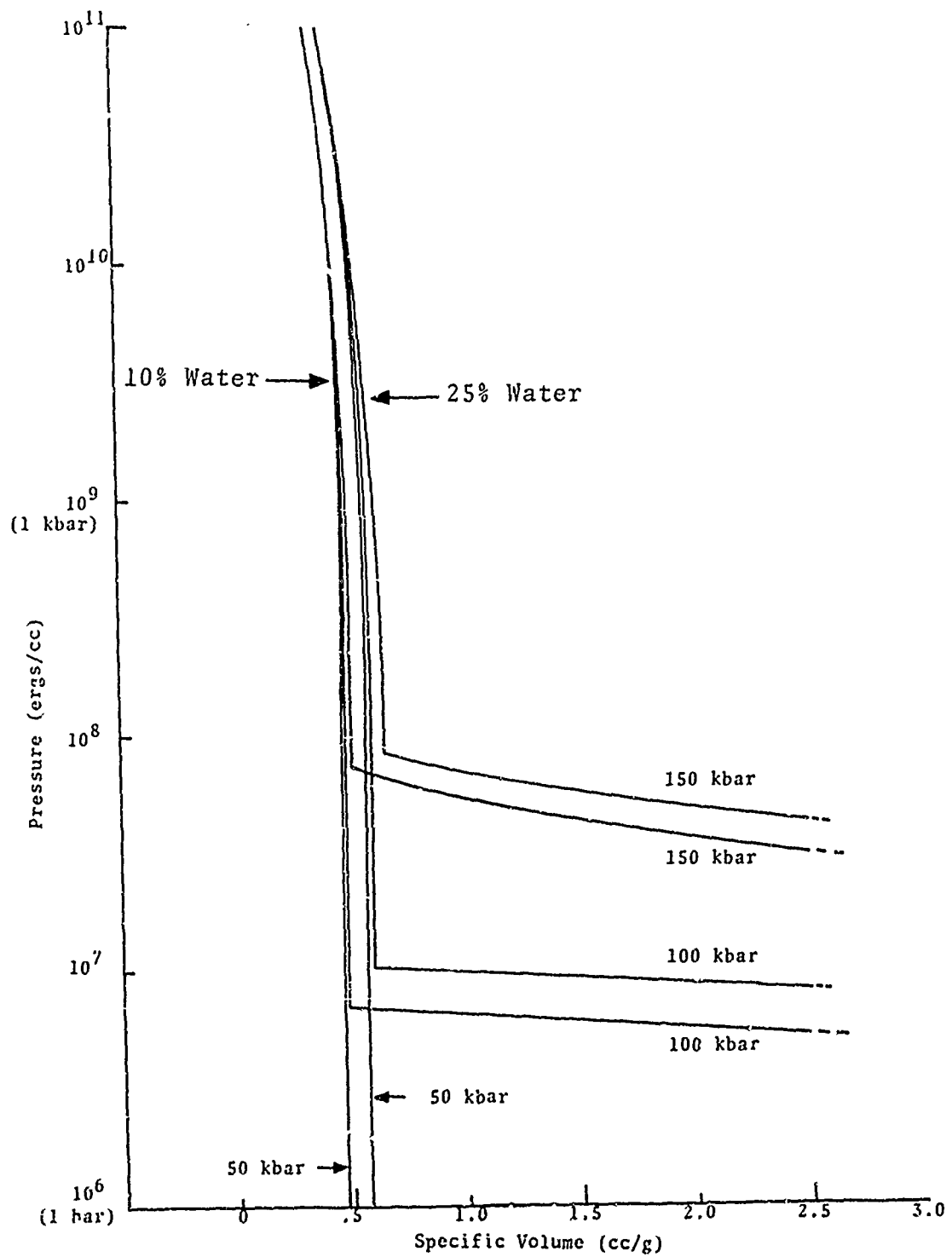


Fig. 4.9--Release adiabats of two PTEQ water/tuff mixtures showing the effect of vaporization of the water.

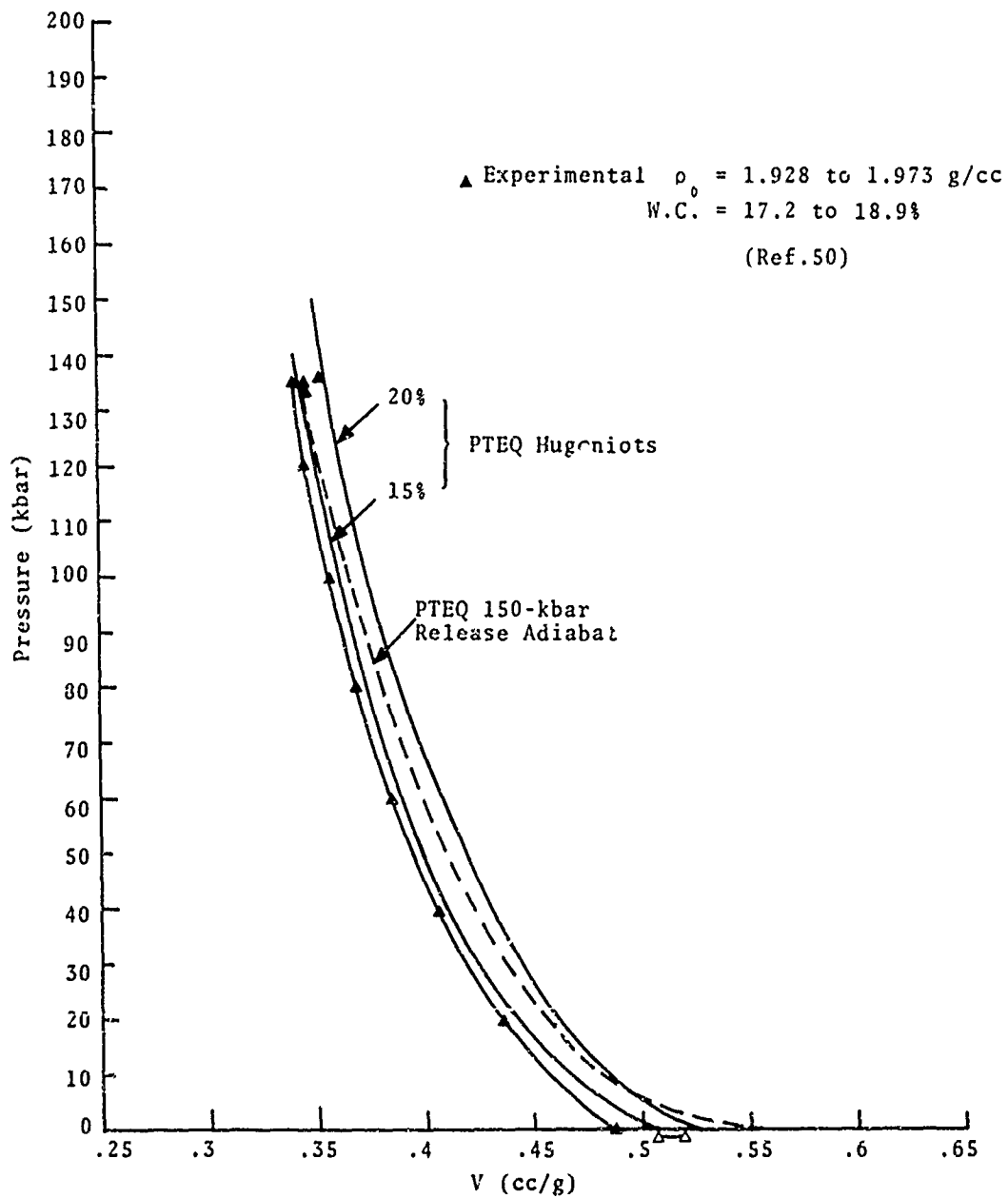


Fig. 4.10--Experimental release adiabat data⁽⁵⁰⁾ compared to PTEQ predictions.

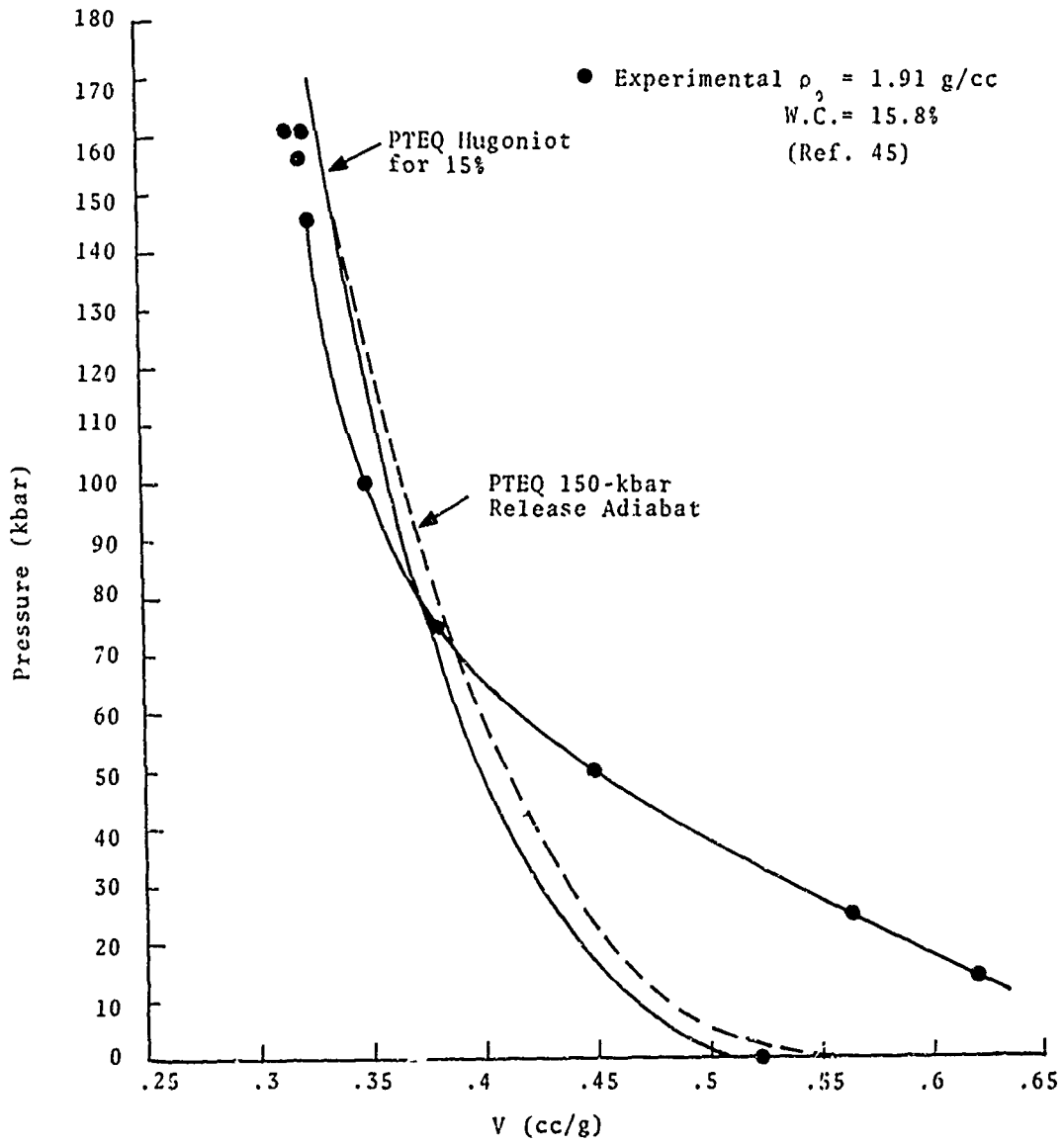


Fig. 4.11--Experimental release adiabat data⁽⁴⁵⁾ compared to PTEQ predictions.

4.3.2 Additional Comments

It is evident from the results presented in this section that a rational calculation of PTEQ states for tuff/water mixtures has been demonstrated. The computer time to determine p from a given V and E is approximately 10 milliseconds on the UNIVAC 1108. This is at least an order of magnitude slower than could be achieved if a table of equilibrium states were used in conjunction with a rapid table look-up scheme.⁽⁵⁴⁾ Thus, in numerical experiments wherein core storage capacity is no limitation, such tables could be readily computed from the PTEQ iteration program.

Still another possibility is that the PTEQ calculations can be employed as the basis of an analytic model for wet tuff. In a manner analogous to that presented in Section III, analytic expressions for the mix could be developed using the percentage water as an explicit parameter.

TABLE 4.1

PTEQ HUGONIOTS FOR 5, 10, 15, 20, 25, 30% WATER (BY MASS)/TUFF MIXTURES

AIX = Energy of Mix, ergs/g
 TVOL = Specific Volume of mix, cc/g
 P = Pressure, ergs/cc
 Theta = Temperature, °K
 Rho Water = Density of Water, g/cc
 Rho Tuff = Density of Tuff, g/cc
 SIE Water = Energy of Water, ergs/g
 SIE Tuff = Energy of Tuff, ergs/g

5 PERCENT WATER (F = .05)

F	AIX	TVOL	P	THETA	RHO WATER	RHO TUFF	SIE WATER	SIE TUFF
1	3.600+08	4.170+01	1.045+10	3.661+02	1.321+00	2.569+00	1.405+09	3.009+08
2	7.200+08	3.951+01	2.030+10	4.005+02	1.331+00	2.675+00	2.754+09	6.067+08
3	1.080+09	3.961+01	3.608+10	4.286+02	1.441+00	2.704+00	4.011+09	9.241+08
4	1.440+09	3.789+01	4.267+10	4.540+02	1.478+00	2.753+00	5.163+09	1.244+09
5	1.800+09	3.728+01	4.916+10	4.774+02	1.510+00	2.797+00	6.227+09	1.567+09
6	2.160+09	3.675+01	5.594+10	4.997+02	1.537+00	2.836+00	7.249+09	1.892+09
7	2.520+09	3.627+01	6.054+10	5.211+02	1.561+00	2.873+00	8.241+09	2.219+09
8	2.880+09	3.585+01	6.586+10	5.420+02	1.583+00	2.906+00	9.205+09	2.547+09
9	3.240+09	3.544+01	7.113+10	5.617+02	1.604+00	2.934+00	1.014+10	2.877+09
10	3.600+09	3.508+01	7.596+10	5.820+02	1.622+00	2.964+00	1.107+10	3.207+09
11	3.960+09	3.475+01	8.071+10	6.019+02	1.639+00	2.997+00	1.198+10	3.538+09
12	4.320+09	3.443+01	8.542+10	6.217+02	1.655+00	3.024+00	1.289+10	3.869+09
13	4.680+09	3.411+01	9.011+10	6.415+02	1.669+00	3.049+00	1.377+10	4.202+09
14	5.040+09	3.387+01	9.420+10	6.608+02	1.684+00	3.074+00	1.465+10	4.534+09
15	5.400+09	3.361+01	9.851+10	6.802+02	1.697+00	3.098+00	1.552+10	4.868+09
16	5.760+09	3.336+01	1.027+11	6.995+02	1.710+00	3.121+00	1.638+10	5.201+09
17	6.120+09	3.313+01	1.069+11	7.188+02	1.724+00	3.143+00	1.724+10	5.535+09
18	6.480+09	3.293+01	1.110+11	7.386+02	1.738+00	3.165+00	1.806+10	5.870+09
19	6.840+09	3.273+01	1.150+11	7.572+02	1.744+00	3.186+00	1.893+10	6.204+09
20	7.200+09	3.248+01	1.190+11	7.764+02	1.755+00	3.206+00	1.977+10	6.539+09
21	7.560+09	3.228+01	1.229+11	7.957+02	1.765+00	3.226+00	2.065+10	6.874+09
22	7.920+09	3.204+01	1.267+11	8.149+02	1.775+00	3.246+00	2.143+10	7.209+09
23	8.280+09	3.190+01	1.306+11	8.341+02	1.773+00	3.265+00	2.225+10	7.545+09
24	8.640+09	3.172+01	1.343+11	8.533+02	1.773+00	3.283+00	2.306+10	7.880+09
25	9.000+09	3.153+01	1.381+11	8.725+02	1.802+00	3.301+00	2.390+10	8.216+09
26	9.360+09	3.138+01	1.418+11	8.918+02	1.811+00	3.319+00	2.471+10	8.552+09
27	9.720+09	3.122+01	1.455+11	9.111+02	1.819+00	3.336+00	2.553+10	8.888+09
28	1.008+10	3.107+01	1.491+11	9.304+02	1.827+00	3.353+00	2.634+10	9.224+09
29	1.044+10	3.091+01	1.527+11	9.494+02	1.835+00	3.370+00	2.715+10	9.560+09
30	1.080+10	3.077+01	1.563+11	9.682+02	1.843+00	3.387+00	2.796+10	9.897+09
31	1.116+10	3.062+01	1.598+11	9.866+02	1.850+00	3.403+00	2.877+10	1.023+10
32	1.152+10	3.048+01	1.633+11	1.008+03	1.857+00	3.419+00	2.957+10	1.057+10
33	1.188+10	3.034+01	1.668+11	1.028+03	1.864+00	3.434+00	3.038+10	1.091+10
34	1.224+10	3.021+01	1.703+11	1.047+03	1.871+00	3.449+00	3.118+10	1.124+10
35	1.260+10	3.011+01	1.731+11	1.070+03	1.876+00	3.462+00	3.200+10	1.158+10
36	1.296+10	2.994+01	1.755+11	1.093+03	1.883+00	3.477+00	3.282+10	1.191+10
37	1.332+10	2.986+01	1.803+11	1.104+03	1.884+00	3.492+00	3.367+10	1.225+10
38	1.368+10	2.973+01	1.837+11	1.129+03	1.886+00	3.506+00	3.446+10	1.259+10
39	1.404+10	2.961+01	1.869+11	1.148+03	1.894+00	3.521+00	3.523+10	1.293+10
40	1.440+10	2.949+01	1.902+11	1.167+03	1.901+00	3.535+00	3.604+10	1.326+10
41	1.476+10	2.938+01	1.937+11	1.187+03	1.915+00	3.550+00	3.684+10	1.360+10
42	1.512+10	2.926+01	1.970+11	1.206+03	1.921+00	3.564+00	3.763+10	1.394+10
43	1.548+10	2.914+01	2.004+11	1.226+03	1.926+00	3.577+00	3.842+10	1.428+10
44	1.584+10	2.904+01	2.037+11	1.245+03	1.936+00	3.591+00	3.921+10	1.461+10

TABLE 4.i (Continued)

5 Percent Water (Cont.)

45	1.620+10	2.894-01	2.070+11	1.265+03	1.934+00	3.604+00	4.000+10	1.495+10
46	1.656+10	2.683-01	2.103+11	1.295+03	1.943+00	3.618+00	4.080+10	1.529+10
47	1.692+10	2.873-01	2.135+11	1.304+03	1.949+00	3.631+00	4.159+10	1.562+10
48	1.728+10	2.863-01	2.168+11	1.324+03	1.954+00	3.643+00	4.238+10	1.596+10
49	1.764+10	2.854-01	2.200+11	1.344+03	1.959+00	3.656+00	4.317+10	1.630+10
50	1.800+10	2.844-01	2.232+11	1.364+03	1.964+00	3.669+00	4.396+10	1.664+10
51	1.836+10	2.835-01	2.264+11	1.384+03	1.969+00	3.681+00	4.476+10	1.697+10
52	1.872+10	2.825-01	2.296+11	1.404+03	1.974+00	3.694+00	4.555+10	1.731+10
53	1.908+10	2.816-01	2.328+11	1.424+03	1.979+00	3.706+00	4.634+10	1.765+10
54	1.944+10	2.807-01	2.359+11	1.444+03	1.984+00	3.718+00	4.714+10	1.799+10
55	1.980+10	2.799-01	2.391+11	1.464+03	1.989+00	3.730+00	4.793+10	1.832+10
56	2.016+10	2.790-01	2.422+11	1.485+03	1.993+00	3.742+00	4.873+10	1.866+10
57	2.052+10	2.781-01	2.453+11	1.505+03	1.997+00	3.753+00	4.952+10	1.900+10
58	2.088+10	2.773-01	2.484+11	1.525+03	2.002+00	3.765+00	5.032+10	1.933+10
59	2.124+10	2.765-01	2.515+11	1.546+03	2.006+00	3.776+00	5.111+10	1.967+10
60	2.160+10	2.757-01	2.546+11	1.566+03	2.011+00	3.788+00	5.191+10	2.001+10
61	2.196+10	2.749-01	2.577+11	1.587+03	2.015+00	3.799+00	5.271+10	2.035+10
62	2.232+10	2.741-01	2.607+11	1.607+03	2.019+00	3.810+00	5.350+10	2.068+10
63	2.268+10	2.733-01	2.638+11	1.628+03	2.024+00	3.821+00	5.430+10	2.102+10
64	2.304+10	2.726-01	2.668+11	1.648+03	2.027+00	3.832+00	5.510+10	2.136+10
65	2.340+10	2.718-01	2.698+11	1.669+03	2.031+00	3.843+00	5.590+10	2.169+10
66	2.376+10	2.711-01	2.728+11	1.690+03	2.035+00	3.853+00	5.670+10	2.203+10
67	2.412+10	2.704-01	2.758+11	1.711+03	2.039+00	3.864+00	5.750+10	2.237+10
68	2.448+10	2.697-01	2.788+11	1.731+03	2.043+00	3.875+00	5.830+10	2.270+10
69	2.484+10	2.690-01	2.818+11	1.752+03	2.047+00	3.885+00	5.910+10	2.304+10
70	2.520+10	2.683-01	2.848+11	1.773+03	2.051+00	3.895+00	5.990+10	2.338+10
71	2.556+10	2.676-01	2.878+11	1.794+03	2.054+00	3.906+00	6.070+10	2.371+10
72	2.592+10	2.669-01	2.907+11	1.815+03	2.058+00	3.916+00	6.150+10	2.405+10
73	2.628+10	2.662-01	2.937+11	1.836+03	2.062+00	3.926+00	6.231+10	2.439+10
74	2.664+10	2.656-01	2.966+11	1.857+03	2.065+00	3.936+00	6.311+10	2.472+10
75	2.700+10	2.649-01	2.996+11	1.878+03	2.069+00	3.946+00	6.392+10	2.506+10
76	2.736+10	2.643-01	3.025+11	1.899+03	2.072+00	3.956+00	6.472+10	2.540+10

TABLE 4.1 (Continued)

10 PERCENT WATER (F = .10)

K	AIX	TVUL	P	THETA	RHO WATER	RHO TUFF	SIE WATER	SIE TUFF
1	3.500+08	4.307-01	1.614+10	3.598+02	1.294+00	2.546+00	1.251+09	2.610+08
2	7.200+08	4.171-01	2.474+10	3.927+02	1.365+00	2.617+00	2.470+09	5.456+08
3	1.080+09	4.075-01	3.194+10	4.200+02	1.413+00	2.672+00	3.578+09	8.025+08
4	1.440+09	4.000-01	3.823+10	4.445+02	1.449+00	2.719+00	4.620+09	1.087+09
5	1.800+09	3.938-01	4.406+10	4.673+02	1.480+00	2.761+00	5.614+09	1.376+09
6	2.160+09	3.880-01	4.951+10	4.890+02	1.506+00	2.799+00	6.573+09	1.670+09
7	2.520+09	3.830-01	5.467+10	5.099+02	1.530+00	2.833+00	7.505+09	1.946+09
8	2.880+09	3.785-01	5.959+10	5.302+02	1.551+00	2.866+00	8.415+09	2.265+09
9	3.240+09	3.745-01	6.433+10	5.501+02	1.570+00	2.896+00	9.308+09	2.586+09
10	3.600+09	3.705-01	6.910+10	5.690+02	1.589+00	2.926+00	1.018+10	2.869+09
11	3.960+09	3.671-01	7.351+10	5.884+02	1.606+00	2.953+00	1.104+10	3.173+09
12	4.320+09	3.638-01	7.782+10	6.075+02	1.621+00	2.979+00	1.189+10	3.479+09
13	4.680+09	3.608-01	8.233+10	6.265+02	1.636+00	3.004+00	1.274+10	3.785+09
14	5.040+09	3.579-01	8.615+10	6.453+02	1.649+00	3.028+00	1.357+10	4.092+09
15	5.400+09	3.552-01	9.018+10	6.641+02	1.662+00	3.051+00	1.440+10	4.401+09
16	5.760+09	3.526-01	9.415+10	6.827+02	1.675+00	3.073+00	1.522+10	4.709+09
17	6.120+09	3.501-01	9.834+10	7.014+02	1.687+00	3.094+00	1.603+10	5.019+09
18	6.480+09	3.478-01	1.019+11	7.199+02	1.698+00	3.115+00	1.684+10	5.329+09
19	6.840+09	3.455-01	1.057+11	7.384+02	1.709+00	3.136+00	1.764+10	5.640+09
20	7.200+09	3.434-01	1.094+11	7.569+02	1.719+00	3.156+00	1.844+10	5.952+09
21	7.560+09	3.413-01	1.131+11	7.754+02	1.729+00	3.175+00	1.923+10	6.263+09
22	7.920+09	3.393-01	1.167+11	7.939+02	1.739+00	3.194+00	2.002+10	6.575+09
23	8.280+09	3.374-01	1.203+11	8.123+02	1.749+00	3.212+00	2.081+10	6.888+09
24	8.640+09	3.355-01	1.238+11	8.308+02	1.758+00	3.230+00	2.160+10	7.201+09
25	9.000+09	3.337-01	1.274+11	8.493+02	1.766+00	3.248+00	2.238+10	7.514+09
26	9.360+09	3.320-01	1.308+11	8.679+02	1.775+00	3.265+00	2.316+10	7.828+09
27	9.720+09	3.303-01	1.343+11	8.862+02	1.783+00	3.282+00	2.393+10	8.141+09
28	1.008+10	3.287-01	1.377+11	9.047+02	1.791+00	3.298+00	2.471+10	8.455+09
29	1.044+10	3.271-01	1.411+11	9.233+02	1.799+00	3.314+00	2.548+10	8.789+09
30	1.080+10	3.256-01	1.445+11	9.419+02	1.806+00	3.330+00	2.625+10	9.084+09
31	1.116+10	3.241-01	1.478+11	9.603+02	1.814+00	3.346+00	2.702+10	9.398+09
32	1.152+10	3.227-01	1.511+11	9.789+02	1.821+00	3.361+00	2.778+10	9.713+09
33	1.188+10	3.212-01	1.544+11	9.975+02	1.828+00	3.377+00	2.855+10	1.003+10
34	1.224+10	3.199-01	1.577+11	1.016+03	1.835+00	3.392+00	2.931+10	1.034+10
35	1.260+10	3.185-01	1.609+11	1.035+03	1.842+00	3.406+00	3.008+10	1.066+10
36	1.296+10	3.172-01	1.641+11	1.053+03	1.848+00	3.421+00	3.084+10	1.097+10
37	1.332+10	3.162-01	1.668+11	1.076+03	1.852+00	3.432+00	3.167+10	1.129+10
38	1.368+10	3.147-01	1.705+11	1.091+03	1.861+00	3.449+00	3.236+10	1.160+10
39	1.404+10	3.137-01	1.732+11	1.113+03	1.865+00	3.460+00	3.316+10	1.192+10
40	1.440+10	3.125-01	1.763+11	1.132+03	1.871+00	3.474+00	3.395+10	1.223+10
41	1.473+10	3.113-01	1.795+11	1.150+03	1.877+00	3.488+00	3.470+10	1.255+10

TABLE 4.1 (Continued)

10 Percent Water (Cont.)

42	1.513+10	3.101-01	1.827+11	1.169+03	1.883+00	3.501+00	3.546+10	1.287+10
43	1.548+10	3.090-01	1.858+11	1.167+03	1.889+00	3.515+00	3.621+10	1.318+10
44	1.594+10	3.079-01	1.890+11	1.206+03	1.895+00	3.528+00	3.696+10	1.350+10
45	1.620+10	3.068-01	1.921+11	1.225+03	1.901+00	3.541+00	3.771+10	1.381+10
46	1.656+10	3.057-01	1.952+11	1.243+03	1.906+00	3.554+00	3.847+10	1.413+10
47	1.692+10	3.046-01	1.983+11	1.262+03	1.912+00	3.567+00	3.922+10	1.445+10
48	1.728+10	3.036-01	2.013+11	1.281+03	1.917+00	3.579+00	3.997+10	1.476+10
49	1.764+10	3.026-01	2.043+11	1.300+03	1.922+00	3.592+00	4.072+10	1.508+10
50	1.800+10	3.016-01	2.073+11	1.319+03	1.927+00	3.604+00	4.147+10	1.540+10
51	1.836+10	3.006-01	2.103+11	1.337+03	1.932+00	3.616+00	4.222+10	1.571+10
52	1.872+10	2.997-01	2.135+11	1.356+03	1.937+00	3.628+00	4.297+10	1.603+10
53	1.908+10	2.987-01	2.165+11	1.375+03	1.942+00	3.640+00	4.373+10	1.635+10
54	1.944+10	2.978-01	2.194+11	1.394+03	1.947+00	3.652+00	4.449+10	1.666+10
55	1.980+10	2.969-01	2.224+11	1.413+03	1.952+00	3.664+00	4.523+10	1.698+10
56	2.016+10	2.960-01	2.254+11	1.433+03	1.956+00	3.675+00	4.598+10	1.730+10
57	2.052+10	2.951-01	2.283+11	1.452+03	1.961+00	3.687+00	4.673+10	1.761+10
58	2.088+10	2.943-01	2.313+11	1.471+03	1.965+00	3.698+00	4.748+10	1.793+10
59	2.124+10	2.934-01	2.342+11	1.490+03	1.970+00	3.709+00	4.824+10	1.825+10
60	2.160+10	2.926-01	2.371+11	1.509+03	1.974+00	3.720+00	4.899+10	1.856+10
61	2.196+10	2.918-01	2.400+11	1.529+03	1.978+00	3.731+00	4.974+10	1.888+10
62	2.232+10	2.910-01	2.429+11	1.548+03	1.983+00	3.742+00	5.049+10	1.920+10
63	2.268+10	2.902-01	2.458+11	1.567+03	1.987+00	3.753+00	5.124+10	1.951+10
64	2.304+10	2.894-01	2.486+11	1.587+03	1.991+00	3.763+00	5.200+10	1.983+10
65	2.340+10	2.886-01	2.515+11	1.606+03	1.995+00	3.774+00	5.275+10	2.014+10
66	2.376+10	2.878-01	2.544+11	1.626+03	1.999+00	3.784+00	5.350+10	2.046+10
67	2.412+10	2.871-01	2.572+11	1.645+03	2.003+00	3.795+00	5.426+10	2.078+10
68	2.448+10	2.863-01	2.600+11	1.665+03	2.007+00	3.805+00	5.501+10	2.109+10
69	2.484+10	2.856-01	2.629+11	1.684+03	2.011+00	3.815+00	5.577+10	2.141+10
70	2.520+10	2.849-01	2.657+11	1.704+03	2.014+00	3.826+00	5.652+10	2.173+10
71	2.556+10	2.842-01	2.685+11	1.724+03	2.016+00	3.838+00	5.728+10	2.204+10
72	2.592+10	2.835-01	2.713+11	1.743+03	2.022+00	3.846+00	5.803+10	2.236+10
73	2.628+10	2.828-01	2.741+11	1.763+03	2.026+00	3.854+00	5.879+10	2.267+10
74	2.664+10	2.821-01	2.769+11	1.783+03	2.029+00	3.865+00	5.954+10	2.299+10
75	2.700+10	2.814-01	2.797+11	1.802+03	2.033+00	3.875+00	6.030+10	2.331+10
76	2.736+10	2.808-01	2.824+11	1.822+03	2.036+00	3.885+00	6.105+10	2.362+10
77	2.772+10	2.801-01	2.852+11	1.842+03	2.040+00	3.894+00	6.181+10	2.394+10
78	2.808+10	2.795-01	2.880+11	1.862+03	2.043+00	3.904+00	6.257+10	2.425+10
79	2.844+10	2.788-01	2.907+11	1.882+03	2.047+00	3.913+00	6.333+10	2.457+10
80	2.880+10	2.782-01	2.934+11	1.902+03	2.050+00	3.923+00	6.408+10	2.489+10
81	2.916+10	2.776-01	2.962+11	1.922+03	2.054+00	3.932+00	6.483+10	2.520+10
82	2.952+10	2.770-01	2.989+11	1.942+03	2.057+00	3.941+00	6.558+10	2.552+10
83	2.988+10	2.764-01	3.016+11	1.962+03	2.060+00	3.951+00	6.633+10	2.583+10

TABLE 4.1 (Continued)

15 PERCENT WATER (F = .15)

K	AIX	TVOL	P	THEIA	RHO WATER	RHO TUFF	SIE WATER	SIE TUFF
1	3.600+08	4.538-01	1.421+10	3.547+02	1.274+00	2.529+00	1.078+09	2.333+08
2	7.200+08	4.392-01	2.206+10	3.858+02	1.343+00	2.595+00	2.179+09	4.626+08
3	1.080+09	4.270-01	4.119+02	2.865+02	1.370+00	2.647+00	3.176+09	7.085+08
4	1.440+09	4.211-01	3.448+10	4.355+02	1.426+00	2.691+00	4.160+09	9.600+08
5	1.800+09	4.143-01	3.996+10	4.574+02	1.455+00	2.731+00	5.087+09	1.220+09
6	2.160+09	4.085-01	4.498+10	4.783+02	1.481+00	2.767+00	5.984+09	1.485+09
7	2.520+09	4.033-01	4.980+10	4.985+02	1.504+00	2.800+00	6.859+09	1.754+09
8	2.880+09	3.986-01	5.441+10	5.180+02	1.525+00	2.831+00	7.714+09	2.027+09
9	3.240+09	3.944-01	5.885+10	5.372+02	1.543+00	2.860+00	8.555+09	2.302+09
10	3.600+09	3.902-01	6.334+10	5.555+02	1.562+00	2.889+00	9.377+09	2.511+09
11	3.960+09	3.866-01	6.749+10	5.741+02	1.578+00	2.915+00	1.019+10	2.840+09
12	4.320+09	3.832-01	7.154+10	5.925+02	1.593+00	2.940+00	1.100+10	3.141+09
13	4.680+09	3.801-01	7.549+10	6.108+02	1.607+00	2.964+00	1.180+10	3.424+09
14	5.040+09	3.710-01	7.937+10	6.290+02	1.621+00	2.987+00	1.259+10	3.709+09
15	5.400+09	3.743-01	8.317+10	6.470+02	1.633+00	3.010+00	1.337+10	3.994+09
16	5.760+09	3.716-01	8.690+10	6.649+02	1.645+00	3.031+00	1.415+10	4.280+09
17	6.120+09	3.650-01	9.057+10	6.828+02	1.657+00	3.052+00	1.492+10	4.568+09
18	6.480+09	3.664-01	9.418+10	7.006+02	1.668+00	3.072+00	1.569+10	4.856+09
19	6.840+09	3.642-01	9.774+10	7.184+02	1.679+00	3.092+00	1.645+10	5.145+09
20	7.200+09	3.620-01	1.013+11	7.362+02	1.689+00	3.111+00	1.721+10	5.435+09
21	7.560+09	3.599-01	1.047+11	7.539+02	1.699+00	3.130+00	1.796+10	5.725+09
22	7.920+09	3.578-01	1.082+11	7.716+02	1.708+00	3.148+00	1.871+10	6.016+09
23	8.280+09	3.550-01	1.115+11	7.893+02	1.718+00	3.166+00	1.946+10	6.308+09
24	8.640+09	3.539-01	1.148+11	8.069+02	1.726+00	3.184+00	2.021+10	6.600+09
25	9.000+09	3.520-01	1.182+11	8.246+02	1.735+00	3.201+00	2.095+10	6.892+09
26	9.360+09	3.502-01	1.215+11	8.423+02	1.743+00	3.217+00	2.169+10	7.185+09
27	9.720+09	3.485-01	1.248+11	8.599+02	1.752+00	3.234+00	2.243+10	7.478+09
28	1.008+10	3.468-01	1.280+11	8.776+02	1.759+00	3.250+00	2.316+10	7.772+09
29	1.044+10	3.452-01	1.312+11	8.953+02	1.767+00	3.266+00	2.390+10	8.066+09
30	1.080+10	3.436-01	1.344+11	9.130+02	1.775+00	3.281+00	2.463+10	8.360+09
31	1.116+10	3.420-01	1.375+11	9.307+02	1.782+00	3.296+00	2.536+10	8.654+09
32	1.152+10	3.405-01	1.407+11	9.484+02	1.789+00	3.311+00	2.609+10	8.949+09
33	1.188+10	3.391-01	1.438+11	9.662+02	1.796+00	3.326+00	2.682+10	9.244+09
34	1.224+10	3.377-01	1.469+11	9.839+02	1.803+00	3.341+00	2.754+10	9.540+09
35	1.260+10	3.363-01	1.499+11	1.002+03	1.809+00	3.355+00	2.827+10	9.835+09
36	1.296+10	3.349-01	1.530+11	1.019+03	1.816+00	3.369+00	2.899+10	1.013+10
37	1.332+10	3.336-01	1.560+11	1.037+03	1.822+00	3.383+00	2.972+10	1.043+10
38	1.368+10	3.323-01	1.590+11	1.055+03	1.828+00	3.396+00	3.044+10	1.072+10
39	1.404+10	3.310-01	1.620+11	1.073+03	1.834+00	3.410+00	3.116+10	1.102+10
40	1.440+10	3.301-01	1.644+11	1.094+03	1.838+00	3.421+00	3.194+10	1.131+10
41	1.476+10	3.286-01	1.679+11	1.109+03	1.846+00	3.436+00	3.260+10	1.161+10
42	1.512+10	3.277-01	1.704+11	1.129+03	1.850+00	3.447+00	3.337+10	1.190+10
43	1.548+10	3.265-01	1.733+11	1.148+03	1.856+00	3.460+00	3.410+10	1.220+10
44	1.584+10	3.254-01	1.762+11	1.165+03	1.862+00	3.473+00	3.481+10	1.250+10

TABLE 4.1 (Continued)

15 Percent Water (Cont.)

45	1.620*10	3.242-01	1.792*11	1.183*03	1.867*00	3.485*00	3.553*10	1.280*10
46	1.656*10	3.231-01	1.821*11	1.201*03	1.873*00	3.498*00	3.624*10	1.309*10
47	1.692*10	3.220-01	1.851*11	1.219*03	1.878*00	3.510*00	3.696*10	1.339*10
48	1.728*10	3.209-01	1.880*11	1.236*03	1.884*00	3.523*00	3.767*10	1.369*10
49	1.764*10	3.199-01	1.909*11	1.254*03	1.889*00	3.535*00	3.838*10	1.399*10
50	1.800*10	3.189-01	1.937*11	1.272*03	1.894*00	3.547*00	3.910*10	1.428*10
51	1.836*10	3.178-01	1.966*11	1.290*03	1.899*00	3.559*00	3.981*10	1.458*10
52	1.872*10	3.169-01	1.995*11	1.308*03	1.904*00	3.570*00	4.052*10	1.488*10
53	1.908*10	3.159-01	2.023*11	1.326*03	1.909*00	3.582*00	4.124*10	1.518*10
54	1.944*10	3.149-01	2.051*11	1.344*03	1.914*00	3.594*00	4.195*10	1.547*10
55	1.980*10	3.140-01	2.080*11	1.362*03	1.918*00	3.605*00	4.266*10	1.577*10
56	2.016*10	3.131-01	2.108*11	1.380*03	1.923*00	3.616*00	4.337*10	1.607*10
57	2.052*10	3.122-01	2.136*11	1.398*03	1.928*00	3.627*00	4.409*10	1.637*10
58	2.088*10	3.113-01	2.163*11	1.416*03	1.932*00	3.638*00	4.480*10	1.667*10
59	2.124*10	3.104-01	2.191*11	1.435*03	1.936*00	3.649*00	4.551*10	1.696*10
60	2.160*10	3.095-01	2.219*11	1.453*03	1.941*00	3.660*00	4.622*10	1.726*10
61	2.196*10	3.087-01	2.246*11	1.471*03	1.945*00	3.671*00	4.693*10	1.756*10
62	2.232*10	3.078-01	2.274*11	1.489*03	1.949*00	3.681*00	4.765*10	1.786*10
63	2.268*10	3.070-01	2.301*11	1.508*03	1.954*00	3.692*00	4.836*10	1.816*10
64	2.304*10	3.062-01	2.328*11	1.526*03	1.958*00	3.702*00	4.907*10	1.845*10
65	2.340*10	3.054-01	2.355*11	1.544*03	1.962*00	3.713*00	4.978*10	1.875*10
66	2.376*10	3.046-01	2.383*11	1.563*03	1.966*00	3.723*00	5.050*10	1.905*10
67	2.412*10	3.038-01	2.410*11	1.581*03	1.970*00	3.733*00	5.121*10	1.935*10
68	2.448*10	3.031-01	2.436*11	1.599*03	1.974*00	3.743*00	5.192*10	1.964*10
69	2.484*10	3.023-01	2.463*11	1.618*03	1.978*00	3.753*00	5.263*10	1.994*10
70	2.520*10	3.016-01	2.490*11	1.636*03	1.981*00	3.763*00	5.335*10	2.024*10
71	2.556*10	3.008-01	2.517*11	1.655*03	1.985*00	3.773*00	5.406*10	2.054*10
72	2.592*10	3.001-01	2.543*11	1.673*03	1.989*00	3.783*00	5.477*10	2.084*10
73	2.628*10	2.994-01	2.570*11	1.692*03	1.993*00	3.792*00	5.549*10	2.113*10
74	2.664*10	2.987-01	2.596*11	1.711*03	1.996*00	3.802*00	5.620*10	2.143*10
75	2.700*10	2.980-01	2.623*11	1.729*03	2.000*00	3.812*00	5.691*10	2.173*10
76	2.736*10	2.973-01	2.649*11	1.748*03	2.004*00	3.821*00	5.763*10	2.203*10
77	2.772*10	2.966-01	2.675*11	1.766*03	2.007*00	3.831*00	5.834*10	2.232*10
78	2.808*10	2.960-01	2.701*11	1.785*03	2.011*00	3.840*00	5.906*10	2.262*10
79	2.844*10	2.953-01	2.727*11	1.804*03	2.014*00	3.849*00	5.977*10	2.292*10
80	2.880*10	2.947-01	2.753*11	1.823*03	2.017*00	3.859*00	6.048*10	2.322*10
81	2.916*10	2.940-01	2.779*11	1.841*03	2.021*00	3.867*00	6.120*10	2.351*10
82	2.952*10	2.934-01	2.805*11	1.860*03	2.024*00	3.877*00	6.191*10	2.381*10
83	2.988*10	2.927-01	2.831*11	1.879*03	2.027*00	3.886*00	6.263*10	2.411*10
84	3.024*10	2.921-01	2.857*11	1.898*03	2.031*00	3.894*00	6.334*10	2.441*10
85	3.060*10	2.915-01	2.883*11	1.917*03	2.034*00	3.903*00	6.406*10	2.470*10
86	3.096*10	2.909-01	2.908*11	1.935*03	2.037*00	3.912*00	6.478*10	2.500*10
87	3.132*10	2.903-01	2.934*11	1.954*03	2.040*00	3.921*00	6.549*10	2.530*10
88	3.168*10	2.897-01	2.960*11	1.973*03	2.044*00	3.930*00	6.621*10	2.559*10
89	3.204*10	2.891-01	2.985*11	1.992*03	2.047*00	3.938*00	6.693*10	2.589*10
90	3.240*10	2.885-01	3.011*11	2.011*03	2.050*00	3.947*00	6.764*10	2.619*10

TABLE 4.1 (Continued)

20 PERCENT WATER (F = .20)

K	AIX	IVOL	P	THETA	RHO WATER	RHO TUFF	SIE WATER	SIE TUFF
1	3.600+08	4.769-01	1.274+10	3.505+02	1.257+00	2.517+00	9.463+08	2.134+08
2	7.200+08	4.614-01	1.990+10	3.799+02	1.325+00	2.577+00	1.944+09	4.143+08
3	1.080+09	4.507-01	2.591+10	4.047+02	1.370+00	2.625+00	2.877+09	6.305+08
4	1.440+09	4.422-01	3.141+10	4.272+02	1.405+00	2.668+00	3.771+09	6.571+08
5	1.800+09	4.351-01	3.647+10	4.482+02	1.435+00	2.706+00	4.634+09	1.091+09
6	2.160+09	4.270-01	4.122+10	4.682+02	1.460+00	2.740+00	5.474+09	1.331+09
7	2.520+09	4.235-01	4.574+10	4.875+02	1.482+00	2.772+00	6.294+09	1.577+09
8	2.880+09	4.187-01	5.006+10	5.064+02	1.504+00	2.802+00	7.099+09	1.822+09
9	3.240+09	4.142-01	5.424+10	5.248+02	1.521+00	2.830+00	7.890+09	2.078+09
10	3.600+09	4.102-01	5.828+10	5.429+02	1.537+00	2.856+00	8.659+09	2.333+09
11	3.960+09	4.062-01	6.238+10	5.602+02	1.554+00	2.883+00	9.436+09	2.591+09
12	4.320+09	4.027-01	6.619+10	5.779+02	1.564+00	2.907+00	1.020+10	2.850+09
13	4.680+09	3.994-01	6.992+10	5.954+02	1.583+00	2.930+00	1.095+10	3.112+09
14	5.040+09	3.963-01	7.358+10	6.128+02	1.596+00	2.952+00	1.170+10	3.375+09
15	5.400+09	3.934-01	7.716+10	6.301+02	1.608+00	2.974+00	1.244+10	3.640+09
16	5.760+09	3.906-01	8.069+10	6.473+02	1.620+00	2.995+00	1.318+10	3.906+09
17	6.120+09	3.879-01	8.416+10	6.644+02	1.631+00	3.015+00	1.391+10	4.173+09
18	6.480+09	3.854-01	8.757+10	6.815+02	1.642+00	3.035+00	1.464+10	4.441+09
19	6.840+09	3.830-01	9.094+10	6.985+02	1.653+00	3.054+00	1.536+10	4.710+09
20	7.200+09	3.807-01	9.426+10	7.155+02	1.663+00	3.072+00	1.608+10	4.980+09
21	7.560+09	3.784-01	9.755+10	7.325+02	1.672+00	3.091+00	1.680+10	5.251+09
22	7.920+09	3.763-01	1.008+11	7.494+02	1.682+00	3.108+00	1.751+10	5.523+09
23	8.280+09	3.742-01	1.040+11	7.663+02	1.691+00	3.126+00	1.822+10	5.795+09
24	8.640+09	3.723-01	1.072+11	7.832+02	1.699+00	3.143+00	1.893+10	6.068+09
25	9.000+09	3.703-01	1.103+11	8.001+02	1.708+00	3.159+00	1.963+10	6.392+09
26	9.360+09	3.685-01	1.134+11	8.170+02	1.716+00	3.175+00	2.034+10	6.716+09
27	9.720+09	3.667-01	1.165+11	8.339+02	1.724+00	3.191+00	2.104+10	7.041+09
28	1.008+10	3.649-01	1.196+11	8.508+02	1.732+00	3.207+00	2.174+10	7.366+09
29	1.044+10	3.633-01	1.226+11	8.676+02	1.739+00	3.222+00	2.244+10	7.691+09
30	1.080+10	3.616-01	1.256+11	8.845+02	1.747+00	3.237+00	2.313+10	8.017+09
31	1.116+10	3.600-01	1.286+11	9.014+02	1.754+00	3.252+00	2.383+10	8.342+09
32	1.152+10	3.585-01	1.316+11	9.183+02	1.761+00	3.267+00	2.452+10	8.667+09
33	1.188+10	3.570-01	1.345+11	9.353+02	1.768+00	3.281+00	2.521+10	8.992+09
34	1.224+10	3.555-01	1.374+11	9.522+02	1.774+00	3.295+00	2.590+10	9.317+09
35	1.260+10	3.540-01	1.404+11	9.691+02	1.781+00	3.309+00	2.659+10	9.642+09
36	1.296+10	3.525-01	1.432+11	9.861+02	1.787+00	3.323+00	2.728+10	9.967+09
37	1.332+10	3.513-01	1.461+11	1.003+03	1.794+00	3.336+00	2.797+10	1.021+10
38	1.368+10	3.499-01	1.490+11	1.020+03	1.800+00	3.350+00	2.866+10	1.049+10
39	1.404+10	3.486-01	1.518+11	1.037+03	1.806+00	3.363+00	2.934+10	1.077+10
40	1.440+10	3.474-01	1.546+11	1.054+03	1.812+00	3.376+00	3.003+10	1.104+10
41	1.476+10	3.461-01	1.574+11	1.071+03	1.817+00	3.389+00	3.071+10	1.133+10
42	1.512+10	3.452-01	1.597+11	1.091+03	1.821+00	3.399+00	3.144+10	1.160+10
43	1.548+10	3.437-01	1.630+11	1.105+03	1.822+00	3.414+00	3.208+10	1.188+10
44	1.584+10	3.428-01	1.653+11	1.125+03	1.832+00	3.424+00	3.280+10	
45	1.620+10	3.417-01	1.680+11	1.142+03	1.837+00	3.436+00	3.349+10	

TABLE 4.1 (Continued)

20 Percent Water (Cont.)

46	1.656+10	3.704-01	1.728+11	1.159+03	1.843+00	3.448+00	3.417+10	1.216+10
47	1.692+10	3.394-01	1.735+11	1.176+03	1.848+00	3.440+00	3.485+10	1.244+10
48	1.728+10	3.357-01	1.763+11	1.195+03	1.854+00	3.472+00	3.553+10	1.272+10
49	1.764+10	3.322-01	1.791+11	1.210+03	1.859+00	3.484+00	3.621+10	1.300+10
50	1.800+10	3.362-01	1.818+11	1.227+03	1.864+00	3.496+00	3.689+10	1.329+10
51	1.836+10	3.351-01	1.845+11	1.244+03	1.869+00	3.507+00	3.756+10	1.357+10
52	1.872+10	3.341-01	1.872+11	1.261+03	1.874+00	3.519+00	3.824+10	1.385+10
53	1.908+10	3.331-01	1.899+11	1.278+03	1.879+00	3.530+00	3.892+10	1.413+10
54	1.944+10	3.321-01	1.926+11	1.295+03	1.884+00	3.542+00	3.960+10	1.441+10
55	1.980+10	3.311-01	1.953+11	1.312+03	1.888+00	3.554+00	4.027+10	1.469+10
56	2.016+10	3.302-01	1.980+11	1.330+03	1.893+00	3.563+00	4.095+10	1.497+10
57	2.052+10	3.292-01	2.006+11	1.347+03	1.898+00	3.574+00	4.162+10	1.525+10
58	2.088+10	3.283-01	2.033+11	1.364+03	1.902+00	3.585+00	4.230+10	1.553+10
59	2.124+10	3.274-01	2.059+11	1.381+03	1.906+00	3.596+00	4.298+10	1.581+10
60	2.160+10	3.265-01	2.085+11	1.398+03	1.911+00	3.608+00	4.365+10	1.609+10
61	2.196+10	3.256-01	2.111+11	1.414+03	1.915+00	3.617+00	4.433+10	1.638+10
62	2.232+10	3.248-01	2.138+11	1.433+03	1.919+00	3.627+00	4.500+10	1.666+10
63	2.268+10	3.239-01	2.164+11	1.450+03	1.924+00	3.637+00	4.568+10	1.694+10
64	2.304+10	3.231-01	2.189+11	1.468+03	1.928+00	3.648+00	4.635+10	1.722+10
65	2.340+10	3.222-01	2.215+11	1.485+03	1.932+00	3.658+00	4.703+10	1.750+10
66	2.376+10	3.214-01	2.241+11	1.502+03	1.936+00	3.668+00	4.771+10	1.778+10
67	2.412+10	3.206-01	2.267+11	1.520+03	1.940+00	3.678+00	4.838+10	1.806+10
68	2.448+10	3.198-01	2.292+11	1.537+03	1.944+00	3.688+00	4.905+10	1.834+10
69	2.484+10	3.191-01	2.318+11	1.555+03	1.948+00	3.697+00	4.973+10	1.863+10
70	2.520+10	3.183-01	2.343+11	1.572+03	1.951+00	3.707+00	5.041+10	1.891+10
71	2.556+10	3.175-01	2.369+11	1.590+03	1.955+00	3.717+00	5.108+10	1.919+10
72	2.592+10	3.168-01	2.394+11	1.607+03	1.959+00	3.726+00	5.176+10	1.947+10
73	2.628+10	3.160-01	2.419+11	1.625+03	1.963+00	3.736+00	5.243+10	1.975+10
74	2.664+10	3.153-01	2.443+11	1.642+03	1.966+00	3.745+00	5.311+10	2.003+10
75	2.700+10	3.146-01	2.469+11	1.660+03	1.970+00	3.755+00	5.379+10	2.031+10
76	2.736+10	3.139-01	2.494+11	1.677+03	1.974+00	3.764+00	5.446+10	2.059+10
77	2.772+10	3.132-01	2.519+11	1.695+03	1.977+00	3.772+00	5.514+10	2.087+10
78	2.808+10	3.125-01	2.544+11	1.713+03	1.981+00	3.782+00	5.581+10	2.116+10
79	2.844+10	3.118-01	2.569+11	1.730+03	1.984+00	3.791+00	5.649+10	2.144+10
80	2.880+10	3.111-01	2.594+11	1.748+03	1.987+00	3.800+00	5.717+10	2.172+10
81	2.916+10	3.105-01	2.619+11	1.766+03	1.991+00	3.809+00	5.784+10	2.200+10
82	2.952+10	3.098-01	2.643+11	1.783+03	1.994+00	3.818+00	5.852+10	2.228+10
83	2.988+10	3.092-01	2.668+11	1.801+03	1.997+00	3.827+00	5.919+10	2.256+10
84	3.024+10	3.085-01	2.692+11	1.819+03	2.001+00	3.836+00	5.987+10	2.284+10
85	3.060+10	3.079-01	2.717+11	1.837+03	2.004+00	3.844+00	6.055+10	2.312+10
86	3.096+10	3.073-01	2.741+11	1.855+03	2.007+00	3.853+00	6.122+10	2.340+10
87	3.132+10	3.066-01	2.766+11	1.872+03	2.010+00	3.862+00	6.190+10	2.368+10
88	3.168+10	3.060-01	2.790+11	1.890+03	2.013+00	3.870+00	6.258+10	2.396+10
89	3.204+10	3.054-01	2.814+11	1.908+03	2.017+00	3.879+00	6.325+10	2.424+10
90	3.240+10	3.048-01	2.839+11	1.926+03	2.020+00	3.887+00	6.393+10	2.452+10
91	3.276+10	3.042-01	2.863+11	1.944+03	2.023+00	3.895+00	6.461+10	2.480+10
92	3.312+10	3.036-01	2.887+11	1.962+03	2.026+00	3.904+00	6.529+10	2.508+10
93	3.348+10	3.031-01	2.911+11	1.980+03	2.029+00	3.912+00	6.597+10	2.537+10
94	3.384+10	3.025-01	2.935+11	2.002+03	2.032+00	3.920+00	6.664+10	2.565+10
95	3.420+10	3.020-01	2.959+11	2.022+03	2.035+00	3.928+00	6.732+10	2.593+10
96	3.456+10	3.016-01	2.978+11	2.035+03	2.038+00	3.935+00	6.800+10	2.621+10
97	3.492+10	3.011+01	3.011+11	2.050+03	2.042+00	3.946+00	6.868+10	2.650+10

TABLE 4.1 (Continued)

25 PERCENT WATER (F = .25)

X	AY	TVUL	C	THETA	RHO WATER	RHO TUFF	STIE WATER	STIE TUFF
1	3.600+08	5.001-C1	1.145+10	3.470+C2	1.246+00	2.505+00	8.308+02	2.004+08
2	7.200+08	4.837-C1	1.815+10	3.747+C2	1.303+00	2.563+00	1.753+09	3.758+08
3	1.040+09	4.721-C1	2.373+10	3.987+C2	1.353+00	2.608+00	2.611+09	5.691+08
4	1.440+09	4.637-C1	2.836+10	4.197+C2	1.398+00	2.646+00	3.441+09	7.732+08
5	1.800+09	4.555-C1	3.258+10	4.398+C2	1.441+00	2.684+00	4.245+09	9.848+08
6	2.160+09	4.495-C1	3.625+10	4.589+C2	1.491+00	2.717+00	5.031+09	1.203+09
7	2.520+09	4.433-C1	4.023+10	4.774+C2	1.463+00	2.748+00	5.600+09	1.426+09
8	2.880+09	4.383-C1	4.377+10	4.954+C2	1.483+00	2.776+00	6.557+09	1.654+09
9	3.240+09	4.341-C1	4.670+10	5.131+C2	1.501+00	2.803+00	7.303+09	1.886+09
10	3.600+09	4.297-C1	5.025+10	5.299+C2	1.519+00	2.830+00	8.036+09	2.121+09
11	3.960+09	4.255-C1	5.479+10	5.470+C2	1.534+00	2.854+00	8.763+09	2.352+09
12	4.320+09	4.221-C1	5.915+10	5.643+C2	1.549+00	2.877+00	9.483+09	2.599+09
13	4.680+09	4.187-C1	6.312+10	5.804+C2	1.562+00	2.900+00	1.020+10	2.841+09
14	5.040+09	4.155-C1	6.757+10	5.974+C2	1.574+00	2.921+00	1.090+10	3.093+09
15	5.400+09	4.125-C1	7.197+10	6.140+C2	1.587+00	2.942+00	1.161+10	3.331+09
16	5.760+09	4.098-C1	7.571+10	6.304+C2	1.598+00	2.963+00	1.231+10	3.578+09
17	6.120+09	4.069-C1	7.894+10	6.468+C2	1.609+00	2.982+00	1.300+10	3.827+09
18	6.480+09	4.042-C1	8.213+10	6.632+C2	1.620+00	3.001+00	1.369+10	4.077+09
19	6.840+09	4.017-C1	8.513+10	6.794+C2	1.630+00	3.020+00	1.438+10	4.328+09
20	7.200+09	3.994-C1	8.918+10	6.957+C2	1.640+00	3.038+00	1.506+10	4.580+09
21	7.560+09	3.971-C1	9.312+10	7.113+C2	1.649+00	3.055+00	1.574+10	4.833+09
22	7.920+09	3.948-C1	9.477+10	7.231+C2	1.659+00	3.073+00	1.642+10	5.087+09
23	8.280+09	3.927-C1	9.742+10	7.443+C2	1.667+00	3.089+00	1.709+10	5.342+09
24	8.640+09	3.907-C1	1.009+11	7.608+C2	1.675+00	3.106+00	1.777+10	5.598+09
25	9.000+09	3.887-C1	1.074+11	7.766+C2	1.684+00	3.122+00	1.845+10	5.854+09
26	9.360+09	3.868-C1	1.068+11	7.927+C2	1.692+00	3.138+00	1.911+10	6.112+09
27	9.720+09	3.848-C1	1.093+11	8.086+C2	1.700+00	3.153+00	1.977+10	6.369+09
28	1.008+10	3.831-C1	1.127+11	8.250+C2	1.709+00	3.169+00	2.044+10	6.627+09
29	1.044+10	3.814-C1	1.161+11	8.411+C2	1.715+00	3.184+00	2.110+10	6.886+09
30	1.080+10	3.797-C1	1.180+11	8.572+C2	1.722+00	3.198+00	2.177+10	7.145+09
31	1.116+10	3.781-C1	1.208+11	8.733+C2	1.729+00	3.213+00	2.243+10	7.405+09
32	1.152+10	3.766-C1	1.236+11	8.895+C2	1.736+00	3.227+00	2.309+10	7.665+09
33	1.188+10	3.749-C1	1.264+11	9.056+C2	1.743+00	3.241+00	2.375+10	7.925+09
34	1.224+10	3.733-C1	1.292+11	9.218+C2	1.749+00	3.255+00	2.440+10	8.186+09
35	1.260+10	3.716-C1	1.320+11	9.379+C2	1.756+00	3.268+00	2.506+10	8.447+09
36	1.296+10	3.700-C1	1.347+11	9.541+C2	1.762+00	3.282+00	2.571+10	8.709+09
37	1.332+10	3.685-C1	1.374+11	9.703+C2	1.768+00	3.295+00	2.637+10	8.971+09
38	1.368+10	3.670-C1	1.402+11	9.865+C2	1.774+00	3.308+00	2.702+10	9.233+09
39	1.404+10	3.655-C1	1.429+11	1.023+C2	1.737+00	3.321+00	2.767+10	9.495+09
40	1.440+10	3.640-C1	1.455+11	1.039+C2	1.785+00	3.333+00	2.833+10	9.753+09
41	1.475+10	3.627-C1	1.482+11	1.055+C2	1.792+00	3.346+00	2.898+10	1.002+10
42	1.512+10	3.614-C1	1.509+11	1.071+C2	1.797+00	3.358+00	2.963+10	1.028+10
43	1.548+10	3.601-C1	1.535+11	1.087+C2	1.803+00	3.370+00	3.028+10	1.055+10
44	1.584+10	3.588-C1	1.562+11	1.103+C2	1.805+00	3.380+00	3.093+10	1.081+10

TABLE 4.1 (Continued)

25 Percent Water (Cont.)

45	1.620+10	1.588-C1	1.588+11	1.570+C2	1.614+CC	3.394+CC	3.159+10	1.107+10
46	1.656+10	1.585-C1	1.603+11	1.610+CC	1.817+CC	3.404+CC	3.226+10	1.133+10
47	1.697+10	1.560-C1	1.674+11	1.635+C2	1.822+CC	3.415+CC	3.291+10	1.160+10
48	1.729+10	1.557-C1	1.650+11	1.657+C2	1.837+CC	3.426+CC	3.356+10	1.186+10
49	1.764+10	1.546-C1	1.646+11	1.688+C2	1.837+CC	3.438+CC	3.421+10	1.212+10
50	1.800+10	1.535-C1	1.733+11	1.694+C2	1.842+CC	3.449+CC	3.485+10	1.239+10
51	1.836+10	1.524-C1	1.739+11	1.700+C2	1.842+CC	3.461+CC	3.550+10	1.266+10
52	1.872+10	1.514-C1	1.759+11	1.717+CC	1.841+CC	3.472+CC	3.614+10	1.292+10
53	1.908+10	1.503-C1	1.770+11	1.737+C2	1.852+CC	3.483+CC	3.678+10	1.319+10
54	1.944+10	1.493-C1	1.785+11	1.743+CC	1.852+CC	3.494+CC	3.743+10	1.345+10
55	1.980+10	1.483-C1	1.801+11	1.765+CC	1.861+CC	3.505+CC	3.807+10	1.372+10
56	2.016+10	1.472-C1	1.817+11	1.792+C2	1.852+CC	3.516+CC	3.871+10	1.398+10
57	2.052+10	1.463-C1	1.832+11	1.798+C2	1.877+CC	3.526+CC	3.936+10	1.425+10
58	2.088+10	1.454-C1	1.847+11	1.814+CC	1.875+CC	3.537+CC	4.000+10	1.451+10
59	2.124+10	1.444-C1	1.862+11	1.831+CC	1.875+CC	3.547+CC	4.064+10	1.478+10
60	2.160+10	1.435-C1	1.877+11	1.847+CC	1.858+CC	3.558+CC	4.129+10	1.505+10
61	2.196+10	1.425-C1	1.892+11	1.863+CC	1.888+CC	3.568+CC	4.193+10	1.531+10
62	2.232+10	1.417-C1	1.907+11	1.882+CC	1.892+CC	3.578+CC	4.257+10	1.558+10
63	2.268+10	1.408-C1	1.922+11	1.898+CC	1.895+CC	3.588+CC	4.321+10	1.584+10
64	2.304+10	1.400-C1	1.937+11	1.913+CC	1.900+CC	3.598+CC	4.385+10	1.611+10
65	2.340+10	1.391-C1	1.952+11	1.925+CC	1.900+CC	3.608+CC	4.450+10	1.638+10
66	2.375+10	1.382-C1	1.967+11	1.946+CC	1.913+CC	3.618+CC	4.514+10	1.664+10
67	2.412+10	1.374-C1	1.982+11	1.962+CC	1.913+CC	3.628+CC	4.578+10	1.691+10
68	2.448+10	1.365-C1	1.997+11	1.979+CC	1.915+CC	3.637+CC	4.642+10	1.717+10
69	2.484+10	1.356-C1	2.012+11	1.993+CC	1.927+CC	3.647+CC	4.706+10	1.744+10
70	2.520+10	1.348-C1	2.027+11	1.995+CC	1.924+CC	3.656+CC	4.771+10	1.771+10
71	2.556+10	1.340-C1	2.042+11	1.998+CC	1.920+CC	3.666+CC	4.835+10	1.797+10
72	2.592+10	1.332-C1	2.057+11	1.995+CC	1.932+CC	3.675+CC	4.899+10	1.824+10
73	2.628+10	1.324-C1	2.072+11	1.997+CC	1.932+CC	3.684+CC	4.963+10	1.850+10
74	2.664+10	1.315-C1	2.087+11	1.993+CC	1.933+CC	3.694+CC	5.027+10	1.877+10
75	2.700+10	1.307-C1	2.102+11	1.995+CC	1.943+CC	3.703+CC	5.091+10	1.904+10
76	2.736+10	1.298-C1	2.117+11	1.992+CC	1.945+CC	3.712+CC	5.155+10	1.930+10
77	2.772+10	1.290-C1	2.132+11	1.995+CC	1.950+CC	3.721+CC	5.219+10	1.957+10
78	2.808+10	1.281-C1	2.147+11	1.993+CC	1.957+CC	3.730+CC	5.284+10	1.984+10
79	2.844+10	1.273-C1	2.162+11	1.995+CC	1.957+CC	3.740+CC	5.348+10	2.010+10
80	2.880+10	1.264-C1	2.177+11	1.993+CC	1.953+CC	3.749+CC	5.412+10	2.037+10
81	2.916+10	1.256-C1	2.192+11	1.995+CC	1.963+CC	3.758+CC	5.476+10	2.063+10
82	2.952+10	1.247-C1	2.207+11	1.992+CC	1.963+CC	3.767+CC	5.540+10	2.090+10
83	2.988+10	1.239-C1	2.222+11	1.995+CC	1.970+CC	3.776+CC	5.604+10	2.117+10
84	3.024+10	1.230-C1	2.237+11	1.993+CC	1.970+CC	3.785+CC	5.668+10	2.143+10
85	3.060+10	1.222-C1	2.252+11	1.995+CC	1.977+CC	3.794+CC	5.732+10	2.170+10
86	3.096+10	1.213-C1	2.267+11	1.992+CC	1.977+CC	3.803+CC	5.796+10	2.196+10
87	3.132+10	1.205-C1	2.282+11	1.995+CC	1.980+CC	3.812+CC	5.860+10	2.222+10
88	3.168+10	1.196-C1	2.297+11	1.993+CC	1.983+CC	3.821+CC	5.924+10	2.248+10
89	3.204+10	1.188-C1	2.312+11	1.995+CC	1.983+CC	3.830+CC	5.988+10	2.274+10
90	3.240+10	1.180-C1	2.327+11	1.992+CC	1.988+CC	3.839+CC	6.052+10	2.300+10
91	3.276+10	1.171-C1	2.342+11	1.995+CC	1.995+CC	3.848+CC	6.116+10	2.326+10
92	3.312+10	1.163-C1	2.357+11	1.992+CC	1.995+CC	3.857+CC	6.180+10	2.352+10
93	3.348+10	1.154-C1	2.372+11	1.995+CC	1.995+CC	3.866+CC	6.244+10	2.378+10
94	3.384+10	1.146-C1	2.387+11	1.992+CC	1.995+CC	3.875+CC	6.308+10	2.404+10
95	3.420+10	1.137-C1	2.402+11	1.995+CC	1.995+CC	3.884+CC	6.372+10	2.430+10
96	3.456+10	1.129-C1	2.417+11	1.992+CC	1.995+CC	3.893+CC	6.436+10	2.456+10
97	3.492+10	1.120-C1	2.432+11	1.995+CC	1.995+CC	3.902+CC	6.500+10	2.482+10
98	3.528+10	1.112-C1	2.447+11	1.992+CC	1.995+CC	3.911+CC	6.564+10	2.508+10
99	3.564+10	1.103-C1	2.462+11	1.995+CC	1.995+CC	3.920+CC	6.628+10	2.534+10
100	3.600+10	1.095-C1	2.477+11	1.992+CC	1.995+CC	3.929+CC	6.692+10	2.560+10

TABLE 4.1 (Continued)

25 Percent Water (Cont.)

92	3.312+10	3.707-01	2.777+11	1.351+03	1.931+00	3.949+00	6.183+10	2.356+10
93	3.348+10	3.194-01	2.755+11	1.855+03	1.920+03	3.852+00	6.293+10	2.394+10
94	3.384+10	3.189-01	2.773+11	1.315+03	1.935+03	3.862+00	6.354+10	2.421+10
95	3.420+10	3.187-01	2.773+11	1.822+03	1.955+03	3.865+00	6.416+10	2.442+10
96	3.456+10	3.177-01	2.773+11	1.893+03	1.978+00	3.878+00	6.475+10	2.472+10
97	3.492+10	3.172-01	2.773+11	1.972+03	1.986+03	3.861+00	6.536+10	2.494+10
98	3.528+10	3.155-01	2.773+11	1.355+03	1.958+03	3.893+00	6.598+10	2.522+10
99	3.564+10	3.323-01	2.742+11	1.920+03	2.009+00	3.896+00	6.659+10	2.544+10
100	3.600+10	3.315-01	2.769+11	1.935+03	2.007+00	3.968+00	6.720+10	2.573+10
101	3.636+10	3.315-01	2.778+11	1.955+03	2.015+00	3.911+00	6.781+10	2.595+10
102	3.672+10	3.302-01	2.816+11	1.965+03	2.013+00	3.923+00	6.842+10	2.623+10
103	3.708+10	3.302-01	2.826+11	1.986+03	2.020+00	3.925+00	6.903+10	2.645+10
104	3.744+10	3.291-01	2.858+11	1.986+03	2.018+00	3.937+00	6.964+10	2.674+10
105	3.780+10	3.291-01	2.867+11	1.958+03	2.028+00	3.940+00	7.025+10	2.695+10
106	3.816+10	3.260-01	2.902+11	2.019+03	2.024+00	3.952+00	7.087+10	2.724+10
107	3.852+10	3.260-01	2.911+11	2.030+03	2.063+03			
108	3.888+10	3.270-01	2.944+11	2.051+03	2.083+03			
109	3.924+10	3.270-01	2.954+11	2.083+03	2.095+03			
110	3.960+10	3.259-01	2.987+11	2.095+03	2.116+03			
111	3.996+10	3.259-01	2.997+11	2.116+03	2.128+03			
112	4.032+10	3.249-01	3.030+11	2.128+03				

TABLE 4.1 (Continued)

30 PERCENT WATER (F = .30)

K	AIX	TVUL	P	THETA	RNG GALLR	RNG TUFF	SIE. MATEC	SIE. TUFF
1	3.000+00	5.248-01	1.057+10	3.443+02	1.231+00	2.496+00	7.612+08	1.881+08
2	7.200+05	5.061-01	1.670+10	3.702+02	1.293+00	2.550+00	1.594+09	3.456+08
3	1.850+09	4.441-01	2.141+10	3.926+02	1.335+00	2.593+00	2.388+09	5.112+08
4	1.440+07	4.846-01	2.671+10	4.129+02	1.373+00	2.631+00	3.158+09	7.029+08
5	1.600+06	4.768-01	3.115+10	4.321+02	1.401+00	2.666+00	3.910+09	8.759+08
6	2.160+09	4.701-01	3.535+10	4.504+02	1.425+00	2.697+00	4.645+09	1.095+09
7	2.520+09	4.642-01	3.935+10	4.681+02	1.446+00	2.726+00	5.368+09	1.297+09
8	3.800+09	4.589-01	4.315+10	4.853+02	1.466+00	2.754+00	6.060+09	1.508+09
9	3.200+09	4.541-01	4.690+10	5.022+02	1.483+00	2.780+00	6.763+09	1.721+09
10	3.600+09	4.494-01	5.067+10	5.184+02	1.501+00	2.805+00	7.476+09	1.939+09
11	3.960+09	4.445-01	5.416+10	5.348+02	1.516+00	2.829+00	8.164+09	2.158+09
12	4.320+09	4.416-01	5.758+10	5.510+02	1.530+00	2.851+00	8.845+09	2.380+09
13	4.680+09	4.381-01	6.093+10	5.670+02	1.543+00	2.873+00	9.521+09	2.605+09
14	5.040+09	4.346-01	6.421+10	5.829+02	1.555+00	2.894+00	1.019+10	2.832+09
15	5.400+09	4.316-01	6.743+10	5.986+02	1.567+00	2.914+00	1.086+10	3.060+09
16	5.760+09	4.286-01	7.060+10	6.145+02	1.579+00	2.934+00	1.152+10	3.291+09
17	6.120+09	4.258-01	7.372+10	6.302+02	1.590+00	2.953+00	1.218+10	3.523+09
18	6.480+09	4.231-01	7.680+10	6.458+02	1.600+00	2.971+00	1.284+10	3.756+09
19	6.840+09	4.205-01	7.984+10	6.614+02	1.610+00	2.989+00	1.349+10	3.991+09
20	7.200+09	4.180-01	8.263+10	6.770+02	1.620+00	3.007+00	1.414+10	4.227+09
21	7.560+09	4.157-01	8.580+10	6.925+02	1.629+00	3.024+00	1.479+10	4.464+09
22	7.920+09	4.134-01	8.873+10	7.080+02	1.638+00	3.041+00	1.543+10	4.702+09
23	8.280+09	4.112-01	9.162+10	7.234+02	1.646+00	3.057+00	1.607+10	4.941+09
24	8.640+09	4.091-01	9.445+10	7.389+02	1.655+00	3.073+00	1.671+10	5.181+09
25	9.000+09	4.070-01	9.733+10	7.543+02	1.663+00	3.089+00	1.735+10	5.421+09
26	9.360+09	4.051-01	1.001+11	7.698+02	1.671+00	3.104+00	1.799+10	5.663+09
27	9.720+09	4.031-01	1.029+11	7.852+02	1.679+00	3.119+00	1.862+10	5.905+09
28	1.008+10	4.013-01	1.057+11	8.006+02	1.686+00	3.134+00	1.926+10	6.147+09
29	1.044+10	3.993-01	1.065+11	8.160+02	1.693+00	3.149+00	1.989+10	6.391+09
30	1.080+10	3.977-01	1.112+11	8.314+02	1.700+00	3.163+00	2.052+10	6.635+09
31	1.116+10	3.960-01	1.139+11	8.468+02	1.707+00	3.177+00	2.115+10	6.879+09
32	1.152+10	3.944-01	1.166+11	8.622+02	1.714+00	3.191+00	2.178+10	7.124+09
33	1.188+10	3.928-01	1.192+11	8.776+02	1.721+00	3.205+00	2.241+10	7.370+09
34	1.224+10	3.912-01	1.219+11	8.931+02	1.727+00	3.218+00	2.303+10	7.616+09
35	1.260+10	3.897-01	1.245+11	9.085+02	1.734+00	3.231+00	2.366+10	7.862+09
36	1.296+10	3.882-01	1.271+11	9.239+02	1.740+00	3.244+00	2.428+10	8.109+09
37	1.332+10	3.866-01	1.298+11	9.394+02	1.746+00	3.257+00	2.490+10	8.356+09
38	1.368+10	3.853-01	1.323+11	9.548+02	1.752+00	3.270+00	2.553+10	8.603+09
39	1.404+10	3.840-01	1.349+11	9.703+02	1.758+00	3.282+00	2.615+10	8.851+09
40	1.440+10	3.826-01	1.375+11	9.857+02	1.765+00	3.295+00	2.677+10	9.099+09
41	1.476+10	3.813-01	1.400+11	1.001+03	1.769+00	3.307+00	2.739+10	9.347+09
42	1.512+10	3.800-01	1.426+11	1.017+03	1.774+00	3.319+00	2.801+10	9.596+09
43	1.548+10	3.787-01	1.451+11	1.032+03	1.778+00	3.331+00	2.863+10	9.845+09
44	1.584+10	3.775-01	1.476+11	1.046+03	1.785+00	3.343+00	2.925+10	1.009+10

TABLE 4.1 (Continued)

30 Percent Water (Cont.)

45	1.620+10	3.767-01	1.496+11	1.066+03	1.766+00	3.351+00	2.990+10	4.334+10
46	1.656+10	3.751-01	1.526+11	1.079+03	1.776+00	3.366+00	3.048+10	1.059+10
47	1.642+10	3.742-01	1.546+11	1.097+03	1.796+00	3.375+00	3.113+10	1.084+10
48	1.728+10	3.727-01	1.575+11	1.110+03	1.806+00	3.388+00	3.172+10	1.109+10
49	1.724+10	3.719-01	1.596+11	1.128+03	1.805+00	3.397+00	3.236+10	1.134+10
50	1.650+10	3.709-01	1.619+11	1.133+03	1.813+00	3.408+00	3.298+10	1.159+10
51	1.636+10	3.698-01	1.644+11	1.159+03	1.819+00	3.419+00	3.360+10	1.184+10
52	1.672+10	3.687-01	1.666+11	1.175+03	1.823+00	3.430+00	3.421+10	1.209+10
53	1.918+10	3.676-01	1.693+11	1.190+03	1.828+00	3.441+00	3.483+10	1.234+10
54	1.944+10	3.666-01	1.717+11	1.206+03	1.833+00	3.451+00	3.544+10	1.259+10
55	1.980+10	3.655-01	1.742+11	1.221+03	1.837+00	3.462+00	3.605+10	1.284+10
56	2.016+10	3.645-01	1.766+11	1.237+03	1.842+00	3.472+00	3.667+10	1.309+10
57	2.052+10	3.635-01	1.790+11	1.252+03	1.846+00	3.483+00	3.728+10	1.334+10
58	2.088+10	3.625-01	1.814+11	1.266+03	1.850+00	3.493+00	3.789+10	1.360+10
59	2.124+10	3.615-01	1.838+11	1.280+03	1.855+00	3.503+00	3.850+10	1.385+10
60	2.160+10	3.605-01	1.862+11	1.299+03	1.859+00	3.514+00	3.912+10	1.410+10
61	2.196+10	3.597-01	1.886+11	1.314+03	1.863+00	3.524+00	3.973+10	1.435+10
62	2.232+10	3.587-01	1.910+11	1.330+03	1.868+00	3.534+00	4.034+10	1.460+10
63	2.268+10	3.578-01	1.933+11	1.346+03	1.872+00	3.543+00	4.095+10	1.486+10
64	2.304+10	3.569-01	1.957+11	1.361+03	1.876+00	3.553+00	4.156+10	1.511+10
65	2.340+10	3.561-01	1.981+11	1.377+03	1.880+00	3.563+00	4.217+10	1.536+10
66	2.376+10	3.552-01	2.004+11	1.393+03	1.884+00	3.572+00	4.279+10	1.561+10
67	2.412+10	3.543-01	2.027+11	1.409+03	1.888+00	3.582+00	4.340+10	1.587+10
68	2.448+10	3.535-01	2.051+11	1.424+03	1.892+00	3.591+00	4.401+10	1.612+10
69	2.484+10	3.527-01	2.074+11	1.440+03	1.896+00	3.601+00	4.462+10	1.637+10
70	2.520+10	3.519-01	2.097+11	1.456+03	1.899+00	3.610+00	4.523+10	1.662+10
71	2.556+10	3.510-01	2.120+11	1.472+03	1.903+00	3.619+00	4.584+10	1.688+10
72	2.592+10	3.503-01	2.143+11	1.487+03	1.907+00	3.628+00	4.645+10	1.713+10
73	2.628+10	3.495-01	2.166+11	1.503+03	1.910+00	3.636+00	4.706+10	1.738+10
74	2.664+10	3.487-01	2.189+11	1.519+03	1.914+00	3.647+00	4.767+10	1.763+10
75	2.700+10	3.479-01	2.212+11	1.535+03	1.918+00	3.656+00	4.828+10	1.789+10
76	2.736+10	3.472-01	2.235+11	1.551+03	1.921+00	3.664+00	4.889+10	1.814+10
77	2.772+10	3.464-01	2.258+11	1.567+03	1.925+00	3.673+00	4.950+10	1.839+10
78	2.808+10	3.457-01	2.280+11	1.582+03	1.928+00	3.682+00	5.011+10	1.864+10
79	2.844+10	3.451-01	2.303+11	1.598+03	1.932+00	3.691+00	5.073+10	1.890+10
80	2.880+10	3.444-01	2.325+11	1.614+03	1.935+00	3.699+00	5.134+10	1.915+10
81	2.916+10	3.436-01	2.346+11	1.630+03	1.938+00	3.708+00	5.195+10	1.940+10
82	2.952+10	3.429-01	2.370+11	1.646+03	1.942+00	3.716+00	5.256+10	1.966+10
83	2.988+10	3.422-01	2.393+11	1.662+03	1.945+00	3.725+00	5.317+10	1.991+10
84	3.024+10	3.415-01	2.415+11	1.678+03	1.948+00	3.733+00	5.378+10	2.016+10
85	3.060+10	3.408-01	2.438+11	1.694+03	1.952+00	3.742+00	5.439+10	2.041+10
86	3.096+10	3.401-01	2.460+11	1.710+03	1.955+00	3.750+00	5.500+10	2.067+10
87	3.132+10	3.395-01	2.482+11	1.726+03	1.958+00	3.758+00	5.561+10	2.092+10
88	3.168+10	3.388-01	2.504+11	1.742+03	1.961+00	3.766+00	5.622+10	2.117+10
89	3.204+10	3.382-01	2.526+11	1.758+03	1.964+00	3.775+00	5.683+10	2.142+10
90	3.240+10	3.375-01	2.549+11	1.774+03	1.967+00	3.783+00	5.744+10	2.168+10
91	3.276+10	3.369-01	2.571+11	1.790+03	1.970+00	3.791+00	5.805+10	2.193+10

TABLE 4.1 (Continued)

30 Percent Water (Cont.)

92	3.312+10	2.593+11	1.806+03	1.973+00	3.799+00	5.866+10	2.216+10
93	3.348+10	2.615+11	1.822+03	1.976+00	3.807+00	5.927+10	2.241+10
94	3.364+10	2.637+11	1.838+03	1.979+00	3.815+00	5.968+10	2.269+10
95	3.370+10	2.655+11	1.855+03	1.984+00	3.822+00	6.049+10	2.294+10
96	3.356+10	2.680+11	1.871+03	1.985+00	3.830+00	6.111+10	2.319+10
97	3.392+10	2.702+11	1.867+03	1.988+00	3.838+00	6.172+10	2.345+10
98	3.528+10	2.711+11	1.907+03	1.986+00	3.841+00	6.233+10	2.366+10
99	3.564+10	2.694+11	1.999+03	2.020+00	3.906+00	6.631+10	2.583+10
100	3.600+10	2.921+11	2.021+03	2.019+00	3.908+00	6.697+10	2.586+10
101	3.636+10	2.873+11	2.035+03	2.022+00	3.919+00	6.760+10	2.593+10
102	3.672+10	2.957+11	2.050+03	2.029+00	3.929+00	6.824+10	2.602+10
103	3.708+10	2.972+11	2.072+03	2.026+00	3.932+00	6.890+10	2.645+10
104	3.744+10	2.953+11	2.087+03	2.031+00	3.942+00	6.954+10	2.673+10

V. 1-D COMPOSITE CONFIGURATIONS*

5.1 INTRODUCTION

In developing the homogenized equations of state in the preceding sections the explicit treatment of material interfaces was avoided. In order to assess the effect of local material discontinuities, detailed calculation of stress wave propagation effects in composite materials is required. In keeping with the philosophy adopted at the outset of the project, the models for the component materials of the composite configuration were initially selected to be very simple and then modified to introduce additional physical effects. Even if its component materials are linear fluids a composite medium will disperse a wave by internal reflections at material interfaces. For a fluid modeled by a non-linear dependence on the specific volume, $p(V)$, this "geometric dispersion" will be counteracted by a sharpening of the wave front provided the bulk modulus increases with increasing pressure. This is also the situation when realistic thermodynamic models, $p(V,E)$, are employed. For non-linear volumetric and thermodynamic models for the component materials, the dispersion effects will therefore be complicated by energy dissipation resulting from irreversible shock heating.

These three fluid models of the component materials are considered, in this section, for laminated configurations in which the stress pulse is propagated normal to the laminates. The component materials represent water, compacted dry tuff and completely saturated wet tuff. As the dispersion relations for these fluid models are better defined and as more complete material models are developed it will be fruitful to add to the models treated in the composite calculations.

* Author: T. D. Riney

In selecting the composite configurations for the 1-D computer calculations it is desirable to initially establish a well-defined pulse in a homogeneous material. The laminated composite structure shown in Fig. 5.1 is designed with a left end block of homogenized wet tuff for this purpose. The midsection consists of N bilaminates of alternating layers of compacted dry tuff and water. A right end block of homogenized wet tuff is added so that the pulse transmitted through the structure can also be inspected under well-defined conditions. The equation of state for wet tuff is constructed by imposing pressure equilibrium, or pressure-thermal equilibrium, between the water and tuff components mixed in the same water mass fraction

$$F = \frac{M_1}{M_1 + M_2} = \frac{h_{01} \rho_{01}}{h_{01} \rho_{01} + h_{02} \rho_{02}} \quad (5.1)$$

The replacement of the laminated mid-section by wet tuff provides an associated homogeneous medium and pulse propagation though this material serves as a standard for the comparison of transmitted pulses.

The 1-D Lagrangian continuum mechanics computer program (SKIPPER) that was used for these calculations is in no way restricted to purely fluid models. Each material laminate is subdivided into a number of small zones, each containing a constant-mass element. Difference equations expressing conservation of mass, momentum and energy are solved in conjunction with prescribed constitutive relations appropriate to each zone material.⁽⁵⁵⁾ These normally include (1) a thermodynamic equation of state describing the isotropic response of the material, (2) a von Neumann artificial viscosity to insure computational stability, (3) a stress-strain relationship describing the deviatoric behavior

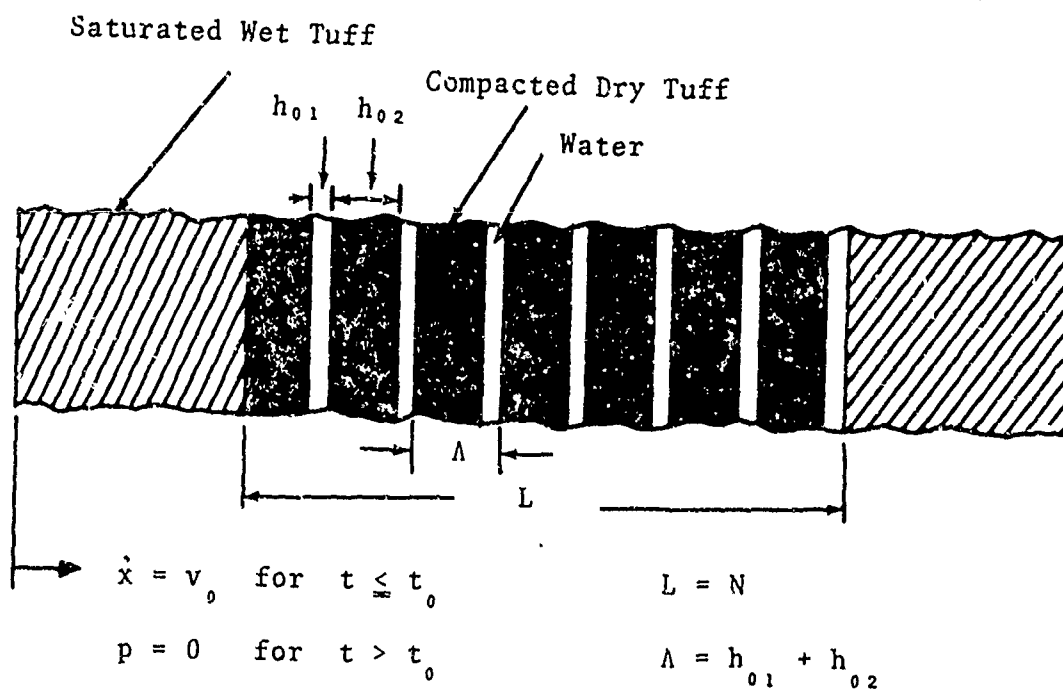


Fig. 5.1--Schematic of bilaminated composite structure.

of the material, (4) a flow rule to determine if a zone is deforming elastically or plastically. The SKIPPER code was implemented by restructuring and modifying a version of the RIP code, developed at S³ under the DASA-sponsored PREDIX study,⁽⁵⁶⁾ from which all subroutines dealing with radiation had been removed.

In the numerical experiments it is desirable to follow a pulse through a large number, N , of bilaminates. SKIPPER is structured to permit the finite difference grid to shift with the pulse as it propagates through the laminated mid-section so that calculations are only made in active regions of the composite structure. At any point in the calculation an homogenized end block may be introduced on the right-hand side of the grid and the pulse propagated into it after traversing the midsection. The calculation may also be restarted from a point in time prior to the introduction of this end block, additional bilaminates inserted for the pulse to propagate through, and then an homogenized right-hand end block introduced into the grid. By this procedure it is possible to conserve computer time both by restricting the calculations to the active part of the laminated structure, and by avoiding the necessity for repeating the early stages of calculations in which only N is varied.

5.2 LINEAR FLUID MODEL

It is of interest to first consider the case in which the material components are represented as simple linear fluids

$$p = A \frac{V - V_0}{V_0} \quad (A, V_0 \text{ constants}) \quad (5.2)$$

Such an idealized medium does not describe a real material but it has the convenient property of propagating finite amplitude waves without undergoing a change of shape. To see this, consider a permanent wave moving at constant velocity c_0 into an undisturbed medium, Fig. 5.2. Let * denote an arbitrary point on the wave profile where the particle velocity, pressure, and density are u , p , ρ respectively. Then conservation of mass and momentum yield

$$\rho(c_0 - u) = \rho_0 c_0 \quad (= \dot{m}, \text{ mass swept past point * in unit time})$$

$$p = \dot{m}u$$

Combining, we get

$$\rho(c_0 - p/\dot{m}) = \dot{m}$$

or

$$p = \rho_0 c_0^2 (1 - \rho_0/\rho) \quad (5.3)$$

which reduces to Eq. (5.2) upon setting $A = \rho_0 c_0^2$. Since (5.3) is obtained for each point *, regardless of the amplitude and shape of the wave, it follows that a steady finite amplitude wave (in an isentropic process) can only exist for the highly idealized linear equation of state.

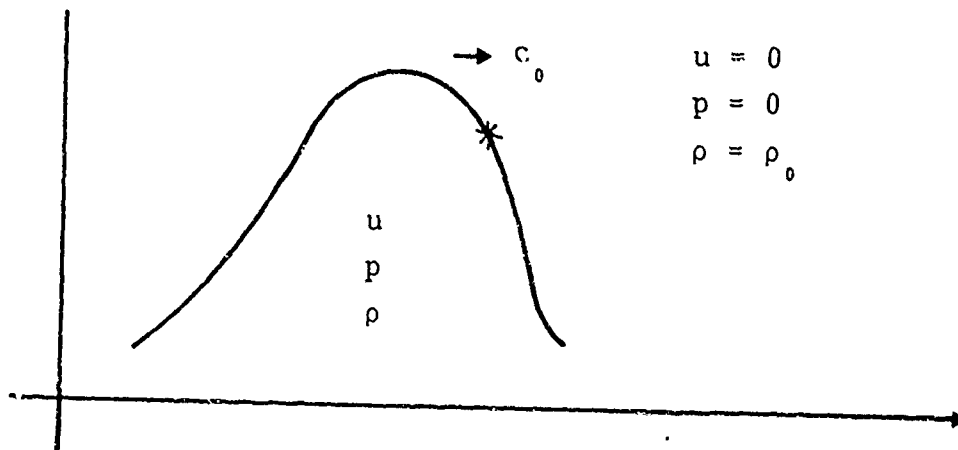


Fig. 5.2--Permanent wave in a linear medium.

5.2.1 Effect of Artificial Viscosity

Lagrangian finite difference codes, including SKIPPER, use an artificial viscosity, or q-term,

$$q = \begin{cases} q_0 \rho \left(\frac{\dot{V}}{V} \Delta X \right)^2 + q_L \rho c \left| \frac{\dot{V}}{V} \Delta X \right|, & \text{for } \frac{\dot{V}}{V} < 0 \\ 0, & \text{for } \frac{\dot{V}}{V} \geq 0 \end{cases} \quad (5.4)$$

which is normally added to the hydrodynamic pressure in the governing equations to permit stable numerical calculations in the presence of shocks. The quadratic term is required for the treatment of non-linear material models in which the wave velocity increases with increased pressure; the quadratic coefficient of q_0 is selected to offset the associated tendency to steepen the wave front and to smear the shock front over three or four finite difference zones. The linear term damps out spurious oscillations in essentially uniform flow regions and the coefficient q_L is selected on the basis of numerical experiments. For non-linear materials the values

$$q_0 = 1.6 \quad q_L = 0.25 \quad (5.5)$$

have been found to give satisfactory results for a wide range of pressures and materials. (55)

For a linear medium there is no tendency for the wave front to steepen to thereby balance the smearing effect of the artificial viscosity. It is therefore required to investigate whether the calculational procedure used in SKIPPER can indeed isolate physically real geometric dispersion effects from the inherent numerical dispersion due to the artificial viscosity, zoning, etc. The initial 1-D calculations were directed toward this question.

To isolate the effect of the q-term, the computer code was applied to an elastic homogeneous medium characterized by Eq. (5.2) with the following choices for the bulk modulus and initial bulk modulus:

$$A = 9.06 \times 10^{10} \text{ ergs/cc} \quad V_0 = 0.50 \text{ cc/g} \quad (5.6)$$

The medium was 0.7 cm wide and was zoned into 220 zones, all of width $\Delta X = 3.18 \times 10^{-3}$ cm. The pulse of amplitude p_0 and duration t_0 was introduced at $X = 0$ by the velocity boundary condition defined by:

$$v_0 = 10^5 \text{ cm/sec} \quad t_0 = 0.5 \times 10^{-6} \text{ sec} \quad (5.7)$$

producing a pressure of amplitude

$$p_0 = \rho_0 v_0 c_0 = v_0 \sqrt{A/V_0} = 42.4 \text{ kbar} \quad (5.8)$$

The calculation describing the propagation of this initially square pulse through the homogeneous medium was repeated for the following choice of coefficients occurring in Eq. (5.4):

Run No.:	401	402	404	408	410	411	412
$(q_L/.25)$:	1	0	.3	1	0	.1	.05
$(q_0/1.6)$:	1	0	.3	0	1	.1	.03

The first calculation, Run 401, used the values of q_L and q_0 commonly employed for non-linear media, Eq. (5.5). The time variation of the pressure pulse, $p(t)$, propagated to distances of 0.03 cm (zone 10) and 0.56 cm (zone 175) in the linear medium are shown in Fig. 5.3. The spreading of the pulse is severe. The progressive damping of the high frequency components, corresponding to a continuous rounding of the initially square pulse, is vividly demonstrated by the Fourier transform,

$$P(\omega) = \int_{-\infty}^{+\infty} p(t) e^{-i\omega t} dt$$

PULSE IN ZONE 10

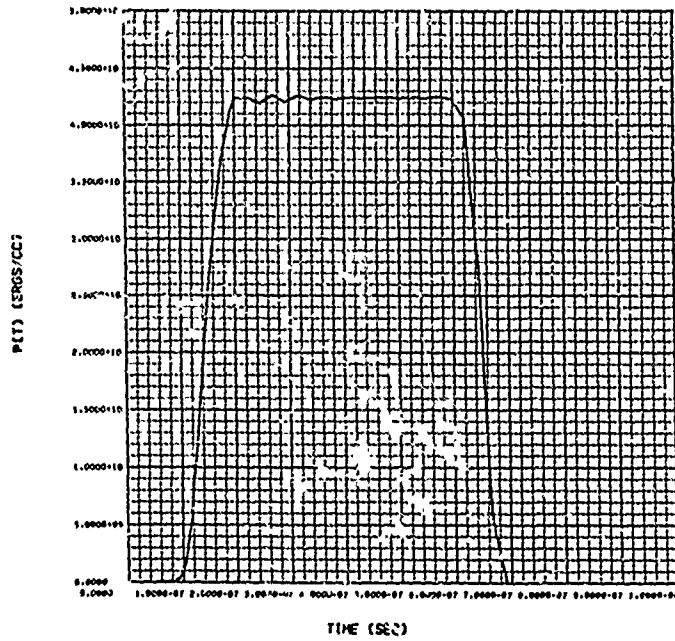


Fig. 5.3(a)--Zone 10

PULSE IN ZONE 175

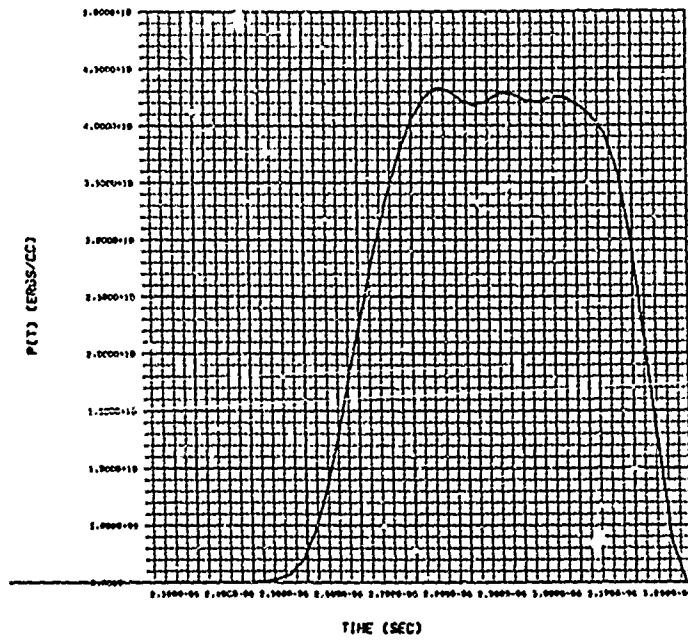


Fig. 5.3(b)--Zone 175

Fig. 5.3--Effect of artificial viscosity ($q_0 = 1.6$, $q_L = 0.25$) on the pulse transmitted through a linear medium to the two indicated positions.

of these two transmitted pulses, Fig. 5.4. This attenuation of the high frequency components is due to the numerics entirely. The second calculation, Run 402 with no artificial viscosity, resulted in numerical oscillations.

None of the choices of q_0 and q_L attempted was satisfactory. One must compromise between the oscillations in the pulse that are acceptable (small q -coefficients) and the spreading of the pulse as it propagates (large q -coefficients). On this basis the choice for Run 412 ($q_0 = 0.48$ and $q_L = 0.0757$) is considered preferable to the others for a linear medium.

5.2.2 Laminated Composite

Even though the q -method cannot accurately treat linear fluid models, SKIPPER was used for one calculation for the laminated structure, Fig. 5.1, in which the materials were modeled in the form of Eq. (5.2).

For the materials in the laminated mid-section, the pressures are given by

$$p_1 = A_1 \frac{V_{01} - V_1}{V_{01}}, \quad p_2 = A_2 \frac{V_{02} - V_2}{V_{02}}. \quad (5.9)$$

The homogenized model for the end blocks is obtained by assuming that these materials are mixed in the mass ratio F , Eq. (5.1). The assumption that the two components of the mixture are in pressure equilibrium then determines the constants V_0 and A required in the linear model of the end blocks (see Section 4.2):

TRANSFORM OF PULSE IN ZONE 10

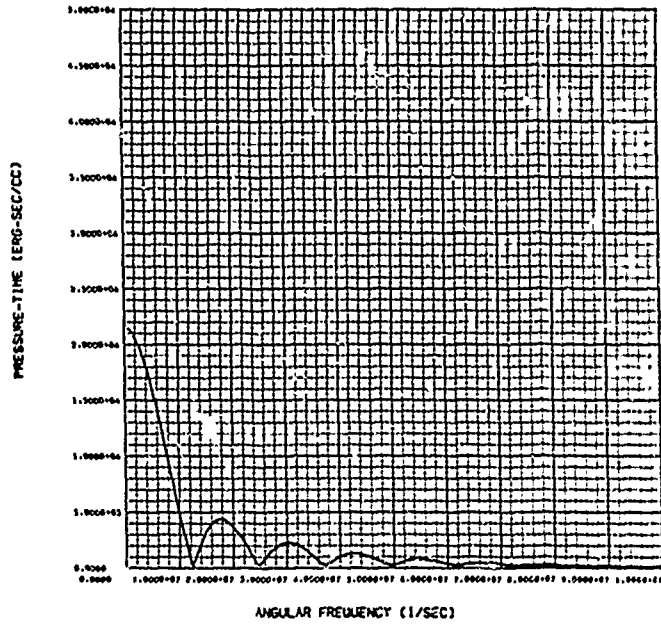


Fig. 5.4(a)--Zone 10

TRANSFORM OF PULSE IN ZONE 175

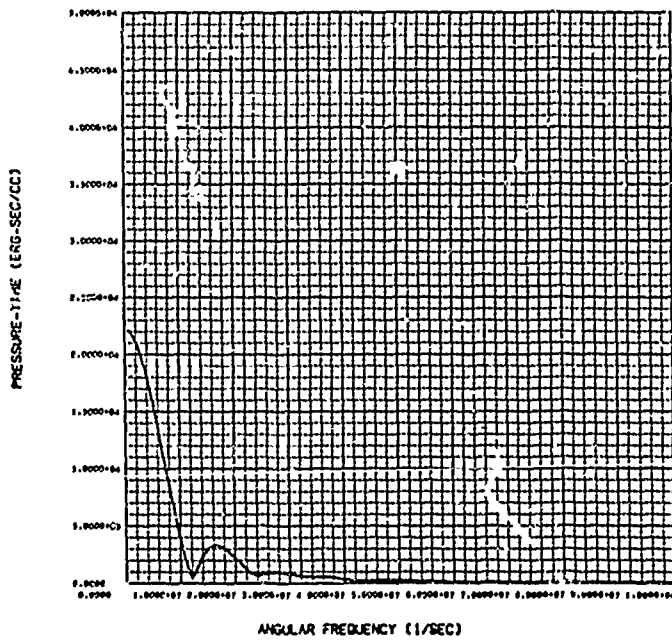


Fig. 5.4(b)--Zone 175

Fig. 5.4--Attenuation of high frequency components of a pulse propagating in a linear medium as a consequence of artificial viscosity ($q_0 = 1.6$, $q_L = 0.25$).

$$V_0 = FV_{01} + (1-F)V_{02} \quad (5.10)$$

$$A = \frac{V_0}{\frac{FV_{01}}{A_1} + \frac{(1-F)V_{02}}{A_2}} \quad (5.11)$$

The bulk moduli of laminate materials 1 and 2 were, respectively, selected to match the Raleigh line of the Hugoniot curves of water and compacted tuff at 50 kbar. These values are listed in Table 5.1 together with the associated parameters for the homogenized end blocks that were computed, (5.10) and (5.11),

TABLE 5.1
PARAMETERS USED IN THE CALCULATION FOR A COMPOSITE
CONFIGURATION OF LINEAR FLUID MODELS

Material	A (ergs/cc)	ρ_0 (g/cc)
Water	1.524×10^{11}	1.0
Compacted Dry Tuff	2.548×10^{11}	2.4
Saturated Wet Tuff (F = .15)	2.079×10^{11}	1.9835

The initial widths of the layers of water and compacted tuff in each bilaminate were

$$h_{01} = 0.0297 \text{ cm} \quad h_{02} = 0.0703 \text{ cm} \quad (5.12)$$

corresponding to a bilaminate width and water mass ratio of

$$\Lambda = 0.1 \text{ cm} \quad F = 0.15 \quad (5.13)$$

The end blocks were chosen to be 0.25 cm wide and the mid-section consisted of ten bilaminates, $N = 10$.

The input loading was defined by the imposed velocity

$$v_0 = 7.786 \times 10^4 \text{ cm/sec} \quad t_0 = 0.5 \times 10^{-6} \text{ sec} \quad (5.14)$$

producing a pressure pulse of amplitude and velocity

$$p_0 = v_0 \sqrt{A \rho_0} = 50 \text{ kbar} \quad c_0 = \sqrt{AV_0} = 0.324 \times 10^6 \text{ cm/sec} \quad (5.15)$$

in the left end block. The initial pulse length is equivalent to $c_0 t_0 / \Lambda = 1.62$ bilaminates. Acoustical matching of the computational zones was realized by using 5 zones per water laminate, 14 zones per compacted tuff laminate, and 51 zones in each saturated wet tuff end block for a total of 290 zones.

In Fig. 5.5 the pulse propagated to two positions in the left and right homogenized end blocks of wet tuff are shown. Although the details of the calculation in the linearized models are known to be smeared by the numerics, the gross effect of the propagation through the ten bilaminate midsection is apparent. Since the rise time of the transmitted pulse far exceeds that attributable to the numerics it must be due to geometric dispersion. The pulse is also lengthened and the peak pressure is actually increased above the initial value.

The increase in the amplitude of the pulse transmitted through the laminated structure is a consequence of the particular combination of impedance mismatch of the laminates, laminate widths and pulse length. The complex form of the pressure profile, inside the laminated midsection is illustrated at three instants in time by plots in Fig. 5.6. In Fig. 5.6(a) the pulse is amplified upon propagating from the left end block into the first tuff layer. The trough apparent in Fig. 5.6(b) occurs at the first water layer.

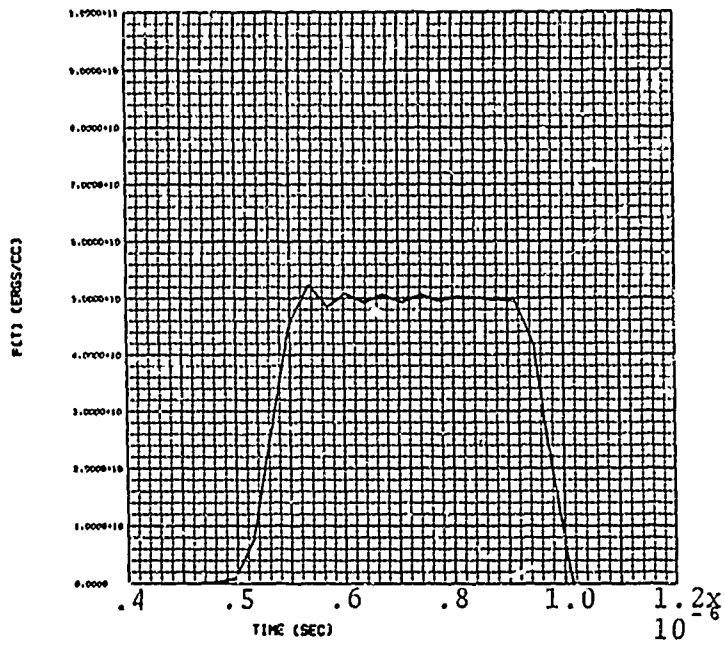


Fig. 5.5(a)

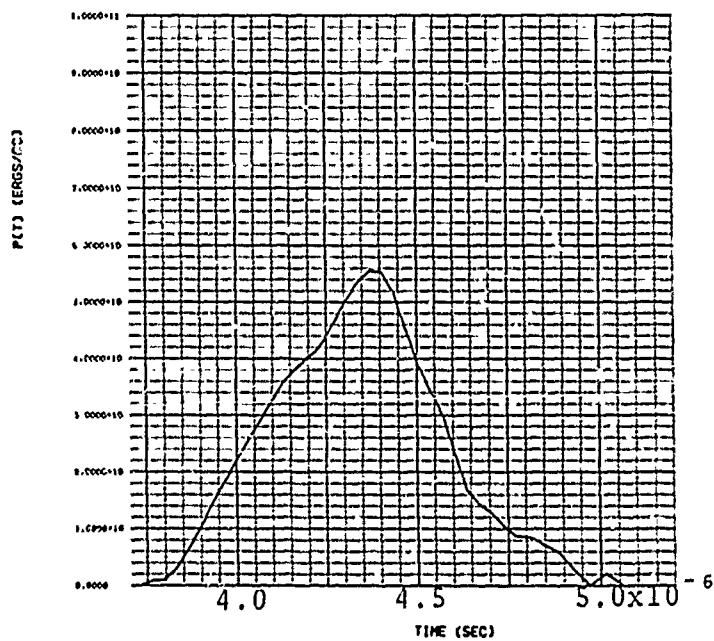


Fig. 5.5(b)

Fig. 5.5--Pressure vs time plots at zones in the homogenized end blocks located (a) in front and (b) behind the laminated structure of linear fluids.

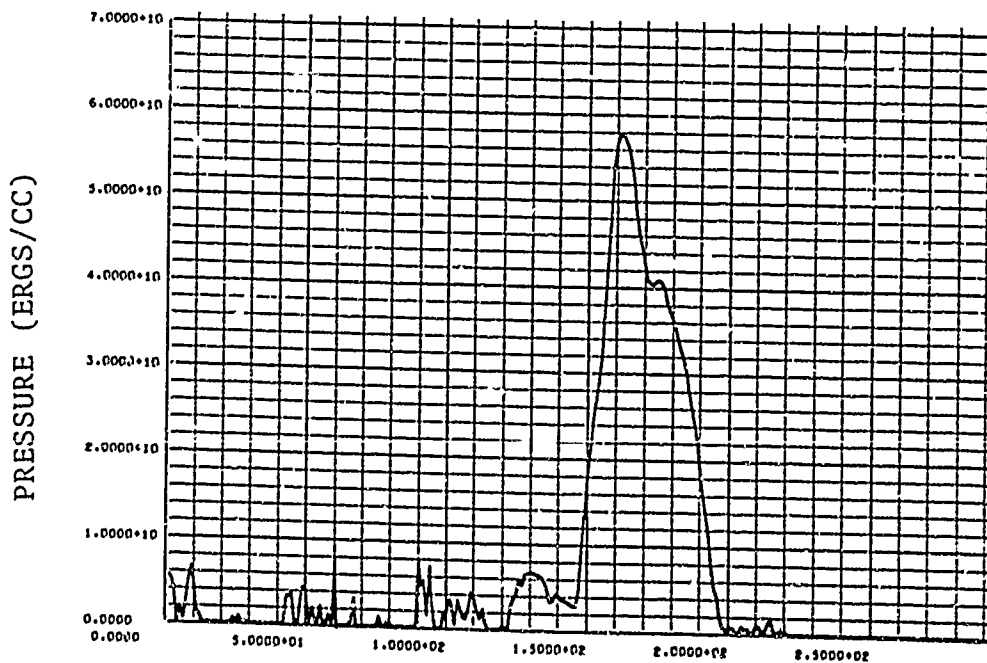
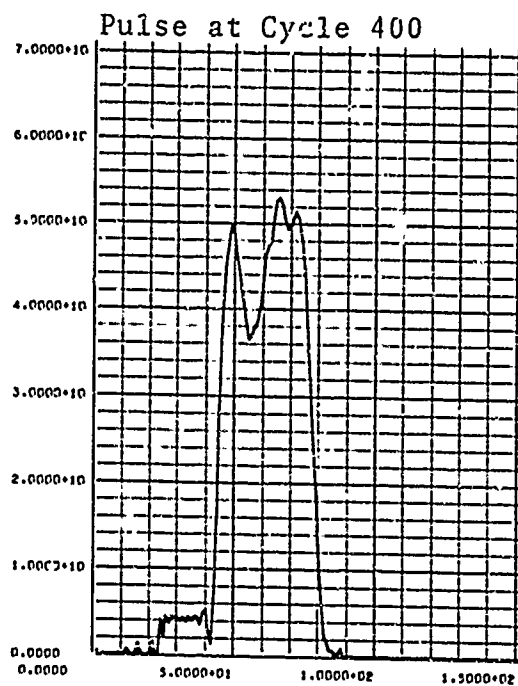
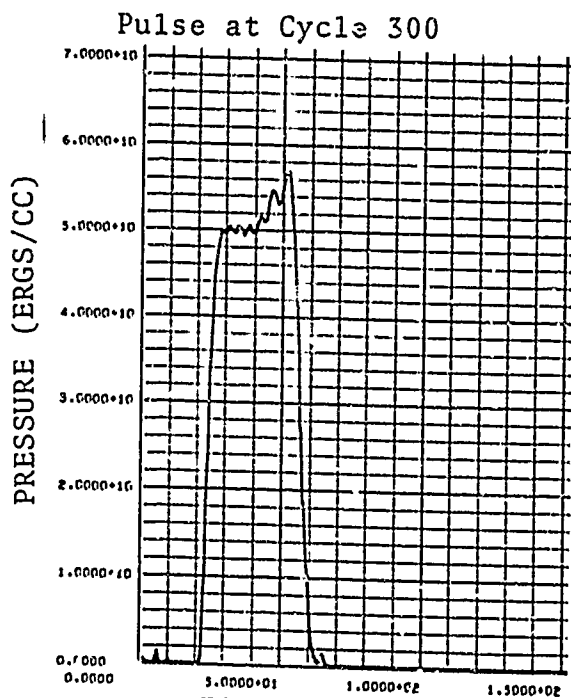


Fig. 5.6--Pressure profiles at three instants in time for the linear laminated structure considered. The numbers on the horizontal axes denote the grid zone number.

In Fig. 5.6(c) the profile is shown just prior to entering the right end block.

The calculated time of arrival of the pulse at each zone of the configuration is depicted in Fig. 5.7. The wave velocity for the homogenized wet tuff, Eq. (5.16) may be used to predict the time of arrival of the pulse at the rear of the first end block, the rear of the laminated portion of the structure, and the rear of the second end block may be predicted from this value. These values (0.77, 3.86 and 4.63 μ sec respectively) are denoted by points 1, 2 and 3 in Fig. 5.7. The agreement with the calculated value at point 2 shows that the substructure of the laminate has negligible effect on the average wave speed in this linear problem, although it was seen to significantly affect the transmitted pulse shape.

If one simply divides the length of the laminated structure by the total times for a signal to cross each layer the corresponding estimate for the mean propagation velocity is given by $\bar{c}_0 = 0.341 \times 10^6$ cm/sec. This estimate would predict that the signal would arrive at the rear end block at 3.71 sec which does not agree with the calculated arrival time at point 2 in Fig. 5.7.

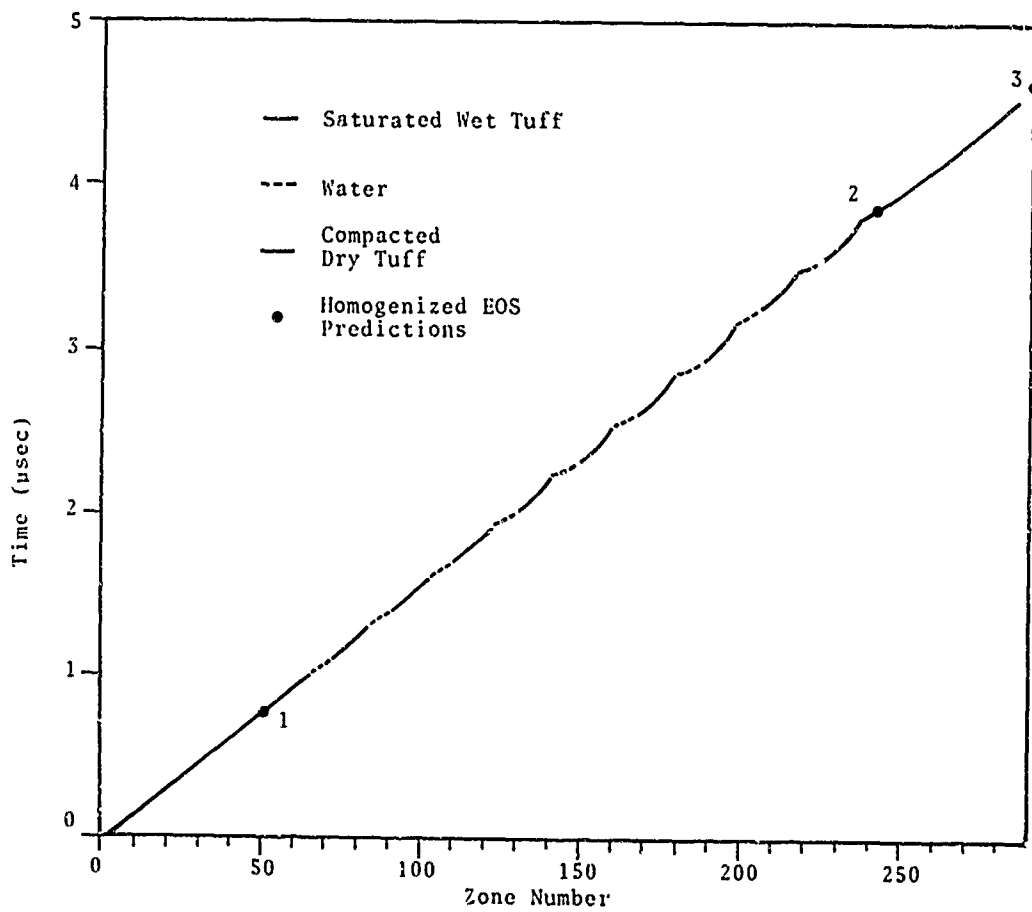


Fig. 5.7--Position of the front of the pulse vs time for the laminated structure with components described by a linear model.

5.3 VOLUMETRIC FLUID MODELS

5.3.1 Preliminary Considerations

The SKIPPER code was used to study wave propagation in the laminated structure, Fig. 5.1, when each component is represented by a non-linear volumetric fluid model of the form

$$p = A\mu + B\mu^2 + F\mu^3; \quad \mu = V_0/V-1 \quad (5.16)$$

For the water and compacted dry tuff laminates the parameters are based on fits to Hugoniot data for pressures below 200 kbar (Eqs. 2.11 and 3.3); the condition of pressure equilibrium was imposed on those fits to construct an associated homogenized equation of state for the saturated wet tuff end blocks with water mass ratio of $F = .15$ (Eq. 4.23). The parameters for the components of the laminated structure of volumetric fluids are listed in Table 5.2.

TABLE 5.2

PARAMETERS USED IN THE CALCULATIONS FOR COMPOSITE CONFIGURATIONS OF VOLUMETRIC FLUID MODELS

Material	A(ergs/cc)	B(ergs/cc)	F(ergs/cc)	ρ_0 (g/cc)
Water	2.19534×10^{10}	5.2138×10^{10}	2.3181×10^{11}	1.0
Compacted Dry Tuff	2.4576×10^{11}	2.98697×10^{11}	6.14886×10^{10}	2.4
Saturated Wet Tuff ($F = .15$)	5.96758×10^{10}	6.31245×10^{11}	-2.60228×10^{11}	1.9835

The dimensions of each bilaminate ($h_{01} = 0.0297$ cm, $h_{02} = 0.0703$ cm) and the mass function of the water ($F = 0.15$) were the same as for the calculation for the structure with linear models, Eq. (5.12) and (5.13). The amplitude of the applied velocity loading was unchanged but the duration of

loading was varied,

$$v_0 = 7.786 \times 10^4 \text{ cm/sec} \quad t_0 \text{ varied} \quad (5.17)$$

This velocity loading introduces a shock of velocity and magnitude

$$D_{wt} = 0.367 \times 10^6 \text{ cm/sec} \quad p_{wt} = 57.1 \text{ kbar} \quad (5.18)$$

in the volumetric fluid model for the left end block of wet tuff.

Preliminary calculations were made to test the numerics of SKIPPER for the non-linear volumetric models. The usual choice for the coefficients in the q-term, Eq. (5.5), was found to maintain the desired three-zone spread for the shock front propagating in the homogeneous wet tuff. Two calculations were made for the laminated structure with $N = 10$ and $t_0 = 0.5 \times 10^{-6}$ sec to test the effect of resolution. In one, the zoning was the same as it was in the earlier calculation for the linear fluids: 5 zones in each water laminate, 14 in each compacted dry tuff laminate, and 50 in each saturated wet tuff end block. In the other calculation, the number of zones was doubled but the results were essentially identical. In subsequent calculations $5 + 14 = 19$ zones have been used in each bilaminate if $t_0 \geq 0.5 \times 10^{-6}$ sec, and 38 zones in each bilaminate for $t_0 < 0.5 \times 10^{-6}$ sec.

5.3.2 Pulse Propagation Normal to Laminates

In the SKIPPER studies of laminated structures with a large number of bilaminates ($N = 30$) the value of t_0 was varied while keeping the other parameters fixed. The purpose is to study the effect of the ratio of the length of the input pulse length to the width of the bilaminate of the

structural midsection,

$$\xi \equiv \frac{D_w t_0}{\Lambda} \quad (5.19)$$

Calculations were completed to $N = 30$ for three values of finite pulse duration, $t = 0.25, 0.5$ and 1.0×10^{-6} sec. These correspond, respectively, to input pulse lengths of 0.94, 1.84 and 3.67 bilaminate widths.

A calculation was also made in which the midsection was replaced by the same homogenized wet tuff as the end blocks ($F = 0.15$). Although the input pulse was $t_0 = 0.5$, the results can be used as a standard of comparison for each of the three laminated calculations for the laminated midsection by invoking hydrodynamic scaling.

In Fig. 5.8, a series of computer plots are shown depicting the pressure profile of the pulse transmitted to four mass depths into the laminated structure for the case where $t_0 = 0.5 \times 10^{-6}$ sec,

$$\xi = 1.84 \quad (5.20)$$

The pulse is shown as its front reaches depths corresponding to 10, 15, 25, and 35 bilaminates. At these instants, the pulse shape is quite irregular, but a general form is discernible from one instant to the other. The front of the pulse is rounded near its peak by the dispersion effect of the laminates, and the pulse is divided into two principal parts. The corresponding pressure profiles for the homogeneous wet tuff medium is superimposed for the first three of these plots. The substructure of the laminated composite results in an amplification of the peak pressure of the transmitted shock. The velocity of propagation is also increased.

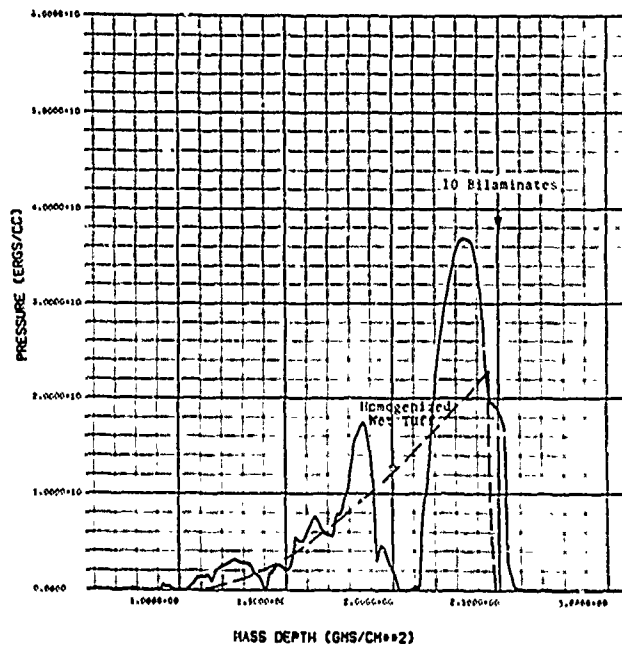


Fig. 5.8(a) -- $t = 3.62 \mu\text{sec}$

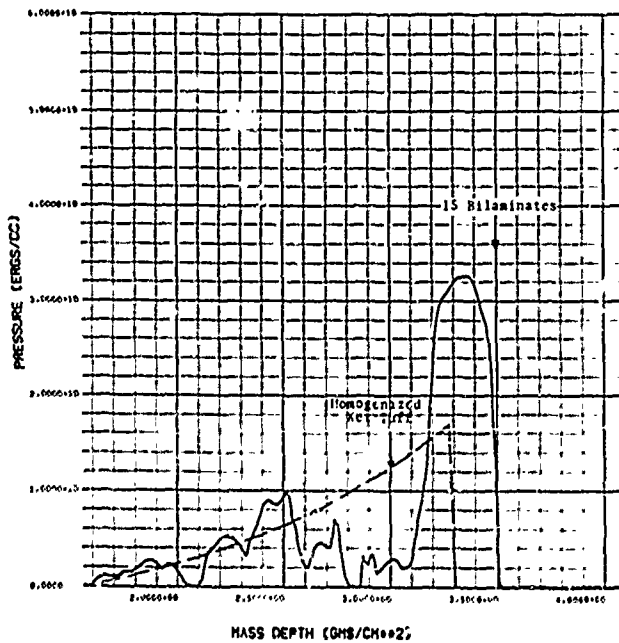


Fig. 5.8(b) -- $t = 5.09 \mu\text{sec}$

Fig. 5.8--Pressure profiles in a water/tuff laminated structure shown at instants when the input pulse, of duration $\tau_0 = 0.5 \mu\text{sec}$, has propagated to depths of
 (a) 10 bilaminates, (b) 15 bilaminates.

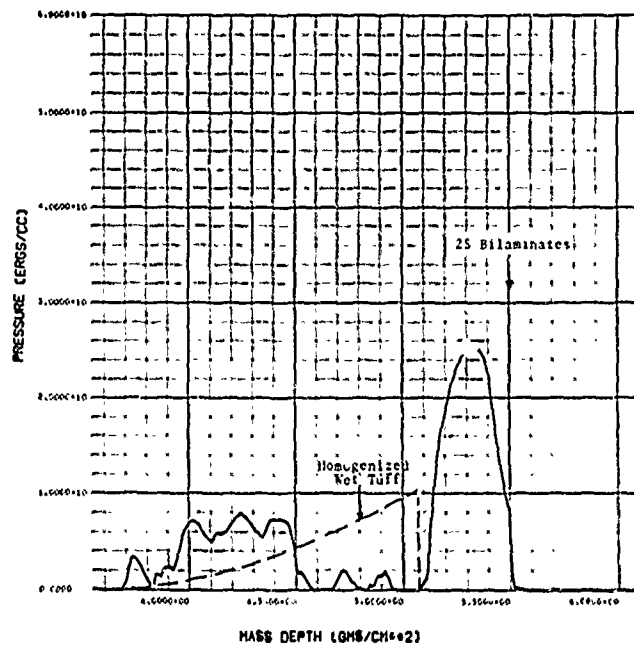


Fig. 5.8(c) -- $t = 8.52 \mu\text{sec}$

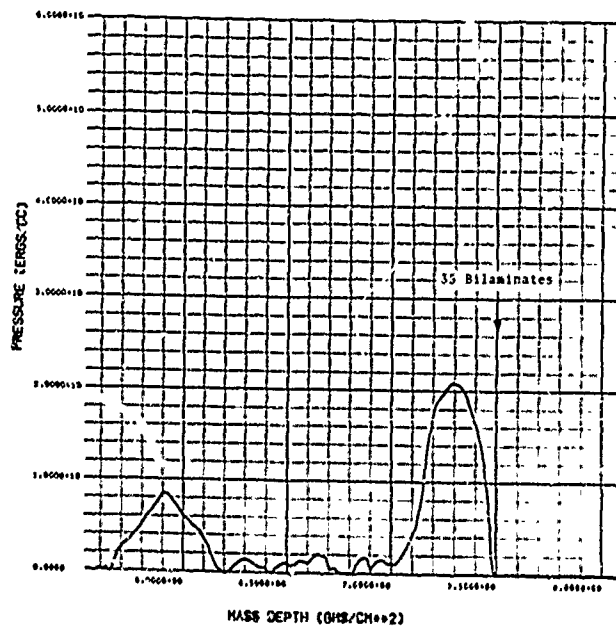


Fig. 5.8(d) -- $t = 12.0 \mu\text{sec}$

Fig. 5.8--Pressure profiles in a water/tuff laminated structure shown at instants when the input pulse, of duration $t_0 = 0.5 \mu\text{sec}$, has propagated to depths of (c) 25 bilaminates, (d) 35 bilaminates.

An alternate method of examining the pulse propagated through the laminated structure is to allow the pulse to be transmitted into an homogenized wet tuff end block on the right side. In Fig. 5.9 computer plots are shown depicting the pressure pulse transmitted to a fixed distance into an homogenized wet tuff end block after being propagated through a laminated midsection of 10, 15, 20 and 30 bilaminates, respectively. Here again, the general shape of the transmitted pulse, $p(t)$, is seen to be preserved and the amplitude and velocity of the transmitted pulse is significantly greater than if it were propagated entirely through an homogenized wet tuff medium of the same total width. This is clearly demonstrated in Figs. 5.9(a) and 5.9(c) by superimposing the corresponding $p(t)$ for the homogenized wet tuff medium onto the computer plots for the laminated structure.

In Fig. 5.10 the pressure pulse of initial duration $t_0 = 1.0 \times 10^{-6}$ sec,

$$\xi = 3.67 \quad (5.21)$$

is shown after being transmitted through the laminated midsection into an homogenized wet tuff end block on the right side of the structure. The transmitted pulse, after 10 and 30 bilaminates, is compared with the corresponding (scaled) pulse transmitted through an homogenized medium. The amplification of the pulse in the composite structure is again observed.

In Fig. 5.11 the pressure pulse of initial duration $t_0 = 0.25 \times 10^{-6}$ sec,

$$\xi = 0.94 \quad (5.22)$$

is shown after being transmitted through the midsections consisting of 15 and 30 bilaminates to a point in a right end block.

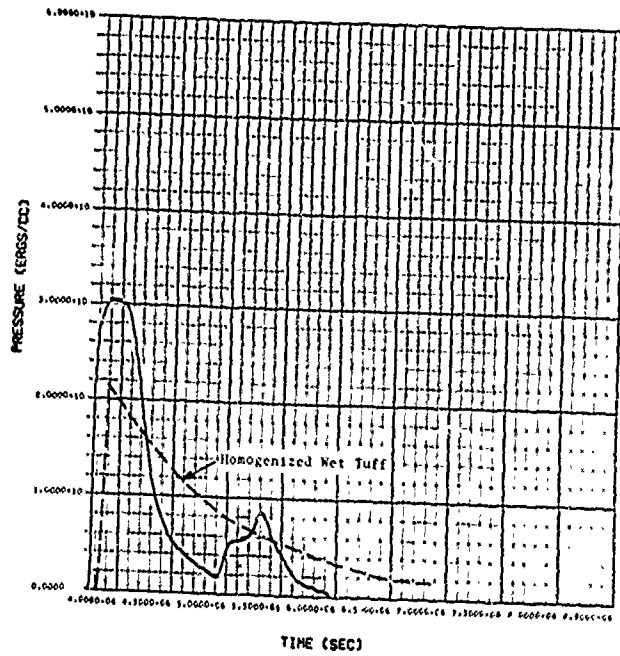


Fig. 5.9(a)--10 bilaminates

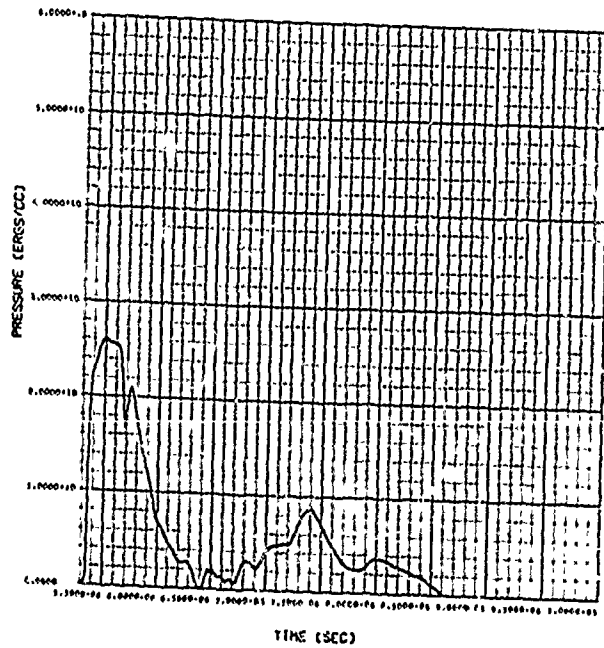


Fig. 5.9(b)--15 bilaminates

Fig. 5.9--Pressure pulse transmitted into an homogenized wet tuff end block after propagation through a laminated water/tuff midsection of indicated number of bilaminates. The input pulse is of duration $t_0 = 0.5 \mu\text{sec}$.

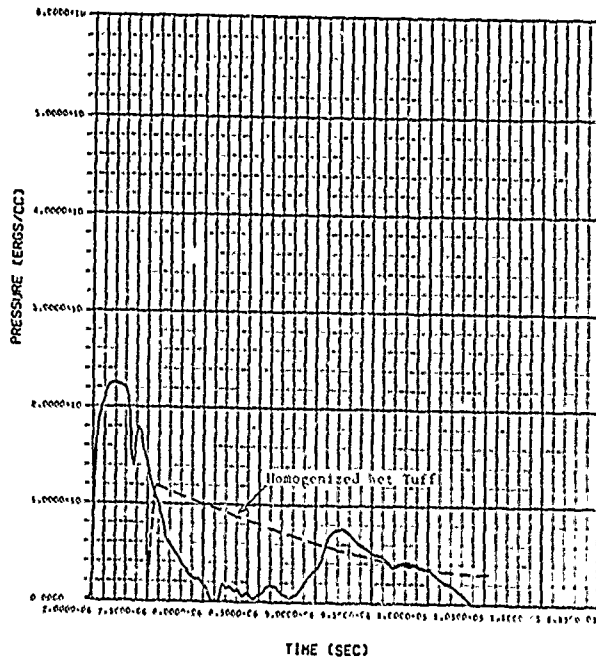


Fig. 5.9(c)--20 bilaminates

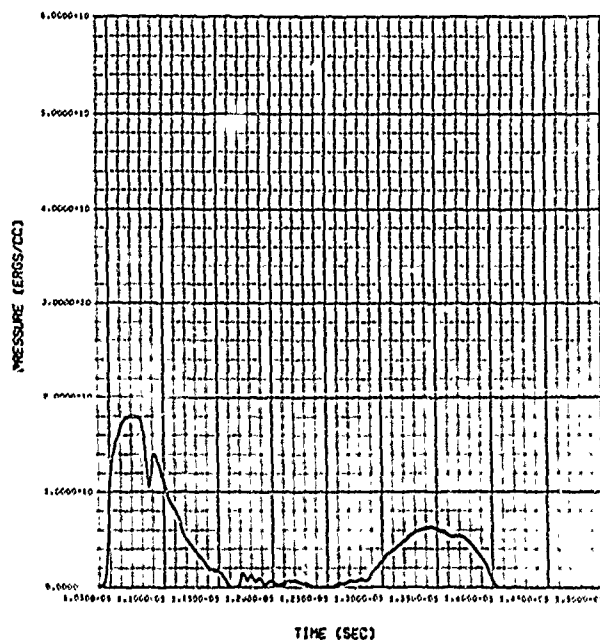


Fig. 5.9(d)--30 bilaminates

Fig. 5.9--Pressure pulse transmitted into an homogenized wet tuff end block after propagation through a laminated water/tuff midsection of indicated number of bilaminates. The input pulse is of duration $t_0 = 0.5 \mu\text{sec}$.

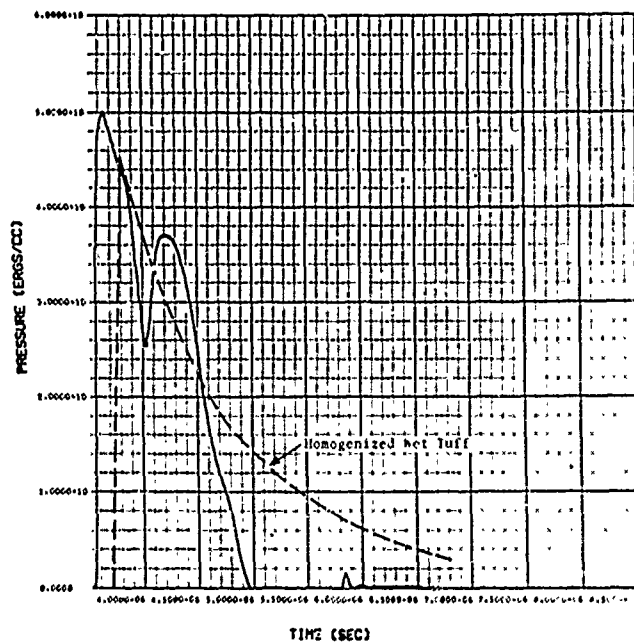


Fig. 5.10(a)--10 bilaminates

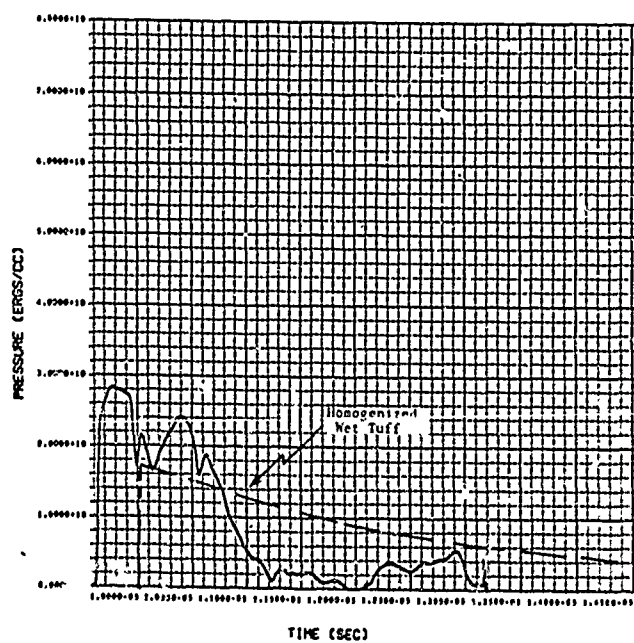


Fig. 5.10(b)--30 bilaminates

Fig. 5.10--Pressure pulse transmitted into an homogenized wet tuff end block after propagation through a water/tuff laminated structure of indicated number of bilaminates. The input pulse is of duration $t_0 = 1.0 \mu\text{sec}$.

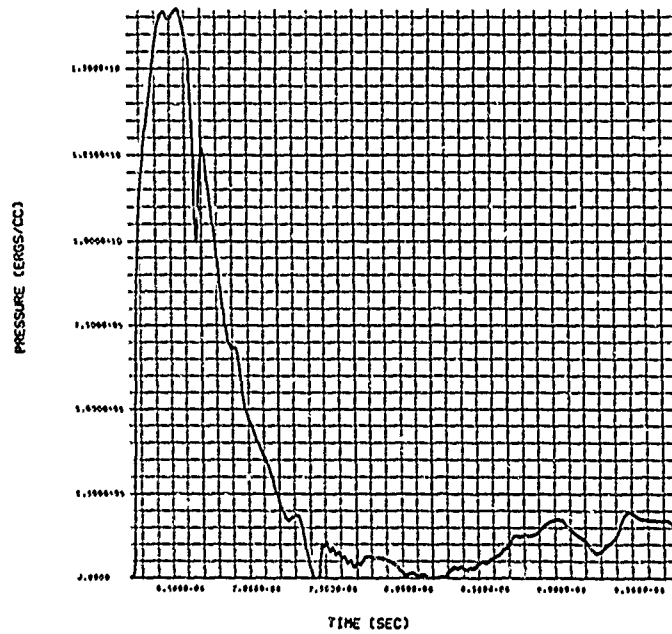


Fig. 5.11(a)--15 bilaminates

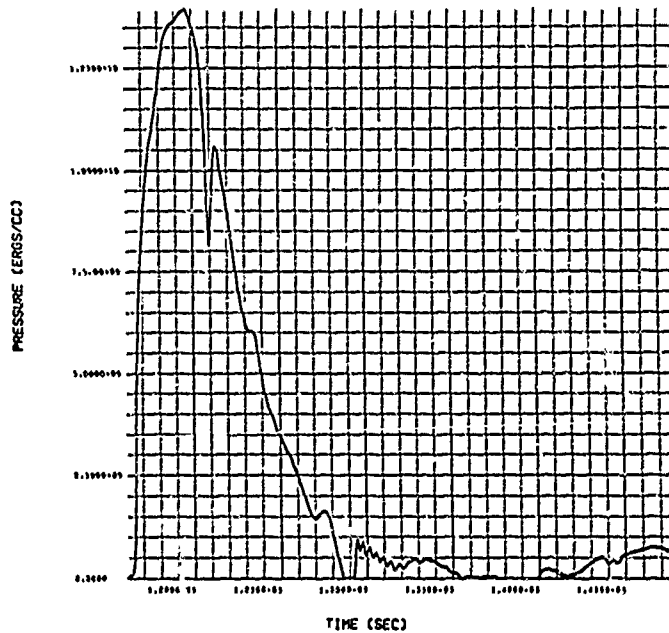


Fig. 5.11(b)--30 bilaminates

Fig. 5.11--Pressure pulse transmitted into an homogenized wet tuff end block after propagation through the indicated number of water/tuff bilaminates. The input pulse is of duration $t_0 = 0.25 \mu\text{sec}$.

A summary of these calculations is given in Fig. 5.12 which compares the peak pulses transmitted to the right hand end block with the peak pressures calculated for the homogenized wet tuff medium. It was observed earlier that the amplitude of the pulse transmitted through the laminated composite was greater than for the homogenized medium with the corresponding load duration, $t_0 = 0.5 \times 10^{-6}$ sec. It is seen from Fig. 5.12 that the composite medium transmits a higher pressure amplitude even for the shorter duration of load, $t_0 = 0.25 \times 10^{-6}$ sec.

By invoking hydrodynamic scaling it is possible to compare these results on the basis of the same load duration, $t_0 = 0.5 \times 10^{-6}$ sec, but for varying values of the sub-structure of the composite medium. The result of this transformation of the calculations is shown in Fig. 5.13. The pressure attenuation for all three values of the ratio ξ are observed to lie on essentially the same curve. The attenuation of the pulse in a laminated composite of non-linear fluids is relatively insensitive to the dimensions of the substructure in the range studied. On the other hand, the attenuation for the composite medium is far less severe than for the homogenized medium, at least for the substructure dimensions studied.

5.3.3 Step Pulse Normal to Laminates

In seeking an explanation for the greater amplitude of the pulse propagated through the composite media, Fig. 5.13, it is desirable to treat the laminated structure when subjected to a step pulse, $t_0 = \infty$,

$$\xi = \infty \quad (5.23)$$

The assumption that pressure equilibrium would be attained at some distance behind the shock front in the laminated

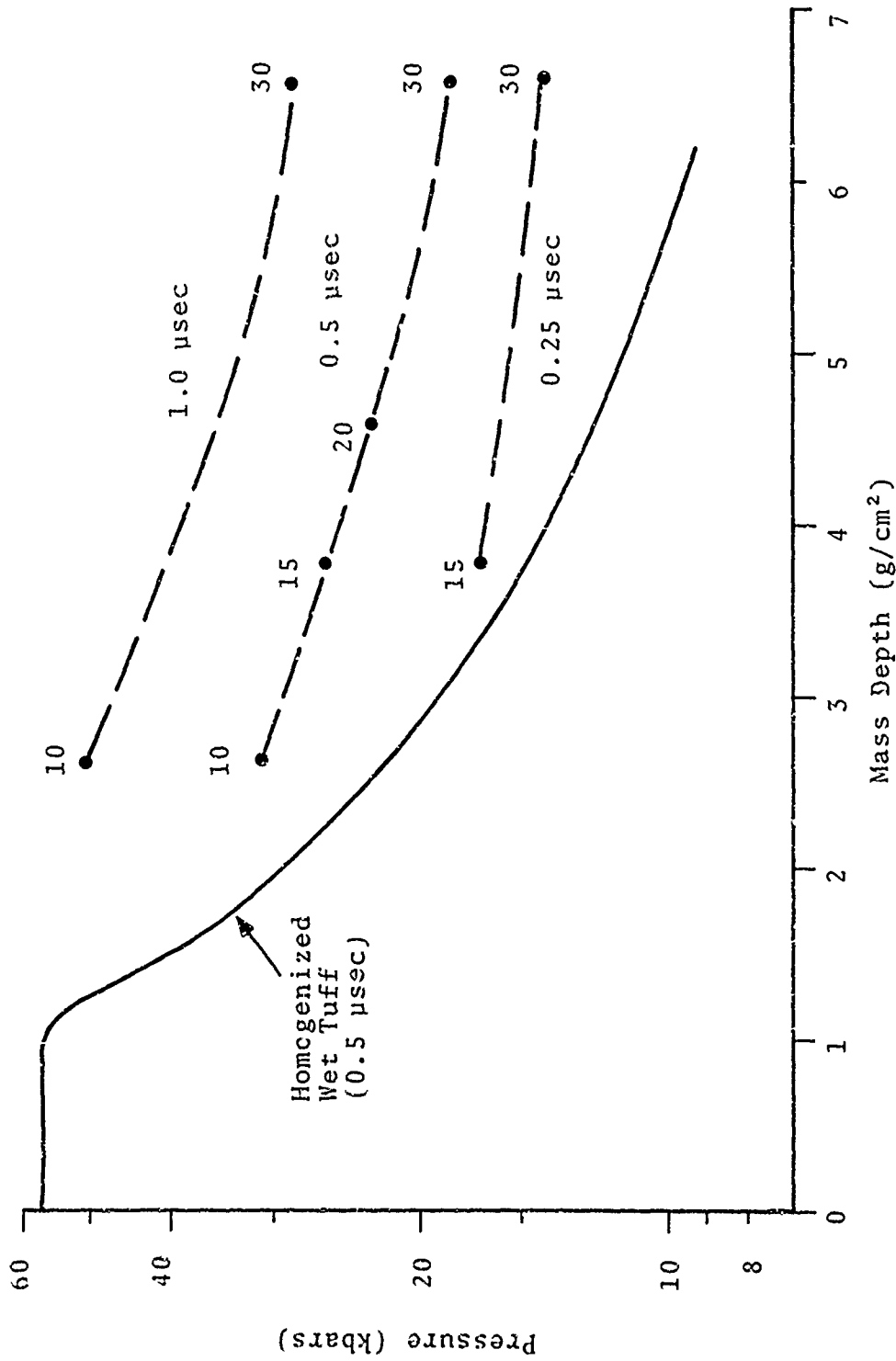


Fig. 5.12--Peak pressures transmitted through the water/tuff laminated structure of non-linear volumetric fluids to a fixed depth in a right-hand homogenized end block. The duration of the input pulse is indicated and the numbers refer to the number of bilaminates in the structure's midsection, N.

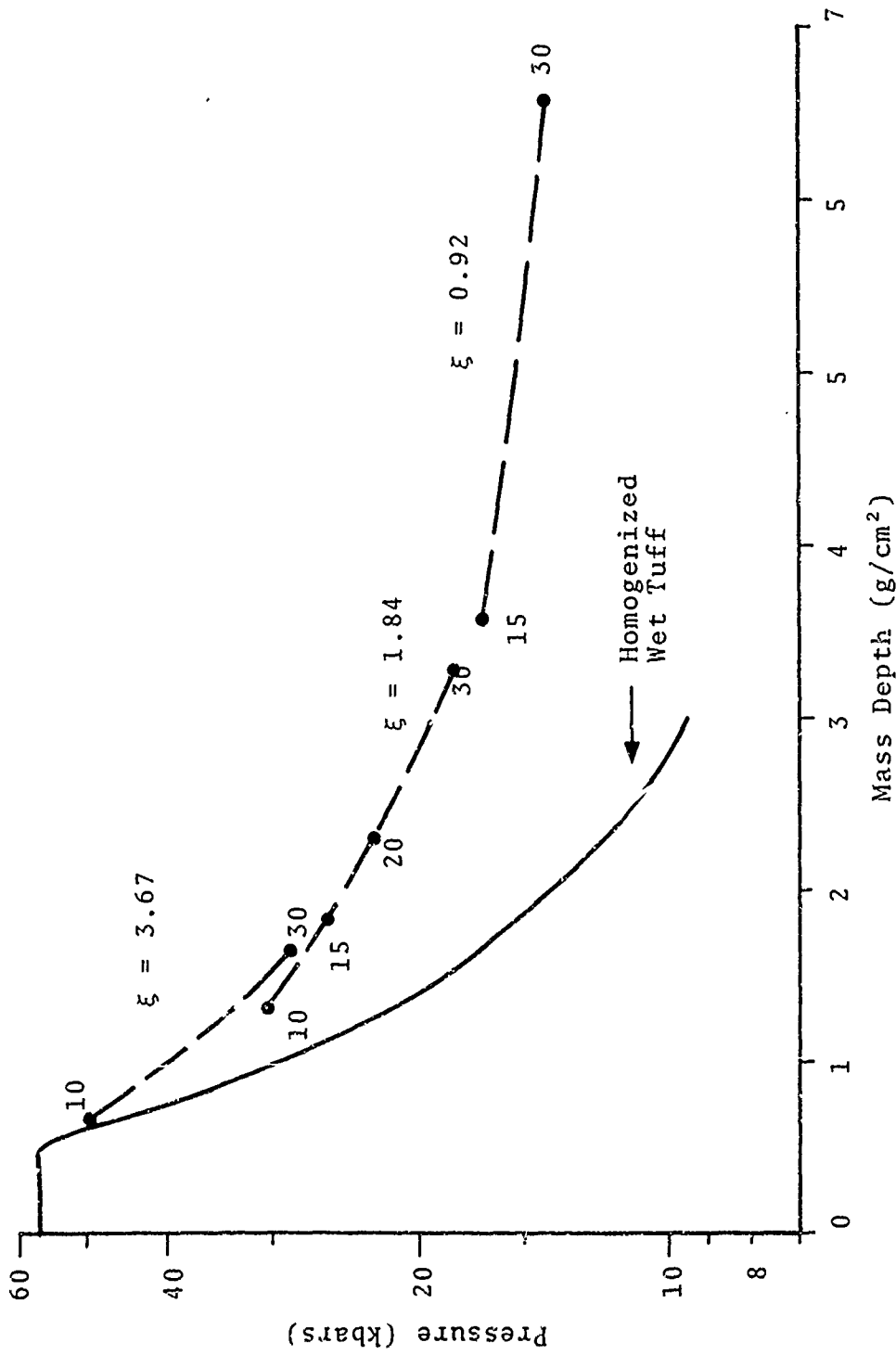


Fig. 5.13--Peak pressures transmitted through a structure with a laminated water/tuff midsection compared with an homogenized wet tuff medium. The components are non-linear volumetric fluids and the results are all scaled to the same input pulse, $t_0 = 0.5 \mu\text{sec}$; the points refer to the number of bilaminates, N.

midsection is equivalent to assuming that the final state is that determined by imposing the Hugoniot conditions on the equivalent homogenized wet tuff medium. From (5.17) and (5.18) the expected equilibrium values for the particle velocity, shock velocity, and pressure behind the front are as follows:

$$\begin{aligned}u_e &= 0.07786 \text{ cm}/\mu\text{sec} & D_e &= 0.367 \text{ cm}/\mu\text{sec} \\p_e &= 57.1 \text{ kbar} & & (5.24)\end{aligned}$$

In Fig. 5.14 pressure vs mass depth plots are shown at two instants for a SKIPPER calculation in which the pulse has been propagated through the homogenized left end block and twenty-four water/tuff bilaminates in the midsection of the structure. In Fig. 5.15 the time variation of the pressure is shown at the center of the first and sixteenth water laminates. For the first water laminate in the midsection, Fig. 5.15(a), the mean pressure of the oscillations is indicated by the dashed line, $\bar{p} = 55.5$ kbar. This deviation from eventual equilibrium pressure is due to the non-linearity of the $p(V)$ relations for the laminate materials.

The spatial periodicity of the oscillations about the value \bar{p} in Fig. 5.15 corresponds to a width of two bilaminates. The time variation of the oscillations is 0.47 μsec as illustrated in Fig. 5.15. A discussion of the approximate periodicity of the oscillation will be given in Section 6.3. The amplitude of the oscillations continuously decreases with time as a consequence of the conversion of the kinetic energy into heat energy.

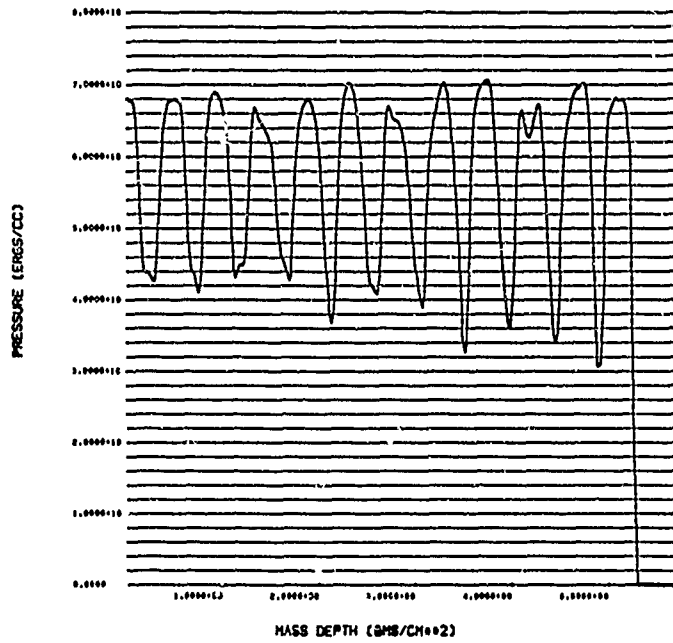


Fig. 5.14(a) -- $t = 7.10 \text{ usec}$

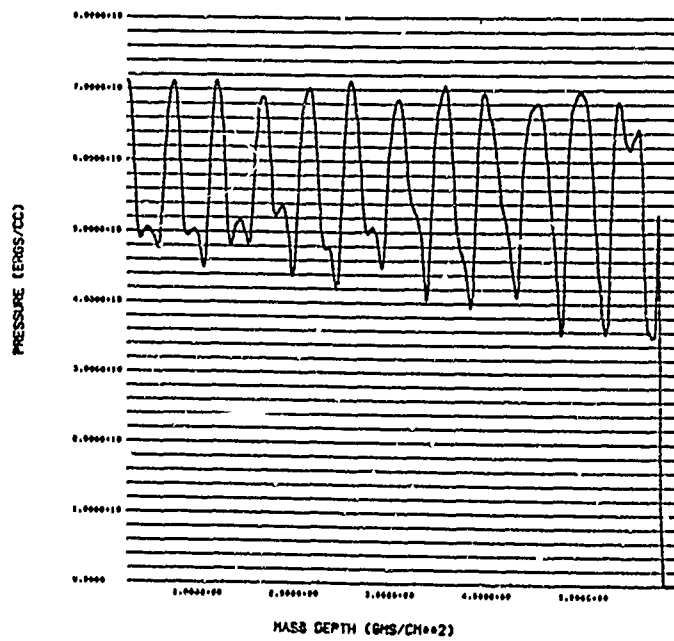


Fig. 5.14(b) -- $t = 7.51 \text{ usec}$

Fig. 5.14--The pressure profile produced by step loading the laminated structure to the indicated time. The water and tuff components are described by non-linear volumetric fluid models.

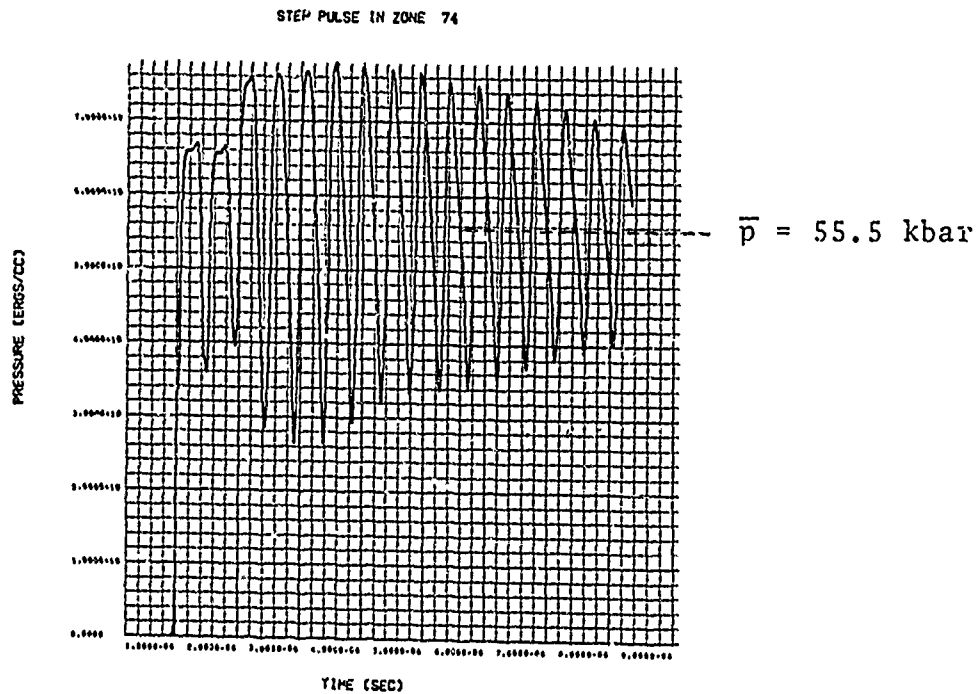


Fig. 5.15(a)--First Bilaminate

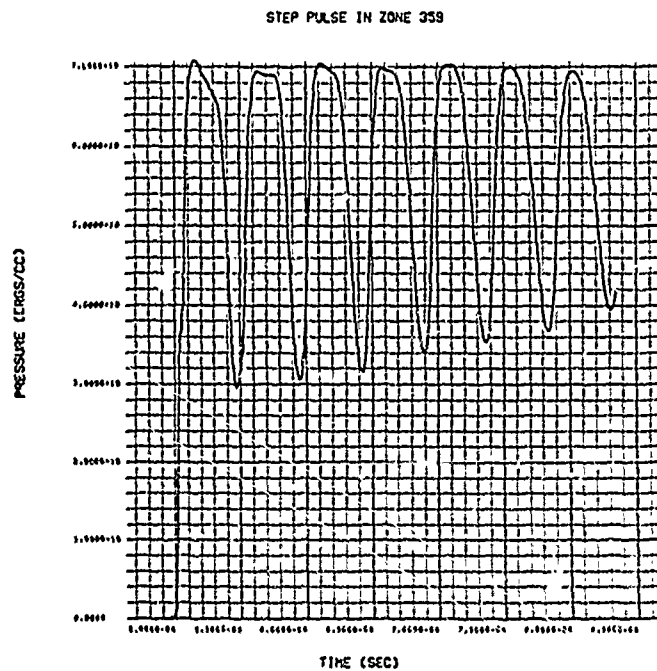


Fig. 5.15(b)--Sixteenth Bilaminate

Fig. 5.15--Pressure as a function of time at the center of the indicated water laminates in the extended water/tuff bilaminate structure. The component materials are treated as volumetric fluids.

5.4 THERMODYNAMIC FLUID MODEL

If a material is shocked from p_1, V_1 to p_2, V_2 and then the compression relieved back to V_1 the residual heat due to the shock processing is

$$\Delta E = \frac{1}{2}(p_1 + p_2)(V_2 - V_1) - \int_{V_1}^{V_2} p \, dV \quad (5.25)$$

When a non-linear material oscillates about some equilibrium pressure, p_e , there will be a corresponding conversion of kinetic energy into heat by this mechanism during each oscillation.

For a volumetric fluid the pressure release is forced to occur along the Hugoniot since variations in internal energy from the Hugoniot value are ignored in computing the pressure, $p = p(V)$. The amount of kinetic energy dissipated into heat during an oscillation (per gram of processed material) is represented in Fig. 5.16(a) by the area between the Rayleigh line and the Hugoniot curve. It is this periodic dissipation mechanisms that causes the attenuation of the $p(t)$ curves shown in Fig. 5.15. The final equilibrium pressure is the same as that determined by imposing the Hugoniot conditions on the associated homogenized volumetric wet tuff medium, i.e. Eq. (5.24)

For a realistic thermodynamic fluid,

$$p = p(V, E) \quad E = E(V, T) \quad (5.26)$$

the permissible (p, V) points are not confined to the Hugoniot (H_0) through $(0, V_0)$ since changes in the internal energy are reflected in the value of the pressure. The schematic in Fig. 5.16(b) illustrates the path that would

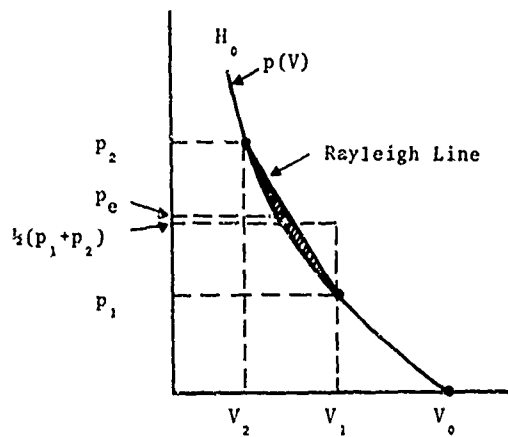


Fig. 5.16(a)

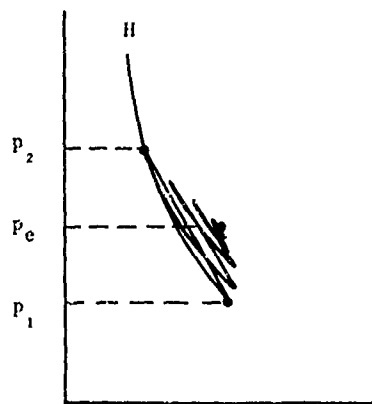


Fig. 5.16(b)

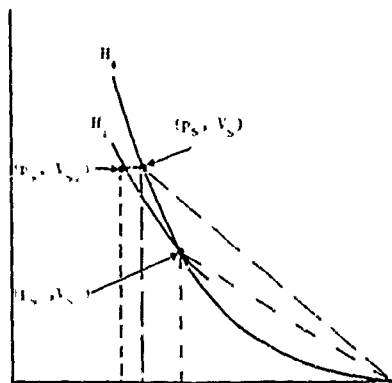


Fig. 5.16(c)

Fig. 5.16--Schematics showing (a) hatched area representing the amount of kinetic energy (per gram) converted into heat during the indicated oscillation of a volumetric fluid material, (b) the locus of p-V points assumed by a thermodynamic fluid subjected to oscillatory loading, and (c) effect of a double shock.

be traced out by such a fluid undergoing repeated shocking and unloading. Starting at point (p_1, V_1) , which in general will not lie on H_0 , the material particle is shocked along a Rayleigh line to a point (p_2, V_2) which lies on H , the Hugoniot which is centered on (p_1, V_1) . The compression is released along an adiabat through (p_2, V_2) to (p_3, V_3) with a net gain in internal energy ΔE given by Eq. (5.25). The augmented internal energy will tend to increase the mean pressure during the next oscillation. The amplitude of the excursions from the increasing mean (to the asymptotic value p_e) may be expected to decrease because of this conversion of kinetic energy to heat. Subsequent shocking and unloading, along the appropriate Rayleigh lines and adiabats, will produce a p-V path which may be expected to move to the right of the Hugoniot (H) through (p_1, V_1) , as indicated schematically in Fig. 5.16(b).

If the material particle reaches the shock pressure p_s in a single shock it will lie on H_0 and the associated internal energy is

$$E_1 = \frac{1}{2} p_s (V_0 - V_s) \quad (5.27)$$

If, on the other hand, the particle reaches the pressure p_s in two successive shocks as shown in Fig. 5.16(c), the internal energy is only

$$E_2 = \frac{1}{2} p_{s1} (V_0 - V_{s1}) + \frac{1}{2} (p_s + p_{s1}) (V_{s1} - V_{s2}) \quad (5.28)$$

In this case the point (p_s, V_s) lies on the Hugoniot, H , and is to the left of the Hugoniot H_0 . Subsequent oscillations, such as indicated in Fig. 5.16(b) may or may not be sufficient to move the final equilibrium point (p_e, V_e) to the right of the H_0 curve. In any case the final temperature in the doubly shocked material will be less than if it reached

its maximum pressure in a single shock. For a highly compressible material such as water at low pressure, this can be a very significant effect.

The calculation for a bilaminated structure subjected to the step pulse loading

$$v_0 = 7.786 \times 10^4 \text{ cm/sec} \quad t > 0$$

was repeated for the case where the water and tuff layers in the midsection were represented as thermodynamic fluids, Eq. (5.26). The equations of state for the water and compacted tuff laminates were the dual forms developed in Sections II and III respectively. Only the condensed states of water occur under the present step loading. In order to allow direct comparison with the corresponding calculation for laminates modeled as volumetric fluids, Eq. (5.23), the left end block through which the pulse is transmitted before entering the midsection was again modeled as an homogenized wet tuff volumetric fluid. The second form of the water and tuff equations of state, Eq. (5.26), is not required for the wave propagation calculations with SKIPPER, but it was used to calculate the temperature in the water and tuff laminates.

In Fig. 5.17 the variation of the pressure and the temperature with time are both depicted at a point located at the center of the first water layer in the midsection of the water/tuff bilaminate structure. Comparison of Fig. 5.17(a) with Fig. 5.15(a), shows that the substitution of the thermodynamic fluid models for the water and tuff has had only a small effect on the pressure for this particular situation. The mean pressure is reduced from $\bar{p} = 55.5$ kbar to $\bar{p} = 53.2$ kbar so that the final expected final equilibrium pressure is approximated by

$$p_e = 57.1 - 2.2 = 54.9 \text{ kbar} \quad (5.29)$$

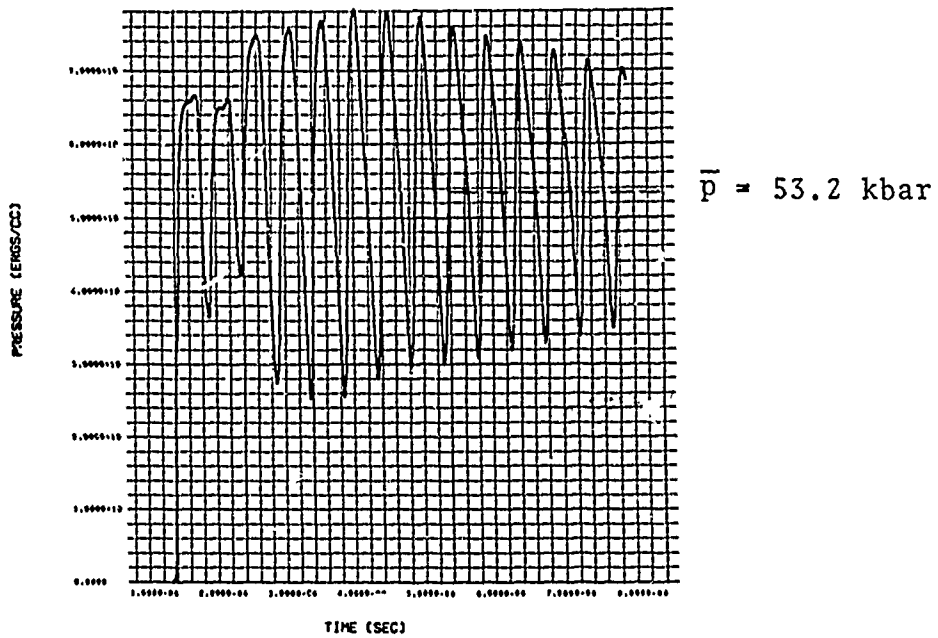


Fig. 5.17(a)--Pressure vs time

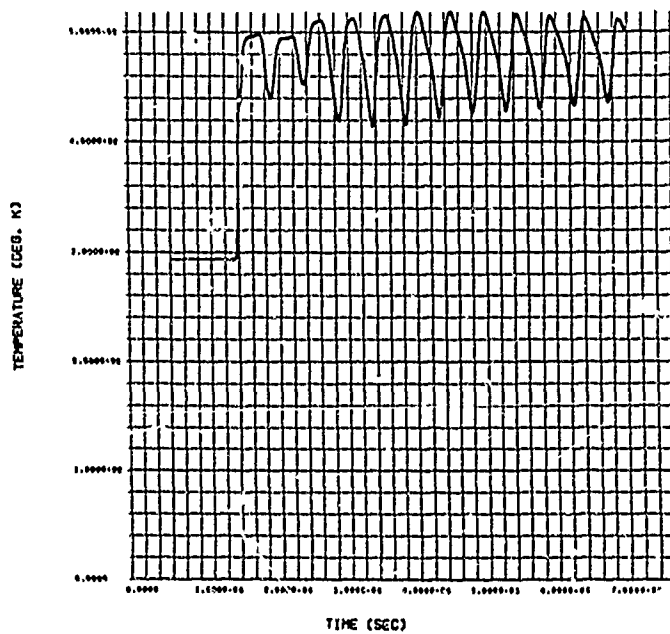


Fig. 5.17(b)--Temperature vs time

Fig. 5.17--Time variation of (a) pressure, and (b) temperature at the center of the first water laminate in the extended bilaminated structure subjected to a step pulse. The laminates are treated as thermodynamic fluids.

In Fig. 5.17(b) the temperature in the first water layer is also seen to approach an asymptotic value. The same is true for the tuff laminates. Examination of the numerical data has led to the following estimates for the equilibrium values for the individual laminates:

$$\text{Water: } T_e = 473 \text{ }^\circ\text{K} \quad \text{Tuff: } T_e = 477 \text{ }^\circ\text{K} \quad (5.30)$$

No heat transfer was permitted in the SKIPPER calculation. The values are very different from those that would be anticipated from homogenized equations of state.

For the imposed velocity loading the corresponding homogenized PTEQ equation of state for wet tuff, mass fraction $F = 0.15$, would yield the following values for the equilibrium particle velocity, shock velocity, pressure and temperature:

$$\begin{aligned} u_e^* &= 0.07786 \text{ cm}/\mu\text{sec} & D_e^* &= 0.365 \text{ cm}/\mu\text{sec} \\ p_e^* &= 56.2 \text{ kbar} & T_e^* &= 526 \text{ }^\circ\text{K} \end{aligned} \quad (5.31)$$

On the other hand, if the individual tuff and water components were shocked directly to the equilibrium pressure, Eq. (5.29), the corresponding Hugoniot temperatures would be

$$\begin{aligned} (p_{H_0} = 54.9 \text{ kbar}) \quad \text{Water: } & 574 \text{ }^\circ\text{K} \\ \text{Tuff: } & 487^\circ\text{K} \end{aligned} \quad (5.32)$$

The SKIPPER results, Eq. (5.30), at first sight seem incompatible with these values since a much higher temperature might be expected in the water laminates in the absence of any heat transfer to the tuff laminates. This discrepancy, however, can be explained in terms of the substructure in the laminated composite.

The front of the step pulse enters a water laminate by crossing an interface from a compacted dry tuff laminate. In the tuff the pressure will be on the order of 70 kbar, e.g., Fig. 5.14, but because of the impedance mismatch at the tuff/water interface, the initial shock transmitted into the water will be only about 35 kbar. Subsequent reflection of this first shock at the next water/tuff interface will essentially double the shock strength. The fact that the water is shocked in a two-step process is verified by the inflection in the rise portion of the $p(\tau)$ plot for a particle located at the center of the first water layer, Fig. 5.17(b). A rough estimate of the difference between the single and double shock Hugoniot energies, $E_1 - E_2$ can be made by neglecting the difference $V_s - V_{s_2}$ in Eqs. (5.27) and (5.28) and considering the water to be shocked to 35 kbar and then to the expected equilibrium value, say 54.9 kbar. The double shocking reduces the internal energy at the mean pressure by about 2/3 to 3/4 of its single shock value. This is of the required magnitude to explain the apparent discrepancy in the equilibrium temperature of the water layers. The tuff layers appear to undergo a single shock in reaching their initial shocked state, but even if it were doubly shocked there would be much less effect than for the more compressible water.

This simple calculation for a step pulse has shown that the temperature attained in a composite material can depend strongly on its substructure.

5.5 FOURIER SYNTHESIS METHOD

The artificial viscosity term in SKIPPER was found to damp out high frequency components of waves propagating in linear materials. To avoid this difficulty a Fourier-synthesis code, WARP, has been developed to study pulse propagation in any linear composite material for which a dispersion relation is known, i.e., a material for which the velocity of propagation as a function of the wave length is known for steady harmonic waves. The pulse is decomposed into its harmonic components, the phase change experienced by each component calculated, and then the contributions of all the resulting harmonics summed to predict the transmitted pulse. Since the input dispersion relation can be determined by either theoretical or experimental means, the WARP code offers a useful tool for studying the influence of the material and dimensional parameters on the dispersion of a pulse transmitted through a linear composite material.

5.5.1 Analysis

In the Fourier synthesis of a pulse transmitted through a medium from the dispersion relation for the medium, one first takes the transform of the incoming pulse of duration $0 < t < t_0$

$$P_1(\omega) = F[p_1(t)] = \int_0^t p(t) e^{-i\omega t} dt \quad (5.33)$$

To each harmonic component, $P_1(\omega)d\omega$, the medium will act as a filter described by a transfer function $T(\omega)$ and the transform of the transmitted component is

$$P_2(\omega) = P_1(\omega)T(\omega) \quad (5.34)$$

The output pulse is then simply

$$p_1(t) = F^{-1}[P_2(\omega)] = \frac{1}{2\pi} \int_{-\infty}^{\infty} P_2(\omega) T(\omega) e^{i\omega t} d\omega \quad (5.35)$$

In general, the transfer function $T(\omega)$ will be of the form

$$T(\omega) = A(\omega) e^{i\theta(\omega)} \quad (A, \theta \text{ real}) \quad (5.36)$$

where $A(\omega)$ is the attenuation factor and θ is the phase shift. Alternately, $T(\omega)$ can be written as

$$T(\omega) = e^{i\phi(\omega)} \quad (5.37)$$

where

$$\theta = \text{Real part of } \phi \quad A = \exp(\text{Imaginary part of } \phi) \quad (5.38)$$

The dispersion relation for the medium, assumed known, provides an expression for the wave number, $k = \omega/C$, for an harmonic dilatation wave traversing the medium. Here $C = C(\omega)$ is the associated phase velocity. The corresponding transfer function for a length L of the laminated medium is defined by (5.35) and

$$\phi(\omega) = k(\omega)L = \frac{\omega L}{C(\omega)} \quad (5.39)$$

If the given dispersion relation admits the possibility of complex solutions for $k(\omega)$, harmonic components will in general experience both attenuation and phase shift. Normally, however, there will be frequencies for which $\phi(\omega)$ is real and for these components there will be no attenuation experienced.

Substitution of (5.37) into (5.33) yields

$$p_2(t) = \frac{1}{2\pi} \int_{-\infty}^{\infty} P_1(\omega) \exp\left[i\omega\left(\frac{L}{C(\omega)} + t\right)\right] d\omega \quad (5.40)$$

5.5.2 The WARP Computer Program

A WARP computer program was constructed to evaluate the output pulse from (5.38) using any prescribed expression for the phase velocity, $C(\omega)$. The Cooley-Tukey algorithm for discrete Fourier transformation is used in this code.⁽⁵⁷⁾ This method, by its speed and accuracy, is superior to alternate algorithms for calculating Fourier transforms.⁽⁵⁸⁾ There is a possibility of enhancing the operation of the Cooley-Tukey algorithm by the use of a base 8 iteration,⁽⁵⁹⁾ but this is not required at the present time.

The WARP code has been tested for the non-dispersive propagation of a pulse, and simple dispersion relations are being tested in it currently. In particular, calculations have been initiated using the Rytov⁽⁶⁰⁾ solutions for the phase velocity, C , of a steady harmonic wave propagating in an infinite medium composed of alternating laminates of two elastic materials. His solution applied to treat the propagation of an harmonic dilatation wave in a direction normal to the layering becomes

$$\begin{aligned} \cos[\omega(h_1+h_2)/C] &= \cos[\omega h_1/c_1] \cos[\omega h_2/c_2] \\ &- \frac{1+I^2}{2I} \sin[\omega h_1/c_1] \sin[\omega h_2/c_2] \quad (5.41) \end{aligned}$$

Here h_1 and h_2 are the laminate materials, I is the impedance ratio defined by

$$I = \frac{c_1 (\lambda_2 + 2\mu_2)}{c_2 (\lambda_1 + 2\mu_1)} \quad (5.42)$$

and c_1, c_2 are the dilatation velocities of the elastic constituents,

$$c_1 = \sqrt{\frac{\lambda_1 + 2\mu_1}{\rho_1}} \quad c_2 = \sqrt{\frac{\lambda_2 + 2\mu_2}{\rho_2}} \quad (5.43)$$

Parametric studies are planned to examine the influence of the material and dimensional parameters on the geometric dispersion of a square pulse propagating through a structure of alternating elastic laminates.

VI. 2-D COMPOSITE CONFIGURATIONS*

6.1 INTRODUCTION

In the preceding calculations, only waves propagating normal to material interfaces were considered; no motion was permitted parallel to the tuff/water bilaminate planes. In this section the opposite situation, in which the wave propagates in the direction of the bilaminates, will be treated. In addition, the intermediate case of a wave propagating through a tuff matrix with periodic parallel pores filled with water will be considered. Each of these involves deformation in two spatial dimensions and numerical solutions were obtained using the 2-D Lagrangian continuum mechanics computer program CRAM.

The numerical technique employed in CRAM is an extension to two space coordinates of the basic finite difference formulation used in the 1-D SKIPPER code. Shocks are approximated by the von Neumann artificial viscosity method.⁽⁵⁶⁾ CRAM can be used to treat multi-material configurations in either cylindrical (2-D axisymmetric) or rectangular (2-D planar) geometry. A variety of choices for the constitutive relation is available for each component material. The code has been previously applied to studies of structural response to energy deposition⁽⁶¹⁾ and armor penetration.⁽⁶²⁾

* Author: T. D. Riney

6.2 WAVE PROPAGATION PARALLEL TO BILAMINATES

6.2.1 Simplified Analytic Solutions

Two analytical treatments have been presented for approximating the Hugoniot of a laminated composite in which the shock propagates in a direction parallel to the material interfaces. Tsou and Chou⁽⁶³⁾ have considered the case in which the two materials are assumed to be firmly bonded together and Torvik⁽⁶⁴⁾ has considered the situation in which there is no bond. The latter case is more appropriate to the situation in which one of the laminates is water and it is of interest to compare his simplified theory with the detailed calculation using the CRAM computer code.

The left boundary of the composite has a constant velocity $\dot{x} = v_0$ imposed (Fig. 6.1(a)); because of symmetry it is only necessary to consider the section shown in Fig. 6.1(b). Torvik assumes that a steady shock front is eventually attained which propagates at a constant velocity D in the two materials. The transition region (S in Fig. 6.1(b)) of two-dimensional flow is assumed to be followed by steady one-dimensional flow, and the Hugoniot jump conditions may be written which account for the change in the thickness of each material laminate. Pressure equilibrium is assumed behind the transition region and the following relations may be written ($i = 1, 2$):

$$h_{0i} \rho_{0i} D = h_{fi} \rho_{fi} (D - u_j) \quad (6.1)$$

$$p(h_{0i} + h_{fi}) = 2h_{0i} \rho_{0i} D u_i \quad (6.2)$$

$$p = A_i \mu_i + B_i \mu_i^2 + F_i \mu_i^3; \quad \mu_i = \frac{\rho_{fi}}{\rho_{0i}} - 1 \quad (6.3)$$

Symmetry demands equality of the sums of the initial and

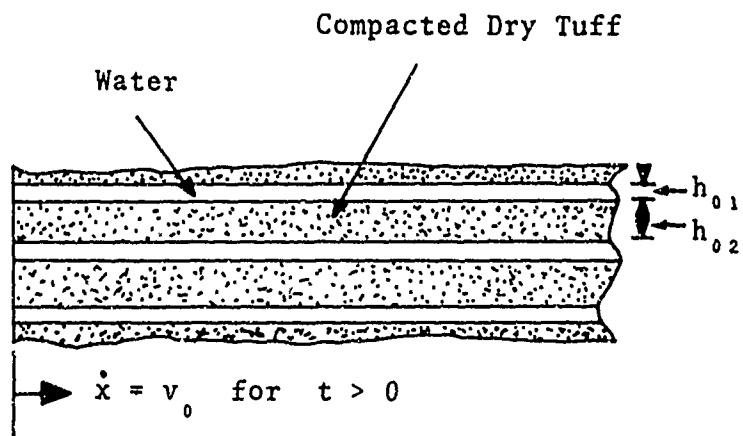


Fig. 6.1(a)

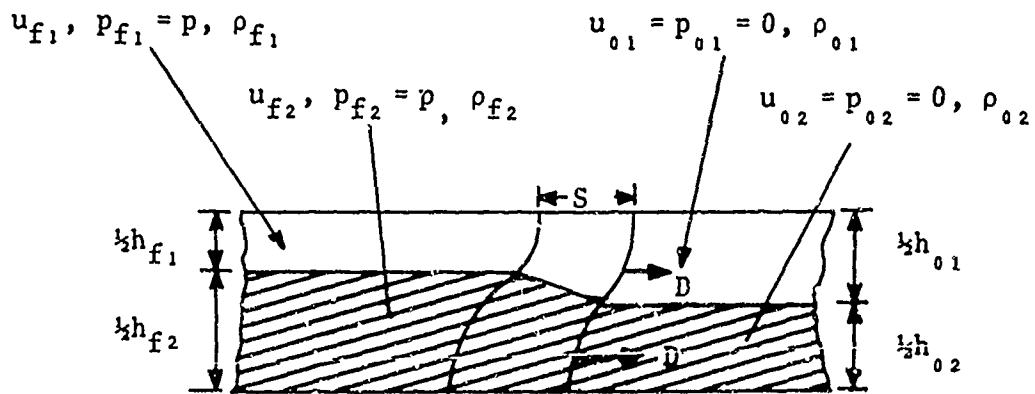


Fig. 6.1(b)

Fig. 6.1--Laminated structure subjected to velocity step loading at left boundary. Subscripts 1 and 2 denote water and compacted tuff, respectively.

final laminate thicknesses

$$h_{01} + h_{02} = h_{f1} + h_{f2} \quad (6.4)$$

and the velocity loading is replaced by the averaged boundary condition

$$u_1 h_{f1} + u_2 h_{f2} = v_0 (h_{f1} + h_{f2}) \quad (6.5)$$

In writing Eq. (6.3) we have assumed that the compacted tuff and water laminates, and the associated homogenized wet tuff material, are non-linear volumetric fluids. The associated constants in the equations of state, the mass fraction of the water in the composite ($F = 0.15$), and the dimensions of the laminates ($h_{01} = 0.297$ cm, $h_{02} = 0.0703$ cm) are all assumed to be the same as for the calculations presented in Section 5.3, i.e., Table 5.2.

The above system of eight equations has been evaluated using a multi-dimensional Newton-Raphson method with the required functional derivatives computed numerically. The predicted shock pressure as a function of the imposed velocity loading, v_0 , is depicted in Fig. 6.2 for a water/tuff laminate in which the mass fraction of water is $F = 0.15$. Curves depicting shock pressure vs v_0 for the associated homogenized wet tuff and for the isolated water and compacted tuff component materials are also shown in Fig. 6.2 for comparison purposes. The corresponding curves showing the pressure as a function of the shock velocity, D , are presented in Fig. 6.3.

The calculation of the Hugoniot for the homogenized wet tuff equation of state assumes there is no diffusion of the water through the tuff. Since relative motion is permitted in Torvik's laminate model, there is less constraint on the materials and a smaller pressure is to be expected when using this model. This is seen to be the case by the results in Figs. 6.2 and 6.3.

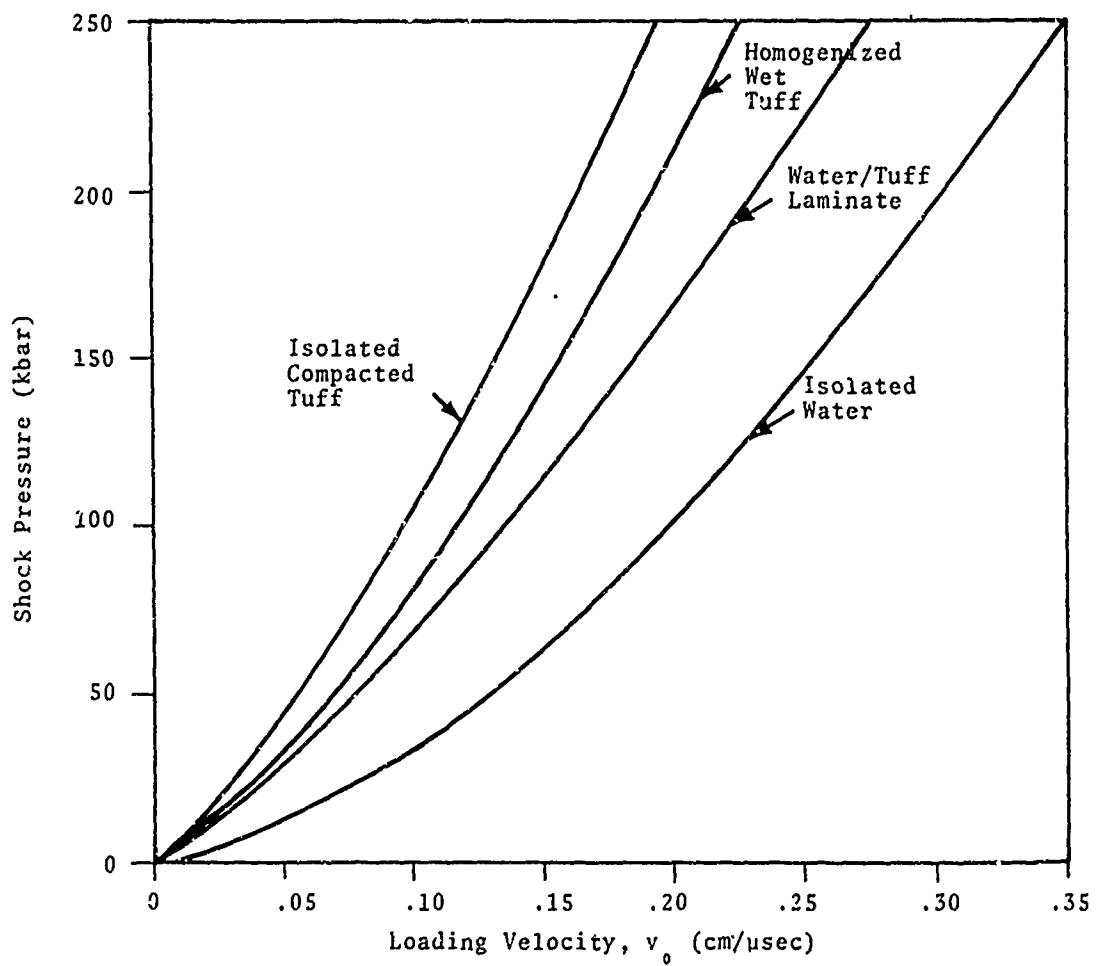


Fig. 6.2--Predicted shock pressures for a water and compacted tuff composite ($F = 0.15$) compared with the values for the isolated components at indicated magnitude of velocity loading.

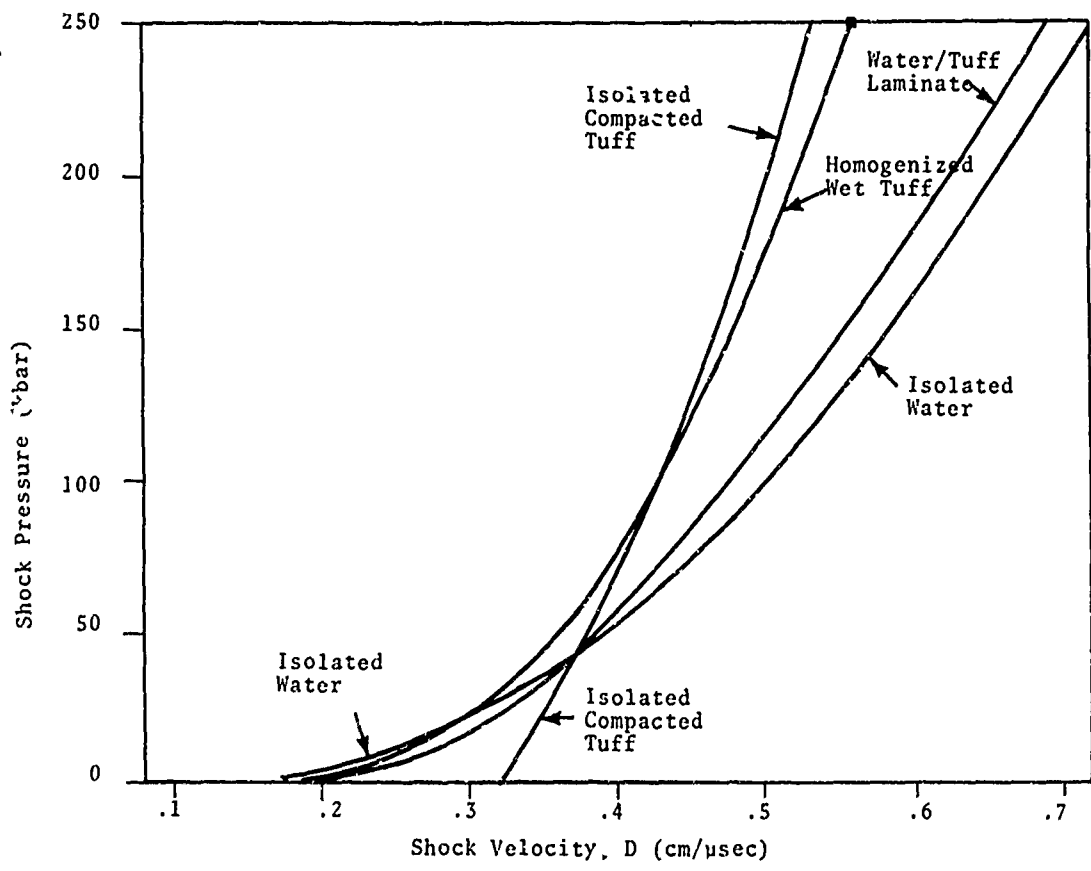


Fig. 6.3--Predicted shock pressure vs shock velocity curves for a water and compacted tuff composite (F = 0.15) compared with the corresponding curves for the isolated component materials.

The laminate model allows for a change in the thicknesses of the water and tuff laminates during their traversal of a transition region at the shock front. The predicted relative changes in the water and tuff laminate widths as they traverse the shock transition region are shown in Fig. 6.4 for $F = 0.15$. At an imposed velocity $v_0 > 0.7$ cm/ μ sec the water layers increase in thickness and the compacted tuff layers decrease in thickness by a corresponding amount. The converse is true for $v_0 < 0.7$ cm/ μ sec. This cross-over velocity is near the value for which the CRAM run was made.

6.2.2 Detailed Computer Solutions

Torvik's simplified analysis of a shock wave propagating parallel to the water/tuff laminates is based on the assumption that a constant steady-state shock and transition region are attained. It is of interest to see if these basic assumptions are valid.

The 2-D Lagrangian CRAM code was used to calculate the full time-dependent flow induced in the water/tuff laminated medium, Fig. 6.1(a). The constants in the equations of state for the volumetric fluid models for the water and tuff components, and the dimensions of the laminates, are the same as in Table 5.2. The configuration was loaded by a longitudinal step pulse by subjecting the left boundary to the velocity

$$v_0 = 7.786 \times 10^4 \text{ cm/sec} \quad (t > 0). \quad (6.6)$$

The section of symmetry between the mid-planes of adjacent tuff and water laminates, corresponding to $k = 1$ and $k = 16$ grid lines in the finite difference mesh, were treated as reflective boundaries and the interface between

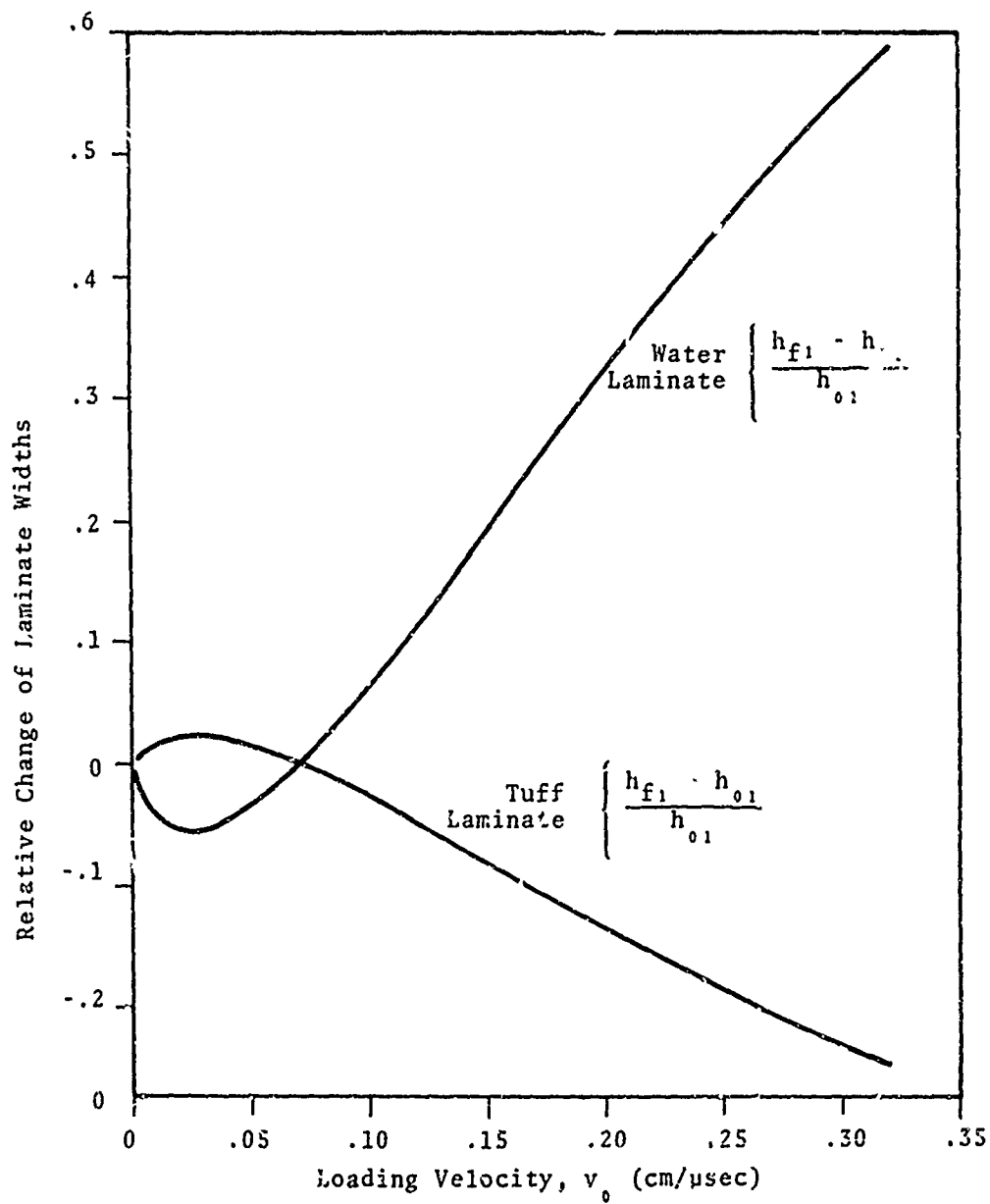


Fig. 6.4--Predicted relative changes in the widths of the laminates behind the steady state longitudinal shock in a water and compacted tuff composite ($F = 0.15$).

the layers was treated as a slip surface to permit relative motion between the tuff and water, Fig. 6.5.

The sequence of pressure contours shown in Fig. 6.6 illustrates the formation and propagation of a steady shock front. Initially, the shock velocity in the tuff is greater than that in the water, $t = 0.05$ and $0.13 \mu\text{sec}$. An essentially steady front is finally obtained, however, in which the shock front in the water layer has a slight lead over the front in the tuff, $t = 0.34$, 0.45 and $0.55 \mu\text{sec}$.

The attainment of a steady state shock is verified by plotting the time variation of the position of the front at the mid-plane of the tuff layer ($k = 2$) and the mid-plane of the water layer ($k = 16$). This information has been extracted from the CRAM data and is plotted in Fig. 6.7. The numerical data are seen to converge towards the curve calculated from the simple steady-state water/tuff laminate model, $D = 0.388 \text{ cm}/\mu\text{sec}$. The homogenized wet tuff model is seen to underestimate the shock velocity, $D_{wt} = 0.367 \text{ cm}/\mu\text{sec}$.

The location of the shock front is denoted by S in the sequence of CRAM velocity field plots shown in Fig. 6.8. Near the loading surface (left boundary) the tuff is continuously pushed upward to fill the void left by the water which rushes to the right with a horizontal velocity component much greater than that of the tuff. In this region the CRAM finite difference mesh is seen to be severely distorted. Near the shock front, however, a steady-state situation is attained in which there is very little vertical motion, the velocity vectors for the mesh vertex points lie essentially on the horizontal grid lines. Just behind the shock there is only a very small downward velocity component in the tuff. This is predicted by the simple water/tuff laminate theory which predicts that the tuff laminate's thickness

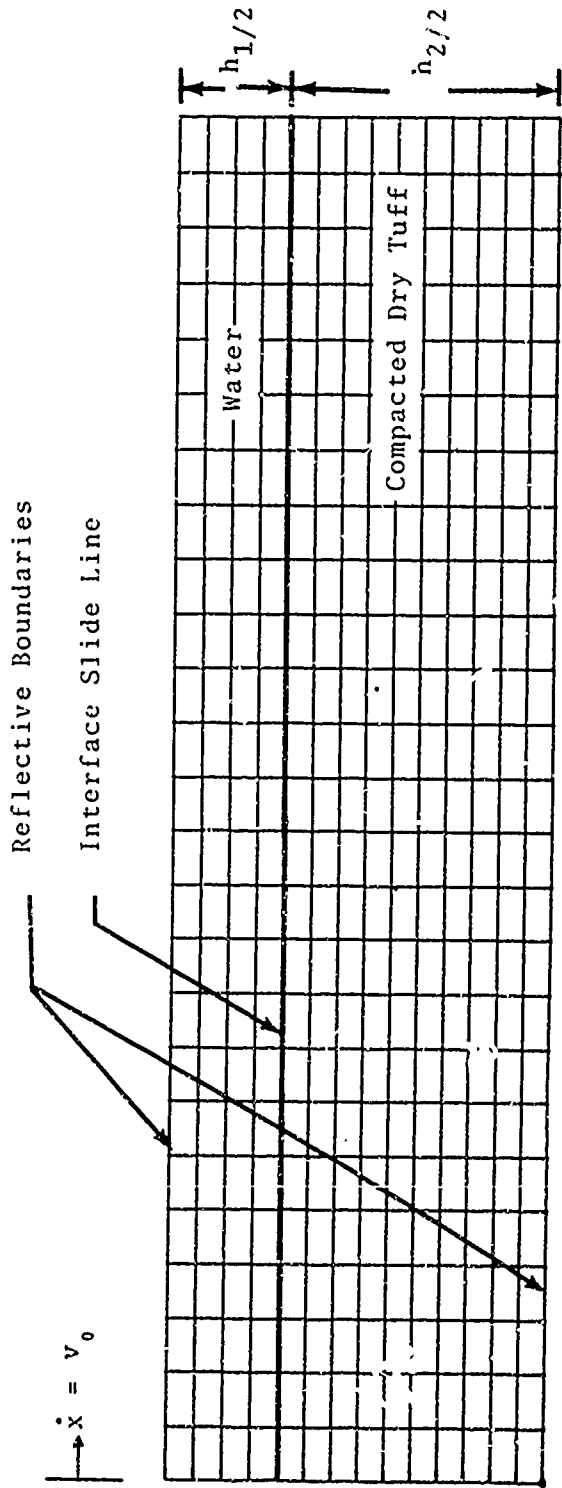


Fig. 6.5(a)

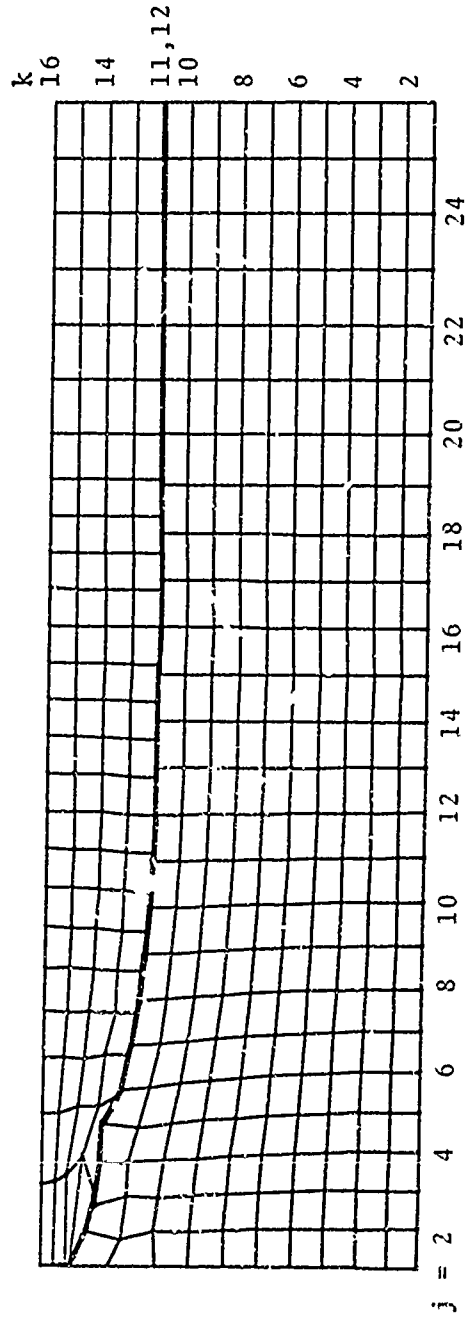


Fig. 6.5(b)

Fig. 6.5--The CRAM grid at (a) the initiation of the calculation and (b) at $t = 0.34 \text{ usec.}$

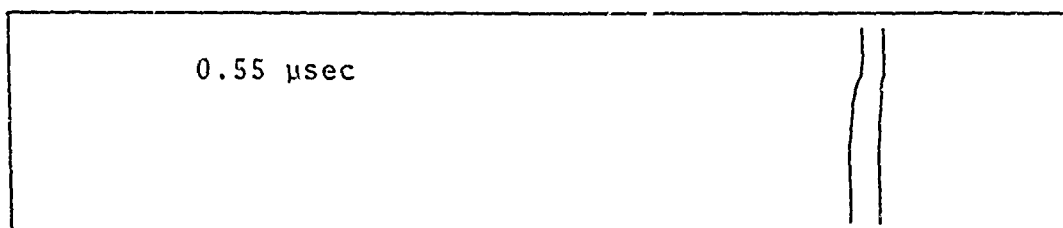
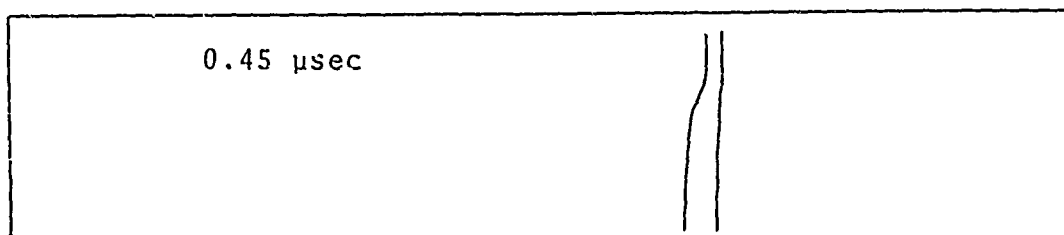
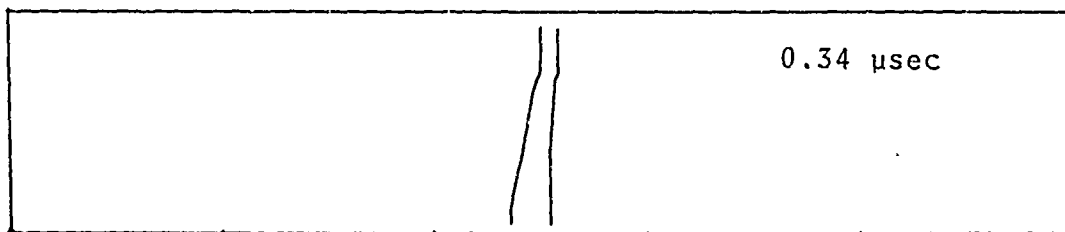
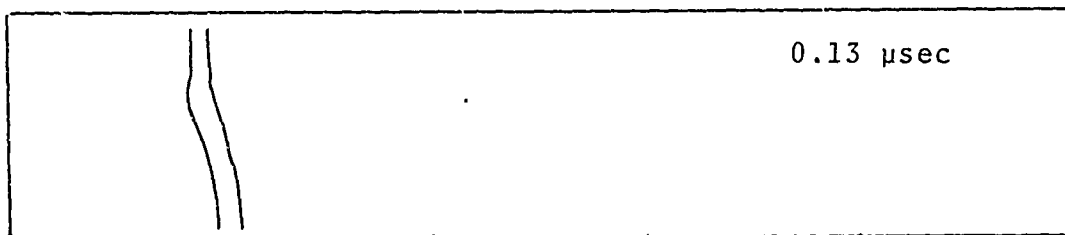
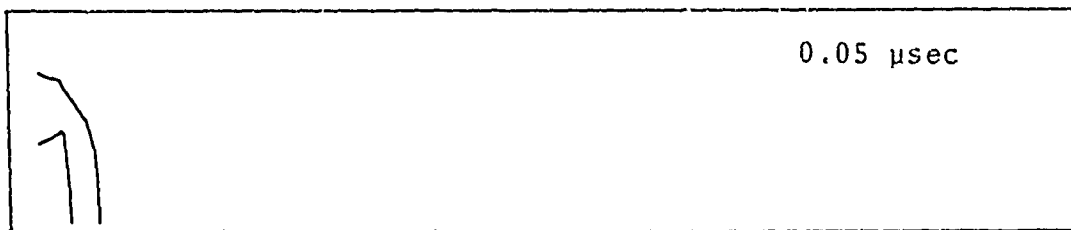


Fig. 6.6--CRAM pressure profiles showing the 20- and 40-kbar isobars near the shock front at indicated times.

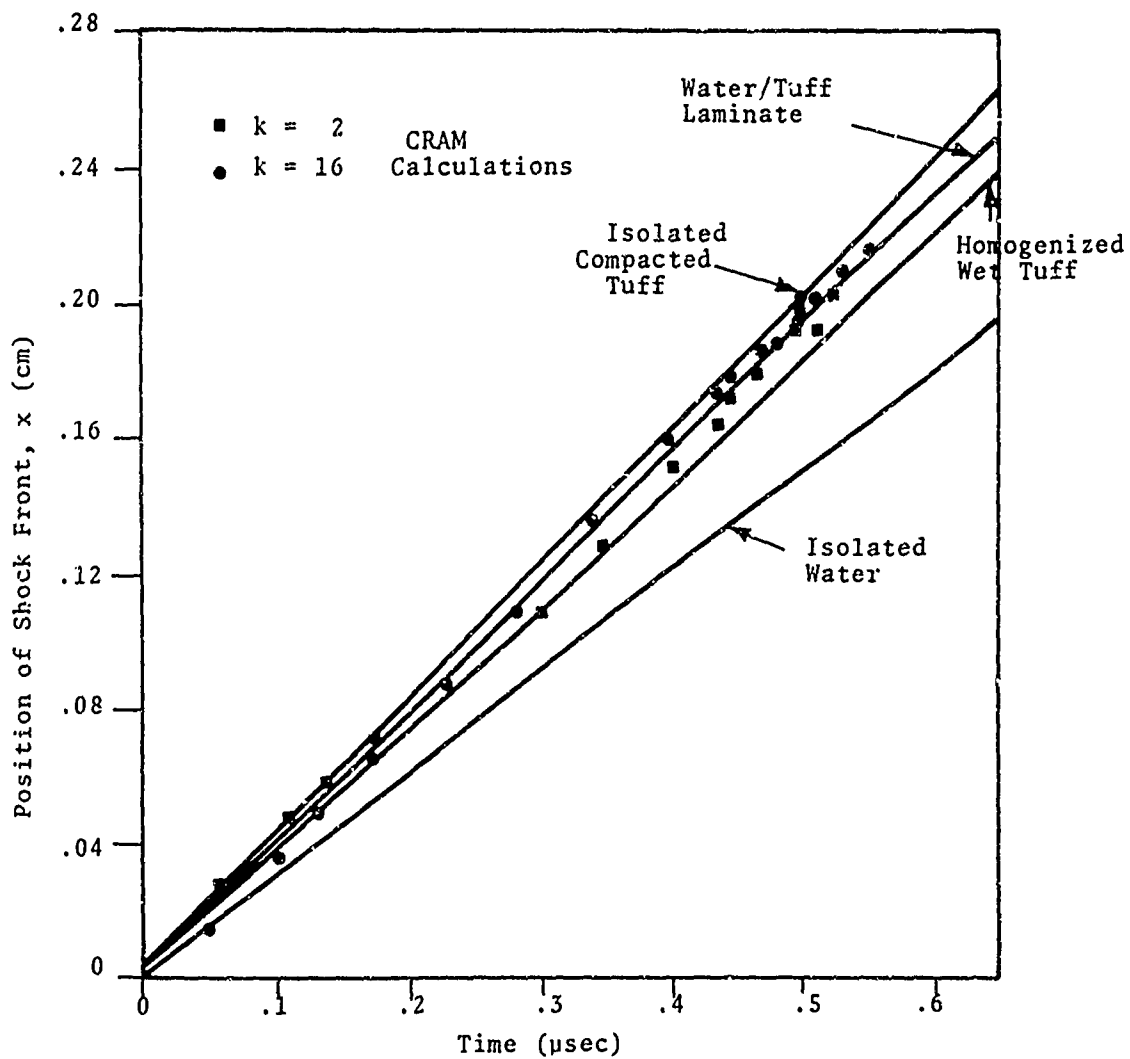


Fig. 6.7--Position of the shock front computed by CRAM compared with the predictions based on the simple composite models ($F = 0.15$). Also shown are the positions for the isolated component materials if subjected to the same velocity step loading.

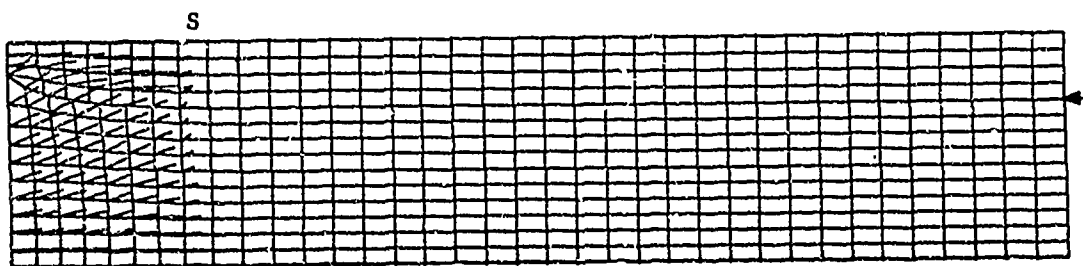


Fig. 6.8(a)-- $t = 0.13 \mu\text{sec}$

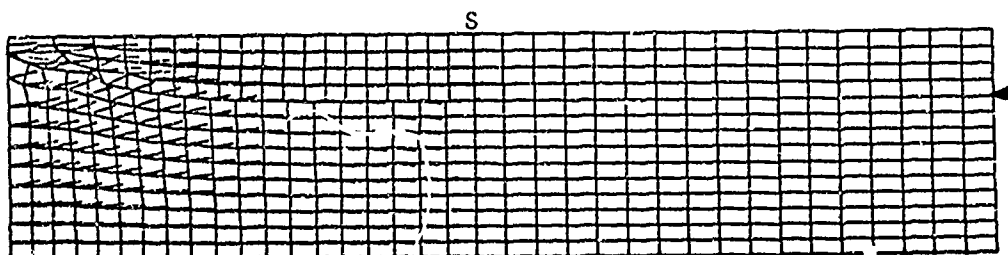


Fig. 6.8(b)-- $t = 0.34 \mu\text{sec}$

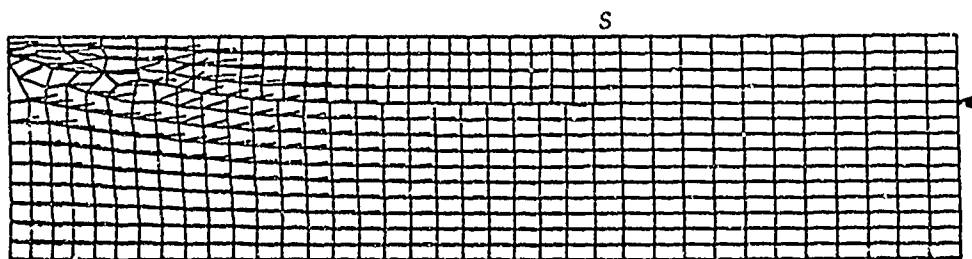


Fig. 6.8(c)-- $t = 0.45 \mu\text{sec}$

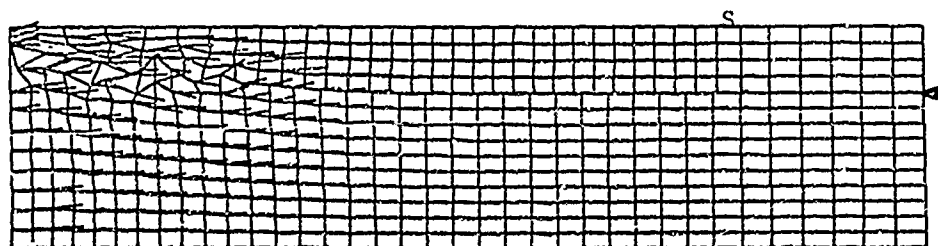


Fig. 6.8(d)-- $t = 0.53 \mu\text{sec}$

Fig. 6.8--The velocity field in the left portion of the CRAM grid at indicated times. The S and arrow symbols denote the positions of the shock front and the water tuff interface respectively.

will be decreased less than one percent from its initial value for $v_0 = 0.07786$ cm/ μ sec, Fig. 6.4.

The horizontal velocity components at the mid-planes of the tuff ($k = 2$) and water ($k = 16$) laminates are plotted in Fig. 6.9 at three stages of the CRAM calculation. Points indicating the values predicted by the steady-state laminate theory ($u_1 = 0.132$ cm/ μ sec, $u_2 = 0.0044$ cm/ μ sec) have also been inserted for comparison. The predictions are in good agreement with the CRAM calculations near the shock front. In each plot the point of intersection of the two profiles locates the position of the loaded surface at that instant in time.

In Fig. 6.10 the pressure profiles along the mid-planes of the tuff and water laminates are presented at the same three instants in time. In each plot, points have been inserted indicating the amplitude and position of the shock front predicted for isolated water, isolated compacted dry tuff, homogenized wet tuff, and the water/tuff laminate if subjected to the same step velocity loading, Eq. (6.6). The prediction of the simple laminate theory, $p = 50.9$ kbar, is seen to give good agreement with the CRAM calculations near the shock front.

The laminate model does not treat the region near the loading surface. The CRAM results there become increasingly inaccurate due to the large distortions of the finite difference mesh, but this difficulty has not affected the calculations near the shock front.

Loading parallel to the planes of a laminated composite represents the most severe test of the applicability of the homogenized wet tuff model for a step pulse. We have seen that the steady-state laminate theory accurately predicts the shock characteristics of the laminate, at least for the conditions for which the CRAM calculation was made.

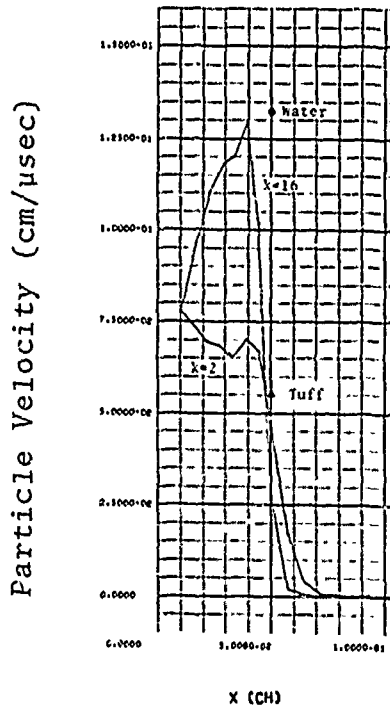


Fig. 6.9(a) -- $t = 0.13 \text{ usec}$

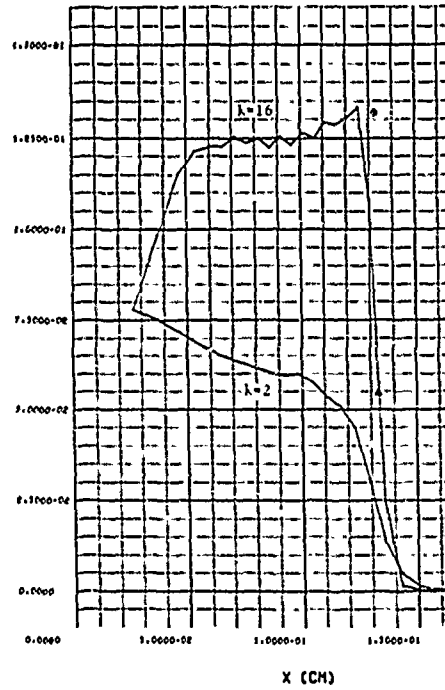


Fig. 6.9(b) -- $t = 0.34 \text{ usec}$

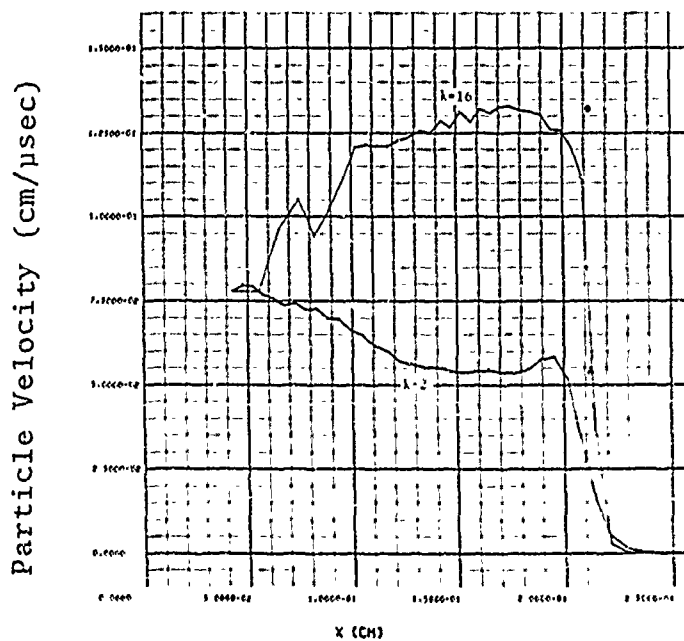


Fig. 6.9(c) -- $t = 0.55 \text{ usec}$

Fig. 6.9--The CRAM horizontal particle velocity profiles at the tuff ($k=2$) and water ($k=16$) mid-planes compared with the predictions of the simple laminate theory ($F=0.15$) at the indicated times.

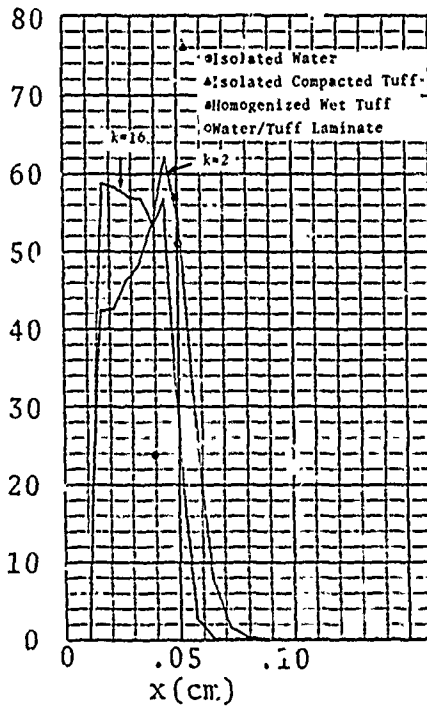
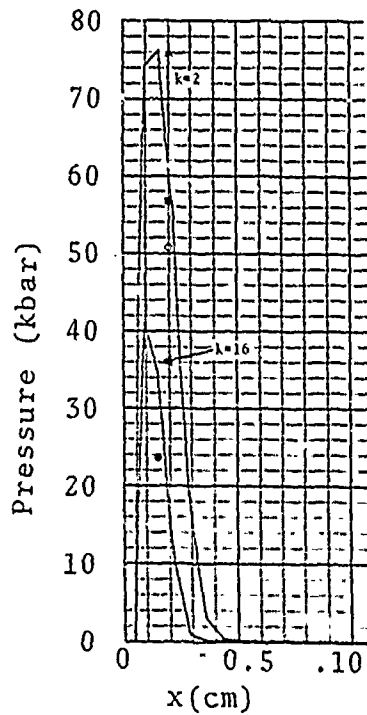


Fig. 6.10(a) -- $t = 0.13 \mu\text{sec}$ Fig. 6.10(b) -- $t = 0.34 \mu\text{sec}$

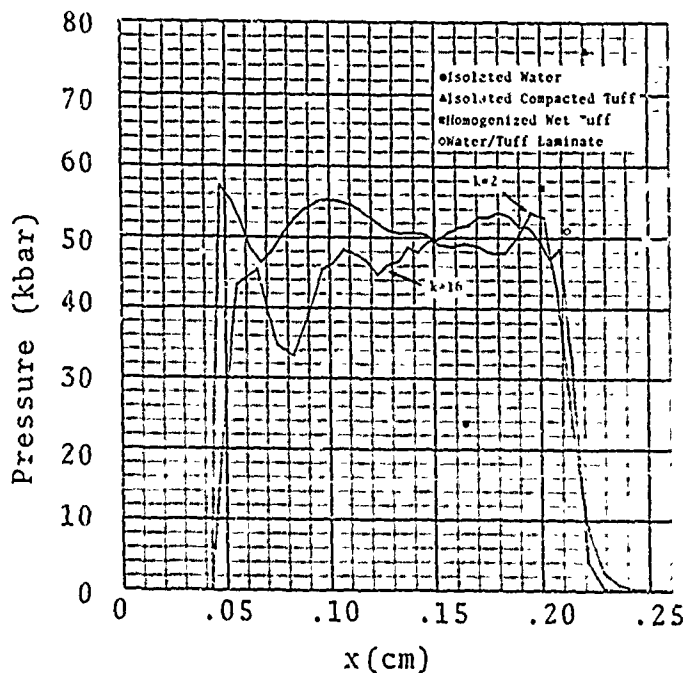


Fig. 6.10(c) -- $t = 0.55 \mu\text{sec}$

Fig. 6.10--CRAM pressure profiles at the tuff ($k=2$) and water ($k=16$) mid-planes compared with the prediction of the simple water/tuff laminate theory ($F = 0.15$) for the indicated times. Note, the left boundary pressures have been incorrectly plotted as zero.

For loading normal to the laminates, no relative motion of the water and tuff is possible and the predictions of the homogenized wet tuff model accurately represent the eventual steady shock conditions (see Section 5.3.3). Consequently, the region between the water/tuff laminate and the homogenized wet tuff curves in Figs. 6.2 and 6.3 appears to represent the range of variation of the Hugoniot of a water and compacted dry tuff composite ($F = 0.15$). These observations are based on calculations in which the material models for the components are non-linear volumetric fluids. From the discussion in Section 5.4 it is clear that the corresponding curves for thermodynamic fluid components may not enclose the equilibrium Hugoniot states of the composite.

6.3 WAVE PROPAGATION TRANSVERSE TO PARALLEL PORES

6.3.1 Computer Solution

The 2-D Lagrangian CRAM code has also been used to calculate the propagation of a step pulse through a compacted tuff matrix with periodic parallel pores that are filled with water, Fig. 6.11(a). The water and tuff responses are again described by the non-linear volumetric fluid models used in Section 6.2, and the pulse is generated by imposing the velocity loading given by Eq. (6.6). The periodicity normal to the direction of propagation is the same as for the laminated structures that have been considered, $\Lambda = 0.1$ cm. The sides of the square cross of the pores are $a = 0.05$ cm and the periodicity in the transverse direction is selected, $\lambda = 0.084$ cm, so that the mass fraction of the water is the same as for the laminated structure, $F = 0.15$. The anticipated equilibrium velocity and amplitude of the shock front are given by Eq. (5.24).

The planes of symmetry of the composite section treated, corresponding to the $k = 1$ and $k = 10$ grid lines in the CRAM finite difference mesh, were treated as reflective boundaries, Fig. 6.11(b). The plane separating the water/tuff region from the tuff region was treated as a slip surface to permit relative motion between the two regions and to minimize attendant zone distortion.

The calculated velocity field plots shown in Fig. 6.12 show the effect of the passage of the shock front over a pore. The first plot, Fig. 6.12(a) shows the upward motion of the tuff when the shock front first reaches the pores. The flow is later directed downward when the wave crosses the pore, Fig. 6.12(b). This upward and downward flow occurs at each pore, Fig. 6.12(c), resulting in a periodic

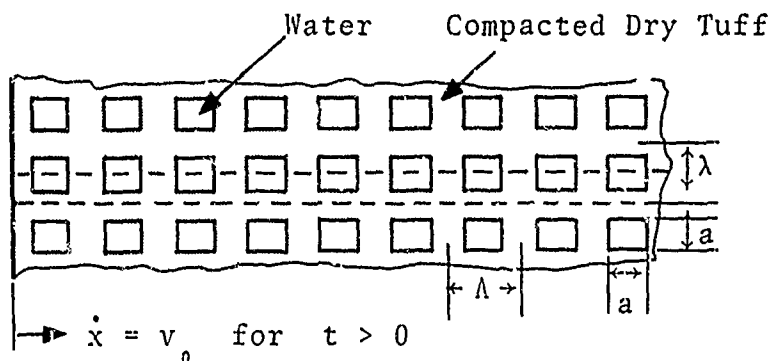


Fig. 6.11(a)

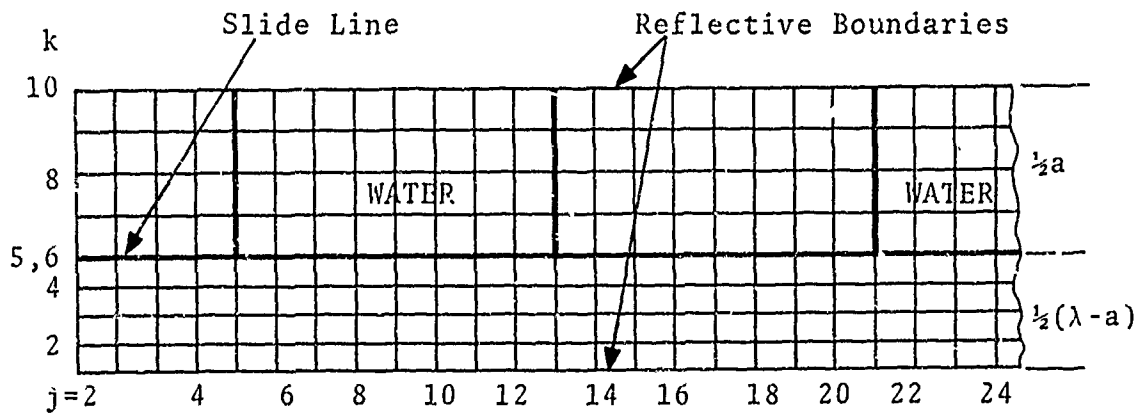


Fig. 6.11(b)

Fig. 6.11--Composite configuration consisting of periodic water-filled pores in a matrix of compacted dry tuff. The symmetric section denoted by the dashed lines in (a) are covered by the grid in (b) for the CRAM calculations.

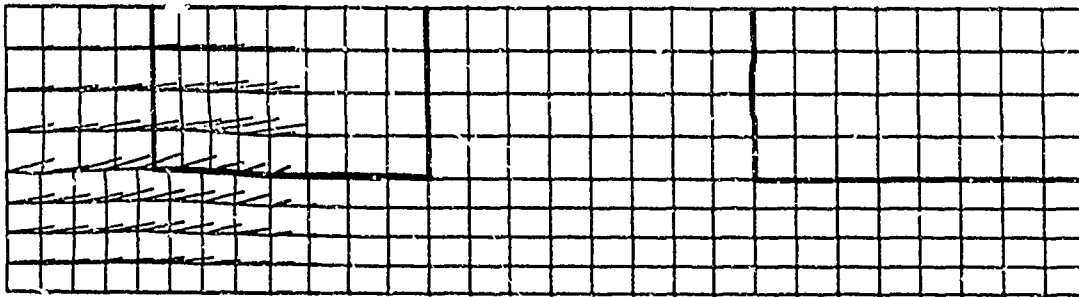


Fig. 6.12(a)-- $t = 0.127 \mu\text{sec.}$

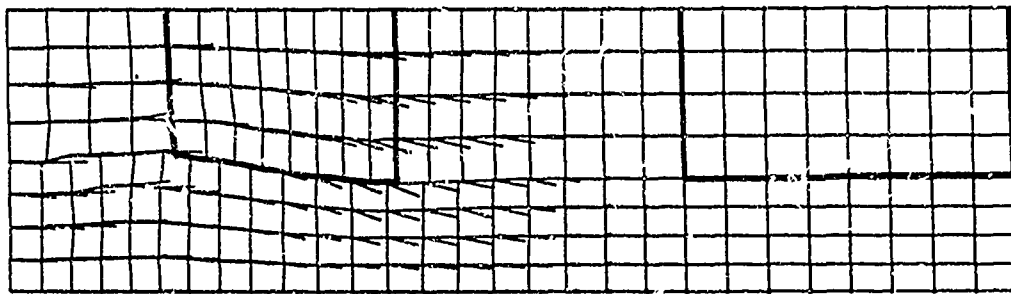


Fig. 6.12(b)-- $t = 0.270 \mu\text{sec.}$

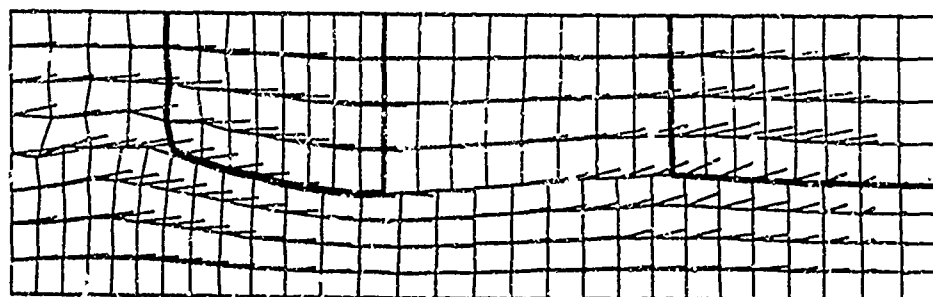


Fig. 6.12(c)-- $t = 0.416 \mu\text{sec.}$

Fig. 6.12--Velocity field calculated with the CRAM code at three instants during the passage of the shock front over a water-filled pore in tuff matrix.

undulating deformation of the composite in the wake of the shock front. This condition is further illustrated in the sequence of CRAM grid plots in Fig. 6.13.

The pressure profiles along the two reflective planes of the symmetric section of the composite are shown in Fig. 6.14 at two instants. The oscillations are essentially centered at the equilibrium value and the wave front is located near the point calculated from $D_{wt} = 0.367 \text{ cm}/\mu\text{sec}$. In Fig. 6.14(b) the wave front has enveloped four pores and the spatial period of the oscillations behind the front are about half that distance, 2Λ . This was also the case for the corresponding 1-D problem, Fig. 5.14.

The spatial periodicity of the oscillations is more apparent in the plots of the particle velocity profiles in the planes of symmetry, Fig. 6.15. The particle velocities are plotted against the j-line number in order to more easily locate the interfaces between the tuff and water/tuff sections of the pore configuration. The average of these two particle velocities for the composite and the expected mean particle velocity are superposed in the CRAM plots.

The temporal variation of the pressure on the velocity loading surface is shown in Fig. 6.16 at the two corners of the symmetrical section. The period of about $0.4 \mu\text{sec}$ is reasonably close to the value computed for the corresponding laminated structure, Fig. 5.15.

6.3.2 Periodicity of Oscillations

The similarity of the residual oscillations in the 1-D and 2-D periodic composites arises from their common equilibrium conditions behind the shock front, Eq. (5.24), and their equal structural periods, $\Lambda = 0.1 \text{ cm}$. Brillouin⁽⁶⁵⁾ has presented methods of detailed analysis of periodic linear structures based on the solution of differential-difference

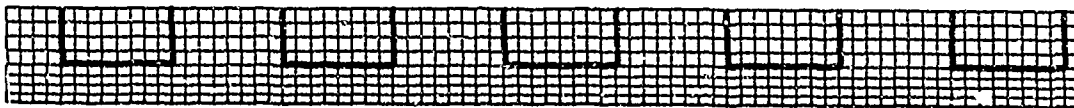


Fig. 6.13(a)-- $t = 0$

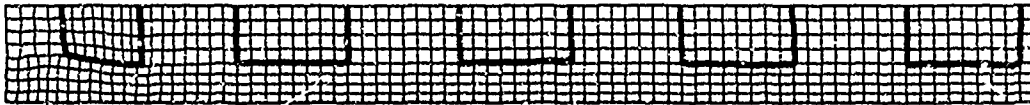


Fig. 6.13(b)-- $t = 0.270 \text{ μsec.}$



Fig. 6.13(c)-- $t = 0.556 \text{ μsec.}$

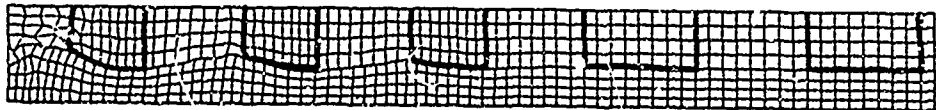


Fig. 6.13(d)-- $t = 0.830 \text{ μsec.}$



Fig. 6.13(e)-- $t = 1.097 \text{ μsec.}$

Fig. 6.13--CRAM finite-difference grid at five instants in the calculation for the periodic pore configuration.

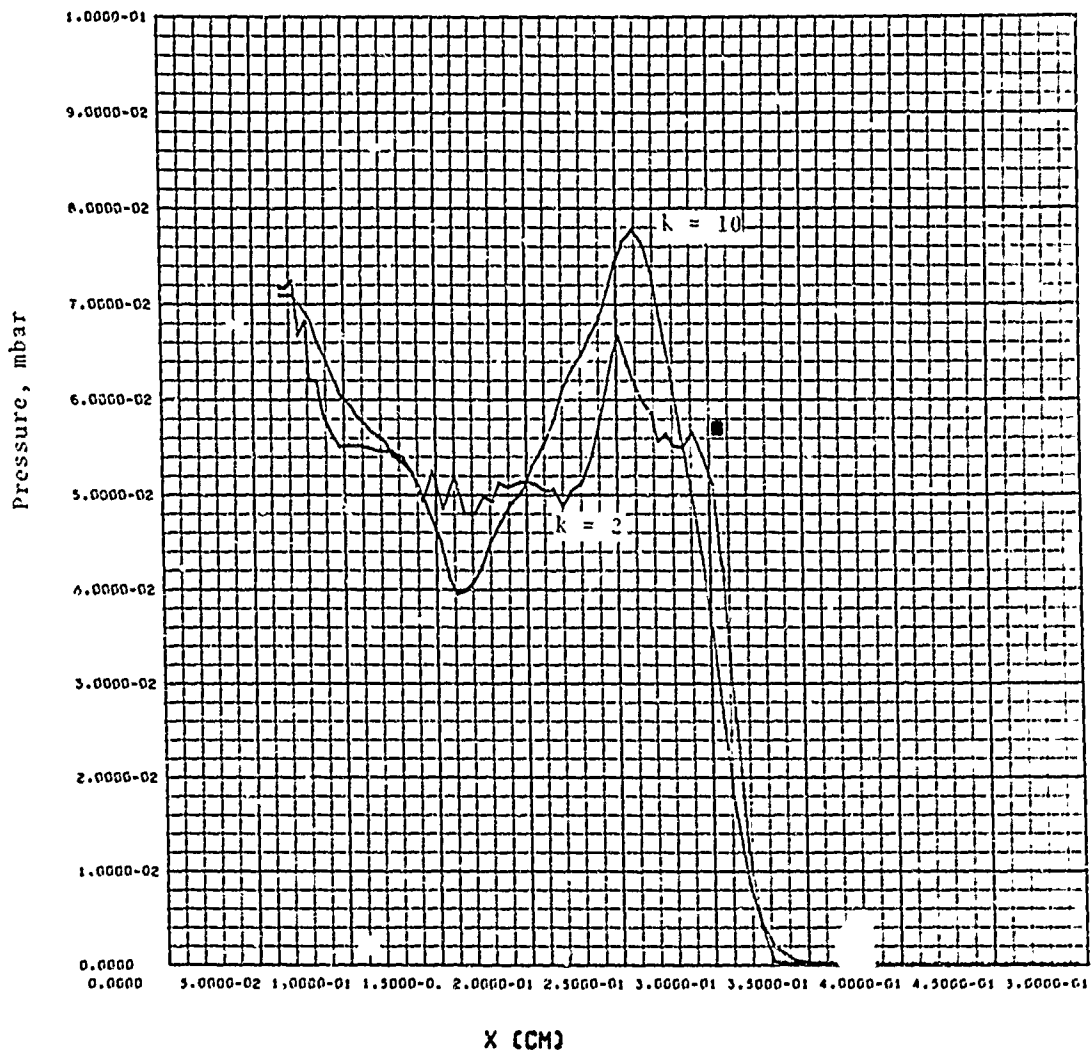


Fig. 6.14(a) -- $t = 0.83 \mu\text{sec}$

Fig. 6.14--Pressure profiles in the symmetry planes in the composite pore configuration at the indicated times. The magnitude and locations of the shock indicated by the point corresponds to a homogenized wet tuff medium.

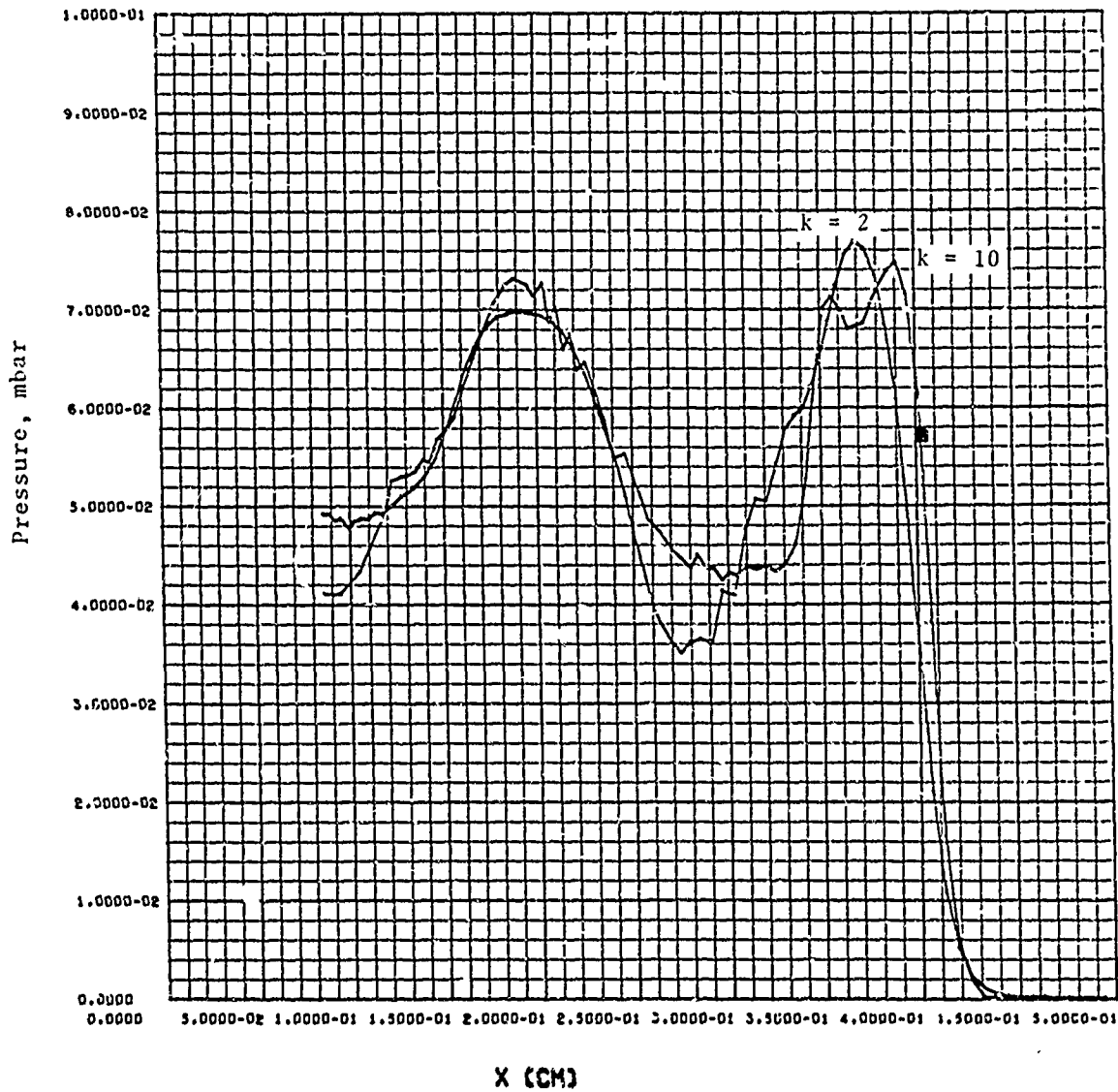


Fig. 6.14(b) -- $t = 1.10 \mu\text{sec}$

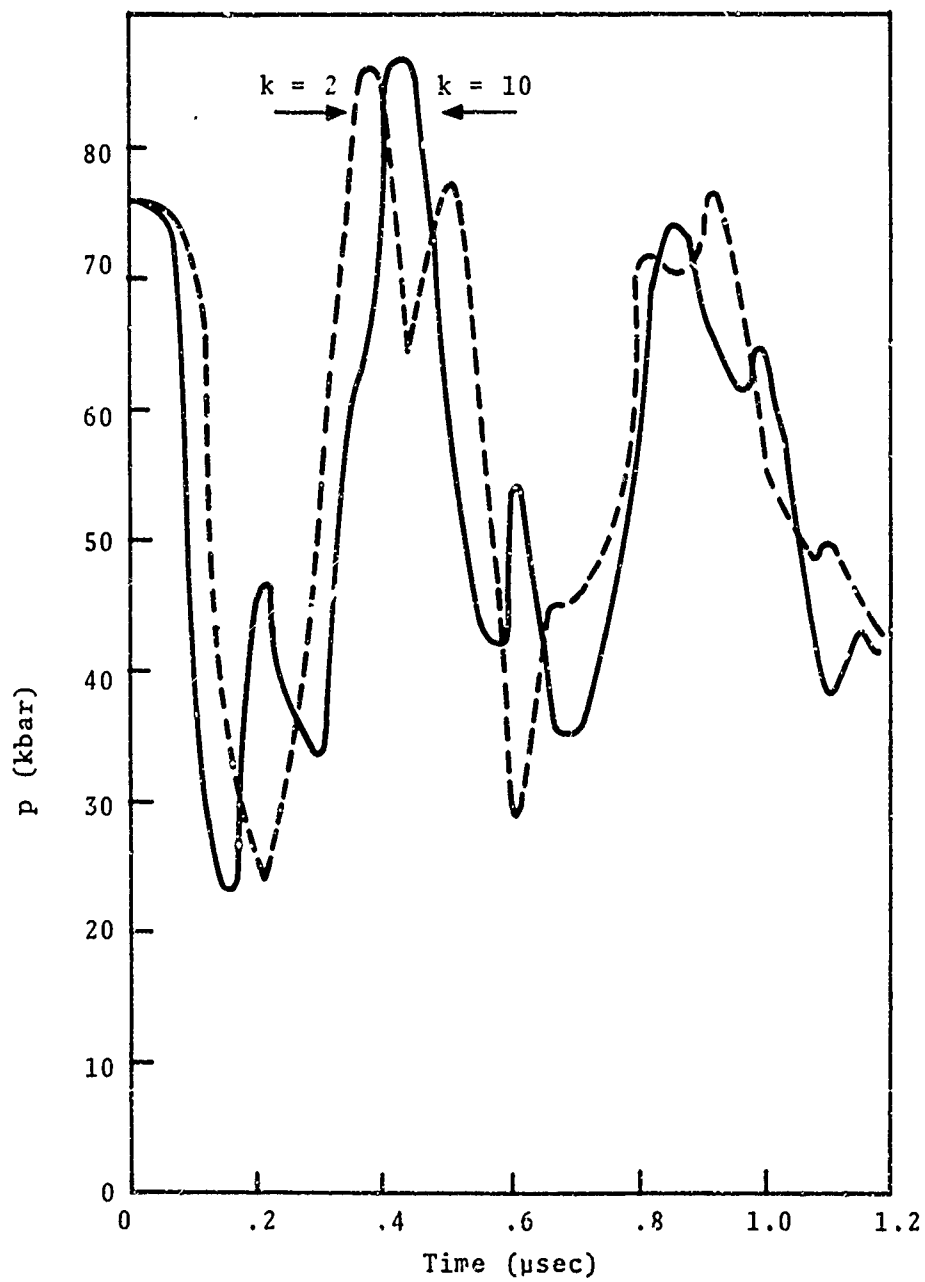


Fig. 6.16--Time variation of the pressure at the two left-hand corners of the symmetrical section of the periodic pore configuration treated with the CRAM code.

equations. Even if the composite is considered as linear, however, the presence of two densities and two elastic moduli would further complicate the methods presented by Brillouin. For this reason an intuitive explanation of the periodicity is given below, though it is perhaps less convincing than an explanation based on a detailed solution of differential-difference equations for periodic structures.

The mean density and sound speed in the water and compacted tuff, corresponding to the equilibrium pressure $p_e = 57.1$ kbar, may be computed from Eqs. (2.11) and (3.3) respectively:

$$\text{Water: } \bar{\rho}_{f_1} = 1.516 \text{ g/cc} \quad \bar{c}_{f_1} = 0.511 \text{ cm}/\mu\text{sec} \quad (6.7)$$

$$\text{Tuff: } \bar{\rho}_{f_2} = 2.85 \text{ g/cc} \quad \bar{c}_{f_2} = 0.390 \text{ cm}/\mu\text{sec}$$

The corresponding values of laminate thickness, bulk modulus $\bar{A} = \bar{\rho} \bar{c}^2$, and "spring constant" $\bar{K} = \bar{A}/\bar{h}$ are

$$\bar{h}_{f_1} = 0.0196 \text{ cm} \quad \bar{A}_{f_1} = 394 \text{ kbar} \quad \bar{K}_{f_1} = 20.1 \text{ kbar/cm} \quad (6.8)$$

$$\bar{h}_{f_2} = 0.0592 \text{ cm} \quad \bar{A}_{f_2} = 433 \text{ kbar} \quad \bar{K}_{f_2} = 7.3 \text{ kbar/cm}$$

In the neighborhood of the equilibrium state the water is stiffer than the tuff. Consequently, the simplest oscillation will be one which the main motion is in the tuff, corresponding to a spatial periodicity of $2(\bar{h}_{f_1} + \bar{h}_{f_2}) \sim 2\lambda$, Fig. 6.17(a). The approximate deflection from the equilibrium state associated with this mode of vibration is represented in Fig. 6.17(b).

The oscillatory strain energy and kinetic energy resident in the symmetric section

$$0 < x < \frac{1}{2}(\bar{h}_{f_1} + \bar{h}_{f_2}) \quad (6.9)$$

may be estimated from the assumed deflection curve, Fig. 6.17(b),

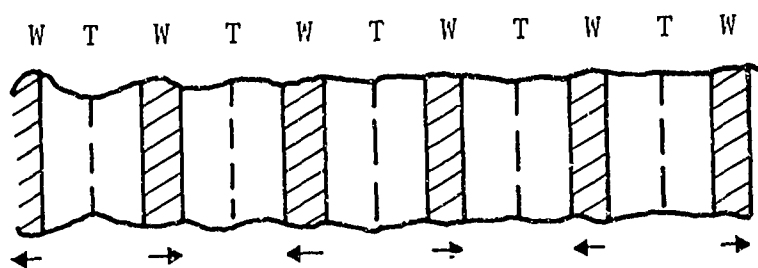


Fig. 6.17(a)

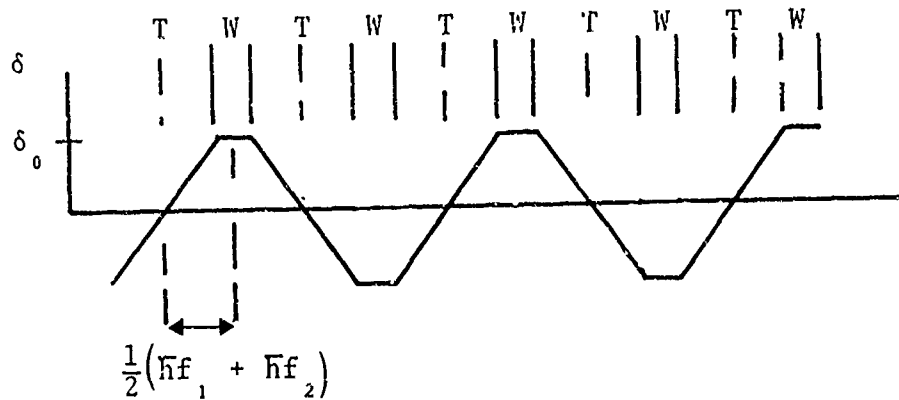


Fig. 6.17(b)

Fig. 6.17--Principal mode of vibration about equilibrium state of 1-D and 2-D periodic water/tuff composites.

$$\delta = \frac{2x}{\bar{h}_{f_2}} \delta_0, \quad \dot{\delta} = \frac{2x}{\bar{h}_{f_2}} \dot{\delta}_0, \quad 0 < x < \frac{1}{2} \bar{h}_{f_2} \quad (6.10)$$

$$\delta = \delta_0, \quad \dot{\delta} = \dot{\delta}_0 \quad \bar{h}_{f_2} < x < \frac{1}{2}(\bar{h}_{f_1} + \bar{h}_{f_2})$$

The corresponding energy components are given by

$$U = k_{f_2} \delta_0^2 \quad (6.11)$$

$$\begin{aligned} K &= \frac{1}{4} m_1 \dot{\delta}_0^2 + \frac{1}{2} \int_0^{\frac{1}{2} \bar{h}_{f_2}} \bar{\rho}_{f_2} \dot{\delta}^2 dx \\ &= \frac{1}{4} \dot{\delta}_0^2 (m_1 + m_2/3) \end{aligned} \quad (6.12)$$

where $m_1 = 0.0297$ g and $m_2 = 0.169$ g are the mass per unit area of the water and tuff laminates. For the linear idealization the total oscillatory energy is conserved, $d(K+U)/dt = 0$, and one obtains

$$\ddot{\delta}_0 + \frac{4 k_{f_2}}{m_1 + m_2/3} \delta_0 = 0 \quad (6.13)$$

The corresponding approximate temporal period of oscillation is

$$\pi \sqrt{\frac{m_1 + m_2/3}{k_{f_2}}} = \pi \sqrt{\frac{.086}{7.3 \times 10^{12}}} = 0.34 \times 10^{-6} \text{ sec} \quad (6.14)$$

An improved approximation can be obtained by replacing k_{f_2} in Eq. (6.14) by the effective spring constant for k_{f_1}

and \bar{K}_{f_2} in series,

$$k = \frac{1}{\frac{1}{\bar{K}_{f_1}} + \frac{1}{\bar{K}_{f_2}}} = 5.1 \text{ kbar/cm}$$

Then the estimated period of oscillation would be 0.41×10^{-6} sec which is as close to the periods calculated for the 1-D (SKIPPER) and 2D (CRAM) composites as one would expect for this crude treatment.

VII. THEORY OF INTERACTING CONTINUA*

7.1 INTRODUCTION

For geologic materials, a practical analytical model must provide an average description of the effects of the constituents, rather than a detailed description of the stress field at each material interface at each instant. It was this basic consideration that led us to concentrate this part of the work towards modifying and applying the theory of interacting continua, or the continuum theory of mixtures, to analyze gross wave propagation and dispersion effects. In the theory of interacting continua, it is assumed that every point of the medium is occupied by a particle of each constituent. Simplified theories were used in the early treatments of diffusion, and these have been presented and compared by Truesdell.⁽⁶⁶⁾ To investigate the propagation of finite amplitude waves, a fuller thermodynamic theory is needed, at least as the basis for empirical assumptions. Various mechanical treatments of acoustic (small amplitude) propagation in porous media have been made—see, for example, Biot⁽⁶⁷⁾—but the more recent development of (irreversible) continuum thermodynamics for finite deformation has initiated applications within the theory of interacting continua.

One approach, Green and Naghdi,^(68,69) is to emphasize the mean properties and motion of the mixture, including interaction forces but not incorporating the individual constituent motions. On this basis, constitutive equations for fluid flow through an elastic solid have been developed by Crochet and Naghdi,⁽⁷⁰⁾ and Green and Steel.⁽⁷¹⁾ Alternatively, the detailed properties and motions of each constituent may be incorporated, and a number of such theories have been recently presented: Green and Naghdi,⁽⁷²⁾ Bowen,⁽⁷³⁾

* Authors: L. W. Morland and S. K. Garg

Müller,⁽⁷⁴⁾ Dunwoody and Müller.⁽⁷⁵⁾ There are conceptual differences between the different authors. These differences arise in the meaning of partial stress and total stress, the interaction contributions to energy and entropy, and the form of the entropy production inequality, including the role of temperature. While an elastic solid-fluid mixture has received some attention, previous references, a more realistic study of finite amplitude ground motions should attempt to describe hysteresis effects by a plasticity or soil mechanics model for the solid constituent. In this first contract period, a purely mechanical model, excluding thermal effects, has been investigated, and in particular the propagation of plane uni-axial waves analyzed to assess the significant features of the model.

Because the theory of interacting continua has apparently not been previously applied to calculate finite amplitude stress wave effects for geologic materials, the general theoretical framework is described in detail in Section 7.2. Some readers may wish only to scan this lengthy section for basic concepts and the concluding discussion. Constitutive laws for a purely mechanical model are formulated in Section 7.3 which relate the partial stresses in the solid material and the fluid constituents to the deformation history of the two constituents. In addition, an interactive body force accounting for the diffusion of the fluid through the pores of the solid matrix is formulated. In Section 7.4 the formulation is specialized to the plane wave case and in Section 7.5 the constitutive laws are specifically adopted to describe completely saturated wet tuff. A finite difference computer code, described in Section 7.6, is implemented to calculate uni-axial wave propagation effects in Section 7.7.

7.2 EQUATIONS OF THEORY OF INTERACTING CONTINUA

In many situations a body of material contains several constituent materials, each preserving its own identity but so diffused through the mixture that every region of space occupied by the mixture, however small on the macroscopic scale, contains some of each constituent. Examples are mixtures of gases, of liquids, of gases and liquids, and of gases and liquids in porous solids. In these situations it is not practical to discuss particle paths for each constituent separately and determine which particle occupies any point of the mixture at a given time. Instead the postulate is made that every point of the mixture body is occupied at every time by a particle of each constituent $\delta^{(\alpha)}$ ($\alpha = 1, \dots, r$). Further, each constituent $\delta^{(\alpha)}$ has a velocity field $\underline{v}^{(\alpha)}(\underline{x}, t)$ through the mixture, where \underline{x} denotes position vector in space (with respect to a fixed Newtonian frame) and t denotes time. In practice $\underline{v}^{(\alpha)}(\underline{x}, t)$ must be interpreted as a mean velocity of $\delta^{(\alpha)}$ particles in some small neighborhood of \underline{x} at time t . The mass of constituent $\delta^{(\alpha)}$ per unit volume of mixture is called its partial density $\rho^{(\alpha)}(\underline{x}, t)$, and the total mass per unit volume of mixture $\rho(\underline{x}, t)$ is given by

$$\rho = \sum \rho^{(\alpha)} . \quad (7.1)$$

Summation will always denote over $\alpha = 1, \dots, r$. Mass concentrations $c^{(\alpha)}(\underline{x}, t)$ may also be defined:

$$c^{(\alpha)} = \rho^{(\alpha)} / \rho , \quad \sum c^{(\alpha)} = 1 . \quad (7.2)$$

Mass production per unit time of $\delta^{(\alpha)}$ is allowed, due to chemical interaction between the constituents, and is denoted

by $\rho_m^{(\alpha)}$ per unit volume of mixture. Results for inert mixtures ($\rho_m^{(\alpha)} = \rho, \alpha = 1, \dots, r$) will also be recorded since they are simpler and will be appropriate to many practical situations.

Let V be any fixed region of space occupied by mixtures at time t , with smooth bounding surface S and outward normal (unit) \underline{n} as shown in Fig. 7.1. The action of

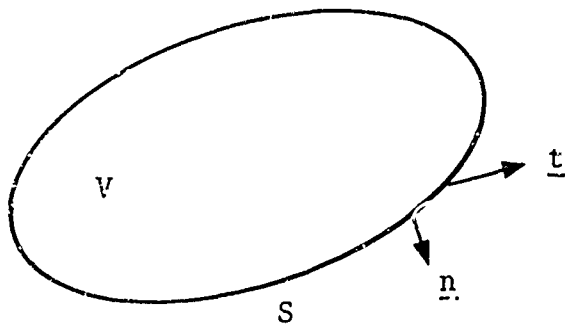


Fig. 7.1--Space region V occupied by mixture

surrounding material on material in V is assumed to be equivalent to a continuously distributed stress vector $\underline{t}(\underline{x}, t)$, defining force per unit area, over S (singular surfaces may be treated and appropriate jump conditions determined analogous to a single constituent theory). It is now postulated that this total stress on S (per unit area) is supported between all the constituents in some division, and defining the partial stress on $\rho_m^{(\alpha)}$ as $\underline{t}^{(\alpha)}(\underline{x}, t)$, that is, the force on $\rho_m^{(\alpha)}$ per unit area of mixture surface, then

$$\underline{t} = \sum \underline{t}^{(\alpha)}. \quad (7.3)$$

This contrasts with a definition of total stress given by

Truesdell,⁽⁷⁶⁾ based on momentum balance for the mixture. The two forms will be compared later. In addition, there is a body force per unit mass of each constituent, $\underline{b}^{(\alpha)}$, due to the external world, for example a gravity attraction, together with interaction body forces $\underline{\beta}^{(\alpha)}$ per unit mass of mixture due to all other constituents. Here these will be assumed to incorporate momentum transfer due to the mass exchange, although Eringen and Ingram⁽⁷⁷⁾ choose to separate the latter from the direct diffusive force. The same separation is made between diffusive couple and angular momentum transfer due to mass exchange. However, constitutive assumptions must ultimately be made for the total quantities, and the separation does not help. Here then $\underline{G}^{(\alpha)}$ denotes the interaction couple on $\underline{s}^{(\alpha)}$ due to all other constituents per unit mass of mixture, and $\underline{\psi}^{(\alpha)}$ denotes the interaction energy transfer to $\underline{s}^{(\alpha)}$ per unit mass of mixture. Heat sources and fluxes will be introduced later. It is convenient to express the interaction couple in terms of an antisymmetric tensor $\underline{\lambda}^{(\alpha)}$ by

$$G_i^{(\alpha)} = \epsilon_{ijk} \lambda_{jk}^{(\alpha)}, \quad \lambda_{ij}^{(\alpha)} = \frac{1}{2} \epsilon_{ijk} G_k^{(\alpha)}, \quad (7.4)^*$$

referred to rectangular Cartesian coordinates.

* Note that

$$\left\{ \begin{array}{l} \epsilon_{ijk} \neq 0 \text{ if and only if } i, j, k \text{ distinct} \\ = 1 \text{ if } i, j, k \text{ in cyclic order} \\ \quad (i, j, k \text{ distinct}) \\ = -1 \text{ if } i, j, k \text{ not in cyclic order} \\ \quad (i, j, k \text{ distinct}) \end{array} \right.$$

Thus, Eq. 7.4(a) $\rightarrow G_x = \lambda_{yz} - \lambda_{zy} = 2\lambda_{yz}$; $G_y = 2\lambda_{zx}$, $G_z = 2\lambda_{xy}$, and hence Eq. 7.4(b).

Mass balance for the constituent $\delta^{(\alpha)}$ instantaneously occupying region V in Fig. 7.1 states that the rate of $\delta^{(\alpha)}$ mass increase inside V plus the $\delta^{(\alpha)}$ mass flux out across S is equal to the rate of $\delta^{(\alpha)}$ mass production inside V , thus

$$\int_V \frac{\partial \rho^{(\alpha)}}{\partial t} dV + \int_S \rho^{(\alpha)} \underline{v} \cdot \underline{n} dS = \int_V m^{(\alpha)} dV . \quad (7.5)$$

Applying the divergence theorem to the surface integral, and assuming all integrands are continuous (the integral law leads directly to the jump condition across a singular surface by the usual "pill-box" argument), leads, on letting $V \rightarrow 0$, to the point form

$$\frac{\partial \rho^{(\alpha)}}{\partial t} + \text{div} \left(\rho^{(\alpha)} \underline{v} \right) = m^{(\alpha)} . \quad (7.6)$$

Introducing the $\delta^{(\alpha)}$ material derivative (time rate of change following an $\delta^{(\alpha)}$ particle)

$$\frac{D^{(\alpha)}}{Dt} = \frac{\partial}{\partial t} + \underline{v} \cdot \text{grad} , \quad = \frac{\partial}{\partial t} + v_j \frac{\partial}{\partial x_j} , \quad (7.7)$$

where x_j ($j = 1, 2, 3$) denotes rectangular Cartesian coordinates, (7.6) may be written

$$\frac{D^{(\alpha)} \rho^{(\alpha)}}{Dt} + \rho^{(\alpha)} \text{div} \underline{v} = m^{(\alpha)} . \quad (7.8)$$

Summing (7.6) over the r constituents and noting that there is no net mass production gives

$$\sum m^{(\alpha)} = 0, \quad \frac{\partial}{\partial t} \sum \rho^{(\alpha)} + \text{div} \sum \rho^{(\alpha)} \underline{v} = 0 . \quad (7.9)$$

Recalling (7.1), (7.9) may be written in the forms

$$\frac{\partial \rho}{\partial t} + \operatorname{div} \rho \underline{v} = 0, \quad \frac{D\rho}{Dt} + \rho \operatorname{div} \underline{v} = 0 \quad (7.10)$$

if a mass average or barycentric velocity \underline{v} and a barycentric rate of change are defined by

$$\rho \underline{v} = \sum^{(\alpha)} \rho^{(\alpha)} \underline{v}^{(\alpha)}, \quad \frac{D}{Dt} = \frac{\partial}{\partial t} + \underline{v} \cdot \operatorname{grad}. \quad (7.11)$$

Now (7.10) describes the mass balance of a body with density ρ and velocity \underline{v} , and \underline{v} is commonly regarded as a velocity of a mixture body (in some mean sense), but it should be noted that there is no mixture body (same set of particles) occupying continuously changing continuous configurations since in general the different constituents are separating by diffusion. A diffusion velocity $\underline{u}^{(\alpha)}(\underline{x}, t)$ of $\delta^{(\alpha)}$ is defined by

$$\underline{u}^{(\alpha)} = \underline{v}^{(\alpha)} - \underline{v}, \quad (7.12)$$

giving the relations

$$\frac{D^{(\alpha)}}{Dt} = \frac{D}{Dt} + \underline{u}^{(\alpha)} \cdot \operatorname{grad}, \quad \sum^{(\alpha)} \rho^{(\alpha)} \underline{u}^{(\alpha)} = 0. \quad (7.13)$$

In particular, with no $\delta^{(\alpha)}$ mass production, $\frac{d^{(\alpha)}}{m} = 0$, (7.6), (7.8) become

$$\frac{\partial \rho^{(\alpha)}}{\partial t} + \operatorname{div} \left(\rho^{(\alpha)} \underline{v}^{(\alpha)} \right) = 0, \quad \frac{D^{(\alpha)} \rho^{(\alpha)}}{Dt} + \rho^{(\alpha)} \operatorname{div} \underline{v}^{(\alpha)} = 0. \quad (7.8')$$

Momentum balance for the $\delta^{(\alpha)}$ constituent instantaneously occupying V states that the rate of increase of $\delta^{(\alpha)}$ momentum inside V plus the flux of $\delta^{(\alpha)}$ momentum out

across S is equal to the total force acting on $\delta^{(\alpha)}$ inside V , thus

$$\begin{aligned} \int_V \frac{\partial}{\partial t} \left(\frac{(\alpha)(\alpha)}{\rho} \underline{v} \right) dV + \int_S \frac{(\alpha)(\alpha)}{\rho} \underline{v} \left(\underline{v} \cdot \underline{n} \right) dS \\ = \int_S \underline{t} dS + \int_V \left(\frac{(\alpha)(\alpha)}{\rho} \underline{b} + \rho \underline{\beta} \right) dV . \end{aligned} \quad (7.14)$$

The interaction body force $\underline{\beta}^{(\alpha)}$ may also be interpreted as the rate of $\delta^{(\alpha)}$ momentum production due to interaction with the other constituents per unit mass of mixture.

Applying the divergence theorem to the first surface integral and using (7.7) shows that

$$\begin{aligned} \int_V \left\{ \frac{D}{Dt} \left(\frac{(\alpha)(\alpha)}{\rho} \underline{v} \right) + \frac{(\alpha)(\alpha)}{\rho} \underline{v} \operatorname{div} \underline{v} - \frac{(\alpha)(\alpha)}{\rho} \underline{b} - \rho \underline{\beta} \right\} dV \\ = \int_S \underline{t} dS . \end{aligned} \quad (7.15)$$

Taking a shrinking sequence of tetrahedrons for V in the usual way, and assuming the integrands are continuous and bounded, establishes the existence of a partial stress tensor $\underline{\underline{\sigma}}^{(\alpha)}$ such that

$$\underline{t} = \underline{\underline{\sigma}} \underline{n} , \quad t_i = \sigma_{ij} n_j \quad (7.16)$$

where \underline{n} is the unit outward normal to the surface element acted on by \underline{t} . Note the difference between (7.16) and a common convention $\underline{t} = \underline{\underline{\sigma}}^T \underline{n}$ where $\underline{\underline{\sigma}}^T$ is the transpose of $\underline{\underline{\sigma}}$. Here σ_{ij} denotes the stress component in the x_i -direction on the surface element with outward normal in the x_j -direction.

Substituting (7.16) into the surface integral of (7.15), applying the divergence theorem and assuming continuity of integrands leads to the point form

$$\frac{(\alpha)}{D} \left(\frac{(\alpha)}{\rho} \frac{(\alpha)}{v} \right) + \frac{(\alpha)}{\rho} \underline{v} \operatorname{div} \underline{v} - \frac{(\alpha)}{\rho} \underline{b} - \rho \underline{\beta} = \operatorname{div} \underline{\sigma} \quad (7.17)$$

where

$$\left[\operatorname{div} \underline{\sigma} \right]_i = \frac{\partial \sigma_{ij}}{\partial x_j} \quad (7.18)$$

On using (7.8), (7.17) may be written

$$\frac{(\alpha)}{\rho} \frac{(\alpha)}{D} \frac{(\alpha)}{v} = \operatorname{div} \underline{\sigma} + \frac{(\alpha)}{\rho} \underline{b} + \rho \underline{\beta} - \frac{(\alpha)}{m} \underline{v} \quad (7.19)$$

In particular, when $\frac{(\alpha)}{m} = 0$,

$$\frac{(\alpha)}{\rho} \frac{(\alpha)}{D} \frac{(\alpha)}{v} = \operatorname{div} \underline{\sigma} + \frac{(\alpha)}{\rho} \underline{b} + \rho \underline{\beta}, \quad (7.19')$$

and $\underline{\beta}$ is purely a diffusive interaction. Defining the total external body force per unit mass of mixture as \underline{b} , given by

$$\rho \underline{b} = \sum \frac{(\alpha)}{\rho} \underline{b}, \quad (7.20)$$

then the momentum balance for the mixture as a whole is obtained by summing the contributions to (7.14) from each constituent in the absence of interaction force contributions, thus

$$\sum \underline{\beta} = 0, \quad (7.21)$$

and the reduction to point form analogous to the derivation of (7.19) gives

$$\sum \left(\rho^{(\alpha)} \frac{D^{(\alpha)} \underline{v}}{Dt} + \frac{(\alpha)}{m} \underline{v} \right) = \text{div } \underline{\sigma} + \rho \underline{b}. \quad (7.22)$$

Here $\underline{\sigma}$ is the total stress tensor which from (7.13), (7.16) satisfies

$$\underline{\sigma} = \sum^{(\alpha)} \underline{\sigma}^{(\alpha)}, \quad \underline{t} = \underline{\sigma} \underline{n}. \quad (7.23)$$

Some algebraic manipulation and use of (7.8), (7.13), (7.11), (7.12), and (7.10) reduces (7.22) to

$$\rho \frac{Dv_i}{Dt} = \rho b_i + \frac{\partial}{\partial x_j} \left\{ \sigma_{ij} - \sum \rho^{(\alpha)} u_i^{(\alpha)} u_j^{(\alpha)} \right\}, \quad (7.24)$$

which has the usual form if a total stress tensor $\underline{\sigma}^*$ is defined by

$$\sigma_{ij}^* = \sigma_{ij} - \sum \rho^{(\alpha)} u_i^{(\alpha)} u_j^{(\alpha)}, \quad \underline{\sigma}^* = \underline{\sigma} - \sum \rho^{(\alpha)} \underline{u}^{(\alpha)} \otimes \underline{u}^{(\alpha)}. \quad (7.25)$$

Truesdell⁽⁷⁶⁾ uses this basis for defining a total stress $\underline{\sigma}^*$, but since a stress boundary condition would relate directly to the total stress vector \underline{t} used in (7.3), the stress tensor $\underline{\sigma}$ defined in (7.23) has direct physical significance while $\underline{\sigma}^*$ involves also the diffusive motion. There seems little point in introducing $\underline{\sigma}^*$.

Angular momentum balance for the constituent $\delta^{(\alpha)}$ instantaneously occupying V states that the rate of increase of $\delta^{(\alpha)}$ angular momentum inside V plus the flux of $\delta^{(\alpha)}$ angular momentum out across S is equal to the total

couple acting on $\overset{(\alpha)}{s}$ inside V , thus

$$\begin{aligned} & \int_V \frac{\partial}{\partial t} \left(\overset{(\alpha)}{\rho} \epsilon_{ijk} x_j \overset{(\alpha)}{v}_k \right) dV + \int_S \overset{(\alpha)}{\rho} \epsilon_{ijk} x_j \overset{(\alpha)}{v}_k \left(\underline{v} \cdot \underline{n} \right) dS \\ &= \int_S \epsilon_{ijk} x_j \overset{(\alpha)}{t}_k dS + \int_V \epsilon_{ijk} \left(\overset{(\alpha)}{\rho} x_j \overset{(\alpha)}{b}_k + \rho x_j \overset{(\alpha)}{\beta}_k \right. \\ & \quad \left. + \overset{(\alpha)}{\rho} \lambda_{jk} \right) dV . \end{aligned} \quad (7.26)^*$$

Here the interaction couple $\overset{(\alpha)}{G}$ (or rate of production of $\overset{(\alpha)}{s}$ angular momentum per unit mass of mixture) has been expressed in terms of the antisymmetric tensor $\overset{(\alpha)}{\lambda}$ by (7.4), and no external body couple is included. Expressing $\underline{t}^{(\alpha)}$ in terms of the stress tensor $\overset{(\alpha)}{\sigma}$ by (7.16) and applying the divergence theorem to the surface integrals and using (7.8) allows (7.26) to be written as

$$\begin{aligned} \epsilon_{ijk} \int_V \left\{ x_j \left[\overset{(\alpha)}{\rho} \frac{D \overset{(\alpha)}{v}_k}{Dt} + \overset{(\alpha)}{m} \overset{(\alpha)}{v}_k - \overset{(\alpha)}{\rho} \overset{(\alpha)}{b}_k - \overset{(\alpha)}{\beta}_k - \frac{\partial \overset{(\alpha)}{\sigma}_{kl}}{\partial x_l} \right] \right. \\ \left. - \overset{(\alpha)}{\sigma}_{kj} - \overset{(\alpha)}{\rho} \lambda_{jk} \right\} dV = 0 . \end{aligned} \quad (7.27)$$

Since the quantity in the bracket [] vanishes identically by the momentum balance (7.19), with the integrand continuous, (7.27) leads to the point form

$$\epsilon_{ijk} \left(\overset{(\alpha)}{\sigma}_{kj} + \overset{(\alpha)}{\rho} \lambda_{jk} \right) = 0 \quad (i = 1, 2, 3) . \quad (7.28)$$

* Angular momentum in vector notation is $\underline{r} \times \underline{v}$. In tensor notation, it is written as $\epsilon_{ijk} x_j \overset{(\alpha)}{v}_k$, where ϵ_{ijk} has been defined previously.

This implies that $\underline{\sigma}^{(\alpha)} + \rho \underline{\lambda}^{(\alpha)T} = \underline{\sigma}^{(\alpha)T} + \rho \underline{\lambda}^{(\alpha)}$, $= \underline{\sigma}^{(\alpha)T} - \rho \underline{\lambda}^{(\alpha)T}$ since $\underline{\lambda}^{(\alpha)}$ is antisymmetric. That is,

$$\sigma_{[ij]}^{(\alpha)} = \frac{1}{2} \left[\sigma_{ij}^{(\alpha)} - \sigma_{ji}^{(\alpha)} \right] = \rho \lambda_{ij}^{(\alpha)}, \quad (7.29)$$

which determines the (non-zero) antisymmetric part of $\underline{\sigma}^{(\alpha)}$. Angular momentum balance for the mixture as a whole is given by the sum of the contributions in (7.26) from each constituent in the absence of the interaction couples, and leads to

$$\sum \lambda_{ij}^{(\alpha)} = 0, \quad \underline{\sigma} = \underline{\sigma}^T. \quad (7.30)$$

That is, the total stress tensor is symmetric (recall the absence of an external body couple). The result (7.29) is independent of $\underline{m}^{(\alpha)}$ and so applies when there is no $\underline{\delta}^{(\alpha)}$ mass production.

Energy balance for the $\underline{\delta}^{(\alpha)}$ constituent instantaneously occupying V states that the rate of increase inside V plus flux out across S of the internal (stored) energy plus kinetic energy of $\underline{\delta}^{(\alpha)}$ is equal to the rate of working of body forces inside V and surface forces on S plus the rate of heat supply inside V and heat flux in across S on $\underline{\delta}^{(\alpha)}$. Let $U^{(\alpha)}$ denote the internal energy per unit mass of $\underline{\delta}^{(\alpha)}$, $r^{(\alpha)}$ the external heat supply to $\underline{\delta}^{(\alpha)}$ per unit mass, and $\psi^{(\alpha)}$ the interaction energy supply to $\underline{\delta}^{(\alpha)}$ per unit mass of mixture from other constituents. Let $\underline{q}^{(\alpha)}$ be the heat flux vector within $\underline{\delta}^{(\alpha)}$, so that $\underline{q}^{(\alpha)} \cdot \underline{n}$ defines the heat flux across unit surface area in the direction of the unit normal \underline{n} carried by $\underline{\delta}^{(\alpha)}$, and let $\underline{q}^{(\hat{\alpha})}$ denote the interaction energy flux into $\underline{\delta}^{(\alpha)}$ from other constituents. Introducing the symmetric and antisymmetric parts of the

velocity gradient tensor, namely the stretching $\underline{\underline{d}}^{(\alpha)}$ and spin $\underline{\underline{\omega}}^{(\alpha)}$, given by

$$\underline{\underline{L}}_{ij}^{(\alpha)} = \frac{\partial v_i^{(\alpha)}}{\partial x_j}, \quad \underline{\underline{d}}^{(\alpha)} = \frac{1}{2} \left(\underline{\underline{L}}^{(\alpha)} + \underline{\underline{L}}^{(\alpha)T} \right), \quad \underline{\underline{\omega}}^{(\alpha)} = \frac{1}{2} \left(\underline{\underline{L}}^{(\alpha)} - \underline{\underline{L}}^{(\alpha)T} \right) \quad (7.31)$$

the energy balance becomes

$$\begin{aligned} & \int_V \frac{\partial}{\partial t} \left(\rho^{(\alpha)} \left[U + \frac{1}{2} \underline{\underline{v}} \cdot \underline{\underline{v}} \right] \right) dV + \int_S \rho^{(\alpha)} \left[U + \frac{1}{2} \underline{\underline{v}} \cdot \underline{\underline{v}} \right] \underline{\underline{v}} \cdot \underline{\underline{n}} dS \\ &= \int_V \left\{ \rho^{(\alpha)} \underline{\underline{b}} \cdot \underline{\underline{v}} + \rho^{(\alpha)} \underline{\underline{r}} + \rho^{(\alpha)} \underline{\underline{\beta}} \cdot \underline{\underline{v}} + \rho^{(\alpha)} \text{tr} \left(\underline{\underline{\lambda}} \underline{\underline{\omega}} \right) + \rho^{(\alpha)} \psi \right\} dV \\ &+ \int_S \left\{ \underline{\underline{t}} \cdot \underline{\underline{v}} - \left(\underline{\underline{q}} + \underline{\underline{q}} \right) \cdot \underline{\underline{n}} \right\} dS. \end{aligned} \quad (7.32)$$

Applying the divergence theorem and using (7.7), (7.16), (7.19), (7.29), (7.31), together with integrand continuity, leads to the point form

$$\begin{aligned} & \frac{D^{(\alpha)}}{Dt} \left(\rho^{(\alpha)} \left[U + \frac{1}{2} \underline{\underline{v}} \cdot \underline{\underline{v}} \right] \right) + \rho^{(\alpha)} \left[U + \frac{1}{2} \underline{\underline{v}} \cdot \underline{\underline{v}} \right] \text{div} \underline{\underline{v}} \\ &= \rho^{(\alpha)} \underline{\underline{r}} + \rho^{(\alpha)} \psi + \frac{1}{2} \rho^{(\alpha)} \frac{D^{(\alpha)}}{Dt} \left(\underline{\underline{v}} \cdot \underline{\underline{v}} \right) + \frac{\rho^{(\alpha)} \underline{\underline{\beta}} \cdot \underline{\underline{v}}}{m} \\ &+ \text{tr} \left(\underline{\underline{\sigma}}^T \underline{\underline{d}} \right) - \text{div} \left(\underline{\underline{q}} + \underline{\underline{q}} \right). \end{aligned} \quad (7.33)$$

Using (7.8) and noting $\text{tr}(\underline{\underline{\sigma}}^T \underline{\underline{d}}) = \text{tr}(\underline{\underline{\sigma}} \underline{\underline{d}})$ since $\underline{\underline{d}}$ is symmetric,

$$\begin{aligned} \rho \frac{(\alpha)}{D} \frac{(\alpha)}{U} + \frac{(\alpha)}{m} \left((\alpha) U - \frac{1}{2} (\alpha) \underline{\underline{v}} \cdot \underline{\underline{v}} \right) &= \frac{(\alpha)}{\rho} r + \rho \psi \\ &+ \text{tr} \left(\underline{\underline{\sigma}} \underline{\underline{d}} \right) - \text{div} \left(\underline{\underline{q}} + \underline{\underline{\hat{q}}} \right). \end{aligned} \quad (7.34)$$

Summing the contributions to (7.32) from each constituent determines the energy balance for the mixture provided that the interaction terms, which make no net contribution, are absent. In point form, the vanishing of this net interaction contribution becomes

$$\sum_{\phi}^{(\alpha)} = \sum \left\{ \rho \left[\underline{\underline{\beta}} \cdot \underline{\underline{v}} + \text{tr} \left(\underline{\underline{\lambda}} \underline{\underline{\omega}} \right) + \psi \right] - \text{div} \underline{\underline{\hat{q}}} \right\} = 0, \quad (7.35)$$

and the mixture energy balance is

$$\begin{aligned} \sum \left\{ \rho \frac{(\alpha)}{D} \frac{(\alpha)}{U} + \frac{(\alpha)}{m} \left((\alpha) U - \frac{1}{2} (\alpha) \underline{\underline{v}} \cdot \underline{\underline{v}} \right) - \frac{(\alpha)}{\rho} r + \text{div} \underline{\underline{q}} \right. \\ \left. - \text{tr} \left[\underline{\underline{\sigma}}^T \left(\underline{\underline{d}} + \underline{\underline{\omega}} \right) \right] \right\} = 0. \end{aligned} \quad (7.36)$$

$\phi^{(\alpha)}$ represents the interaction energy supply to $\delta^{(\alpha)}$ per unit volume of mixture, and (7.35) provides one restriction on the contributing quantities. For the case $m^{(\alpha)} = 0$, the constituent energy balance (7.34) becomes

$$\rho \frac{(\alpha)}{D} \frac{(\alpha)}{U} = \frac{(\alpha)}{\rho} r + \rho \psi + \text{tr} \left(\underline{\underline{\sigma}} \underline{\underline{d}} \right) - \text{div} \left(\underline{\underline{q}} + \underline{\underline{\hat{q}}} \right). \quad (7.37)$$

For each constituent $\delta^{(\alpha)}$ we have the mass balance equation (7.8), three momentum balance equations (7.19), three

angular momentum balance equations (7.29), and an energy balance equation (7.34), giving a total of $8r$ balance equations. The quantities to be determined for each constituent are $\rho^{(\alpha)}$, $m^{(\alpha)}$, three components of $\underline{v}^{(\alpha)}$, nine components of $\underline{\sigma}^{(\alpha)}$, three components of $\underline{\beta}^{(\alpha)}$, three components of $\underline{\lambda}^{(\alpha)}$, $\underline{U}^{(\alpha)}$, three components of $\left(\underline{q}^{(\alpha)} + \underline{\hat{q}}^{(\alpha)}\right)$, $\underline{\psi}^{(\alpha)}$, and the temperature $\theta^{(\alpha)}$ which, though not explicitly arising in the balance equation, will arise in the heat flux law (in general). That is, $26r$ quantities, but recall the restrictions (7.9), (7.21), (7.30), (7.35)—eight in total—arising from the balance laws for the mixture as a whole, showing that $26r-8$ quantities only need be found and the set then completed by the restrictions. Alternatively, the balance laws and restrictions provide $8r+8$ equations for $26r$ quantities. To obtain a balance of equation and unknowns (the usual criterion for a consistent theory) it is required to prescribe $18r-8$ constitutive equations (material properties). This is accomplished by postulating functional relations for $m^{(\alpha)}$ ($r-1$); $\underline{\sigma}^{(\alpha)}$ ($6r$), $\underline{\beta}^{(\alpha)}$ ($3r-3$), $\underline{\lambda}^{(\alpha)}$ ($3r-3$), $\underline{U}^{(\alpha)}$ (r), $\underline{q}^{(\alpha)} + \underline{\hat{q}}^{(\alpha)}$ ($3r$) and $\underline{\psi}^{(\alpha)}$ ($r-1$) in terms of the $\rho^{(\alpha)}$, $\underline{v}^{(\alpha)}$, $\theta^{(\alpha)}$ and quantities derived from these, for example deformation gradients, velocity gradients, and temperature gradients. Prescription of the $\underline{\lambda}^{(\alpha)}$ could be included by prescribing $9r$ components of the $\underline{\sigma}^{(\alpha)}$ subject to the three restrictions. Note that the quantities $\underline{b}^{(\alpha)}$, $\underline{r}^{(\alpha)}$ not discussed above are governed by external environment.

If all constituents have a common temperature $\theta \equiv \theta^{(\alpha)}$, each α , then $r-1$ quantities are eliminated. In this situation, the $r-1$ independent interaction energy supplies $\underline{\psi}^{(\alpha)}$ cannot be prescribed separately, and must be regarded as arising to maintain the common temperature, and will be determined by (7.34), (7.35). Further, for isothermal conditions $\theta \equiv \text{const}$ (prescribed), so that all temperature derivatives vanish, the energy balance (7.34) serves to

determine the $U^{(\alpha)}$ once the 20r quantities $\rho^{(\alpha)}$, $m^{(\alpha)}$, $v^{(\alpha)}$, $\underline{\sigma}^{(\alpha)}$, $\underline{\beta}^{(\alpha)}$, $\underline{\lambda}^{(\alpha)}$ are determined by the 7r balance laws (energy balance excluded), 7 restrictions and 13r-7 constitutive equations for the $m^{(\alpha)}$, $\underline{\sigma}^{(\alpha)}$, $\underline{\beta}^{(\alpha)}$, in terms of kinematic quantities and a fixed temperature parameter. This is therefore a mechanical theory with reference to temperature only as a parameter which defines a family of mechanical constitutive laws. For an adiabatic theory (for example in wave motions when heat conduction time scales are supposed large compared with pulse times), each $q^{(\alpha)} = 0$ and, in the same spirit $\underline{q}^{(\alpha)} = 0$, but there is less motive for setting $\psi^{(\alpha)} = 0$. However, provided that the remaining quantities in (7.34), $U^{(\alpha)}$, $m^{(\alpha)}$, $\underline{\sigma}^{(\alpha)}$ depend only on the temperatures, and not gradients, of all $\theta^{(\alpha)}$, then (7.34) for all α in principle determines the $\theta^{(\alpha)}$ in terms of mechanical quantities and temperature may be eliminated to leave a mechanical theory.

The functional relations describing the constitutive response of the material must satisfy the principle of material frame indifference, that is, be independent of the observer. By observer is meant a rigid frame, defined, say, by a triad of orthogonal vectors, and a clock, and a change of frame is a time dependent rigid rotation and time dependent origin translation. Thus, denoting quantities in a second frame by *,

$$\underline{x}^* = Q(t)\underline{x} + \underline{c}(t), \quad QQ^T = \underline{1}, \quad \det Q = +1. \quad (7.38)$$

The change of time origin, $t^* = t+a$, is neglected as this just shows that t should not occur as an explicit argument in the functionals. Here Q is a proper orthogonal transformation representing rotation and excluding a change from right to left-handed axes; this restriction is not made by

Truesdell⁽⁷⁸⁾ but in many situations the inclusion of $\det Q = -1$ does not impose additional restrictions on the functionals. The meaning of (7.38) is that

$$\underline{x}^* = x_i \underline{e}_i^* , \quad \underline{x} = x_i \underline{e}_i , \quad \underline{e}_i^* = Q^T \underline{e}_i \quad (7.39)$$

in the absence of the translation $\underline{c}(t)$, where $\underline{e}_i, \underline{e}_i^*$ are the triads of unit orthogonal base vectors in the two frames, and x_i, x_i^* the respective components of $\underline{x}, \underline{x}^*$. The physical assertions are that $\binom{(\alpha)}{m}, U, \psi$ are frame indifferent scalars, that is, have the same value in all frames:

$$\binom{(\alpha)}{m}^* = \binom{(\alpha)}{m}, \text{ etc.} \quad (7.40)$$

and $\underline{n}, \binom{(\alpha)}{t}, \binom{(\alpha)}{\underline{\beta}}, \binom{(\alpha)}{\underline{q}}, \binom{(\hat{\alpha})}{\underline{q}}$ are frame indifferent vectors, that is, have a given magnitude and direction with respect to some fixed frame. Since any vector \underline{d} may be expressed in the form $\underline{x}_2 - \underline{x}_1$, representing a line segment between two points x_1, x_2 , then if \underline{d} is frame indifferent \underline{d}^* is the line segment between the same points, given by $\underline{x}_2^* - \underline{x}_1^*$. Thus, from (7.38)

$$\underline{d}^* = Q \underline{d} . \quad (7.41)$$

Since both \underline{n} and $\binom{(\alpha)}{t}$ are frame indifferent vectors and $\binom{(\alpha)}{t} = \binom{(\alpha)}{\underline{\sigma}} \underline{n}$, $\binom{(\alpha)}{\underline{\sigma}}$ is defined to be a frame indifferent second order tensor, and from (6.41) satisfies

$$\binom{(\alpha)}{\underline{\sigma}}^* = Q \binom{(\alpha)}{\underline{\sigma}} Q^T . \quad (7.42)$$

In passing note that particle velocities $\binom{(\alpha)}{v}$ are not frame indifferent vectors and the spins $\binom{(\alpha)}{\underline{\omega}}$ are not frame indifferent tensors. Applying the restrictions (7.40), (7.41), (7.42) to the appropriate quantities provides some limitations

on the forms of functional dependence permitted. The case of a simple material is described by Truesdell.⁽⁷⁸⁾

Further restrictions on the constitutive functionals are obtained by invoking a "second law of thermodynamics." In the case of a single constituent there is not complete agreement on the form (and meaning) of the axiomatized entropy production inequality—contrast Truesdell⁽⁷⁸⁾ and Meixner⁽⁷⁹⁾—and certainly no direct physical interpretation of entropy during an irreversible motion. For mixtures the situation is even more tenuous. Should each constituent have its own entropy or merely the mixture as a whole, does the inequality apply separately to each constituent or just to the mixture as a whole, are first queries. Then, what are the roles of $\frac{(\hat{\alpha})}{q} / \theta$, $\frac{(\hat{\alpha})}{\psi} / \theta$ —are they contributions to entropy flux? Different viewpoints have been adopted by Green and Nagdi,^(68,72) Bowen,⁽⁷³⁾ Müller,⁽⁷⁴⁾ Dunwoody and Müller⁽⁷⁵⁾ for example. Having formulated an entropy production inequality it is asserted that it must be satisfied by all admissible thermodynamic processes, that is, processes satisfying all the balance laws but allowing arbitrary body force and heat supply. However, even the simple theories, for example, a mixture of inviscid fluids with no mass exchange, are still left in a complex form at this point, and it would seem more fruitful to investigate simple models on the basis of empirical evidence, perhaps applicable to particular situations. Mechanical theories of diffusion of fluids through elastic solids have been given by Adkins^(80,81) and Green and Adkins.⁽⁸²⁾

As far as possible the constitutive laws for the $\delta^{(\alpha)}$ constituent should reflect the character of that material existing as a single continuum if the identity of the materials composing the mixture is to be preserved. However, while the interaction terms $\frac{(\alpha)}{m}$, $\frac{(\alpha)}{\beta}$, $\frac{(\alpha)}{\lambda}$, $\frac{(\alpha)}{\psi}$, $\frac{(\hat{\alpha})}{q}$ allow

the $\rho^{(\alpha)}$ equations to depend on the motion and thermal changes in the other constituents, there is a case for insisting that the relations between the partial stress $\sigma^{(\alpha)}$ and the motion of $\rho^{(\alpha)}$ should also be influenced by the other constituents, and similarly for $\bar{u}^{(\alpha)}$, $\bar{q}^{(\alpha)}$. Recall that the partial stress is defined as force per unit area of mixture surface as each constituent is supposed to occupy the entire mixture space, which suggests that the effective stress carried by $\rho^{(\alpha)}$ should be the partial stress appropriately scaled to account for an effective area of cross-section of $\rho^{(\alpha)}$ per unit area of mixture. Similarly, effective density changes of $\rho^{(\alpha)}$ will be given by scaling the partial density changes to allow for effective volume occupied by $\rho^{(\alpha)}$ per unit volume of mixture. To some extent these two new concepts introduced—effective area and effective volume—will depend on the motions (deformations) of all constituents, and a minimal interaction can be incorporated by postulating that the laws holding for $\rho^{(\alpha)}$ as a single continuum should apply to the effective stress, effective density, effective heat flux. Postulates are then required for the two scaling functions. This idea will be developed for mixtures of simple materials on a purely mechanical basis and very restrictive assumptions for the latter postulates. Applications to mixtures of ideal fluids in elastic and plastic-plastic solids under simple deformations are made.

7.3 CONSTITUTIVE LAWS FOR INTERACTING CONTINUA

7.3.1 Formulation of Mechanical Theory

In order to describe the behavior of a (partially) saturated porous solid under dynamic conditions within the framework of a mechanical theory of mixtures (appropriate to isothermal or adiabatic motions), it is necessary to lay down constitutive laws relating the partial stresses in each of the constituents to the deformation history of both (in general) constituents. In addition, a similar law for the interaction body force is required. While the principle of material frame indifference provides some restrictions on the form of the kinematic quantities which may occur in these laws, even for mixtures of isotropic elastic solids and ideal fluids the restricted forms are far too general to fit to available empirical data. We are primarily concerned with finite deformation for which material properties are described in terms of response functions of several arguments, not constant moduli as in linearized approximations.

It is desirable that the individual constitutive laws should reflect the character of the respective materials as single continua if their identity in the mixture is to be preserved. Since the theory of interacting continua postulates that each point is occupied by a particle of each constituent, the basic formulation eliminates all reference to actual mean volume $n^{(\alpha)}$ occupied by $\delta^{(\alpha)}$ per unit volume of mixture, and to actual area of cross-section $M^{(\alpha)}$ per unit cross-section of mixture. Hence, effective densities $\rho^{(\alpha)e}$ and effective stress tensors $\underline{\sigma}^{(\alpha)e}$ are not considered. Conceptually they may be defined in terms of the partial densities $\rho^{(\alpha)}$ and partial stresses $\underline{\sigma}^{(\alpha)}$ by the scaled relations

$$\rho^{(\alpha)} = n^{(\alpha)} \rho^{(\alpha)e}, \quad \underline{\sigma}^{(\alpha)} = M^{(\alpha)} \underline{\sigma}^{(\alpha)e} \quad (\alpha = 1, \dots, r), \quad (7.43)$$

where

$$\sum^{(\alpha)} n = 1, \quad \sum^{(\alpha)} M = 1, \quad 0 \leq n \leq 1, \quad 0 \leq M \leq 1, \quad (7.44)$$

and summation over $\alpha = 1, \dots, r$ is implied. Such scaling is, of course, conceptual, and serves only to introduce the factors $^{(\alpha)}n$, $^{(\alpha)}M$. However, on this basis, a simple model for the mixture can be formulated by assuming the constitutive law for each $^{(\alpha)}s$ as a single-continuum to relate $^{(\alpha)}\sigma^e$ to $^{(\alpha)}\rho^e$ and the isochoric deformation associated with the constituent displacement field $^{(\alpha)}\underline{u}$, the latter unchanged by the volume scaling. This will be called a "dilatation adjusted model." Further interaction through the shear response may be present, but the dilatation interaction is conceptually clearer and will be adopted as a preliminary model for data fitting and wave propagation studies. It should be noted that additional interactions may be incorporated in the interaction body force, but for the initial wave studies in a porous solid containing ideal fluid, a simple diffusive resistance will be assumed.

To develop our model we will focus attention on simple materials exhibiting no explicit time dependence in their response, and in particular on elastic materials (solid or fluid) for which the stress $^{(\alpha)}\sigma^e$ depends only on the current deformation gradient $^{(\alpha)}\underline{F}$ with respect to some reference configuration. History dependence through a scalar parameter such as mean plastic strain or plastic work can be incorporated similarly. If $^{(\alpha)}\underline{X}$ denotes an $^{(\alpha)}s$ particle position in the reference configuration, then in rectangular Cartesian spatial coordinates x_i ($i = 1, 2, 3$), the deformation (motion) of $^{(\alpha)}s$ is described by

$$x_i = ^{(\alpha)}\chi_i \left(^{(\alpha)}\underline{X}, t \right), \quad (7.45)$$

and the deformation gradient is

$${}^{(\alpha)}_{F_{ij}} = \frac{\partial x_i}{\partial X_j} = \delta_{ij} + \frac{\partial u_i}{\partial X_j} \quad (7.46)$$

where δ_{ij} is the Krönecker delta. Mass conservation for ${}^{(\alpha)}_{s}$ (in the absence of mass transfer between constituents due to chemical interaction) requires

$$\frac{(\alpha)}{\rho} J = \frac{(\alpha)}{\rho_0} \quad (7.47)$$

where $\frac{(\alpha)}{\rho_0}$ is the initial partial density and

$$J = \left| \det \left(\frac{(\alpha)}{F} \right) \right|, > 0, \quad (7.48)$$

is the Jacobian of the deformation. A partial density preserving deformation satisfies

$$J \equiv 1. \quad (7.49)$$

Now we may regard the deformation $\frac{(\alpha)}{F}$ as a density preserving deformation $\frac{(\alpha)}{F}^*$ followed by a uniform dilatation J^{-1} ; thus

$$\frac{(\alpha)}{F} = \left\{ \frac{(\alpha)}{J} \right\}^{-1/3} \underline{1} \frac{(\alpha)}{F}^* = \left\{ \frac{(\alpha)}{J} \right\}^{-1/3} \frac{(\alpha)}{F}^*, \quad (7.50)$$

where $\underline{1}$ is the unit tensor. $\frac{(\alpha)}{F}^*$ is defined uniquely by (7.50) and by construction measures the shear deformation. The dilatation adjusted model defines an effective deformation $\frac{(\alpha)}{F}^e$ by

$$\frac{(\alpha)}{F}^e = \left\{ \frac{(\alpha)}{J} \right\}^{-1/3} \frac{(\alpha)}{F}^*, \quad \frac{(\alpha)}{J}^e = \frac{\frac{(\alpha)}{\rho_0} e}{\frac{(\alpha)}{\rho} e} = \frac{\frac{(\alpha)}{n}}{\frac{(\alpha)}{n_0}} \frac{(\alpha)}{J}, \quad (7.51)$$

where n_0 is the initial value of n , and so

$$\tilde{F}^{(\alpha)} e = \left(\frac{n^{(\alpha)}}{n_0^{(\alpha)}} \right)^{1/3} \tilde{F}^{(\alpha)}. \quad (7.52)$$

Then, if the constitutive law for $\delta^{(\alpha)}$ as a single continuum is expressed by

$$\tilde{\sigma}^{(\alpha)} = g_0^{(\alpha)}(\tilde{F}), \quad (7.53)$$

where the response function $g_0^{(\alpha)}$ applies to a reference configuration with initial density ρ_0 , within the mixture the constitutive law for $\delta^{(\alpha)}$ becomes

$$\tilde{\sigma}^{(\alpha)} = \frac{(\alpha)}{M} g_0^{(\alpha)} \left[\left(\frac{n^{(\alpha)}}{n_0^{(\alpha)}} \right)^{1/3} \tilde{F}^{(\alpha)} \right]. \quad (7.54)$$

Thermal expansion effects could be incorporated similarly.

For example, an ideal fluid in isolation satisfies the constitutive law

$$\tilde{\sigma} = p(\rho_0/\rho) \underline{\underline{1}} = -p(J) \underline{\underline{1}}, \quad (7.55)$$

so within the mixture the model predicts a law

$$\tilde{\sigma} = Mp \left(\frac{n}{n_0} \frac{\rho_0}{\rho} \right) \underline{\underline{1}}. \quad (7.56)$$

An isotropic elastic solid is described by

$$\tilde{\sigma} = \phi_0(I_k) \underline{\underline{1}} + \phi_1(I_k) \underline{\underline{B}} + \phi_2(I_k) \underline{\underline{B}}^2 \quad (7.57)$$

where $\tilde{B} = \tilde{F} \tilde{F}^T$ (\tilde{F}^T denotes the transpose of \tilde{F}), ϕ_0, ϕ_1, ϕ_2 are the response functions and I_k ($k = 1, 2, 3$) are the invariants of \tilde{B} :

$$I_1 = \text{tr } \tilde{B}, \quad I_2 = I_3 \text{tr } \tilde{B}^{-1}, \quad I_3 = \det \tilde{B} = J^2, \quad (7.58)$$

where $\text{tr } \tilde{B}$ denotes B_{jj} and \tilde{B}^{-1} is the inverse of \tilde{B} .

Now

$$\begin{aligned} \tilde{B}^e &= \left(\frac{n}{n_0} \right)^{2/3} \tilde{B}, & I_1^e &= \left(\frac{n}{n_0} \right)^{2/3} I_1, & I_2^e &= \left(\frac{n}{n_0} \right)^{4/3} I_2, \\ I_3^e &= \left(\frac{n}{n_0} \right) I_3, \end{aligned} \quad (7.59)$$

so within the mixture the partial stress is given by

$$\tilde{\tau} = M \left\{ \phi_0 \left(I_k^e \right) \tilde{1} + \phi_1 \left(I_k^e \right) \left(\frac{n}{n_0} \right)^{2/3} \tilde{B} + \phi_2 \left(I_k^e \right) \left(\frac{n}{n_0} \right)^{4/3} \tilde{B}^2 \right\}. \quad (7.60)$$

The above description is only complete when the factors $\binom{(\alpha)}{n}$ and $\binom{(\alpha)}{M}$ are prescribed for each constituent and these are constitutive functions for the mixture, specifically describing the interaction. In general they could be functions of the deformations of all constituents (perhaps histories), but we will make the simple postulate that they depend on the current partial densities (changes):

$$\binom{(\alpha)}{M} = \binom{(\alpha)}{M} \binom{(\beta)}{J}, \quad \binom{(\alpha)}{n} = \binom{(\alpha)}{n} \binom{(\beta)}{J} \quad (\alpha, \beta=1, \dots, r). \quad (7.61)$$

This is in accord with the simple concept of interaction only through dilatations. If further we make the restriction that each area scaling $\binom{(\alpha)}{M}$ depends on the dilatations only through the volume scaling of the same constituent, with the same

dependence for each constituent, then

$$M^{(\alpha)} = f\left(\begin{matrix} (\alpha) \\ n \end{matrix}\right), \quad f(0) = 0. \quad (7.62)$$

It now follows, using (6.44), that

$$M = \sum_n \begin{matrix} (\alpha) \\ n \end{matrix}. \quad (7.63)^\dagger$$

The relations (7.61) and (7.63) will be adopted as a preliminary description of the interaction, so that it remains to determine the single set of functions $\begin{matrix} (\alpha) \\ n \end{matrix} \begin{matrix} (\beta) \\ J \end{matrix}$, subject to (known) initial structure of the mixture. That is, in the unstressed state we prescribe the effective densities $\begin{matrix} (\alpha) \\ \rho_0 \end{matrix} e$ and, say, the partial densities (part by mass) $\begin{matrix} (\alpha) \\ \rho_0 \end{matrix}$, so that $\begin{matrix} (\alpha) \\ n_0 \end{matrix}$ is determined by (7.43).

To discuss the determination of the $\begin{matrix} (\alpha) \\ n \end{matrix} \begin{matrix} (\beta) \\ J \end{matrix}$ let us focus on a binary mixture ($\alpha = 1, 2$), and write

$$\begin{matrix} (1) \\ n \end{matrix} \begin{matrix} (1) \\ J \end{matrix}, \begin{matrix} (2) \\ J \end{matrix} = n, \quad \begin{matrix} (2) \\ n \end{matrix} = 1-n, \quad (7.64)$$

so we are concerned with a single function n of two arguments. Now consider quasistatic tests such that, in the absence of external body force and supposing the interaction body force to be zero when diffusion is negligible, the stress, partial stresses, and constituent deformations are uniform through the mixture body. In particular the partial densities

[†]For each fixed s , $f\left(\begin{matrix} (s) \\ n \end{matrix}\right) + \sum_{\alpha \neq s} f\left(\begin{matrix} (\alpha) \\ n \end{matrix}\right) = 1$ where $\begin{matrix} (s) \\ n \end{matrix} = 1 - \sum_{\alpha \neq s} \begin{matrix} (\alpha) \\ n \end{matrix}$.

Thus $f\left(\begin{matrix} (s) \\ n \end{matrix}\right) = \sum_{\alpha \neq s} f\left(\begin{matrix} (\alpha) \\ n \end{matrix}\right)$ for all $\begin{matrix} (s) \\ n \end{matrix}, \begin{matrix} (\alpha) \\ n \end{matrix}$ subject to (7.44).

Hence, $f(n)$ is linear, and in view of $f(0) = 0$ and $\sum f\left(\begin{matrix} (\alpha) \\ n \end{matrix}\right) = 1$ the result (7.63) follows.

are uniform, and if there is no net diffusion from the body,

$$\frac{(\alpha)}{\rho} \equiv \frac{(\alpha)}{\rho_0} \quad (\alpha = 1, 2) \quad (7.65)^*$$

by mass conservation, and hence

$$\frac{(\alpha)}{J} = \frac{\rho_0}{\rho}, = J \quad (\alpha = 1, 2) . \quad (7.66)$$

That is, the partial dilatations of both constituents (or all constituents in general) are the same, equal to the mixture dilatation. Thus the argument of each $n^{(\alpha)}$, hence n , is the pair (J, J) , and it is convenient to define

$$n(J, J) = N(J) . \quad (7.67)$$

Quasistatic tests involve $n^{((1) (2))}$ only on the path $J^{(1)} = J^{(2)}$, but it is possible that in wave motions with small diffusion the dilatation pair $J^{(1)}, J^{(2)}$ will lie in some reasonably narrow strip containing this path, and that $n^{((1) (2))}$ can be expressed, say, in the form

$$n^{((1) (2))} = N\left(\frac{1}{2}[J^{(1)} + J^{(2)}]\right) + k\left(\frac{1}{2}[J^{(1)} - J^{(2)}]\right) \left(\frac{(2)}{J} - \frac{(1)}{J}\right) . \quad (7.68)$$

In principle, the function $k(J)$ would be determined by solutions for small disturbances superposed on equilibrium configurations with different dilatations J . Once $N(J)$ is known, magnitudes of $J^{(2)} - J^{(1)}$ can be estimated from simple wave propagation solutions using the leading term of (7.68) as an approximation to n .

*

$$\frac{(\alpha)}{J} = \frac{(\alpha)}{\rho_0} = \frac{(\alpha)M_0/V_0}{(\alpha)M/V} = V/V_0 \quad \left(\frac{(\alpha)}{M_0} = \frac{(\alpha)}{M}, \text{ no diffusion} \right)$$

Hence, etc.

7.3.2 Interacting Continua under Simple Deformations

First consider a mixture of isotropic elastic solid and ideal fluid described by (7.55) through (7.60), and denote the solid by $\alpha = 1$. In uniform dilatation with equal principal stretches λ , the solid deformation is given by

$$\underline{\underline{B}} = \lambda^2 \underline{\underline{1}}, \quad I_1 = 3\lambda^2, \quad I_2 = 3\lambda^4, \quad I_3 = \lambda^6 = J^2. \quad (7.69)$$

Writing $\underline{\underline{B}} = \underline{\underline{B}}(\lambda)$, it follows from (7.59), (7.69), that

$$\underline{\underline{B}}^{(1)} e = \underline{\underline{B}} \left[\left(\frac{n}{n_0} \right)^{1/3} \lambda \right], \quad (7.70)$$

whence by (7.60) and (7.63)

$$\frac{1}{3} \sigma_{kk}^{(1)} = - n p \left[\frac{n}{n_0} \lambda^3 \right] = - n p \left(\frac{n}{n_0} J \right), \quad (7.71)$$

where $p^{(1)}(J)$ is the pressure in the isolated elastic solid under uniform dilatation with Jacobian J . That is, the uniform dilatation response in the mixture is determined solely by the uniform dilatation response in isolation and n , anticipated by the definitions of n and effective deformation. Finally, for the ideal fluid, from (7.56)

$$\frac{1}{3} \sigma_{kk}^{(2)} = - (1-n) p \left(\frac{1-n}{1-n_0} J \right), \quad (7.72)$$

and the total mixture pressure is given by

$$\frac{1}{3} \sigma_{kk} = - n p \left(\frac{n}{n_0} J \right) - (1-n) p \left(\frac{1-n}{1-n_0} J \right). \quad (7.73)$$

From (7.66), (7.67), a quasistatic deformation of the mixture with no diffusion results in a pressure-dilatation response $p(J)$ where

$$p(J) = N(J) p^{(1)} \left[\frac{N(J)}{N_0} J \right] + [1 - N(J)] p^{(2)} \left[\frac{1-N(J)}{1-N_0} J \right]. \quad (7.74)$$

Thus, given $p^{(1)}(J)$, $p^{(2)}(J)$, (6.74) is an implicit equation for $N(J)$ subject to the initial condition $N(1) = N_0$. Alternatively, a constitutive postulate $N(J)$ will predict the mixture pressure $p(J)$ from $p^{(1)}(J)$, $p^{(2)}(J)$.

In case both constituents are fluids, it can be shown from hydrostatics that the effective pressures $p^{(1)e}$ and $p^{(2)e}$ must be the same. In this case, (7.74) may be replaced by

$$p^{(1)} \left[\frac{N}{N_0} J \right] = p^{(2)} \left[\frac{1-N}{1-N_0} J \right]. \quad (7.75)$$

Thus, given $p^{(1)}(J)$, $p^{(2)}(J)$, (6.75) is an implicit equation for $N(J)$. We will also investigate a "Minimal Principle" based on uniform dilatation response, namely, that for a given equilibrium Jacobian J the value $N(J)$ is such as to minimize the total pressure $p(J)$. That is, the effective density changes in the constituents adjusts to minimize $p(J)$.

Turning to uni-axial strain with longitudinal stretch λ_1 and unit stretch in the lateral directions, the dilatation is given by

$$J = \lambda_1. \quad (7.76)$$

The principal partial stresses in the ideal fluid, within the mixture, are equal, and given by

$$\sigma_1^{(2)} = \sigma_2^{(2)} = \sigma_3^{(2)} = -(1-n) p \left(\frac{1-n}{1-n_0} J^{(2)} \right) = -(1-n) p \left(\frac{1-n}{1-n_0} \lambda_1^{(2)} \right). \quad (7.77)$$

For the elastic solid the deformation invariants are

$$\begin{aligned} I_1^{(1)e} &= \left(\frac{n}{n_0} \right)^{2/3} (\lambda_1^2 + 2), & I_2^{(1)e} &= \left(\frac{n}{n_0} \right)^{4/3} (2\lambda_1^2 + 1), \\ I_3^{(1)e} &= \left(\frac{n}{n_0} \right)^2 \lambda_1^2, \end{aligned} \quad (7.78)$$

and the principal partial stresses are

$$\sigma_1^{(1)} = n \left\{ \phi_0 \left(\frac{(1)}{I_k} e \right) + \phi_1 \left(\frac{(1)}{I_k} e \right) \left(\frac{n}{n_0} \right)^{2/3} \lambda_1^2 + \phi_2 \left(\frac{(1)}{I_k} e \right) \left(\frac{n}{n_0} \right)^{4/3} \lambda_1^4 \right\}, \quad (7.79)$$

$$\sigma_2^{(1)} = \sigma_3^{(1)} = n \left\{ \phi_0 \left(\frac{(1)}{I_k} e \right) + \phi_1 \left(\frac{(1)}{I_k} e \right) \left(\frac{n}{n_0} \right)^{2/3} + \phi_2 \left(\frac{(1)}{I_k} e \right) \left(\frac{n}{n_0} \right)^{4/3} \right\}, \quad (7.80)$$

In view of (7.78) the elastic partial stress $\sigma_1^{(1)}$ within the mixture is not related simply to the respective stress in isolation, even if the response functions depend only on $\frac{(1)}{I_3}$, since λ_1 is still scaled by (n/n_0) and by $(n/n_0)^{1/3}$ in different terms. Thus longitudinal response of the solid is not sufficient to describe that of the mixture even when n is known, but the three separate response functions must be given.

Before leaving the isotropic elastic solid-ideal fluid mixture, let us note the linearized infinitesimal strain equations which are derived from (7.55) through (7.60) and

(7.63). Defining the infinitesimal strain tensor for the solid, $\underline{\epsilon}$, by

$$\epsilon_{ij} = \frac{1}{2} \left(\frac{\partial u_i}{\partial x_j} + \frac{\partial u_j}{\partial x_i} \right) \quad (7.81)$$

where \underline{u} is the displacement vector, then neglecting terms of order $\max(\epsilon_{ij})$ in comparison with unity,

$$\stackrel{(1)}{F}_{ij} = \delta_{ij} + \frac{\partial u_i}{\partial x_j}, \quad \stackrel{(1)}{B}_{ij} = \delta_{ij} + 2\epsilon_{ij},$$

$$\stackrel{(1)}{B}_{ij}^{-1} = \delta_{ij} - 2\epsilon_{ij} \quad (7.82)$$

$$\stackrel{(1)}{I}_1 = 3 + 2\epsilon, \quad \stackrel{(1)}{I}_2 = 3 + 4\epsilon, \quad \stackrel{(1)}{I}_3 = 1 + 2\epsilon, \quad (7.83)$$

where ϵ is the dilatation

$$\epsilon = \epsilon_{kk} = \stackrel{(1)}{J} - 1. \quad (7.84)$$

Similarly, the fluid dilatation $e(\ll 1)$ is given by

$$e = \stackrel{(2)}{J} - 1. \quad (7.85)$$

In turn, set

$$n(1 + \epsilon, 1 + e) = n_0(1 + n_1\epsilon + n_2e) \quad (7.86)$$

where the constants n_1, n_2 are supposed to be of order unity or less. Thus, from (7.53), (7.83), (7.86),

$$\stackrel{(1)}{I}_1 e - 3 = \frac{1}{2} \left(\stackrel{(1)}{I}_2 e - 3 \right) = \stackrel{(1)}{I}_3 e - 1 = 2 \left\{ (1+n_1)\epsilon + n_2 e \right\}. \quad (7.87)$$

Now (7.59), (7.62), (7.82) lead to

$$\begin{aligned} \sigma_{ij}^{(1)} = n_0 \left\{ 2 \mu^{(1)} \epsilon_{ij} + \left[\lambda^{(1)} + n_1 \left(\lambda^{(1)} + \frac{2}{3} \mu^{(1)} \right) \right] \epsilon \delta_{ij} \right. \\ \left. + n_2 \left(\lambda^{(1)} + \frac{2}{3} \mu^{(1)} \right) \epsilon \delta_{ij} \right\} \end{aligned} \quad (7.88)$$

where

$$\begin{aligned} \mu^{(1)} &= \left\{ \phi_1 + 2\phi_2 \right\} \epsilon_{ij=0} , \\ \lambda^{(1)} &= 2 \sum_{r=0}^2 \left\{ \frac{\partial \phi}{\partial I_1^r} + 2 \frac{\partial \phi}{\partial I_2^r} + \frac{\partial \phi}{\partial I_3^r} \right\} \epsilon_{ij=0} . \end{aligned} \quad (7.89)$$

Similarly, from (7.56), (7.63), (7.85), (7.86), for the ideal fluid

$$\sigma_{ij}^{(2)} = K^{(2)} \left\{ (1 - n_0 - n_0 n_2) \epsilon - n_0 n_1 \right\} \delta_{ij} , \quad (7.90)$$

where

$$K^{(2)} = - p'(\rho_0/\rho)_{c=0} . \quad (7.91)$$

Notice that the interaction terms representing dependence on the alternative dilatation are respectively for the solid and fluid

$$\frac{(1)}{K} n_0 n_2 \epsilon \delta_{ij} , \quad - \frac{(2)}{K} n_0 n_1 \epsilon \delta_{ij} , \quad (7.92)$$

where $\frac{(1)}{K} = \frac{(1)}{\lambda} + \frac{2}{3} \frac{(1)}{\mu} .$

Combining equations (7.86), (7.88) and (7.90), we obtain the partial stresses in the solid and the fluid as:

$$\sigma_{ij}^{(1)} = n_0 \left\{ \lambda^{(1)} \varepsilon \delta_{ij} + 2\mu^{(1)} \varepsilon_{ij} \right\} + (n - n_0) K^{(1)} \delta_{ij} \quad (7.93)$$

and

$$\sigma_{ij}^{(2)} = (1 - n_0) K^{(2)} e - (n - n_0) K^{(2)} \delta_{ij} . \quad (7.94)$$

The meaning of these equations is quite clear. Let us assume that $K^{(1)} > K^{(2)}$. Application of pressure on the solid tends to reduce the pore volume. Thus the partial fluid pressure consists of two parts, i.e., (1) deformation of the original fluid volume and (2) due to relative reduction in pore volume. Similar interpretation may be applied to the partial solid pressure. In uni-axial strain ε_1 and e_1 ,

$$\sigma^{(1)} = n_0 \left\{ \left(K^{(1)} + \frac{4}{3} \mu^{(1)} \right) \varepsilon_1 + K^{(1)} (n_1 \varepsilon_1 + n_2 e_1) \right\} , \quad (7.95)$$

$$\sigma^{(2)} = (1 - n_0) K^{(2)} e_1 - n_0 K^{(2)} (n_2 e_1 + n_1 \varepsilon_1) . \quad (7.96)$$

Now consider the solid to be elastic-plastic so that the allowed shear stress is restricted. This is an essential qualitative feature when large non-isotropic stresses occur, and, albeit oversimplified, provides the most simple realistic model. For uni-axial strain and spherically symmetric deformation it is sufficient to postulate elastic dilatation (no permanent volume change) and a yield criterion to describe plastic response (no flow rule is required). In both cases there are two non-vanishing principle stresses, σ_1 (in the longitudinal or radial direction respectively) and $\sigma_2 = \sigma_3$ in the lateral directions, together with a longitudinal

(radial) principal stretch λ_1 , and in the spherical geometry equal lateral stretches $\lambda_2 = \lambda_3$ (unity in uni-axial strain). Both the Tresca and von Mises yield criteria reduce to

$$s(\sigma_2 - \sigma_1) = Y, \quad s = \pm 1, \quad (7.97)$$

describing yield in the opposite shear senses, where Y is the yield stress in shear. For simplicity we will neglect work hardening and assume Y is constant. Now we postulate an elastic relation between mean stress increment and dilatation increment, of the form

$$\frac{1}{3} d(\sigma_1 + 2\sigma_2) = K dJ, \quad (7.98)$$

where K is a function of the current deformation invariants in general, but we assume a simplified dependence

$$K = K(J). \quad (7.99)$$

The incremental relation (7.98) may be alternatively expressed as a rate law with respect to time or any monotonic parameter describing the loading path since the material is not rate-dependent. Note that (7.98) is a restricted form of the isotropic elastic response given by (7.57) which relates σ_{kk} to J only in uniform dilatation, as used in (7.71). However, the restricted form (7.98) in conjunction with (7.99) may be integrated to give

$$\frac{1}{3} (\sigma_1 + 2\sigma_2) = -p(J) \quad (7.100)$$

which holds through both elastic and plastic deformation.

In plastic deformation, the yield criterion (7.97) and dilatation law (7.100) give

$$\left. \begin{aligned} \sigma_1 &= -p(J) - \frac{2}{3} sY, \\ \sigma_2 &= sY + \sigma_1. \end{aligned} \right\} \quad (7.101)$$

Hence, within the mixture, during plastic deformation of the solid,

$$\left. \begin{aligned} \sigma_2 - \sigma_1 &= nsY, \\ \sigma_1 &= -np \left(\frac{n}{n_0} J \right) - \frac{2}{3} nsY \\ &= ns_1 \left(\frac{n}{n_0} J \right). \end{aligned} \right\} \quad (7.102)$$

Thus, the longitudinal (radial) stress-dilatation law within the mixture is determined by the longitudinal (radial) stress-dilatation law during isolated plastic yield, contrasting with general isotropic elastic response (7.79) in uni-axial strain, here a consequence of the foregoing restrictive assumptions. A complete description requires an elastic shear law to replace (7.97) during elastic response when

$$|\sigma_2 - \sigma_1| < Y, \quad (7.103)$$

or for "unloading" from yield states. Using the decomposition (7.50) where $J = \lambda_1 \lambda_2^2$, the shear deformation is given by

$$\hat{F}^* = \begin{pmatrix} \gamma^{2/3} & & 0 \\ & \gamma^{-1/3} & \\ 0 & & \gamma^{-1/3} \end{pmatrix}, \quad \gamma = \frac{\lambda_1}{\lambda_2}, \quad (7.104)$$

and J, γ can be regarded as the two independent strains describing dilatation and shear respectively. We now assume

In plastic deformation, the yield criterion (7.97) and dilatation law (7.100) give

$$\left. \begin{aligned} \sigma_1 &= -p(J) - \frac{2}{3} sY = S_1(J) , \\ \sigma_2 &= sY + \sigma_1 . \end{aligned} \right\} \quad (7.101)$$

Hence, within the mixture, during plastic deformation of the solid,

$$\left. \begin{aligned} \sigma_2 - \sigma_1 &= nsY , \\ \sigma_1 &= -np\left(\frac{n}{n_0} J\right) - \frac{2}{3} nsY \\ &= nS_1\left(\frac{n}{n_0} J\right) . \end{aligned} \right\} \quad (7.102)$$

Thus, the longitudinal (radial) stress-dilatation law within the mixture is determined by the longitudinal (radial) stress-dilatation law during isolated plastic yield, contrasting with general isotropic elastic response (7.79) in uni-axial strain, here a consequence of the foregoing restrictive assumptions. A complete description requires an elastic shear law to replace (7.97) during elastic response when

$$|\sigma_2 - \sigma_1| < Y , \quad (7.103)$$

or for "unloading" from yield states.

From (7.57) the principal stress difference $\sigma_2 - \sigma_1$ is expressed in terms of λ_1 and λ_2 , which may be expressed in an incremental form required for unloading (reloading) from a previous plastic state, and in turn a mixture law is obtained. A simpler elastic model is obtained by expressing $\underline{\sigma}$ as an isotropic tensor function of the stretch tensor $\underline{V} = \underline{B}^{1/2}$ and omitting the term in \underline{V}^2 , that is, setting the

third response function analogous to $\phi_2(I_k)$ in (7.57) to be zero. Then

$$\underline{\sigma} = \psi_0(I_k)\underline{1} + \psi_1(I_k)\underline{V}, \quad (7.104)$$

and the dilatation law (7.100) requires that

$$\psi_0(I_k) = -p(J) - \frac{1}{3}\psi_1(J)I_1, \quad (7.105)$$

where

$$J = I_3 = \det \underline{V}, \quad I_1 = \text{tr } \underline{V}.$$

Now

$$\sigma_1 - \sigma_2 = \psi_1(J)(\lambda_1 - \lambda_2), \quad (7.106)$$

and with the further restriction

$$\psi_1 = \text{const.}, = 2\mu, \quad (7.107)$$

the incremental law required for loading/unloading from previous yield states takes the simple form

$$d(\sigma_1 - \sigma_2) = 2\mu d(\lambda_1 - \lambda_2). \quad (7.108)$$

Allowing $\psi_1(J)$ results in a further dependence on dJ so that the incremental shear response is not uncoupled from dilatation response. Confining attention to (7.108), the mixture law is

$$d\left(\frac{\sigma_1 - \sigma_2}{n}\right) = 2\mu d\left[\left(\frac{n}{n_0}\right)^{\frac{1}{3}} (\lambda_1 - \lambda_2)\right], \quad (7.109)$$

since, by (7.50),

$$\tilde{F}^e = \left(\frac{n}{n_0}\right)^{\frac{1}{3}} \begin{pmatrix} \lambda_1 & & \\ & \lambda_2 & \\ & & \lambda_3 \end{pmatrix}. \quad (7.110)$$

In uni-axial strain $\dot{\lambda}_1 = \dot{\lambda}, \dot{\lambda}_2 = \dot{\lambda}_3 = 0$, and

$$J = \lambda, \quad (7.111)$$

whence the plastic laws (7.102) become

$$\sigma_1 = nS_1 \left(\frac{n}{n_0} \lambda\right), \quad \sigma_2 - \sigma_1 = nsY. \quad (7.112)$$

However, the elastic laws (7.98), modified for the mixture, and (7.109) become

$$d\left(\frac{\sigma_1 + 2\sigma_2}{n}\right) = 3K \left(\frac{n}{n_0} \lambda\right) d\left(\frac{n}{n_0} \lambda\right) \quad (7.113)$$

$$d\left(\frac{\sigma_1 - \sigma_2}{n}\right) = 2\mu d\left[\left(\frac{n}{n_0}\right)^{\frac{1}{3}} \lambda\right]$$

so that

$$d\left(\frac{\sigma_1}{n}\right) = K\left(\frac{n}{n_0} \lambda\right) d\left(\frac{n}{n_0} \lambda\right) + \frac{4}{3} \mu d\left[\left(\frac{n}{n_0}\right)^{\frac{1}{3}} \lambda\right] \quad (7.114)$$

and the combination $K\left(\frac{n}{n_0} \lambda\right) + \frac{4}{3} \mu$ does not determine the longitudinal stress strain gradient between σ_1/n and $\frac{n}{n_0} \lambda$. Thus (7.114) requires separate knowledge of $K(J)$ and ${}^0\mu$, even in this highly simplified model, say from dilatation and uni-axial strain measurements. It must be recalled that the directly related plastic laws (7.112) are a consequence

of the simplified elastic-plastic model proposed. While less restrictive models allow the same extension to mixture laws by dilatation adjustment, direct relations like (7.112) are not anticipated

7.4 PLANE WAVE PROPAGATION

7.4.1 Governing Relations

Wave propagation in mixtures has chiefly been investigated within linearized theories, and in particular for harmonic waves in infinite fluid-saturated elastic solids. Non-linear effects and possible shock formation are thus absent. The present study includes these effects and makes comparison with the opposite dispersion effects due to the constituent interactions through diffusion and the coupled constitutive laws. Attention is restricted to plane wave propagation in uni-axial strain, and the longitudinal stress-strain laws derived from the simple elastic-plastic model and ideal fluid in Section 7.3 are used in illustration.

Now let us consider uni-axial motion in the x -direction. We will assume that the external body force $\underline{b}^{(\alpha)}$ is absent and that there is no mass transfer between the constituents due to chemical interaction. In this case, equations (7.8) and (7.19) expressing conservation of mass and momentum for $\delta^{(\alpha)}$ constituents reduce to

$$\frac{\partial \rho}{\partial t} + v \frac{\partial \rho}{\partial x} + \rho \frac{\partial v}{\partial x} = 0, \quad (7.115)$$

$$\frac{\partial \rho}{\partial t} + w \frac{\partial \rho}{\partial x} + \rho \frac{\partial w}{\partial x} = 0, \quad (7.116)$$

$$\rho \left(\frac{\partial v}{\partial t} + v \frac{\partial v}{\partial x} \right) = \rho \beta + \frac{\partial \sigma_x^{(1)}}{\partial x}, \quad (7.117)$$

$$\rho \left(\frac{\partial w}{\partial t} + w \frac{\partial w}{\partial x} \right) = -\rho \beta + \frac{\partial \sigma_x^{(2)}}{\partial x}. \quad (7.118)$$

Here superscripts (1) and (2) refer to material 1 (tuff) and 2 (water), respectively. Also

$$\begin{aligned} \rho^{(1)} \rho^{(2)} &= \text{partial mass density of tuff (water) ,} \\ \rho &= \text{current mass density of mix } \left(= \frac{\rho^{(1)} \rho^{(2)}}{\rho^{(1)} + \rho^{(2)}} \right) , \end{aligned}$$

$v(w)$ = the particle velocity of tuff (water) ,

β = internal diffusive body force ,

$$\sigma_x^{(1)} \sigma_x^{(2)} = \text{partial longitudinal stress of tuff (water) ,}$$

$$\sigma_y^{(1)} \sigma_y^{(2)} = \text{partial transverse stress of tuff (water) .}$$

This system has to be completed by adjoining the constitutive laws developed in Section 7.3. The principle partial stresses in the fluid, within the mixture, are equal, and given by:

Fluid (e.g., Water):

$$\sigma_x^{(2)} = \sigma_y^{(2)} = - (1-n) p \left(\frac{1-n}{1-n_0} \frac{J^{(2)}}{J} \right) \quad (7.119)$$

where $p^{(2)}$ (J) is the relation expressing the pressure response of the fluid constituent when isolated. The solid is considered to be elastic-plastic so that the difference between its principal partial stresses is restricted.

Solid (e.g., Compacted Try Tuff):

In the plastic regime, we have

$$\sigma_x^{(1)} - \sigma_y^{(1)} = s n Y , \quad s = \pm 1 , \quad (7.120)$$

$$\frac{1}{3} \left[\sigma_x^{(1)} + 2 \sigma_y^{(1)} \right] = - n p \left(\frac{n}{n_0} \frac{J^{(1)}}{J} \right) , \quad (7.121)$$

where $p^{(1)}(J)$ is the relation expressing the pressure response of the isolated solid under uniform dilatation and Y is the maximum shear stress that the isolated solid can sustain. In the elastic regime $\left[\left| \sigma_x^{(1)} - \sigma_y^{(2)} \right| < nY \right]$, the response of the solid is governed by (7.121) and the elastic shear law

$$d \left(\sigma_x^{(1)} - \sigma_y^{(1)} \right) = 2n \mu_1 \left(\frac{n}{n_0} \right) d J^{(1)} \quad (7.122)$$

where $\mu_1(J)$ is the shear modulus of the isolated solid. When the yield stress Y is negligible compared to the applied pressure pulse, the constitutive relation for the solid assumes the simple form:

$$\sigma_x^{(1)} = -n p \left(\frac{n}{n_0} \lambda \right) \quad (7.123)$$

It still remains to prescribe the interaction function $n \left(\frac{(1)}{J}, \frac{(2)}{J} \right)$. As a first approximation (assuming small dilatation difference between the constituents) the function $N \left[\frac{1}{2} \left(\frac{(1)}{J} + \frac{(2)}{J} \right) \right]$ defined by (7.67) and obtained from the data discussed in Section 7.5 is adopted. This serves to estimate the dilatation difference $\frac{(2)}{J} - \frac{(1)}{J}$. A second treatment adopts the expansion (7.68) with different values for k so that a possible effect of different dilatations on the pulse propagation can be observed. Finally, the internal longitudinal body force β must be prescribed. If we suppose the body force, β depends on the two velocity fields and partial densities, frame indifference requires linear dependence on the relative velocity $w - v$ with coefficient depending on the scalars $\rho^{(1)}$, $\rho^{(2)}$ and $w - v$. We will first adopt the most simple form

$$\rho \beta = \rho_0 d (w-v) \quad (7.124)$$

where d is a constant with the dimension of the reciprocal of time. From data given by Ishihara⁽⁸³⁾ for slow diffusion through sands and clays, d takes values in the range $10^2 - 10^1 \text{ sec}^{-1}$, so various values across this range will be used to investigate the effect of a diffusive resistance. The significance of this term depends also on the relative velocity $(w - v)$ and the stress gradient, and hence the pulse rise time. As d increases we would expect the relative velocity to decrease (an opposing force), and solutions for d over the entire range will determine the product $d(w-v)$ in the different situations and assess the significance of the resistance. Negligible (or small) relative velocity which may arise with larger values of d would imply that both constituents have approximately the same velocity field, and then the simplifying approximation of a single velocity field and single constituent described by the total stress-deformation law may be applicable.

7.4.2 Non-Dimensional Formulation

System of equations (7.115) through (7.118) can be more simply expressed in terms of (X, t) where X is a material coordinate for the first material and by eliminating partial densities $\rho^{(1)}, \rho^{(2)}$ in favor of the Jacobians of the deformations

$$\lambda = J^{(1)} = \rho_0^{(1)} / \rho^{(1)}, \quad \gamma = J^{(2)} = \rho_0^{(2)} / \rho^{(2)}. \quad (7.125)$$

Thus, for any function $f(x,t) = \tilde{f}(X,t)$, one has

$$\frac{\partial f}{\partial x} = \frac{1}{\lambda} \frac{\partial \tilde{f}}{\partial X}, \quad \frac{Df}{Dt} = \frac{\partial \tilde{f}}{\partial t}, \quad (7.126)$$

$$\frac{Df}{Dt} = \frac{\partial \tilde{f}}{\partial t} + \frac{(w-v)}{\lambda} \frac{\partial \tilde{f}}{\partial X}.$$

This transformation reduces the equations (7.115) through (7.118) to

$$\frac{\partial \lambda}{\partial t} = \frac{\partial v}{\partial X} , \quad (7.127)$$

$$\left(\frac{\partial}{\partial t} + \frac{w-v}{\lambda} \frac{\partial}{\partial X} \right) \gamma = \frac{\gamma}{\lambda} \frac{\partial w}{\partial X} , \quad (7.128)$$

$$\frac{\partial v}{\partial t} = \frac{\lambda d}{c_0} (w-v) + \frac{1}{\rho_0 c_0} \frac{\partial \sigma_x^{(1)}}{\partial X} , \quad (7.129)$$

$$\left(\frac{\partial}{\partial t} + \frac{w-v}{\lambda} \frac{\partial}{\partial X} \right) w = \frac{-\gamma d}{1-c_0} (w-v) + \frac{1}{\rho_0 (1-c_0)} \frac{\gamma}{\lambda} \frac{\partial \sigma_x^{(2)}}{\partial X} , \quad (7.130)$$

where c_0 and $1-c_0$ denote the initial mass concentrations.

$$c_0 = \frac{\rho_0^{(1)}}{\rho_0} , \quad 1 - c_0 = \frac{\rho_0^{(2)}}{\rho_0} , \quad (7.131)$$

We define a characteristic length, L , to be twice the length of the specimen (ℓ). A convenient measure for a typical wave speed is an acoustic wave speed in material 1 based on the initial partial density $\rho_0^{(1)}$

$$\rho_0^{(1)} S_0^2 = \left. \frac{d p^{(1)}(\bar{\mu})}{d(\bar{\mu})} \right|_{\bar{\mu} = 0} \quad (7.132)^*$$

where $\bar{\mu} = \frac{1}{J} - 1$.

* Utilizing the functional form (7.144) for $p^{(1)}(\bar{\mu})$, (7.132) becomes

$$\rho_0^{(1)} S_0^2 = \Lambda^{(1)} ,$$

where $\Lambda^{(1)}$ is a material constant defined in Section 7.5.

Introducing the non-dimensional variables,

$$\left. \begin{aligned} Z &= X/L & \tau &= S_0 t/L \\ \bar{v} &= v/S_0 & \bar{w} &= w/S_0 \\ \bar{\sigma} &= \sigma / \rho_0 S_0^2 & \bar{d} &= Ld/S_0 \end{aligned} \right\} \quad (7.133)$$

the following system of equations is obtained

$$\frac{\partial \lambda}{\partial \tau} = \frac{\partial \bar{v}}{\partial Z}, \quad (7.134)$$

$$\frac{\partial \gamma}{\partial \tau} + \frac{\bar{w} - \bar{v}}{\lambda} \frac{\partial \gamma}{\partial Z} = \frac{\gamma}{\lambda} \frac{\partial \bar{w}}{\partial Z}, \quad (7.135)$$

$$\frac{\partial \bar{v}}{\partial \tau} = \frac{\lambda \bar{d}}{c_0} (\bar{w} - \bar{v}) + \frac{\partial \bar{\sigma}^{(1)}}{\partial Z}, \quad (7.136)$$

$$\frac{\partial \bar{w}}{\partial \tau} + \frac{\bar{w} - \bar{v}}{\lambda} \frac{\partial \bar{w}}{\partial Z} = \frac{-\gamma \bar{d}}{1 - c_0} (\bar{w} - \bar{v}) + \frac{c_0}{1 - c_0} \frac{\gamma}{\lambda} \frac{\partial \bar{\sigma}^{(2)}}{\partial Z}. \quad (7.137)$$

This governing system is completed by adjoining the constitutive laws (7.68), (7.119), (7.123).

$$\bar{\sigma}^{(1)} = -n \frac{\bar{p}^{(1)}}{\rho_0} \left(\frac{n}{n_0} \lambda \right), \quad (7.138)$$

$$\bar{\sigma}^{(2)} = - (1-n) \frac{\bar{p}^{(2)}}{\rho_0} \left(\frac{1-n}{1-n_0} \gamma \right), \quad (7.139)$$

where

$$n(\lambda, \gamma) = N \left(\frac{\gamma + \lambda}{2} \right) + k \left(\frac{\lambda + \gamma}{2} \right) (\gamma - \lambda). \quad (7.140)$$

The plausible range for d is $10^2 - 10^6 \text{ sec}^{-1}$. Assuming S_0 to be the order of 10^5 cm/sec and L to be the order of 10^0 cm , the range for \bar{d} becomes $10^{-3} - 10^{+1}$. Solutions will be obtained over the entire range of \bar{d} to assess the effect of the diffusive resistance.

7.4.3 Initial and Boundary Conditions

We consider the half-space $Z > 0$ initially at rest.

Thus

$$\left. \begin{array}{l} \bar{v} = \bar{w} = 0 \\ \lambda = \gamma = 1 \end{array} \right\} \text{ at } t = 0 \quad Z > 0 \quad . \quad (7.141)$$

The motion of the material plane $Z = 0$ is prescribed for $\tau \leq \tau_0$ as if both constituents move together

$$\bar{v} = \bar{w} = \bar{V}(\tau) \quad \text{on } Z = 0, \quad \tau \leq \tau_0 \quad . \quad (7.142)$$

For $\tau > \tau_0$, the stresses $\overset{(1)}{\bar{\sigma}}$ and $\overset{(2)}{\bar{\sigma}}$ must be zero at $Z = 0$. For the simplified constitutive laws considered here this yields

$$\lambda = \gamma = 1 \quad \text{at } Z = 0, \quad \tau > \tau_0 \quad . \quad (7.143)$$

7.5 EXPERIMENTAL DATA ANALYSIS

To arrive at an approximation for the interaction function n that is based on experimental data, we consider a body of the mixture to be subjected to quasi-static uniform dilatation. Under isotropic loading no shear stresses are introduced and the hydrostatic pressure in the mixture is given by Eq. (7.74). Thus, given the quasistatic pressure-dilatation response relation for the mixture, $p(J)$ and those of its constituents, ${}^{(1)}p(J)$ and ${}^{(2)}p(J)$, Eq. (7.74) is an implicit equation for $N(J)$ subject to the initial condition $N(1) = N_0$. Least square fits have been made to the data discussed elsewhere in this report for ${}^{(1)}p(J)$ and ${}^{(2)}p(J)$. The fits for Schooner tuff(1), Eq. (3.16) and water (2), Eq. (2.11), are

$$\begin{aligned} {}^{(1)}p(J) &= A \bar{\mu} + B \bar{\mu}^2 + F \bar{\mu}^3 + H \bar{\mu}^4, \\ {}^{(2)}p(J) &= A \bar{\mu} + B \bar{\mu}^2 + F \bar{\mu}^3 \end{aligned} \quad (7.144)$$

where $\bar{\mu} = \frac{1}{J} - 1$.

The parameters A , B , ..., F are listed in Table 7.1 together with the range of validity. In order to use Eq. (7.74), we also require the mixture response $p(J)$. Unfortunately, however the available data for $p(J)$ and ${}^{(1)}p(J)$ is not sufficiently accurate to enable the use of the implicit Eq. (7.74).

As we observed in Section 7.2, in case the strength of tuff can be neglected, both constituents may be regarded as fluids and the simpler equation (7.75) may be utilized to calculate $N_p(J)$. Fortunately, the yield strength of tuff is very small (< 0.6 kbar) and as such use of Eq. (7.75) is justified at least as a first approximation. A computer

TABLE 7.1
 PARAMETERS IN THE FITS OF EXPERIMENTAL p-V DATA FOR THE
 ISOLATED WATER AND COMPACTED DRY TUFF MIXTURE COMPONENTS

Material	P_{\max} (kbar)	ρ_0 (g/cc)	A (ergs/cc)	B (ergs/cc)	F (ergs/cc)	H (ergs/cc)
Water	250	1.0	2.1953×10^{10}	5.2138×10^{10}	2.3181×10^{11}	--
Compacted Dry Tuff	200	2.356	4.8851×10^{10}	1.9868×10^{12}	-4.6715×10^{12}	4.3406×10^{12}

program was written to evaluate $N_p(J)$ through the use of Eq. (7.75). We show the results for two water fractions ($F = 14.4\%$ and $F = 14.8\%$) in Fig. 7.2. Note that mass fraction, F , is related to N_0 through the equation

$$\frac{1}{N_0} = 1 + \frac{F}{1-F} \frac{\rho_0^{(1)}}{\rho_0^{(2)}} \quad (7.145)$$

The function $N_p(J)$ [$F = 14.8\%$] has been fitted to the following theoretical curve.

$$\begin{aligned} N_p(J) = & 0.7089193 - 0.3140556 (J-1) \\ & + 0.1399297 (J-1)^2 + (J-1)^3 \\ & + 5.726582 (J-1)^4 \end{aligned} \quad (7.146)$$

The minimal principle has also been applied to the dilatational law (7.74) to predict $N_m(J)$. Application of the method involves analysis of the right-hand side of Eq. (7.74). In the analysis, for each selected value of J , $p(J)$ is minimized over possible values of N such that

$$\left. \frac{dp(J)}{dN} \right|_{N = N(J)} = 0 \quad (7.147)$$

To conduct this analysis, the computer program FLISTT was developed and applied to the fits $p^{(1)}(J)$, $p^{(2)}(J)$. The predicted curves for $N_m(J)$ ($F = 14.4$ and 14.8%) are shown in Fig. 7.3. The function $N_m(J)$ ($F = 14.8\%$) has been fitted to the analytical curve

$$\begin{aligned} N_m(J) = & 0.71058 - 0.72698(J-1) - 1.71055(J-1)^2 \\ & + 5.26770(J-1)^3 + 14.27141(J-1)^4 \end{aligned} \quad (7.148)$$

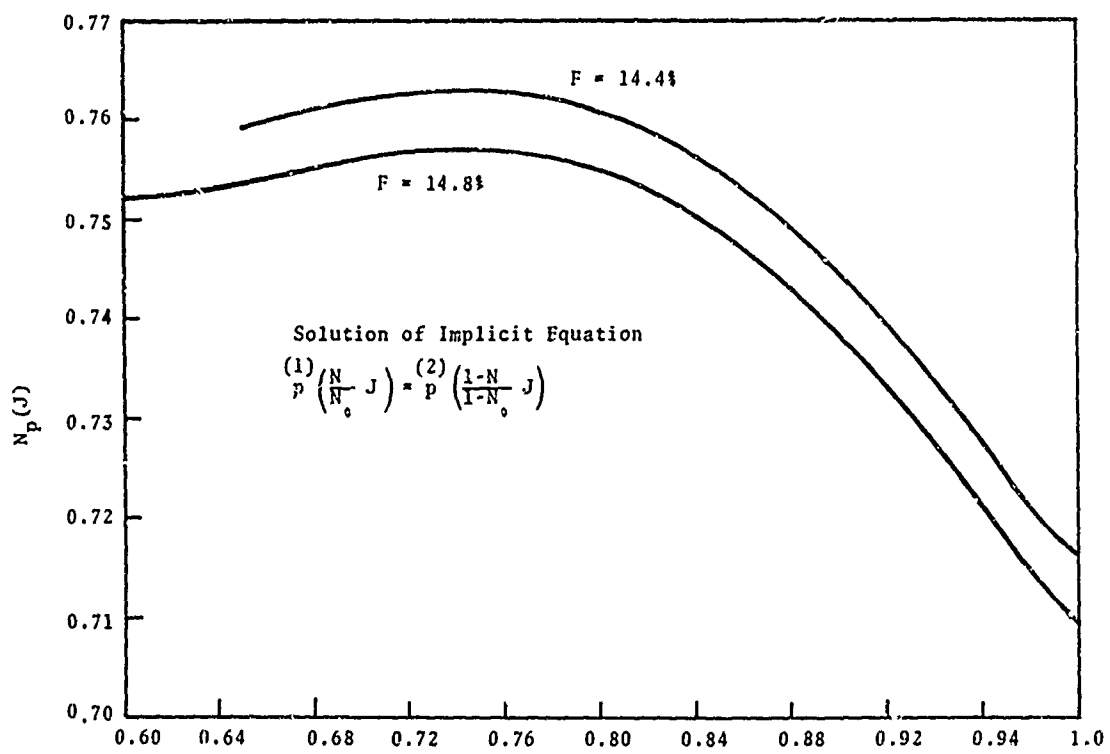


Fig. 7.2-- $N(J)$ for saturated wet tuff calculated on the basis of pressure equilibrium.

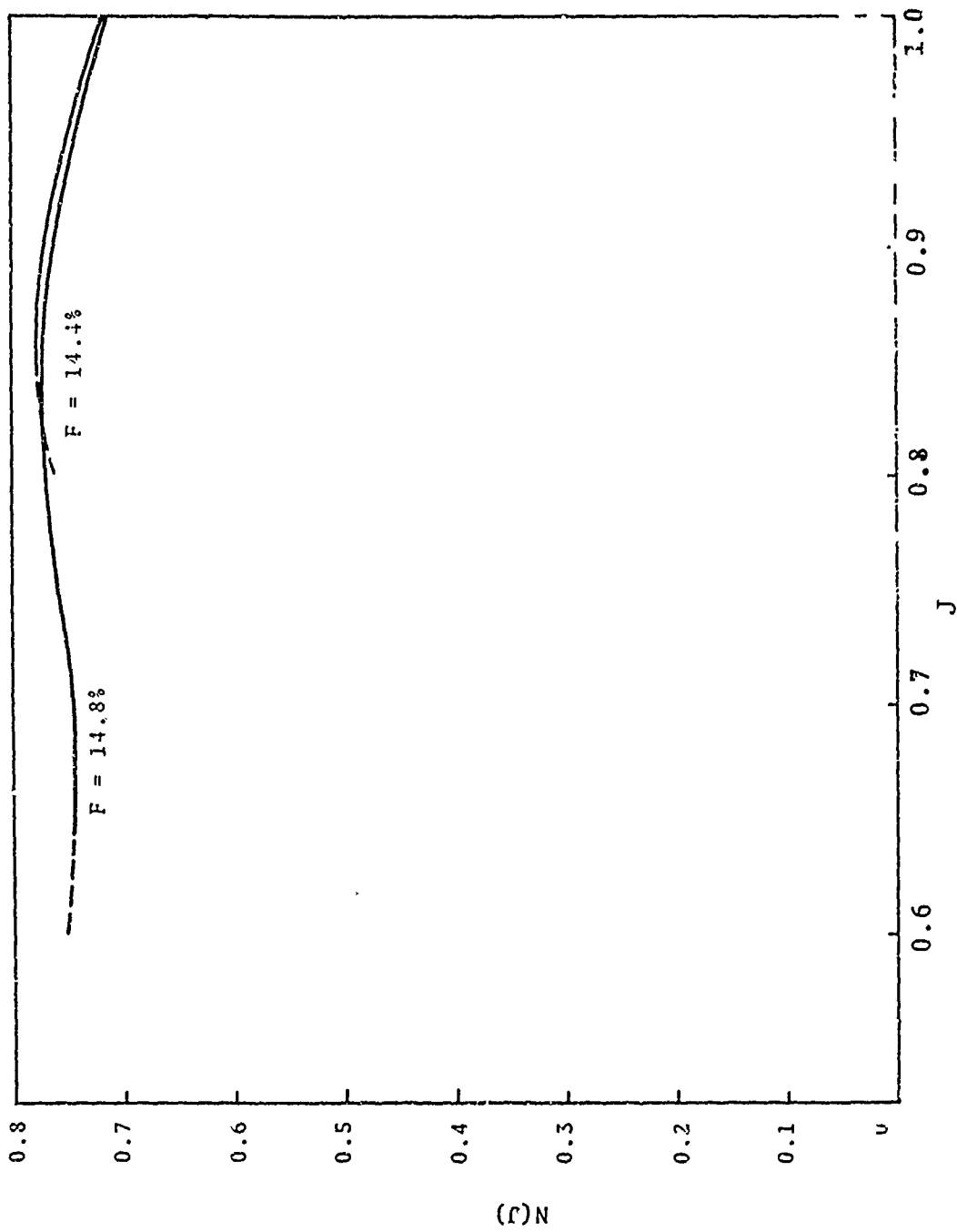


Fig. 7.3--The function $N(J)$ for saturated wet tuffs with the indicated water content fractions.

In Figs. 7.4(a) and 7.4(b), we show the quasi-static mixture response predicted on the basis of pressure equilibrium and minimal principle models. For comparison purposes, the response of the individual components and the experimental data is also plotted therein. Notwithstanding the fact that $N_m(J)$ and $N_p(J)$ are quite different, they predict approximately the same mixture response except in the low pressure regime. We will return to this question in Section 7.7. In the meantime, we observe that there exists a clearer physical motivation for using $N(J)$ calculated on the basis of pressure equilibrium than the one obtained by employing minimal principle.

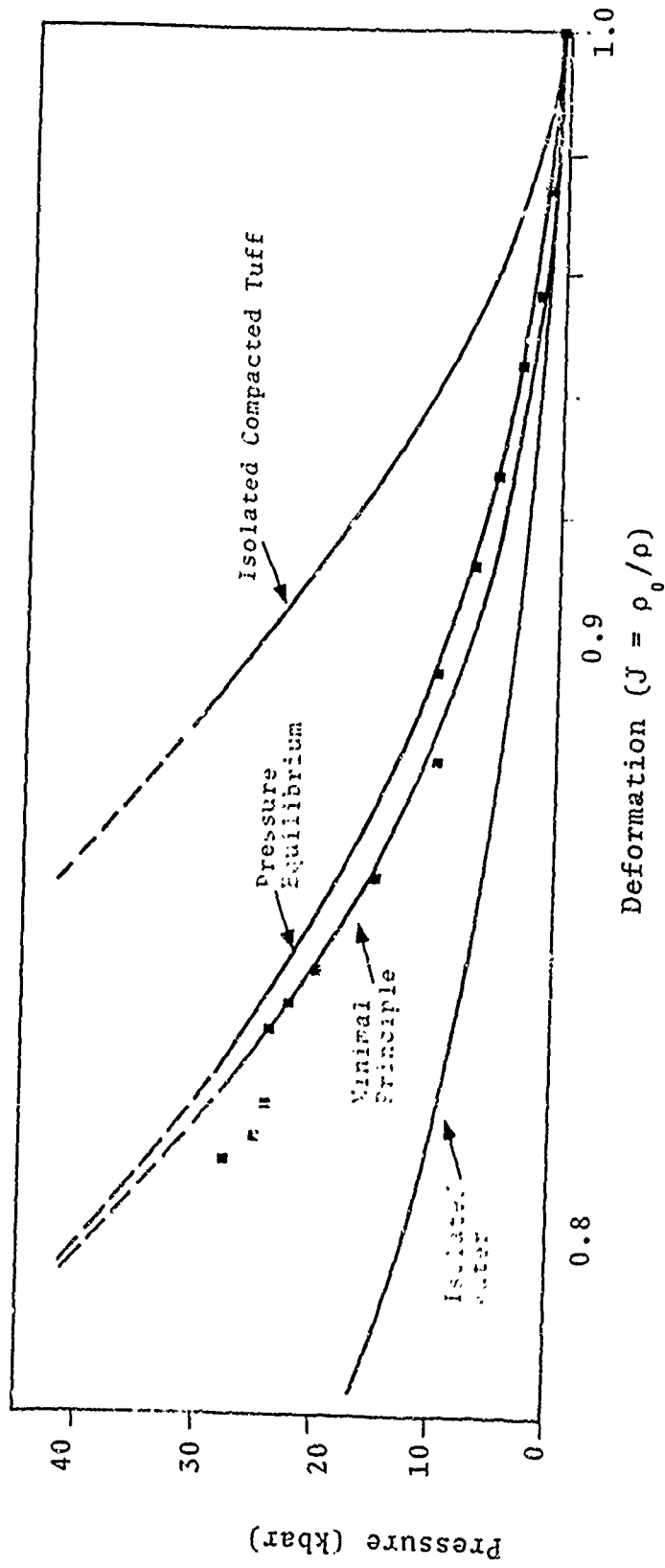


Fig. 7.4(a) -- Comparison of predicted p-V response of saturated wet tuff ($F = 0.144$) with the quasistatic data of Ref. 35.

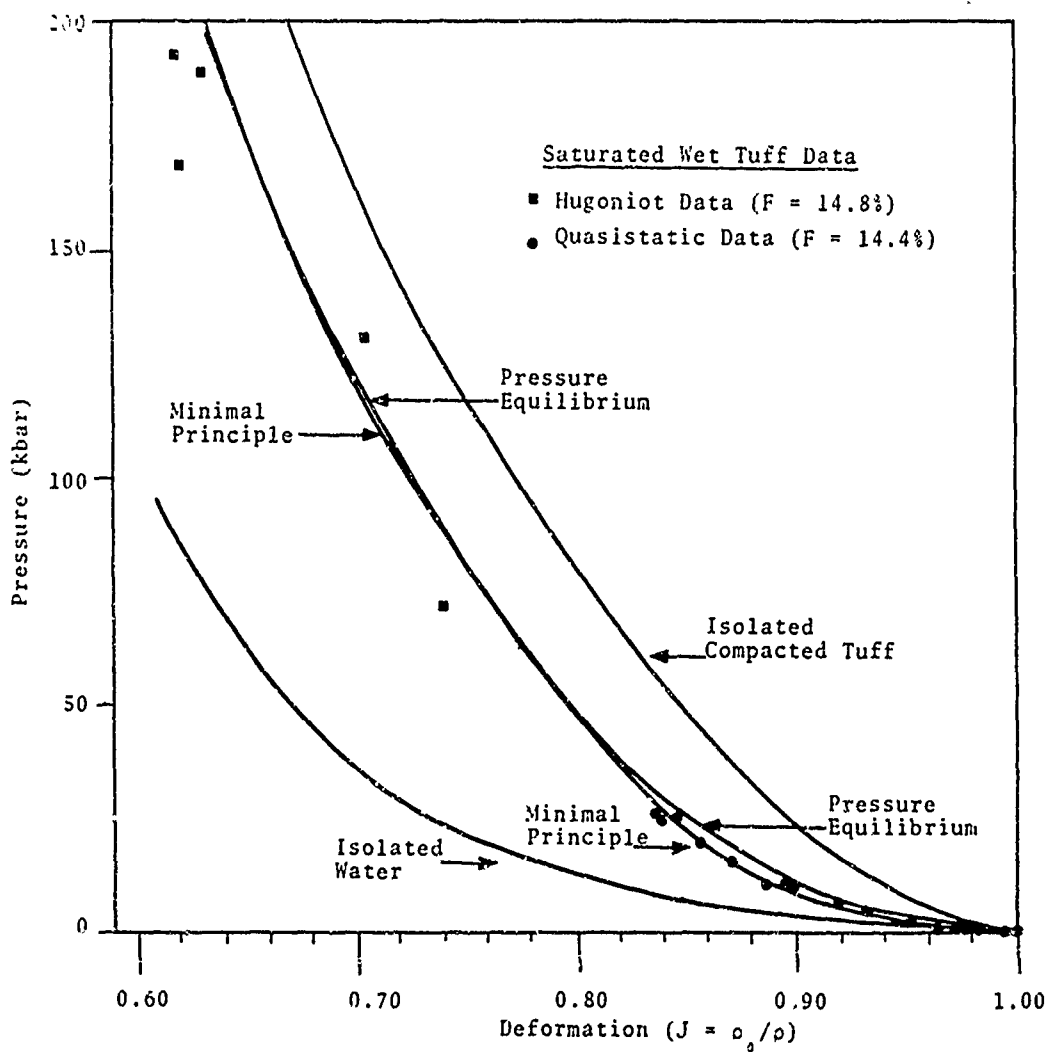


Fig. 7.4(b)--Comparison of predicted p-V response of saturated wet tuff ($F = 0.148$) on the extended pressure range. Data points from the Hugoniot measurement of Ref.38 , and the quasistatic tests of Ref.35 are also shown.

7.6 FINITE DIFFERENCE SCHEME

The system of equations (7.134) through (7.140) is solved by the two-step Lax-Wendroff scheme.⁽⁸⁴⁾ This scheme has second order accuracy $[O(\Delta\tau)^2]$. The provisional values are first calculated at the centers of the rectangular meshes $(j+\frac{1}{2}, n+\frac{1}{2})$ of the $(Z-\tau)$ plane. The final values at mesh points $(j, n+1)$ are then calculated from provisional values. The difference scheme is given below.

7.6.1 Provisional Values at $(j+\frac{1}{2}, n+\frac{1}{2})$

$$\lambda_{j+\frac{1}{2}}^{n+\frac{1}{2}} = \frac{1}{2} (\lambda_{j+1}^n + \lambda_j^n) + \frac{\Delta\tau}{2\Delta Z} (\bar{v}_{j+1}^n - \bar{v}_j^n),$$

$$\begin{aligned} \gamma_{j+\frac{1}{2}}^{n+\frac{1}{2}} = & \frac{1}{2} (\gamma_{j+1}^n + \gamma_j^n) - \frac{\Delta\tau}{2\Delta Z} \left(\frac{\bar{w}_{j+1}^n - \bar{v}_{j+1}^n + \bar{w}_j^n - \bar{v}_j^n}{\lambda_{j+1}^n + \lambda_j^n} \right) \\ & \cdot (\gamma_{j+1}^n - \gamma_j^n) + \frac{\Delta\tau}{2\Delta Z} \frac{\gamma_{j+1}^n + \gamma_j^n}{\lambda_{j+1}^n + \lambda_j^n} (\bar{w}_{j+1}^n - \bar{w}_j^n), \end{aligned}$$

$$\begin{aligned} \bar{v}_{j+\frac{1}{2}}^{n+\frac{1}{2}} = & \frac{1}{2} (\bar{v}_{j+1}^n + \bar{v}_j^n) + \frac{\Delta\tau}{2} \frac{\bar{d}}{c_0} \frac{1}{4} (\lambda_{j+1}^n + \lambda_j^n) \\ & \cdot (\bar{w}_{j+1}^n + \bar{w}_j^n - \bar{v}_{j+1}^n - \bar{v}_j^n) + \frac{\Delta\tau}{2\Delta Z} \left(\frac{(1)}{\sigma_{j+1}} \bar{v}_{j+1}^n - \frac{(1)}{\sigma_j} \bar{v}_j^n \right), \end{aligned}$$

$$\begin{aligned} \bar{w}_{j+\frac{1}{2}}^{n+\frac{1}{2}} = & \frac{1}{2} (\bar{w}_{j+1}^n + \bar{w}_j^n) - \frac{\Delta\tau}{2\Delta Z} \frac{\bar{w}_{j+1}^n + \bar{w}_j^n - \bar{v}_{j+1}^n - \bar{v}_j^n}{\lambda_{j+1}^n + \lambda_j^n} \\ & \cdot (\bar{w}_{j+1}^n - \bar{w}_j^n) - \frac{\bar{d}}{1-c_0} \frac{\Delta\tau}{8} (\gamma_{j+1}^n + \gamma_j^n) (\bar{w}_{j+1}^n + \bar{w}_j^n - \bar{v}_{j+1}^n - \bar{v}_j^n) \\ & + \frac{c_0}{1-c_0} \frac{\Delta\tau}{2\Delta Z} \frac{\gamma_{j+1}^n + \gamma_j^n}{\lambda_{j+1}^n + \lambda_j^n} \left(\frac{(2)}{\sigma_{j+1}} \bar{w}_{j+1}^n - \frac{(2)}{\sigma_j} \bar{w}_j^n \right). \end{aligned} \quad (7.149)$$

7.6.2 Final Values at (j, n+1)

$$\lambda_j^{n+1} = \lambda_j^n + \frac{\Delta\tau}{\Delta Z} \left(\bar{v}_{j+\frac{1}{2}}^{n+\frac{1}{2}} - \bar{v}_{j-\frac{1}{2}}^{n+\frac{1}{2}} \right),$$

$$\begin{aligned} \gamma_j^{n+1} = \gamma_j^n - \frac{\Delta\tau}{\Delta Z} & \frac{\bar{w}_{j+\frac{1}{2}}^{n+\frac{1}{2}} + \bar{w}_{j-\frac{1}{2}}^{n+\frac{1}{2}} - \bar{v}_{j+\frac{1}{2}}^{n+\frac{1}{2}} - \bar{v}_{j-\frac{1}{2}}^{n+\frac{1}{2}}}{\lambda_{j+\frac{1}{2}}^{n+\frac{1}{2}} + \lambda_{j-\frac{1}{2}}^{n+\frac{1}{2}}} \\ & \cdot \left(\gamma_{j+\frac{1}{2}}^{n+\frac{1}{2}} - \gamma_{j-\frac{1}{2}}^{n+\frac{1}{2}} \right) + \frac{\Delta\tau}{\Delta Z} \frac{\gamma_{j+\frac{1}{2}}^{n+\frac{1}{2}} + \gamma_{j-\frac{1}{2}}^{n+\frac{1}{2}}}{\lambda_{j+\frac{1}{2}}^{n+\frac{1}{2}} + \lambda_{j-\frac{1}{2}}^{n+\frac{1}{2}}} \left(\bar{w}_{j+\frac{1}{2}}^{n+\frac{1}{2}} - \bar{w}_{j-\frac{1}{2}}^{n+\frac{1}{2}} \right), \end{aligned}$$

$$\begin{aligned} \bar{v}_j^{n+1} = \bar{v}_j^n + \Delta\tau \frac{\bar{d}}{c_0} \frac{1}{4} & \left(\lambda_{j+\frac{1}{2}}^{n+\frac{1}{2}} + \lambda_{j-\frac{1}{2}}^{n+\frac{1}{2}} \right) \left(\bar{w}_{j+\frac{1}{2}}^{n+\frac{1}{2}} + \bar{w}_{j-\frac{1}{2}}^{n+\frac{1}{2}} - \bar{v}_{j+\frac{1}{2}}^{n+\frac{1}{2}} \right. \\ & \left. - \bar{v}_{j-\frac{1}{2}}^{n+\frac{1}{2}} \right) + \frac{\Delta\tau}{\Delta Z} \left(\frac{(1)}{\sigma} \gamma_{j+\frac{1}{2}}^{n+\frac{1}{2}} - \frac{(1)}{\sigma} \gamma_{j-\frac{1}{2}}^{n+\frac{1}{2}} \right), \end{aligned}$$

$$\begin{aligned} \bar{w}_j^{n+1} = \bar{w}_j^n - \frac{\Delta\tau}{\Delta Z} & \frac{\bar{w}_{j+\frac{1}{2}}^{n+\frac{1}{2}} + \bar{w}_{j-\frac{1}{2}}^{n+\frac{1}{2}} - \bar{v}_{j+\frac{1}{2}}^{n+\frac{1}{2}} - \bar{v}_{j-\frac{1}{2}}^{n+\frac{1}{2}}}{\lambda_{j+\frac{1}{2}}^{n+\frac{1}{2}} + \lambda_{j-\frac{1}{2}}^{n+\frac{1}{2}}} \\ & \cdot \left(\bar{w}_{j+\frac{1}{2}}^{n+\frac{1}{2}} - \bar{w}_{j-\frac{1}{2}}^{n+\frac{1}{2}} \right) - \frac{\bar{d}}{1-c_0} \frac{\Delta\tau}{4} \left(\gamma_{j+\frac{1}{2}}^{n+\frac{1}{2}} + \gamma_{j-\frac{1}{2}}^{n+\frac{1}{2}} \right) \\ & \cdot \left(\bar{w}_{j+\frac{1}{2}}^{n+\frac{1}{2}} + \bar{w}_{j-\frac{1}{2}}^{n+\frac{1}{2}} - \bar{v}_{j+\frac{1}{2}}^{n+\frac{1}{2}} - \bar{v}_{j-\frac{1}{2}}^{n+\frac{1}{2}} \right) + \frac{c_0}{1-c_0} \frac{\Delta\tau}{\Delta Z} \\ & \cdot \frac{\gamma_{j+\frac{1}{2}}^{n+\frac{1}{2}} + \gamma_{j-\frac{1}{2}}^{n+\frac{1}{2}}}{\lambda_{j+\frac{1}{2}}^{n+\frac{1}{2}} + \lambda_{j-\frac{1}{2}}^{n+\frac{1}{2}}} \left(\frac{(2)}{\sigma} \gamma_{j+\frac{1}{2}}^{n+\frac{1}{2}} - \frac{(2)}{\sigma} \gamma_{j-\frac{1}{2}}^{n+\frac{1}{2}} \right). \end{aligned} \tag{7.150}$$

The stresses $\frac{(1)}{\sigma}$ and $\frac{(2)}{\sigma}$ are evaluated by substituting corresponding values of λ and γ in the constitutive relations (7.130) through (7.140). In case it is desired to include elastic-plastic descriptions for tuff, constitutive relation (7.138) is replaced by the (equivalent non-dimensional forms) Eqs. (7.120) through (7.122).

7.6.3 Velocity Boundary Condition

At $Z = 0$ ($j = 1$), the velocities \bar{v}_j^{n+1} and \bar{w}_j^{n+1} are specified.

$$\bar{v}_1^{n+1} = \bar{w}_1^{n+1} = \bar{v}(\tau)$$

To evaluate λ_1^{n+1} , γ_1^{n+1} , it is necessary to employ implicit difference equations. These are obtained by centering at $(1\frac{1}{2}, n+\frac{1}{2})$. Thus

$$\begin{aligned} \lambda_1^{n+1} &= \lambda_2^n + \lambda_1^n - \lambda_2^{n+1} + \frac{\Delta\tau}{\Delta Z} \left(\bar{v}_2^{n+1} + \bar{v}_2^n - \bar{v}_1^n - \bar{v}_1^{n+1} \right), \\ \gamma_1^{n+1} \left(1 - a_1 \frac{\Delta\tau}{\Delta Z} - b_1 \frac{\Delta\tau}{\Delta Z} \right) &= b_1 \frac{\Delta\tau}{\Delta Z} \left(\gamma_2^{n+1} + \gamma_2^n + \gamma_1^n \right) \\ &\quad - a_1 \frac{\Delta\tau}{\Delta Z} \left(\gamma_2^{n+1} + \gamma_2^n - \gamma_1^n \right) - \gamma_2^{n+1} + \gamma_2^n + \gamma_1^n, \quad (7.151) \end{aligned}$$

where

$$a_1 = \frac{\left(\frac{\bar{w}_2^{n+1}}{w_2} + \frac{\bar{w}_2^n}{w_2} + \frac{\bar{w}_1^{n+1}}{w_1} + \frac{\bar{w}_1^n}{w_1} \right) - \left(\frac{\bar{v}_2^{n+1}}{v_2} + \frac{\bar{v}_2^n}{v_2} + \frac{\bar{v}_1^{n+1}}{v_1} + \frac{\bar{v}_1^n}{v_1} \right)}{\lambda_2^{n+1} + \lambda_2^n + \lambda_1^{n+1} + \lambda_1^n},$$

and

$$b_1 = \frac{\frac{\bar{w}_2^{n+1}}{w_2} + \frac{\bar{w}_2^n}{w_2} - \frac{\bar{w}_1^n}{w_1} - \frac{\bar{w}_1^{n+1}}{w_1}}{\lambda_2^{n+1} + \lambda_2^n + \lambda_1^{n+1} + \lambda_1^n}.$$

7.6.4 Artificial Viscosity

In order to smooth out the shocks, a simple quadratic artificial viscosity term was added to the partial pressures.

$${}^{(1)}q_{j+\frac{1}{2}}^{n+\frac{1}{2}} \approx {}^{(1)}q_{j+\frac{1}{2}}^n = \frac{2a^2}{\lambda_j^n + \lambda_{j+1}^n} (\bar{v}_{j+1}^n - \bar{v}_j^n)^2 ,$$

$${}^{(2)}q_{j+\frac{1}{2}}^{n+\frac{1}{2}} \approx {}^{(2)}q_{j+\frac{1}{2}}^n = \frac{2a^2 \rho_0^{(2)}}{{}^{(1)}\rho_0 (\gamma_j^n + \gamma_{j+1}^n)} (\bar{w}_{j+1}^n - \bar{w}_j^n)^2 ,$$

$${}^{(1)}q_j^n = \frac{a^2}{4\lambda_j^n} (\bar{v}_{j+1}^n - \bar{v}_{j-1}^n)^2 ,$$

$${}^{(2)}q_j^n = \frac{a^2 \rho_0^{(2)}}{4 \rho_0 \gamma_j^n} (\bar{w}_{j+1}^n - \bar{w}_{j-1}^n)^2 . \quad (7.152)$$

The artificial viscosity term ${}^{(1)}q$ ${}^{(2)}q$ was evaluated only when $\partial\bar{v}/\partial Z(\partial\bar{w}/\partial Z) < 0$. For $\partial\bar{v}/\partial Z(\partial\bar{w}/\partial Z) \geq 0$, it was set equal to zero. The coefficient "a" was taken to be 2.

7.7 NUMERICAL RESULTS

A FORTRAN code (POROUS) has been written incorporating the finite difference scheme outlined in Section 7.6. Wave propagation was investigated in a water-saturated tuff specimen 0.5 cm long ($\ell = 0.5$ cm, $L = 1.0$ cm). The following values are assumed for various parameters:

$$\bar{v}_0 = 7.786 \times 10^4 / S_0 ,$$

$$\tau_0 = 5 \times 10^{-7} S_0 / L ,$$

$$\bar{v}(\tau) = \begin{cases} \bar{v}_0 , & \tau < \tau_0 , \\ 0.75 \bar{v}_0 (3 - 2\tau/\tau_0) + 0.25 \bar{v}_0 , & \tau \leq \tau_0 \leq \frac{3\tau_0}{2} , \\ 0.25 \bar{v}_0 , & \tau > 3 \tau_0 / 2 , \end{cases}$$

$$\Delta Z = 0.004 ,$$

$$\Delta \tau = 0.0008 ,$$

$$\ell / \Delta Z = 125 \text{ (number of zones)} . \quad (7.153)$$

For sake of convenience, the following discussion is divided into four parts, namely:

- (1) Use of minimal principle versus pressure equilibrium $N(J)$,
- (2) Inclusion of dilatational difference term $k(\lambda - \gamma)$ in the constitutive law ,
- (3) Effect of diffusive resistance ,
- (4) Inclusion of strength effects .

7.7.1 Minimal Principle vs Pressure Equilibrium

To study the effect of using $N_p(J)$ or $N_m(J)$, the constitutive relation (7.140) was taken in the simplified form

$$n(\lambda, \gamma) = N\left(\frac{\lambda + \gamma}{2}\right) .$$

Also d was taken to be $10^6/\text{sec}$. Note that this value for d is used also in Section 7.2 and 7.4. Calculations were run for three different values of $N(J)$, namely

$$(1) \quad N(J) = N_m(J) \quad \text{Eq. (7.148),}$$

$$(2) \quad N(J) = N_p(J) \quad \text{Eq. (7.146),}$$

$$(3) \quad N(J) = N_0 .$$

The effective pressures in the two constituents and the mixture at $\tau = 0.064$ are shown in Figs. 7.5 through 7.7. A comparison of Figs. 7.5 and 7.6 shows that although the mixture pressure (behind the shock) is nearly the same in both cases, the response of individual constituents (and the diffusion of water ahead of the shock in tuff) is quite different. Again, Fig. 7.7 reinforces this observation. Even though the pressure in the two constituents is quite different from that predicted in Figs. 7.5 and 7.6, the mixture response is only slightly different.

The preceding discussion clearly indicates that the mixture pressure behind the shock is relatively insensitive to the form of $N(J)$. This is not too surprising. Let us examine the mixture equations.

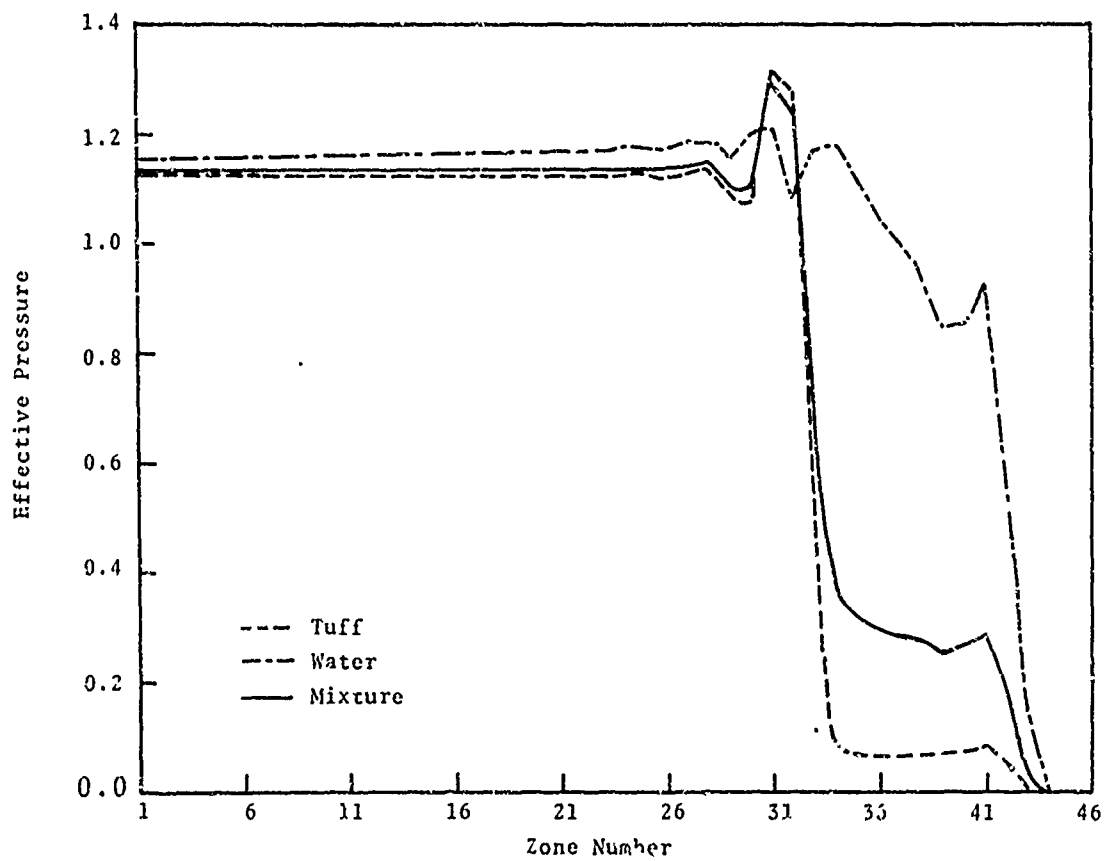


Fig. 7.5--Effective pressures with $n = N_m(J)$. Here $d = 10^6/\text{sec}$, $\tau = 0.064$ and $F = 0.148$.

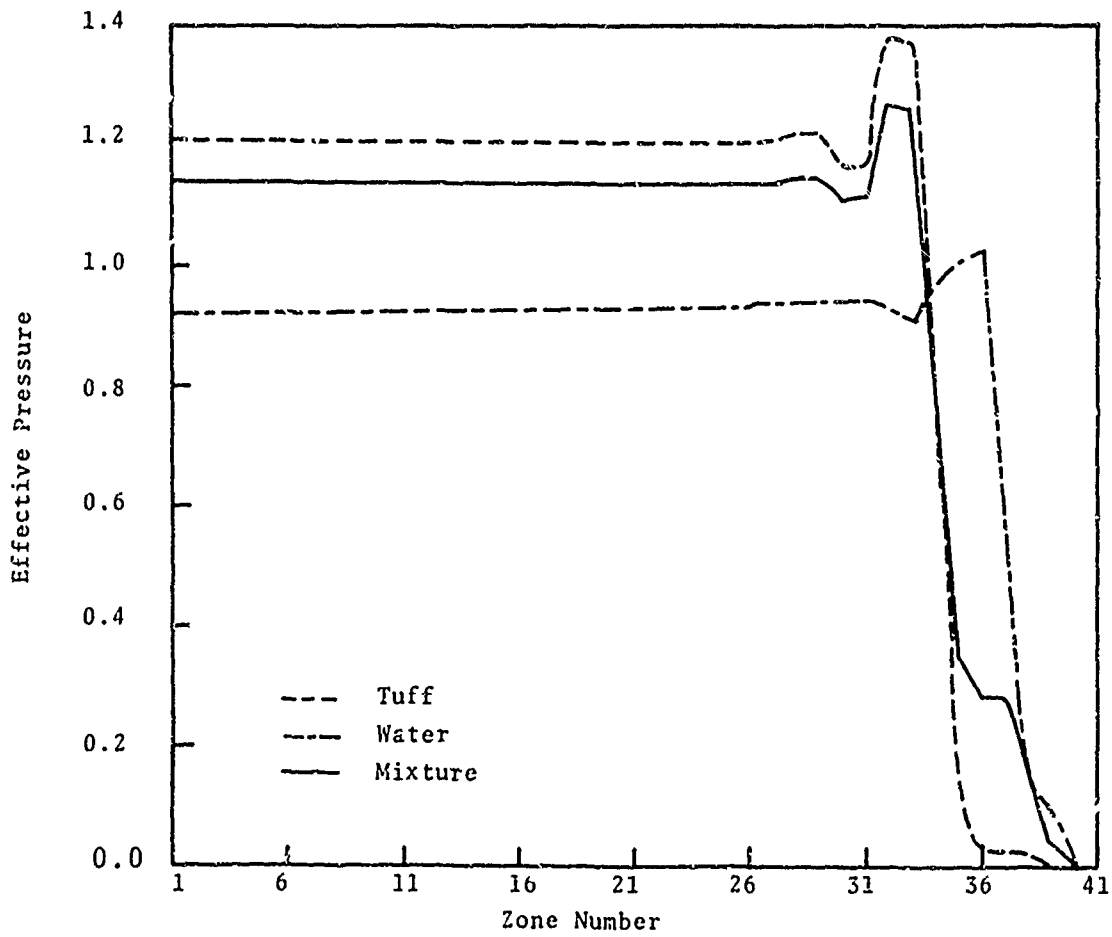


Fig. 7.6--Effective pressures with $n = N_p(J)$. Here $d = 10^6/\text{sec}$, $\tau = 0.064$ and $F = 0.148$.

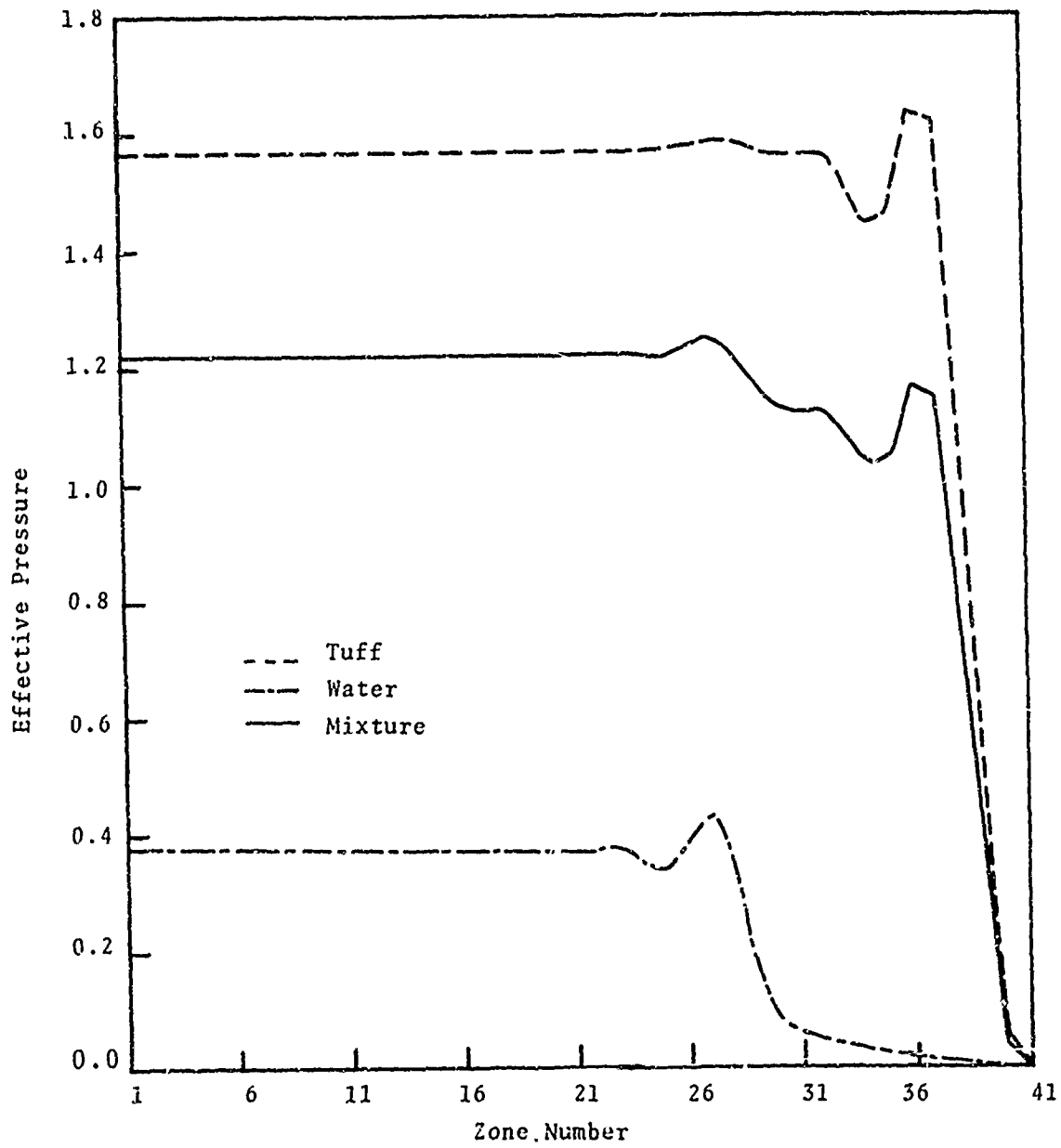


Fig. 7.7--Effective pressures with $n = N_a$. Here $d = 10^6/\text{sec}$, $\tau = 0.064$ and $F = 0.148$.

Equation of Continuity:

$$\frac{\partial \rho}{\partial t} + \frac{\partial(\rho V)}{\partial x} = 0, \quad (7.154)$$

Equation of Momentum:

$$\frac{\partial V}{\partial t} + V \frac{\partial V}{\partial x} = \frac{\partial \sigma}{\partial x} - \frac{\partial}{\partial x} \left[\frac{(1)}{\rho} u_1^2 + \frac{(2)}{\rho} u_2^2 \right], \quad (7.155)$$

where

$$\rho = \frac{(1)}{\rho} + \frac{(2)}{\rho}, \quad (\text{Mixture Density})$$

$$V = \left(\frac{(1)}{\rho} v + \frac{(2)}{\rho} w \right) / \rho, \quad (\text{Mixture Velocity})$$

$$u_1 = v - V, \quad u_2 = w - V,$$

$$\sigma = \frac{(1)}{\sigma} + \frac{(2)}{\sigma}.$$

Behind the shock

$$v \approx w \approx \text{const.}$$

and therefore

$$u_1 \approx u_2 \approx 0.$$

Thus the mixture behaves more or less like a single constituent. It is immaterial how the total stress σ is divided into partial stresses $\frac{(1)}{\sigma}$ and $\frac{(2)}{\sigma}$.

However, when the interest centers on the response of individual constituents and diffusion, the form of $N(J)$ is quite important. It is felt that since pressure equilibrium is physically more reasonable than minimal principle, it should be used to predict $N(J)$.

7.7.2 Inclusion of Dilatational Difference Term $k(\lambda-\gamma)$ in the Constitutive Law

We observed in the preceding that behind the shock, the mixture moves as if it were a single constituent. It is, therefore, reasonable to expect that the effective pressures in the two constituents (water and tuff) behind the shock should be approximately equal. With this in view, we have examined various forms of the dilatational difference term $k(J) (\lambda-\gamma)$ for incorporation into the constitutive law (7.140). We present here (see Figs. 7.8 through 7.10) results for three choices of k , i.e.,

$$(1) \quad k = 1.0 (J-1) ,$$

$$(2) \quad k = 1.2 (J-1) ,$$

$$(3) \quad k = 1.4 (J-1) ,$$

where

$$J = (\lambda+\gamma)/2 .$$

An examination of Figs. 7.6 and 7.8 through 7.10 reveals that for the choice $k = 1.2(J-1)$, the pressures in the two constituents behind the shock are nearly equal. This case also corresponds to least diffusion of water through tuff. We note in passing that inclusion of dilatational difference term does not make too much difference as far as the mixture pressure is concerned.

Calculations were also run for the following two additional choices for the dilatational difference term:

$$(1) \quad (\mu_0 - \mu_c^2) \mu_1 ,$$

$$(2) \quad (\mu_0 - \mu_2^2)(\mu_1 - \mu_1^2) ,$$

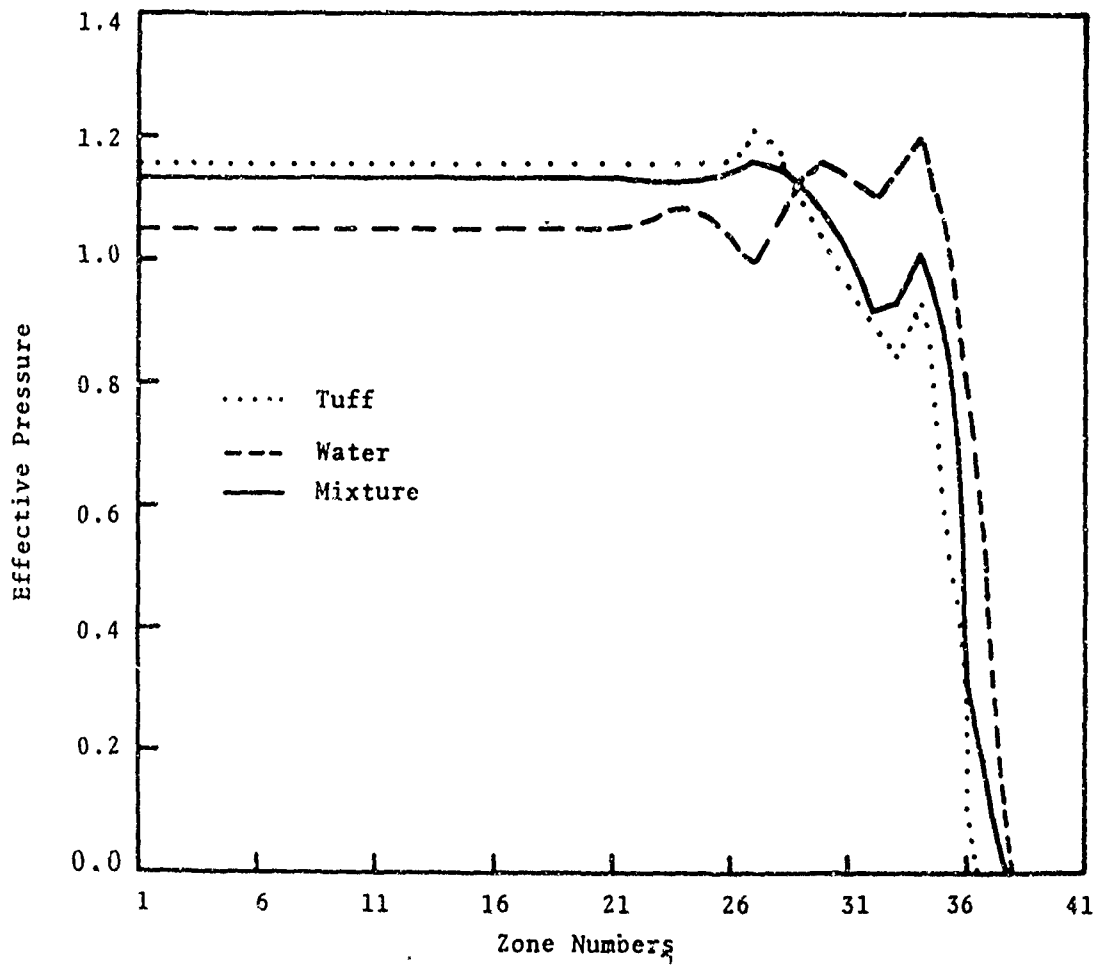


Fig. 7.8--Effective pressures with $n = N(J) + (J-1)(\lambda-\gamma)$.
 Here $d = 10^6/\text{sec}$, $\tau = 0.064$ and $F = 0.148$.

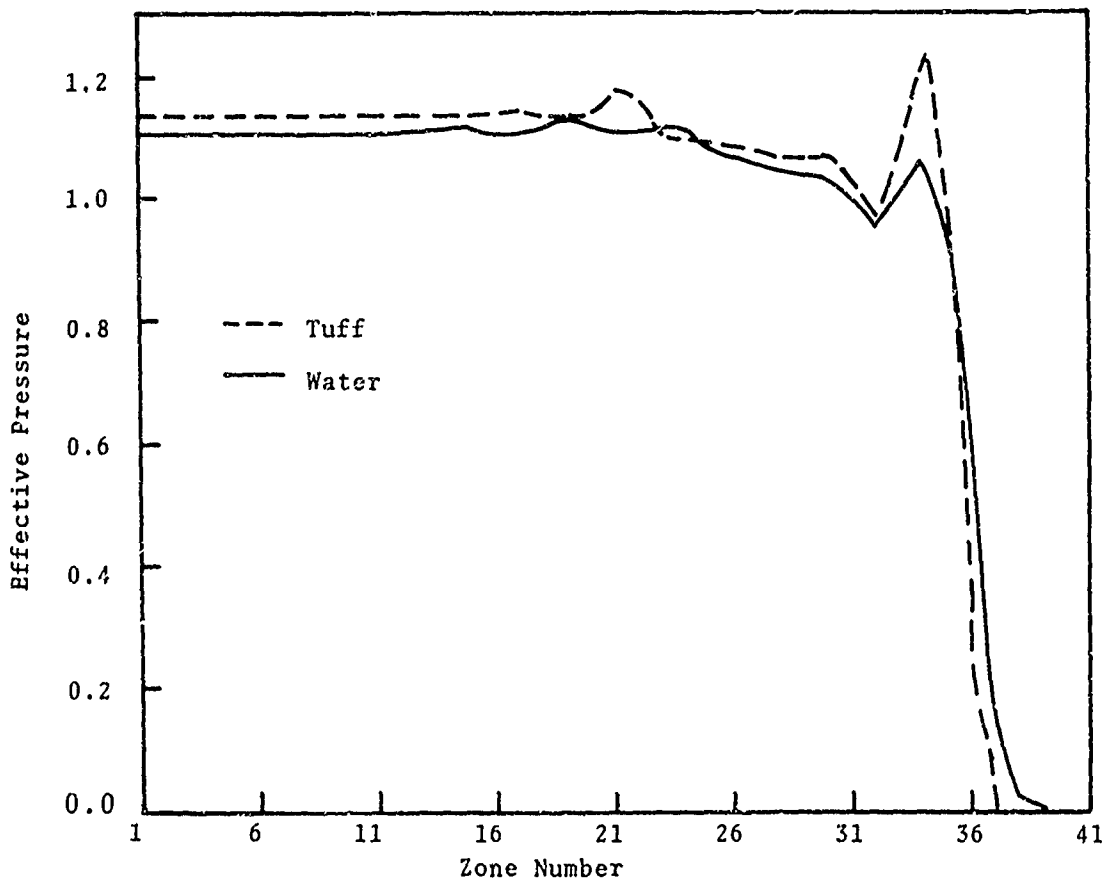


Fig. 7.9--Effective pressures with $n = N(J) + 1.2(J-1)(\lambda-\gamma)$.
 Here $d = 10^6/\text{sec}$, $\tau = 0.064$ and $F = 0.148$.

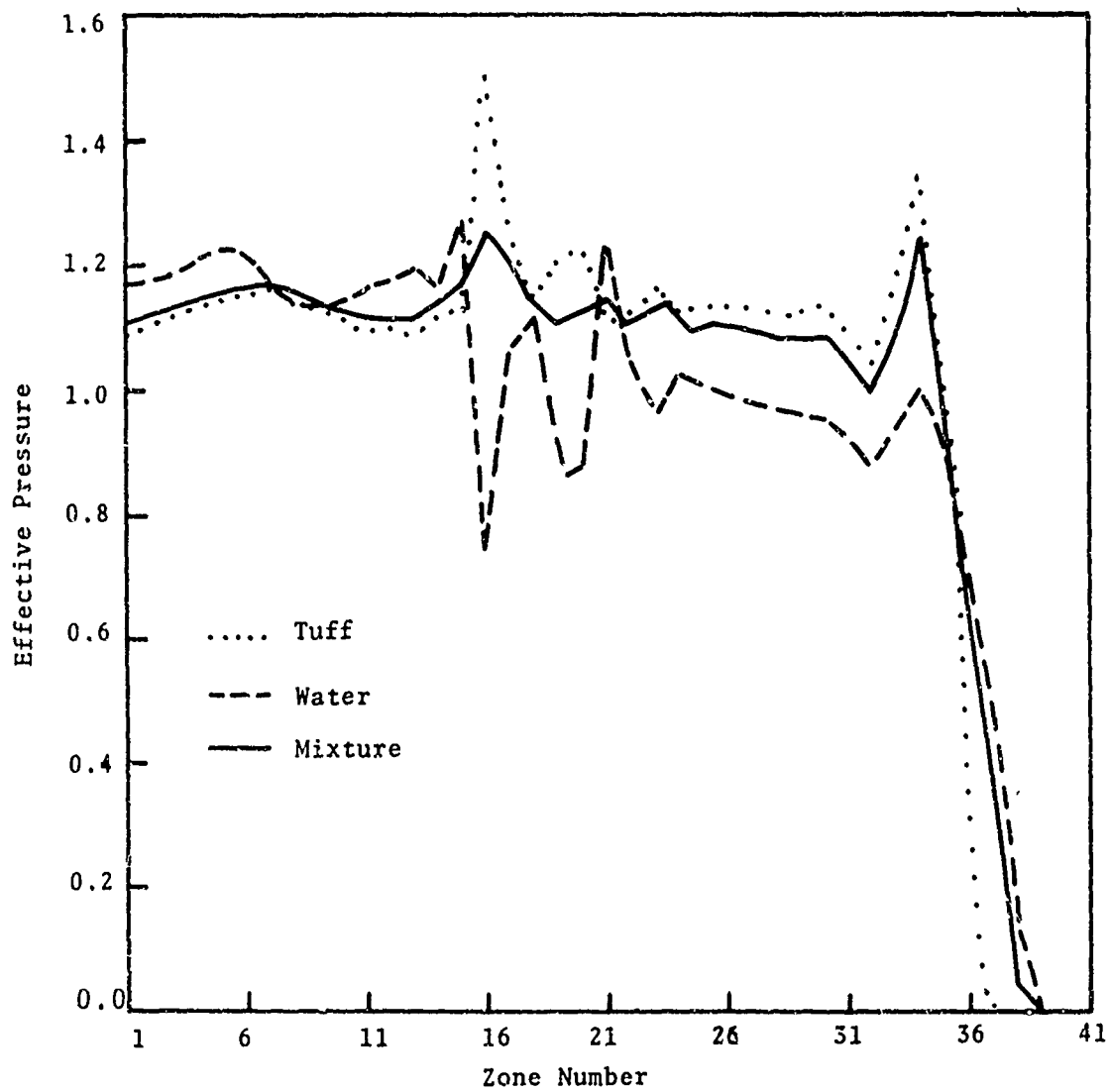


Fig. 7.10--Effective pressures with $n = N(J) + 1.4(J-1)(\lambda-\gamma)$.
 Here $d = 10^6/\text{sec}$, $\tau = 0.064$ and $F = 0.143$.

where

$$\mu_0 = \frac{\lambda + \gamma}{2} - 1 ,$$

and

$$\mu_1 = \lambda - \gamma .$$

The effective pressures at $\tau = 0.064$ are shown in Figs. 7.11 and 7.12. Particle velocities are plotted in Figs. 7.13 and 7.14. The first choice for the dilatational difference term leads to nearly the same results as the case $k = 1.2(J-1)$ discussed above. The second choice for the dilatational difference term yields a slightly higher pressure in water than in tuff. It also leads to somewhat greater diffusion. A look at the velocity profiles is very instructive. The particle velocity far behind the shock is nearly the same in both the materials. However, just behind the shock, the particle velocity in water is much greater than that in tuff. This result is in qualitative agreement with the CRAM code calculations of Section VI. Finally, we observe that in order to correctly predict diffusion and the response of individual constituents in the mixture, it is important to include the dilatational difference term. Presumably it can be tailored to reproduce the experimentally observed phenomena.

7.7.3 Effect of Diffusive Resistance

In order to study the effect of diffusive resistance, calculations were run for the following cases:

- (1) $d = 10^7/\text{sec}$
 $n = N(J) + (\mu_0 - \mu_0^2)(\lambda - \gamma) ,$
- (2) $d = 0$
 $n = N(J) + (\mu_0 - \mu_0^2)(\lambda - \gamma) ,$

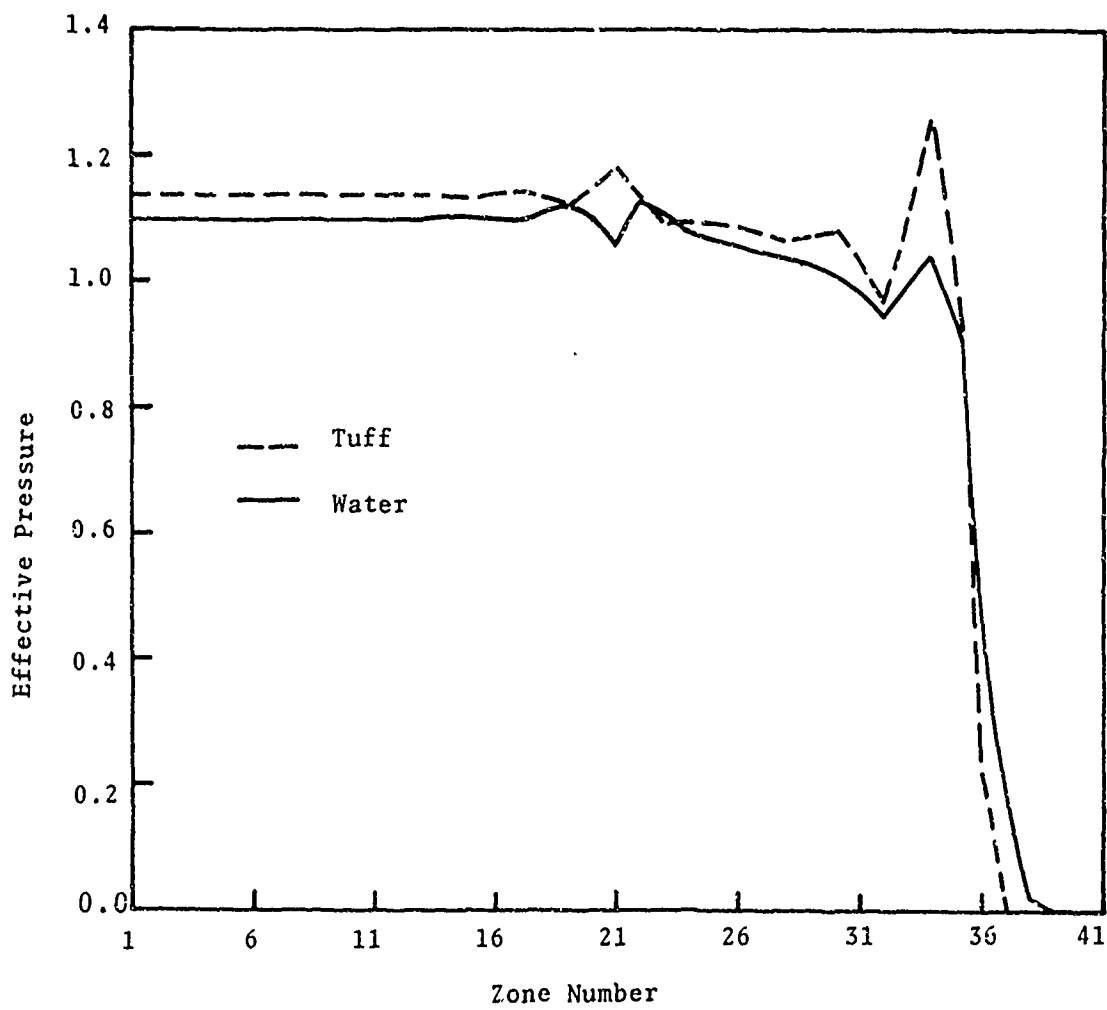


Fig. 7.11--Effective pressures with $n = N(J) + (\mu_0 - \mu_0^2)(\lambda - \gamma)$.
 Here $d = 10^6/\text{sec}$, $\tau = 0.064$ and $F = 0.148$.

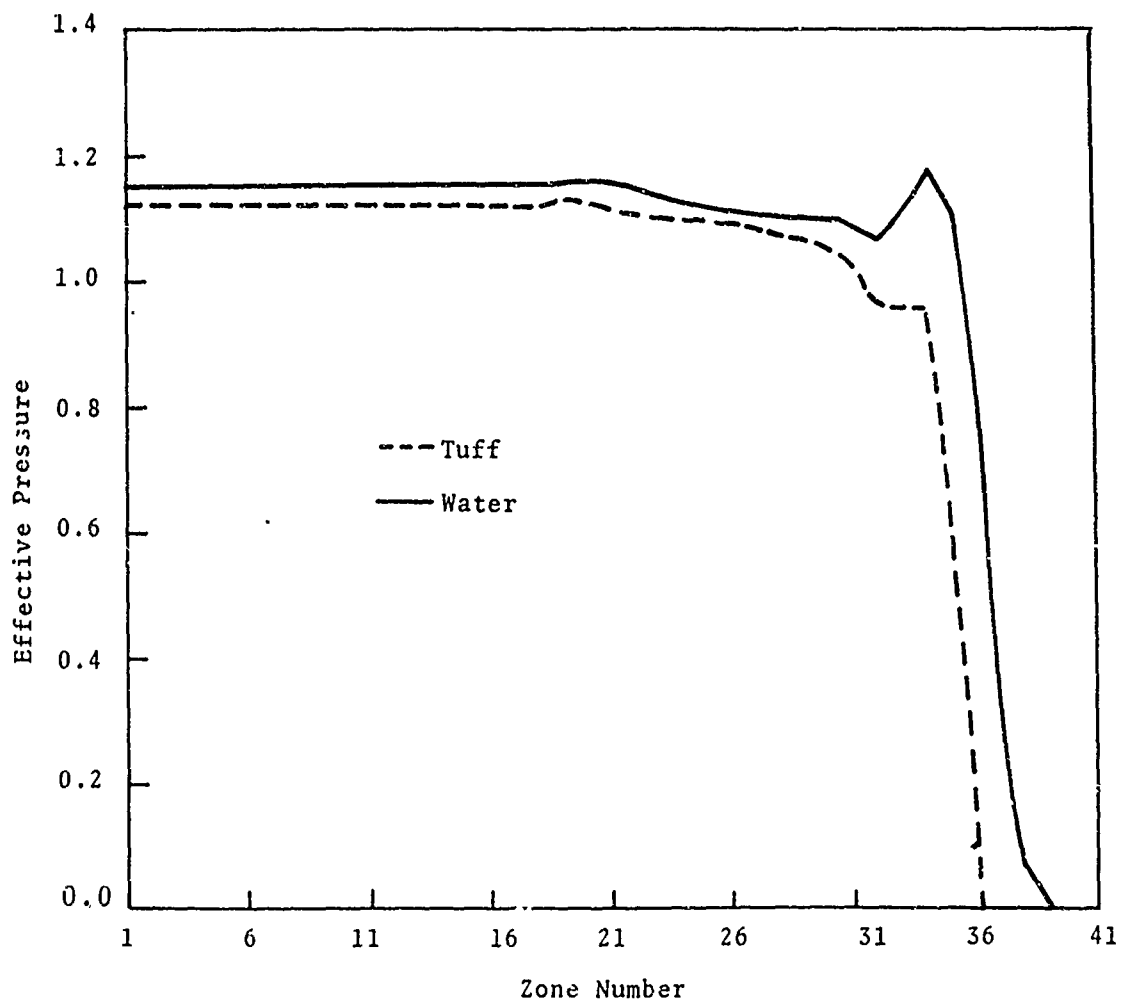


Fig. 7.12--Effective pressures with $n = N(J) + (\mu_0 - \mu_0^2)(\mu_1 - \mu_1^2)$.
 Here $d = 10^6/\text{sec}$, $\tau = 0.064$ and 0.148 .

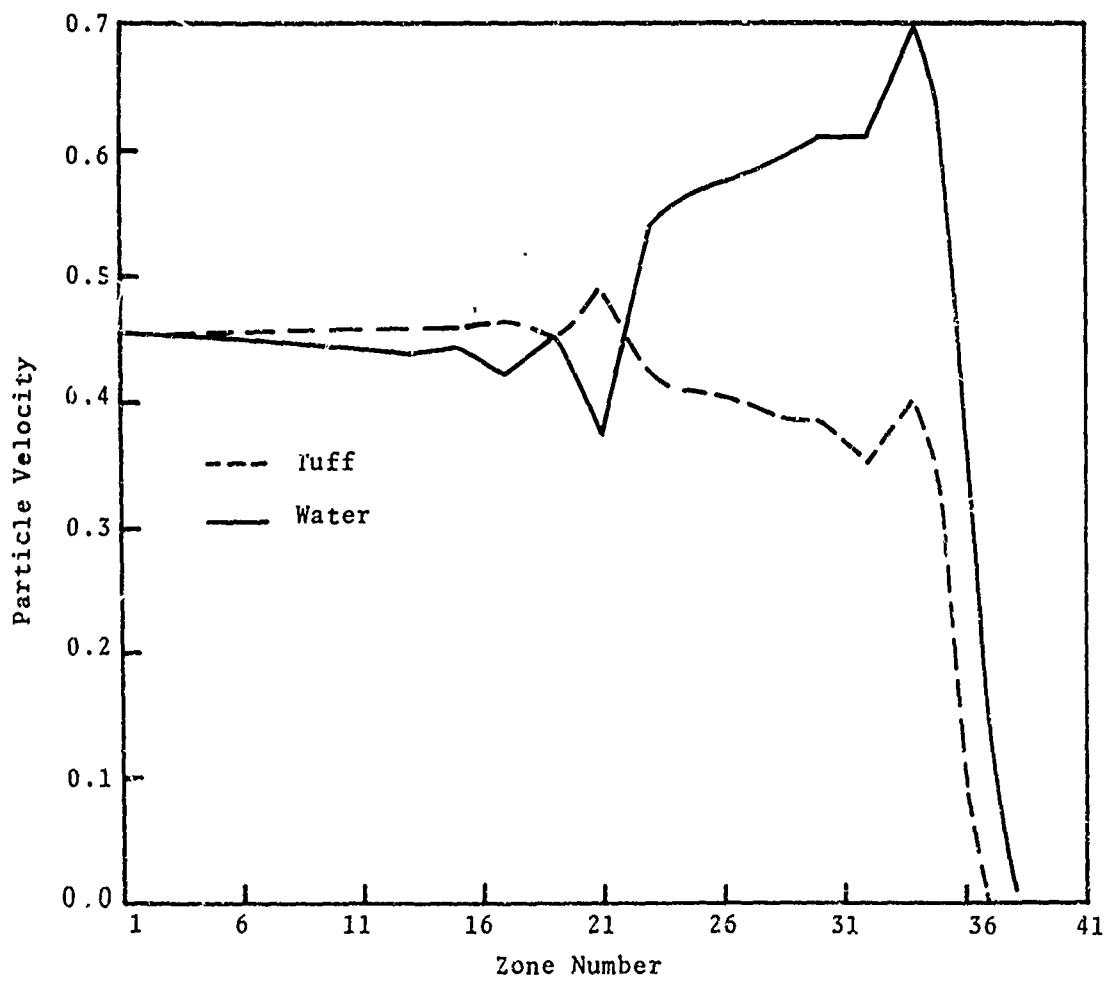


Fig. 7.13--Particle velocities with $n = N(J) + (\mu_0 - \mu_0^2)(\lambda - \gamma)$.
 Here $d = 10^6/\text{sec}$, $\tau = 0.064$ and $F = 0.148$.

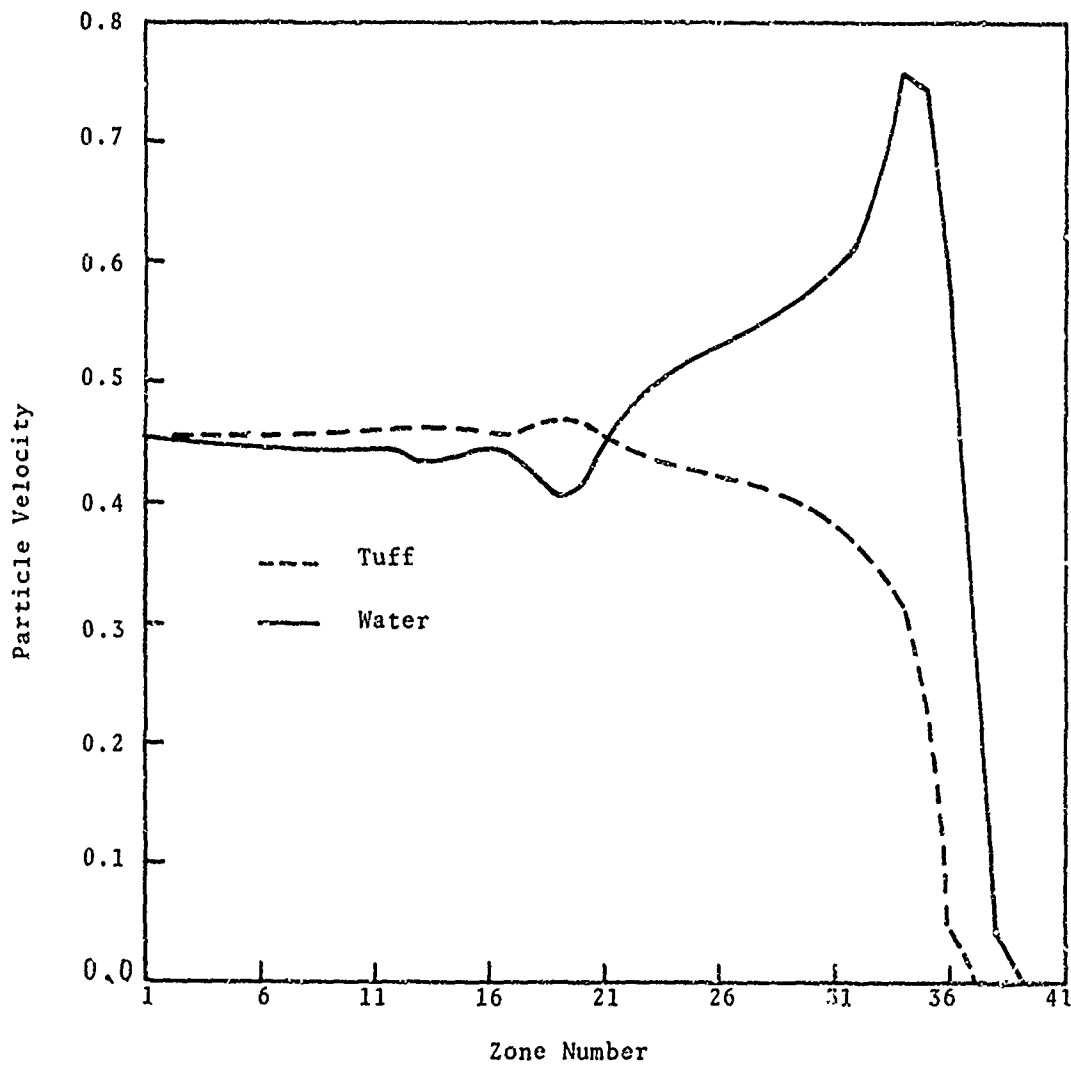


Fig. 7.14--Particle velocities with $n = N(J) + (\mu_0 - \mu^2)(\mu_1 - \mu^2)$.
 Here $d = 10^6/\text{sec}$, $\tau = 0.064$ and $F = 0.148$.

$$(3) \quad d = 0$$

$$n = N(J) + (\mu_0 - \mu_0^2)(\mu_1 - \mu_1^2) .$$

Effective pressure distributions in the two constituents at $\tau = 0.064$ are shown in Figs. 7.15 through 7.17. It is evident from Fig. 7.15 (compare with Fig. 7.11) for this value of d both constituents move together. The small pressure difference in Fig. 7.15 is probably the result of the constitutive assumption for the dilatational difference term. In this case, the mixture motion may be treated as that of a single constituent. Examination of Fig. 6.16 shows that the constitutive assumption for the dilatational interaction term is incorrect. This is obvious on comparing Figs. 7.16 and 7.17. In Fig. 7.17, the pressures behind the shock are nearly equal. Note that in this case, there is a significant amount of diffusion of water through tuff (compare with Fig. 7.12). Thus a decrease in d leads to an increase in diffusion and an increase in it produces a corresponding decrease in diffusion. Also, the constitutive assumption for n of case (3) leads to physically correct results over a range of values of d .

7.7.4 Inclusion of Strength Effects

To illustrate the effect of including elastic-plastic description for tuff, a calculation was run for the following choice of tuff properties:

$$\text{Poisson's Ratio } (\nu) = 0.15 ,$$

$$\text{Yield Stress } (Y) = 5 \text{ kbar} ,$$

$$n = N(J) + (\mu_0 - \mu_0^2)(\mu_1 - \mu_1^2) .$$

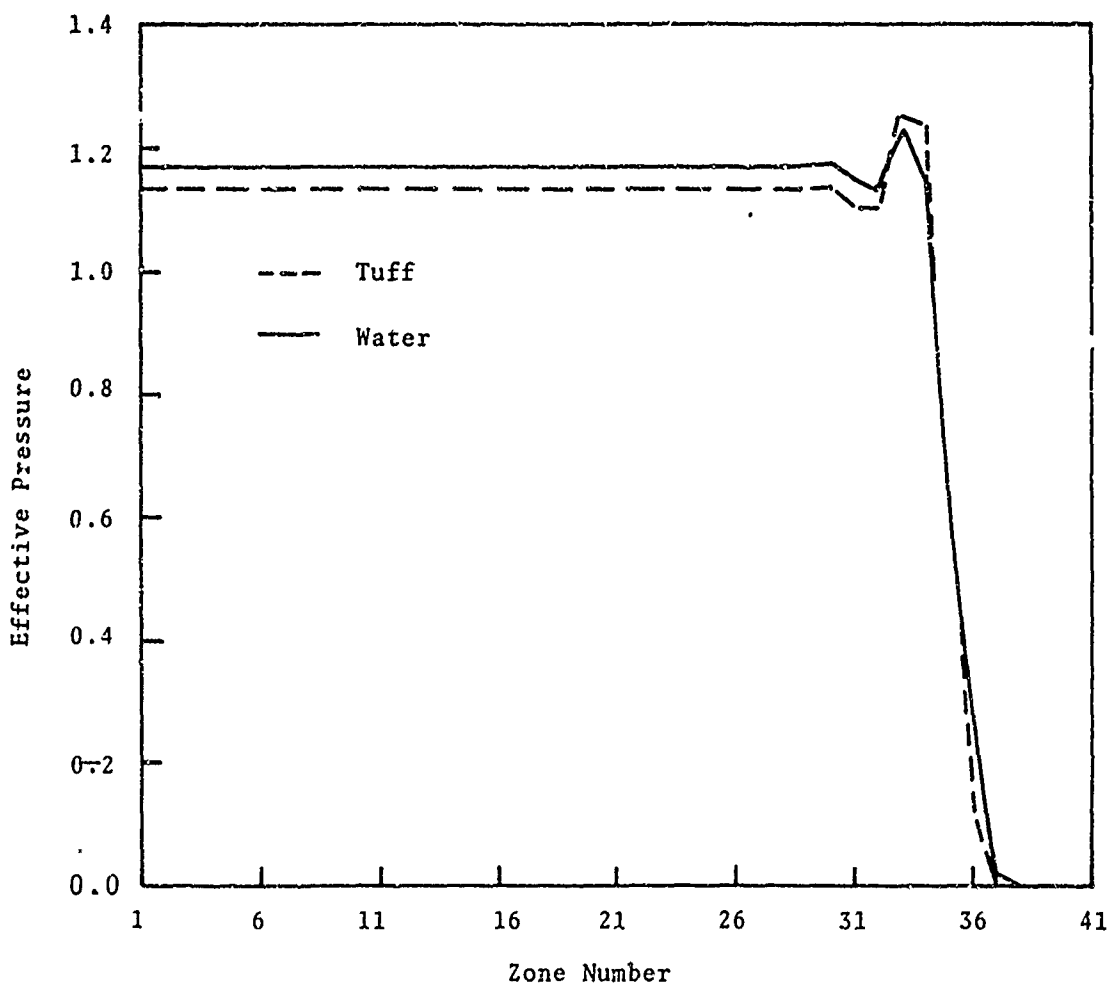


Fig. 7.15--Effective pressures with $n = N(J) + (\mu_0 - \mu_v^2)(\lambda - \gamma)$.
 In this case $d = 10^7/\text{sec}$, $\tau = 0.064$ and
 $F = 0.148$.

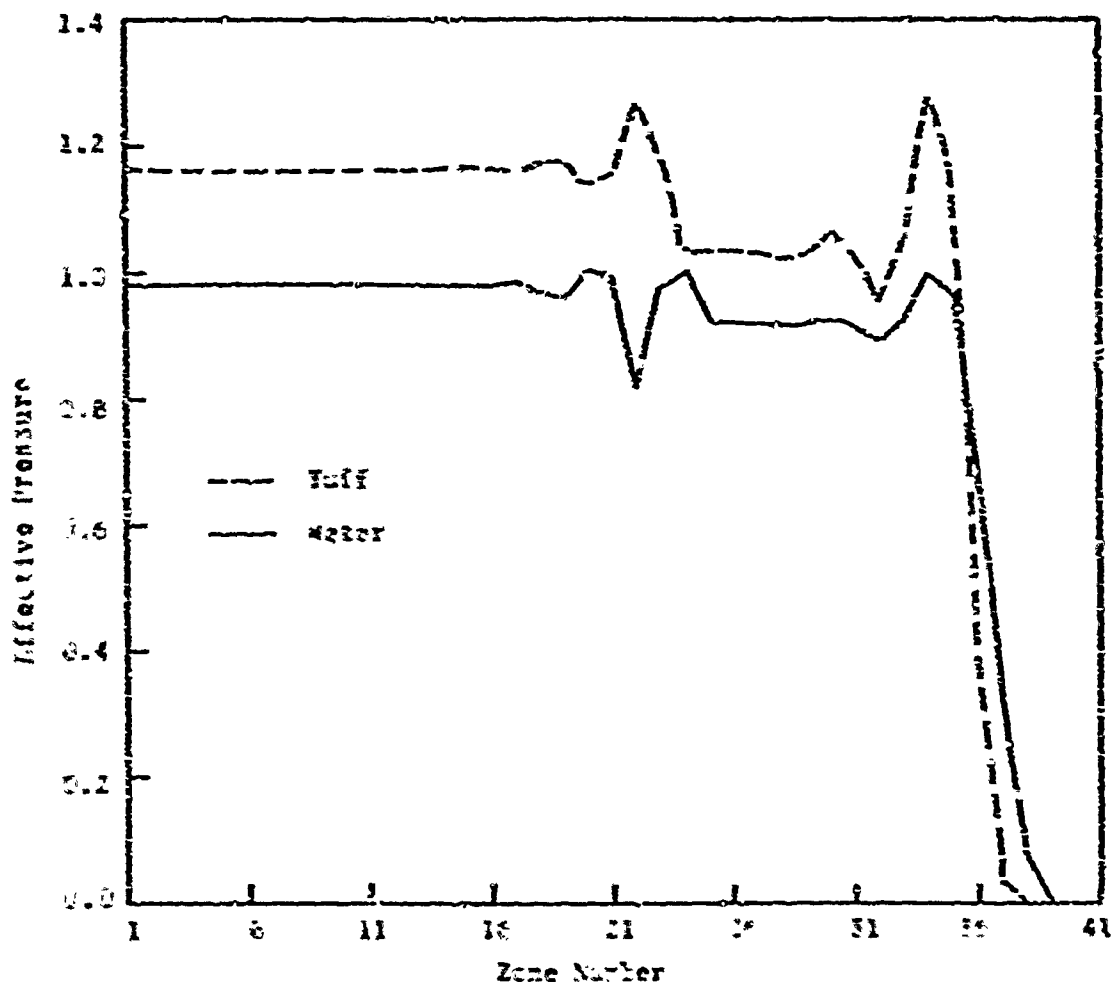


Fig. 7.16--Effective pressures with $n = N(J) + \left(\frac{a_1 - a_2}{J}\right)(\lambda - \nu)$.
 In this case $d = 0$, $\tau = 0.004$ and $F = 0.148$.

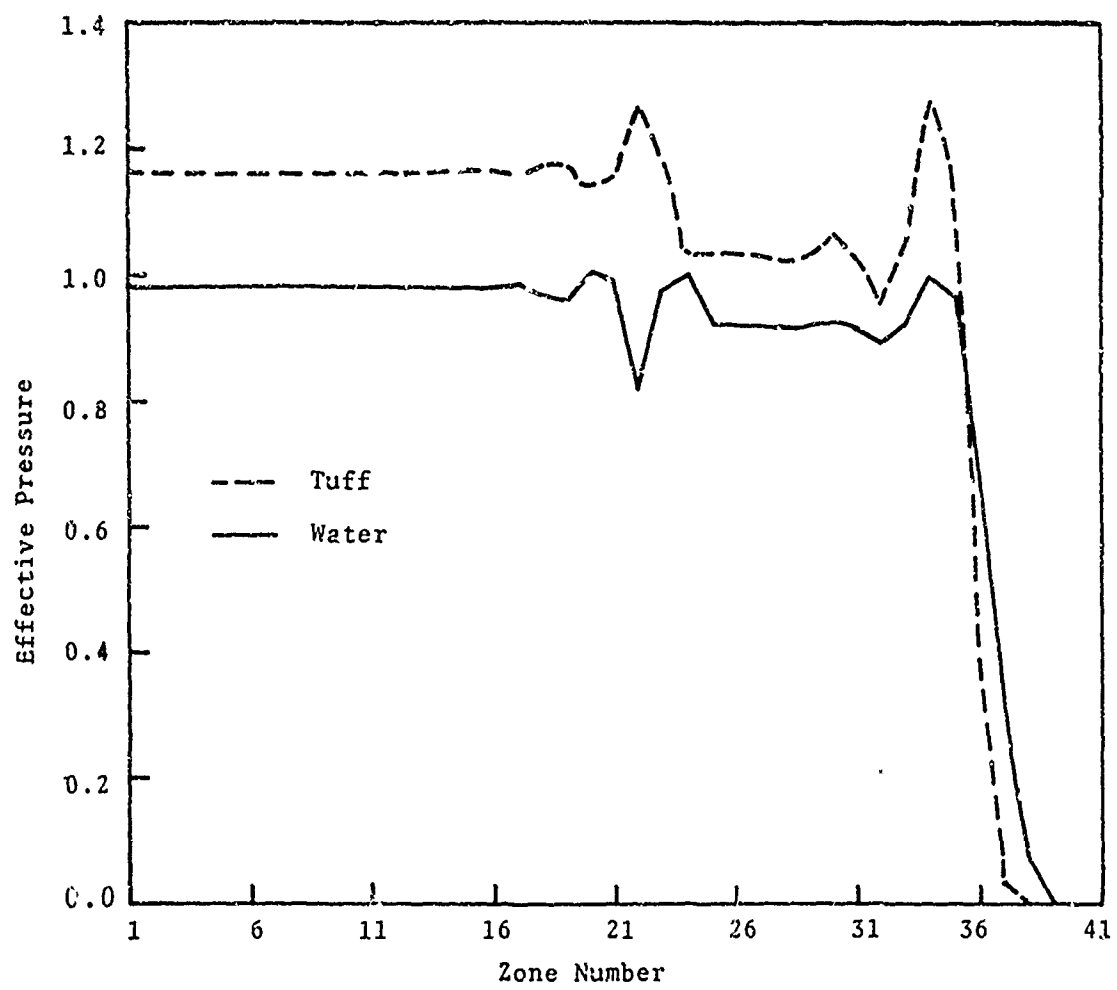


Fig. 7.16--Effective pressures with $n = N(J) + (\mu_0 - \mu_0^2)(\lambda - \gamma)$.
 In this case $d = 0$, $\tau = 0.054$ and $F = 0.148$.

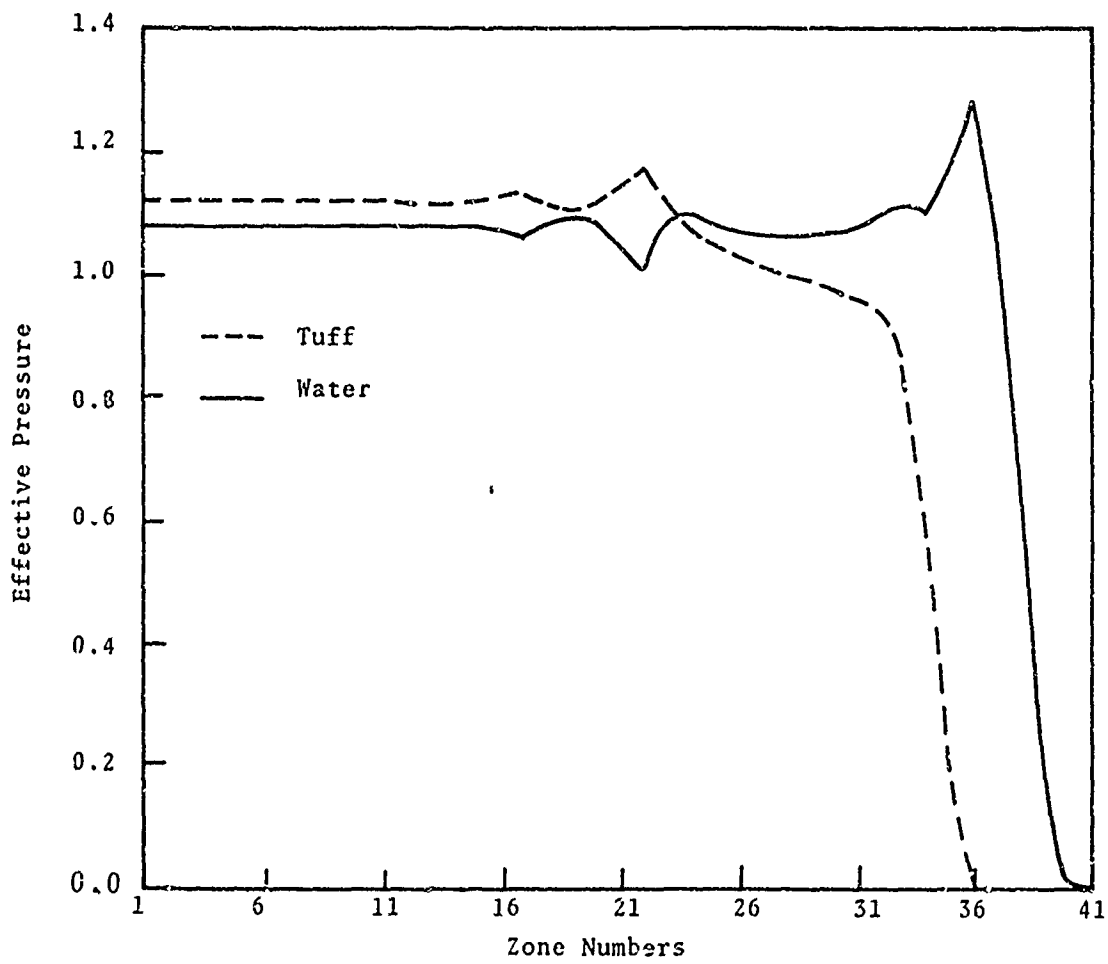


Fig. 7.17--Effective pressures with $n = N(J) + (\mu_0 - \mu_0^2)(\mu_1 - \mu_1^2)$.
 In this case $d = 0$, $\tau = 0.064$ and $F = 0.148$.

The longitudinal stresses in the two components at $\tau = 0.064$ are shown in Fig. 7.18. A comparison with Fig. 7.12 reveals that whereas in the hydrodynamic case longitudinal stress in tuff (behind the shock) is slightly less than that in water, the reverse appears to be true in this case. Also the diffusion is slightly smaller. However, we observe that it is not possible to separate the elastic precursor in tuff from the diffusion of water. Indeed, it appears that diffusion of water through tuff may be much more important than the elastic precursor in tuff.

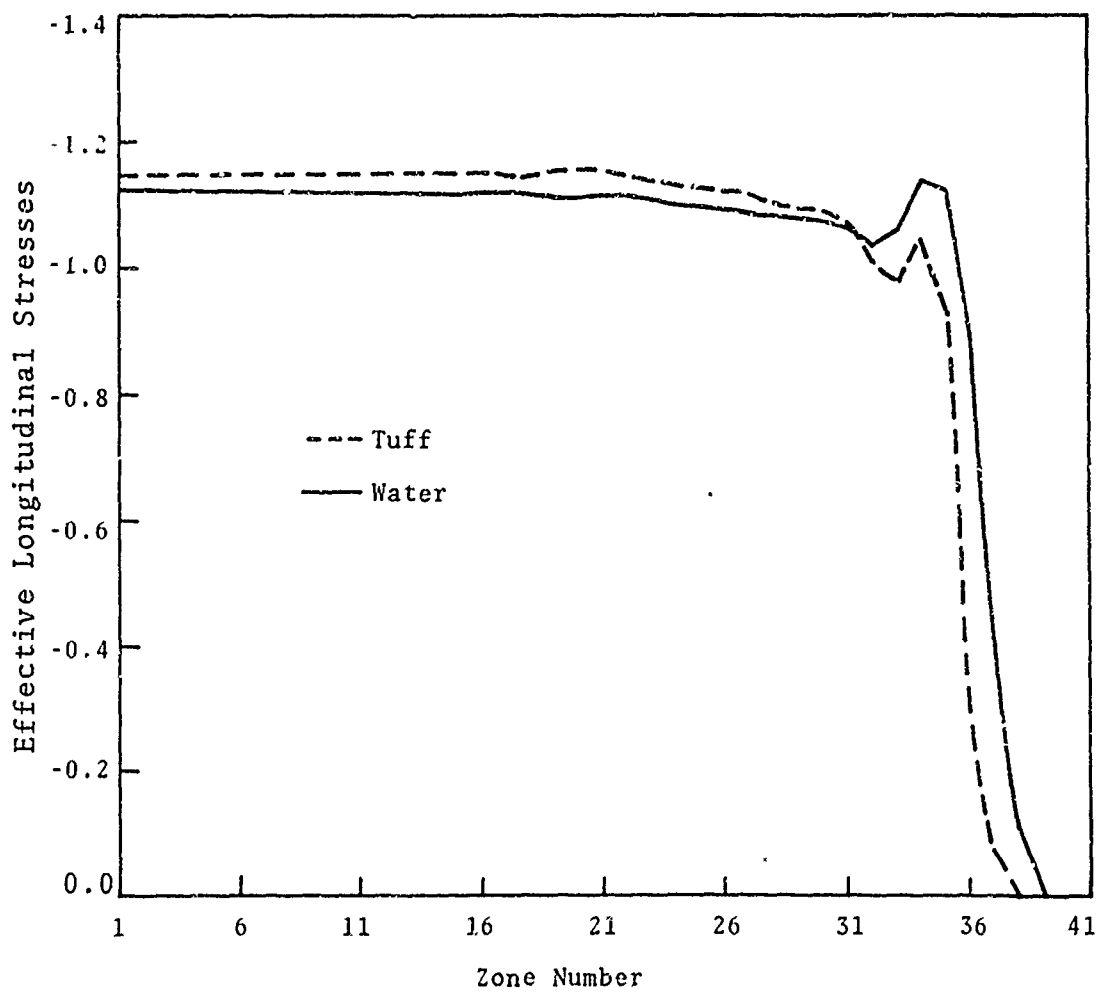


Fig. 7.18--Effective longitudinal stresses with $n = N(J) + (\mu_0 - \mu_0^2)(\mu_1 - \mu_2^2)$, $Y = 5$ kbar and $\nu = 0.15$. Here $d = 10^6$, $\tau = 0.064$ and $F = 0.148$.

VIII. DISCUSSION

The analytic equation of state for pure water presented in Section II provides an essential tool for investigating wave propagation effects in geologic composites when shocked below 250 kbars. Two areas of interest, however, remain to be investigated for pure water substance. As pointed out in Section IV, water in pressure and thermal equilibrium with a geologic material (e.g., tuff), is more susceptible to phase changes in the compressed state. It would be useful to investigate the Water-Ice VII phase transition to ascertain the significance of its inclusion in the equation of state formulation for water.

A second area of interest for pure water is the extension of the present formulation in the expanded state regime so as to include the (thermodynamic) region in the neighborhood of the critical point. This modification should improve the accuracy of calculation of expanded states of material previously shocked to a pressure in the range 150-250 kbars.

Perhaps of greater significance to the construction of adequate material models for calculating stress wave effects in a geologic medium is a more realistic description of the rock matrix. Emphasis here should first be placed on partially saturated materials wherein such factors as matrix crush-up strength, irreversible crush kinetics, enhanced shock heating, and non-equilibrium thermodynamics are taken into account. The available data for the crush-up regime of geologic media are very limited but reasonable estimates for the pertinent parameters can be anticipated; this was found to be the case for compacted tuff in Section III of this report. A phenomenological model for the crush-up

regime has been presented by Herrmann^(85, 86) and this framework, together with an homogenized equation of state for the water saturated material (corresponding to states realized when all the voids are crushed up), provides a point of departure for this analysis.

Work has been initiated along these lines for a partially saturated wet tuff medium. The homogenized PTEQ equation of state will be used to determine the reference saturated wet tuff states associated with complete crush-up. An homogenized reference equation based on pressure equilibrium between the water and tuff components under adiabatic conditions will also be considered.

Detailed numerical calculation for 1-D laminated configurations (Section V) demonstrated that the attenuation of finite-length pulses can be significantly reduced by the presence of substructure in the medium. This unexpected result, obtained for non-linear volumetric models for the water and tuff components, should be investigated further using more realistic material models. Calculations for step pulses have already shown that the presence of a substructure can drastically lower the equilibrium temperature attained by the water laminates when no heat transfer is permitted between the laminates modeled as thermodynamic fluids. This is a consequence of the water reaching initial peak pressure by being subjected to two successive shocks. For a finite-length pulse this mechanism is still present and will affect expanded states of the water.

Such 1-D calculations are extremely useful in providing an understanding of the effect of substructure on wave propagation. Partially saturated geologic media can also be simulated by spaces between the water and rock laminates in an appropriate configuration. The non-equilibrium kinetics and thermodynamics can most economically be

examined by this method in conjunction with analytical approximations accounting for heat transfer between the laminates. These studies would help to establish the relevance of the PTEQ model to field type pulse (msec duration), as well as the limits on the homogenized model for laboratory material tests.

Some 2-D and 3-D calculations should be made to simulate the crush-up of the rock (e.g., tuff) matrix for a partially saturated medium. The shear strength of the matrix and the kinetics of the crush-up mechanism cannot be treated using a laminated configuration. These calculations would provide valuable insight and a check on the validity of the homogenized treatment based on Herrmann's model (and very limited experimental data).

The 2-D calculation of a step pulse propagating parallel to the laminates of a water/tuff composite (Section VI) showed that the particle velocities of the components can be quite different. The Theory of Interacting Continua developed in Section VII explicitly accounts for this relative diffusion within a generalized homogenized model. Although considerable progress was achieved during the present contract period in understanding the nature of the interaction function, n , this effort should be continued and correlated with experimental data. The constitutive relations should be extended to account for mechanical crush-up by considering the rock component to be a porous matrix (e.g., porous tuff). Calculations should be made to study this effect when diffusion of the water through the partially filled pores is allowed.

A major modification of the Theory of Interacting Media that should be made is to develop material models which include the dependence of the partial pressures on the internal energy of the associated component.

In the above discussion the suggested areas of future theoretical effort are clearly indicated from the work of the first ten months' period of this contract. The work has also shown the need for experimental data for the release isentropes of completely saturated geologic materials, e.g., tuff. In extending the modelling to include partially saturated tuff, there will be a corresponding requirement for data describing the loading and release paths in the crush-up regime.

A second area in which experimental data are needed is to evaluate the relative diffusion of an included fluid through the pores of a geologic matrix material. The effect on wave propagation can be studied by using fluids of widely varying viscosity and measuring the profile and attenuation of pulses. A separation of the elastic precursor from any diffusion precursor could also be attained by such tests.

The theoretical and experimental areas suggested are all in accordance with the philosophy of incorporating new physical effects into the material models in a step-by-step procedure. Once the characterization of the isotropic stress component and the crush-up states for partially saturated materials are completed, however, there are various candidates for the next most important mechanism to be incorporated into the models, e.g., it is hazardous to specify intuitively which of these physical effects should be singled out for detailed theoretical analysis (or for associated experimental tests). It is therefore suggested that a series of 1-D spherical calculations be made in which the material parameters governing the candidate physical effects are varied over the range of uncertainty. The sensitivity of the predicted far-field seismic signal to the uncertainties in the material properties can be estimated in this manner. Such information would be a helpful basis for determining the physical effects which warrant subsequent detailed study.

REFERENCES

1. Simmons, G., and E. Herrin, "The Present Status of Seismic Coupling," Proc. of Seismic Coupling Meeting Sponsored by the Advanced Research Projects Agency, Stanford Research Institute, January 1968.
2. Brace, W. F., and J. B. Walsh, "Mechanical Properties of Rock of Importance in Decoupling Analysis," Defense Atomic Support Agency Report DASA 2266, December 1968.
3. Kennedy, G. C., "Pressure-Volume-Temperature Relations in Water at Elevated Temperatures and Pressures," Am. J. Sci. 248, 540 (1950).
4. Bridgman, P. W., "The Phase Diagram of Water to 45,000 kg/cm²," J. Chem. Phys. 5 (1937).
5. Bridgman, P. W., "Pressure-Volume Relations for Seventeen Elements to 100,000 kg/cm²," Am. Acad. Arts Sci. 74, April 1942.
6. Keenan, J. H., and F. G. Keyes, Thermodynamic Properties of Steam, John Wiley and Sons, Inc., New York, January 1967.
7. Keenan, J. H., F. G. Keyes, P. G. Hill and J. G. Moore, Steam Tables, John Wiley and Sons, Inc., New York (1969).
8. Meyer, C. A., et al., 1967 ASME Steam Tables, ASME, New York (1969).
9. Walsh, J. M., and M. H. Rice, "Dynamic Compression of Liquids from Measurements on Strong Shock Waves," J. Chem. Phys. 26, 815-823 (1957).
10. Rice, M. H., and J. M. Walsh, "Equation of State of Water to 250 Kilobars," J. Chem. Phys. 26, 824-830 (1957).
11. Papetti, R. A., and M. Fujisaki, "The Rice and Walsh Equation of State for Water: Discussion, Limitations, and Extensions," J. App. Phys. 39, (1968).
12. Waiker, W. A., and H. M. Sternberg, "The Chapman-Jouguet Isentrope and the Underwater Shockwave Performance of Pentolite," Fourth Symposium on Detonation (October 12-15, 1965), U. S. Naval Ordnance Laboratory, White Oak, Silver Spring, Maryland.

13. Pistorious, C.W.F.T., and W. E. Sharp, "Properties of Water, Part VI. Entropy and Gibbs Free Energy of Water in the Range 10-1000°C and 1-250,000 Bars," Am. J. Sci., 258, 757-768, December 1960.
14. Sharp, W. E., "The Thermodynamic Functions for Water in the Range -10 to 1000°C and 1 to 250,000 Bars," Lawrence Radiation Laboratory Report UCRL-7118, October 1962.
15. Howard, J. C., "Thermodynamic Data for Water," Lawrence Radiation Laboratory Report UCRL-6455-T, April 1961.
16. Papetti, R., Private Communication, December 5, 1969.
17. Bjork, R. L., K. N. Kreyenhagen, and M. H. Wagner, "Compressible Hydrodynamic Analysis of an Underwater Blast," (U), Shock Hydrodynamics, Inc., NRD-TRC-69-6, March 1969.
18. Born, M., "Thermodynamics of Crystals and Melting," J. Chem. Phys., 7, 591-603 (1939).
19. Cowperthwaite, M., and R. Shaw, "A $C_V(T)$ Equation of State for Liquids. Calculation of the Shock Temperature of Carbon Tetrachloride, Nitromethane and Water in the 100 Kbar Region," Submitted for publication to J. Appl. Phys., October 1969. (Work performed at Stanford Research Institute under Contract No. NONR-3760(00)).
20. Walsh, J. M., and R. H. Christian, "Equation of State of Metals from Shock Wave Measurements," Phys. Rev. 97 (6), 1544-1556, March 15, 1955.
21. Snay, H. G., and J. H. Rosenbaum, "Shockwave Parameters in Fresh Water for Pressures up to 95 kilobars," NAVORD Report 2383 (1952).
22. Al'Tshuler, L. V., A. A. Bakanova, and R. F. Trunin, "Phase Transformations of Water Compressed by Strong Shock Waves," Soviet Physics-JETP, p. 614, no. 26 (1957).
23. Schall, R. "Die Zustandsgleichung des Wassers bei hohen Drucken nach Rontgenblitzaufnahmen intensiver Stoßwellen," (The Equation of State of Water at High Pressure in Shockwaves by Means of Flash X-ray Photography), Z. Angew. Physik 2, 252 (1950).

24. Dorsey, N. E., Properties of Ordinary Water Substance, Reinhold, New York (1940).
25. Ahrens, T. J., and V. G. Gregson, "Shock Compression of Crustal Rocks: Data for Quartz, Calcite, and Plagioclase Rocks," J. Geophys. Res. 69 no. 22 (1964).
26. Watanabe, K., H. Ozawa, and I. Tanishita, "New Equation of State for Ordinary Water Substance in the Critical Region," Bulletin of JSME, Vol. II, no. 48, 1145-1160 (1968).
27. Holser, W. T., and G. C. Kennedy, "Properties of Water, Part IV. Pressure-Volume-Temperature Relations of Water in the Range 100-400°C and 100-1400 Bars," Am. J. Sci. 256, 744-751 (1958).
28. Kennedy, G. C., "Properties of Water, Part I. Pressure-Volume-Temperature Relations in Steam to 1000°C and 100 Bars Pressure," Am. J. Sci. 255, 724-730 (1957).
29. Kennedy, G. C., W. L. Knight and W. T. Holser, "Properties of Water, Part III. Specific Volume of Liquid Water to 100°C and 1400 Bars," Am. J. Sci. 256, 590-595 (1958).
30. Holser, W. T., and G. C. Kennedy, "Properties of Water, Part IV. Pressure-Volume-Temperature Relations of Water in the Range 100-400°C and 100-1400 Bars," Am. J. Sci. 256, 744-754 (1958).
31. Holser, W. T., and G. C. Kennedy, "Properties of Water, Part V. Pressure-Volume-Temperature Relations of Water in the Range 400-1000°C and 100-1400 Bars," Am. J. Sci. 257, 71-77 (1959).
32. Sears, F. W., Thermodynamics, the Kinetic Theory of Gases and Statistical Mechanics, Second Edition, Addison-Wesley Publishing Co., Inc., Cambridge, Mass. (1955).
33. Epstein, P. S., Thermodynamics, John Wiley and Sons, New York (1957).
34. Allen, R. T., "Equation of State of Rocks and Minerals," General Dynamics, General Atomic Division, GAMD-7834, March 17, 1967.

35. Stephens, D. R., H. Louis and E. M. Lilley, "Loading-Unloading p-V Curves for Tuffs from the Nevada Test Site," Lawrence Radiation Laboratory, UCRL-50554, February 20, 1969.
36. Stephens, D. R., and E. M. Lilley, "Static P-V Curves of Cracked Consolidated Earth Material to 40 Kilobars," Lawrence Radiation Laboratory, UCRL-14711, March 28, 1966.
37. Stephens, D. R., E. M. Lilley, and H. Louis, "Pressure-Volume Equation of State of Consolidated and Fractured Rocks to 40 kbar," Lawrence Radiation Laboratory, UCRL-71238, March 6, 1969.
38. Shipman, F. H., W. M. Isbell and A. H. Jones, "High Pressure Hugoniot Measurements for Several Nevada Test Site Rocks," General Motors Corp., Defense Atomic Support Agency Report DASA-2200, March 1969.
39. Jones, A. H., and N. H. Froula, "Uniaxial Strain Behavior of Four Geological Materials to 50 Kilobars," General Motors Corporation, Defense Atomic Support Agency Report DASA 2209, March 1969.
40. Petersen, C. F., et al., "Equation of State of Rocks," Stanford Research Institute, SRI-PGU-6618, June 15, 1968.
41. Lombard, D. B., "The Hugoniot Equation of State of Rocks," Lawrence Radiation Laboratory, UCRL-6311, February 28, 1961.
42. Bass, R. C., H. J. Hawk and A. J. Chabai, "Hugoniot Data for some Geologic Materials," Sandia Laboratory, SC-4903 RR, June 1963.
43. Bass, R. C., "Additional Hugoniot Data for Geologic Materials," Sandia Laboratory, SC-RR-66-548, October 1966.
44. Lysne, P. C., "A Comparison of Calculated and Measured Low Stress Hugoniots and Release Adiabats of Dry and Water Saturated Tuff," Sandia Laboratories, Albuquerque, New Mexico (no date).
45. Wiedermann, A. H., and O. E. Curth, "Shock Unloading Characteristics of Porous Geological Materials," IIT Research Institute, Chicago, Illinois, AFWL-TR-66-118, January 1967.

46. Wiedermann, A. H., and O. E. Curth, "Shock Unloading Characteristics of Crushable Rocks," IIT Research Institute, Chicago, Illinois, WL-TDR-64-52, August 1964.
47. Anderson, D. C., and F. B. Porzel, "Close-In Time-of-Arrival Measurements for Yield of Underground Rainier Shot," WT-1495, December 1959, Hugoniot data supplied by Lawrence Radiation Laboratory.
48. Handbook of Chemistry and Physics, 44th Edition, published by the Chemical Rubber Publishing Company.
49. Bakken, L. H., and P. D. Anderson, "The Compleat Equation of State Handbook, . . .," Sandia Report SCL-TM-67-118, 1967.
50. Rosenberg, J. T., T. J. Ahrens and C. F. Petersen, "Dynamic Properties of Rocks," Stanford Research Institute, DASA-2112, July 1968.
51. Schneider, P. J., Temperature Response Charts, John Wiley and Sons, Inc., New York, 1963.
52. Soo, S. L., Fluid Dynamics of Multiphase Systems, Blaisdell Publishing Company, Waltham, Mass., 315-316, (1967).
53. Petersen, C. F., "Shock Wave Studies of Selected Rocks," Stanford Research Institute, Thesis submitted to Stanford University, May 16, 1969.
54. Farmer, O. A., T. E. Springer, and B. B. Fisher, "FORTRAN IV Hydrogen Property Tabular Codes," LASL-LA3381, UC-34, Physics TID-4500, October 1965.
55. Wilkins, M. L., "Calculation of Elastic-Plastic Flow," Lawrence Radiation Laboratory Report UCRL-7322, April 1963.
56. Kruger, R. A., "The Material Response Program, RIP," (presented at the Nuclear Survivability Working Group on Propulsion and Ordnance Systems, Kirtland Air Force Base, December 3, 4, 1969), Systems, Science and Software Report 3SR-120, December 1969.
57. Cooley, J. W., and J. W. Tukey, "An Algorithm for the Machine Calculation of Complex Fourier Series," Math. of Comp., 19, 297 (1965).

58. Gentlemen, W. M., and G. Sande, "Fast Fourier Transforms--for Fun and Profit," Proc., Fall Joint Computer Conference, 1966, 29, 563 (1966).
59. Borgland, G. D., "A Fast Fourier Transform Algorithm Using Base 8 Iterations," Math. of Comp., 22, 275 (1968).
60. Rytov, S. M., "Acoustical Properties of a Thinly Laminated Medium," Soviet Phys. Acoustics, 2, 68-80, (1956).
61. Halda, E. J., and T. D. Riney, "Response of Two-Dimensional Bodies to Energy Deposition--CRAM Applications," Part II, General Electric Technical Report No. 68-001, December 1967.
62. Sedgwick, R. T., "Theoretical Terminal Ballistic Investigation and Studies of Impact at Low and Very High Velocities," Air Force Armament Laboratory Report AFATL-TR-68-61, May 1968.
63. Tsou, F. K., and P. C. Chou, "Analytical Study of Hugoniot in Unidirectional Fiber Reinforced Composites," J. Composite Materials, 3, 500-517 (1969).
64. Torvik, P. J., "Shock Propagation in a Composite Material," Air Force Institute of Technology Report AFII-TR-69-7, June 1969.
65. Brillouin, L., Wave Propagation in Periodic Structures, Dover Publications, Inc., New York, N.Y., 1953.
66. Truesdell, C., "Mechanical Basis of Diffusion," J. Chem. Phys. 37, 10, 2336-2343 (1962).
67. Biot, M. A., "Generalized Theory of Acoustic Propagation in Porous Dissipative Media," J. Acoust. Soc. Am. 34, 9, 1254-1264 (1962).
68. Green, A. E., and P. M. Naghdi, "A Dynamical Theory of Interacting Continua," Int. J. Eng. Sci. 3, 231 (1965).
69. Green, A. E., and P. M. Naghdi, "A Note on Mixtures," Int. J. Eng. Sci. 6, 631-635 (1968).
70. Crochet, M. J., and P. M. Naghdi, "On Constitutive Equations for Flow of Fluid through an Elastic Solid," Int. J. Eng. Sci. 4, 383-401, 1966.

71. Green, A. E., and T. R. Steel, "Constitutive Equations for Interacting Continua," Int. J. Eng. Sci. 4, 483-500 (1966).
72. Green, A. E., and P. M. Naghdi, "A Theory of Mixtures," Arch. Rat. Mech. Anal. 24, 243 (1967).
73. Bowen, R. M., "Toward a Thermodynamics and Mechanics of Mixtures," Arch. Rat. Mech. Anal. 24, 243-262 (1967).
74. Müller, I., "A Thermodynamic Theory of Mixtures of Fluids," Arch. Rat. Mech. Anal. 28, 1-39 (1968).
75. Dunwoody, N. T., and I. Müller, "A Thermodynamic Theory of Two Chemically Reacting Ideal Gases with Different Temperatures," Arch. Rat. Mech. Anal. 29, 344-369 (1968).
76. Truesdell, C., "On The Foundations of Mechanics and Energetics," Continuum Mechanics II (Gordon and Breach) (Translation of author's 1957 paper in Italian) (1965).
77. Eringen, A. C., and J. D. Ingram, "A Continuum Theory of Chemically Interacting Media," Int. J. Eng. Sci. 3, 197, (1965).
78. Truesdell, C., "Elements of Continuum Mechanics," (Springer-Verlag) (1966).
79. Meixner, J., "Processes in Simple Thermodynamic Materials," Arch. Rat. Mech. Anal. 33, 33 (1969).
80. Adkins, J. E., "Diffusion through Isotropic Highly Elastic Solids," Phil. Trans. Roy. Soc., A, 256, 301 (1964).
81. Adkins, J. E., "Diffusion of Fluids through Aelotropic Highly Elastic Solids," Arch. Rat. Mech. Anal. 15, 222 (1964).
82. Green, A. E., and J. E. Adkins, "A Contribution to the Theory of Non-linear Diffusion," Arch. Rat. Mech. Anal. 15, 235 (1964).
83. Ishihara, K., "Propagation of Compressional Waves in a Saturated Soil," Proc. Int. Symp. on Wave Propagation and Dynamic Properties of Earth Materials, Albuquerque, New Mexico, Aug. 1967.

84. Richtmyer, R. D., and K. W. Morton, "Difference Methods for Initial-Value Problems," Interscience, New York (1967).
85. Herrmann, W., "Constitutive Equation for the Dynamic Compaction of Ductile Porous Materials," J. Appl. Phys. 40, 2490, May 1969.
86. Herrmann, W., "On The Dynamic Compaction of Initially Heated Porous Materials," Sandia Laboratory Report SC-DR-68-865, April 1968.
87. Green, S. J., and R. D. Perkins, "Uniaxial Compression Tests at Strain Rates from 10^{-4} /sec to 10^4 /sec on Three Geologic Materials," General Motors Corporation, MSL-68-6, April 1968.
88. Stephens, D. R., "The Hydrostatic Compression of Eight Rocks," Lawrence Radiation Laboratory, J. of Geophysical Research, 69, no. 14, 2967, July 1967.
89. Barnes, H., "Geologic Description of Selected Rock Samples from the Nevada Test Site," U. S. Dept. of the Interior Geological Survey, Tech. Letter: NTS-185, June 21, 1967.
90. Stowe, R. L., "Strength and Deformation Properties of Granite, Basalt, Limestone and Tuff at Various Loading Rates," U. S. Army Eng. Waterways Exp. Sta. Misc. Paper C-69-1, January 1969.
91. Cording, E. J., F. D. Patton, and D. U. Derce, "Rock Bolt Tests in U129 Tunnel Nevada Test Site," Fenix and Scisson, Inc., Summary Report, NVP-38-19, July 26, 1965.
92. Clark, S. P., Handbook of Physical Constants, Geol. Soc. of Amer., Inc., Revised Ed., 1966.
93. Scholz, C. H., "Microfracturing and the Inelastic Deformation of Rock in Compression," J. Geophys. Res., 72, no. 4, 1417, Feb. 15, 1968.
94. Clark, G. B., R. V. Whitman and F. M. Sauer, "Nuclear Geoplosics ...," Part Two, Stanford Research Institute, Defense Atomic Support Agency Report DASA-1285(II), May 1964.

APPENDIX A

DERIVATION OF THE HYDRODYNAMIC EQUATION OF STATE FOR A MIXTURE FROM THE GIVEN EQUATION OF STATE OF THE CONSTITUENT MATERIALS

INTRODUCTION

We consider a mixture which is sufficiently intimate that local temperature equilibrium can be assumed among the constituents as well as the local pressure equilibration. The desired equation of state is that of the mixture, to be used in applications in which dimensions of interest are very large compared to the scale size of the inhomogeneities. Further, from use in standard hydrodynamic applications, it is desirable to determine the pressure P of the mixture as a function of the density $\bar{\rho}$ (or specific volume $\bar{\tau}$) and specific internal energy \bar{E} of the mix.

BASIC EQUATIONS

The known equations of state of the constituents are taken to be of the general form

$$P_i = P_i(\tau_i, E_i) \quad (A.1)$$

$$E_i = E_i(\tau_i, \theta) \quad (A.2)$$

The condition that the specific energy \bar{E} be that given by the energies of the constituents is

$$\bar{E} = \frac{\sum m_i E_i(\tau_i, \theta)}{\sum m_i} \quad (A.3)$$

where m_i is the mass of each constituent, per unit mass of mix. and θ is the temperature.

The condition that the specific volume $\bar{\tau}$ be due to the individual specific volumes is

$$\bar{\tau} = \frac{\sum m_i \tau_i}{\sum m_i} \quad (\text{A.4})$$

and, finally, the condition that the equilibrated pressure \bar{P} be that of each constituent is given by the N equations (for N constituents)

$$\bar{P} = P_i(\tau_i, E_i) \quad i = 1 \text{ to } N \quad (\text{A.5})$$

Equations (A.3), (A.4) and (A.5), assuming that P_i , τ_i , E_i and $E_i(\tau_i, \theta)$ are the known functions implied by Eqs. (A.1) and (A.2), comprise a set of $2N+2$ equations in the $2N+2$ unknowns τ_i , θ and \bar{P} . The objective is to determine the solution of these equations for fixed \bar{E} , $\bar{\tau}$.

SOLUTION BY ITERATION

When Eqs. (A.1) and (A.2) are representative of real media, the above set of equations is ordinarily too complex to solve exactly. An accurate solution is, however, possible by the following iteration method.

It has proved convenient to separate the process into two iterations, which will be described first in general terms: In the first iteration, the τ_i are temporarily held constant and θ is varied until the energy condition, Eq. (A.3), is satisfied to some prescribed accuracy. This iteration procedure gives θ , and also the individual energies E_i . In the second iteration, the resulting E_i are held constant and the τ_i are varied to solve Eq. (A.4) and the N Eqs. (A.5). This iteration gives the N quantities τ_i and also \bar{P} .

The process (the two iterations) is then repeated until a self-consistent set of quantities τ_i, θ, \bar{P} is obtained.

The detailed procedure is as follows. An initial estimate is made for θ and the τ_i . These initial τ_i are, further, adjusted to satisfy the condition (A.4) on over-all specific volume $\bar{\tau}$ (this initial normalization of the τ_i will be seen to be useful in the second iteration, below.)

For the θ iteration (τ_i constant), the right side of Eq. (3) is computed

$$\tilde{E} = \frac{\sum m_i E_i(\tau_i, \theta)}{\sum m_i}$$

using the known E_i functions Eq. (A:2). A refined θ is then computed using

$$\Delta\theta = \frac{\bar{E} - \tilde{E}^*}{C_v}$$

where C_v is an approximate average specific heat. A new \tilde{E} is then computed and an associated new θ . This process is cycled until convergence is obtained. In determining C_v above, once two values of E have been calculated, it is possible to obtain an accurate value of this quantity and speed convergence. For this purpose, a C_v is calculated each cycle from $C_v = \left(\frac{\tilde{E}_1 - E_2}{\theta_1 - \theta_2} \right)$ where 1 and 2 subscripts refer to the last two \tilde{E}, θ points.

* Until $\left| \frac{\tilde{E} - \bar{E}}{\bar{E}} \right| < .2$, a regula falsi iteration is used to refine θ .

For the τ_i iteration, the basic equations are (from the variations of Eqs. (A.4) and (A.5) with θ constant)

$$\bar{P} = P_i + \left(\frac{\partial P_i}{\partial \tau_i} \right)_{E_i} \Delta \tau_i \quad (\text{A.6})$$

$$0 = \sum_i m_i \Delta \tau_i \quad (\text{A.6})$$

The second equation (the derivative of Eq. (A.4)) requires only that the specific volume of the mix remain constant; for this reason it was necessary to assure that the initial specific volume be correct, as done in the pre-iteration adjustment described above. These are $N+1$ equations in $\Delta \tau_i, \bar{P}$ with solution

$$\bar{P} = \frac{\sum P_i \omega_i}{\sum \omega_i} \quad \omega_i \equiv m_i / \left(\frac{\partial P_i}{\partial \tau_i} \right)_{E_i}$$

$$\Delta \tau_i = \frac{\omega_i}{m_i} \left(P_i - \frac{\sum P_i \omega_i}{\sum \omega_i} \right)$$

as is easily verified by substitution. Once a solution is determined, the τ_i are updated

$$\tau_i = \tau_i + \Delta \tau_i$$

and new P_i are determined from Eq. (A.1)

$$P_i = P_i(\tau_i, E_i)$$

Also, it has been found that convergence is faster if we compute improved values of the coefficients $\left(\frac{\partial P_i}{\partial \tau_i}\right)_{E_i}$ each cycle, using points P_i, τ_i from previous cycles, i.e.,

$$\left(\frac{\partial P_i}{\partial \tau_i}\right)_{E_i} = \frac{P_{i,1} - P_{i,2}}{\tau_{i,1} - \tau_{i,2}}$$

in order to have accurate coefficients for the next cycle, in Eq. (A.6). With these new values of P_i and $\left(\frac{\partial P_i}{\partial \tau_i}\right)_{E_i}$ it is now possible to compute improved solutions to Eqs. (A.6) and (A.7) for the next cycle of the iteration. The process is found to be rapidly convergent.

The τ_i iteration gives \bar{P} and new τ_i for fixed E_i . A new θ and set of E_i is then determined from the θ iteration and the τ_i iteration can then be repeated to determine improved τ_i and a new \bar{P} . This process also is found to converge rapidly in experience to date, giving the desired \bar{P} for specified $\bar{\tau}$ and \bar{E} of the mix.

A computer program has been written which performs the above iterations, utilizing (where possible) the results of a similar program which was developed at S³ for another application. The basic program is compatible with state equations of the forms (A.1), (A.2), once those relations are programmed (as subroutines).

APPENDIX B
NTS TUFF DATA

B.1 CRYSTAL OR NONPOROUS DENSITY OF DRY TUFFS

This parameter has also been referred to in the literature as "the grain density," and "the density of the solids." The values that have been found are listed in Table B.1.

TABLE B.1

Crystal Density (g/cc)	Reference
2.3	44
2.0	44
2.6	44
2.7	44
2.37	37
2.597	37
2.122	37
2.21	89
2.23	89
2.43	45
2.409	50
2.33 to 2.49	90

Preceding page blank

B.2 GRAIN SIZE OF DRY TUFFS

Although the grain size has been reported many places in the literature, the best study by far was conducted by Petersen, et al. ⁽⁴⁰⁾ All reported values are listed in Table B.2.

TABLE B.2

Component	Wt. %	Grain Size (mm)	Reference
Tuff	2.6	>9.42	40
	2.8	9.42-6.68	
	3.7	6.68-4.7	
	2.6	4.7-3.96	
	9.5	3.96-1.98	
	25.9	1.98-0.41	
	17.9	0.41-0.15	
	13.2	0.15-0.05	
	21.8	<0.05	
Crystals	5-15	average .2 to .4	50
Glass Fragments	10-70	average .3 to .5	
Lithic Fragments	3-8	average .3 to .5	
Glass Dust Matrix	15-20	.001	
Glass and Crystallites	60	<.01	39
Quartz, Chert, Feldspar	40	.3	
Tuff #1	Range	.01 to 10.	37
Tuff #2	Range	.05 to 10.	
Tuff #3	Range	.1 to 2.	
Tuff #4	Range	.05 to 5.	
Tuff	Range	.005 to 3.	36
Tuff	Average	.01	93

B.3 HYDRODYNAMIC SOUND SPEED FOR DRY TUFFS

The hydrodynamic sound speed, c_0 , found in the literature for porous dry tuffs is presented in Table B.3.

TABLE B.3

c_0 ($\times 10^5$ cm/sec)	Remarks	Reference
1.034	From a fit to high pressure data ($p = .2$ to 1.3 Mbar).	38
1.32 to 1.47	From a fit to low pressure data. ($p = 30$ to 190 kbar).	38
1.25	From an extrapolation of the curve on page 23 of the reference.	41
2.3	For pressures greater than 130 kbar.	43
2.56	From the relation $c_0 = (c_1^2 - 4/3 c_2^2)^{1/2}$, where c_1 and c_2 were measured.	89
2.12		89
1.94		92

B.4 COMPOSITION OF DRY TUFFS

Table B.4 contains the geologic composition of various tuffs as found in the literature.

TABLE B.4

Component	Quantity	Reference
	(Wt. %)	
Sanidine	<1 to 6	} 50
Quartz	<1 to 7	
Plagioclase	<1 to 5	
Biotite	Trace to <1	
Glass Fragments	60 to 70	
Glass Dust Matrix	15 to 20	
Lithic Fragments	3 to 8	
	(Wt. %)	
Glass Shards	85	} 53
Quartz, Feldspar and Lithic	15	
	(Vol. %)	
Feldspar Phenocrysts	6	} 88
Quartz Phenocrysts	8	
Chalcedony Segregations	14	
Matrix (Clay, Chalcedony, Zeolite, etc.)	72	
	(Vol. %)	
Quartz	4	} 36
Plagioclase	1	
Alkali Feldspar	7	
Microlites	10	
Glass	78	

Table B.4 (Continued)

Component	Quantity	Reference
Quartz Matrixal	(Vol. %) 32.5 67.5	} 37
Quartz Matrixal (principally glass)	(Vol. %) 3.5 96.5	} 37
Clinoptilolite Anorthoclase Quartz	(Vol. %) 94. 5 1	} 37

B.5 THERMAL PROPERTIES FOR TUFF-LIKE MATERIALS AND TUFF COMPONENTS

The thermal expansion coefficients of the following materials were found in the Handbook of Physical Constants. (92)

	<u>Linear Expansion Coefficient (α)</u> ($\times 10^{-6}/^{\circ}\text{C}$)
Glass	7.88 to 9.1
Masonry	4.0 to 7.0
Fire Clay Brick	8.1
Cement and Concrete	10. to 14.
Granite	8.3
Sandstone	7.0 to 12.0
Limestone	9.0
Fused Quartz	0.42
	<u>Volumetric Expansion Coefficient (β)</u> ($\times 10^{-6}/^{\circ}\text{C}$)
Quartz	35.3
Porcelain	10.8

The constant pressure specific heat data for the following materials was also found in the Handbook of Physical Constants. (92)

	<u>C_p (cal/g $^{\circ}\text{C}$)</u>
Dry Clay	.22
Glass	.1988
Quartz	.138
Granite	.192
Basalt	.20
Marble	.21

Table B.5 (Continued)

The following are estimated values for nonporous, dry tuff based on the above values for tuff-like materials and the components of tuff.

$$\beta = 27. \times 10^{-6} / ^\circ\text{C}$$

$$C_p = 0.20 \text{ cal/g } ^\circ\text{C}$$

$$C_v = 0.20 \text{ cal/g } ^\circ\text{C}$$

B.6 STRENGTH PARAMETERS OF DRY TUFF

The unconfined compressive strength, Y, and Poisson's ratio, ν , for various porous, dry tuffs, have been measured and calculated in a variety of ways. Table B.6 contains the values found in the literature.

Y (kbars)	ν	ρ (g/cc)	Por.(%)	Remarks	References
.65		1.9	34	Strain Rate = $1. \times 10^3$ /sec	87
.45		1.9	34	Strain Rate = 1.8×10^{-2} /sec	
.36		1.9	34	Strain Rate = 1.6×10^{-4} /sec	
.876	.085	1.76	20.36	p = 0 to .2 kbar	89
	0.16	1.76	20.36	p = 0. to .876 kbar	
.796	.075	1.76	21.08	p = 0 to .5 kbar	
	0.17	1.76	21.08	p = .5 to .796 kbar	
				Stress Rate = 3.5 to 5.2 bars/sec	
	.18	1.76	20.36	From pulse velocity on cores	89
	.28	1.76	21.08		
.223	0.15	1.6		Water content = 4.6%	91
	0.36	2.78			92
	0.11	1.45	42.		
	0.11	1.6	37.		
	0.24	2.2	14		
.214	0.09	2.35	10.3		94
.037	0.12	1.45	42.5		94

UNCLASSIFIED

Security Classification

DOCUMENT CONTROL DATA - R & D		
<i>(Security classification of title, body of abstract and indexing annotation must be entered when the overall report is classified)</i>		
1. ORIGINATING ACTIVITY (Corporate author) Systems, Science and Software P.O. Box 1620 La Jolla, California 92037		2a. REPORT SECURITY CLASSIFICATION Unclassified
		2b. GROUP
3. REPORT TITLE Stress Wave Effects in Inhomogeneous and Porous Earth Materials		
4. DESCRIPTIVE NOTES (Type of report and inclusive dates) Formal Report (Period 15 May 1969 - 14 March 1970)		
5. AUTHOR(S) (First name, middle initial, last name) T.D. Riney, S.K. Garg, J.W. Kirsch, L.W. Morland, C.R. Hastings		
6. REPORT DATE March 31, 1970	7a. TOTAL NO. OF PAGES 297	7b. NO. OF REFS 94
8a. CONTRACT OR GRANT NO. DASA 01-69-C-0159	9a. ORIGINATOR'S REPORT NUMBER(S) 3SR-267	
b. PROJECT NO. (ARPA Order No. 1438)		
c. Program Code No. 9F10	9b. OTHER REPORT NO(S) (Any other numbers that may be assigned this report) DASA 2498	
10. DISTRIBUTION STATEMENT This document has been approved for Public Release and Sale; Its Distribution is Unlimited.		
11. SUPPLEMENTARY NOTES	12. SPONSORING MILITARY ACTIVITY Director Advanced Research Projects Agency Washington, D.C. 20301	
13. ABSTRACT The studies described in this report are directed to the construction of reliable techniques for calculating stress wave propagation in a geologic medium in the pressure range from 300 kbar down to a few bars. The medium is considered to be a composite consisting of rock matrix with water in its pores and a description of its wave propagation characteristics is sought in terms of the behavior of the isolated rock and water components. Nevada tuff is selected for the rock matrix in order to be specific in formulating its equation of state from available experimental data. The equation of state for water is constructed in convenient analytic forms for the expanded and condensed states as well as the transition through the steam dome. The shock pressure of saturated wet tuff media with varied mass fractions of water is treated under three assumptions related to the homogeneity of the media: (1) complete homogenization--equation of state for wet tuff is calculated under the assumption that the water and tuff components are in local pressure and thermal equilibrium; (2) no homogenization--detailed wave propagation calculations for composite water/tuff configurations of varied substructure; and (3) theory of interacting continua--generalized homogenized treatment in which the individual responses of the water and tuff components are treated without explicit consideration of the substructure of the composite.		

DD FORM 1 NOV 65 1473

UNCLASSIFIED
Security Classification

14. KEY WORDS	LINK A		LINK B		LINK C	
	ROLE	WT	ROLE	WT	ROLE	WT
Composite materials						
Stress waves in geologic media						
Water equation of state						
Underground explosions						
Nevada tuff						
Seismic waves						
Rock and soil models						
Porous media						
Decoupling						